

FIBRE FORMATION, CHARACTERISATION AND CARBONISATION OF BIO-BASED PRECURSORS



By

Bongkot Hararak

A thesis submitted to
the University of Birmingham for the degree of
DOCTOR OF PHILOSOPHY

School of Metallurgy and Materials
College of Engineering and Physical Sciences
University of Birmingham

March 2020

UNIVERSITY OF
BIRMINGHAM

University of Birmingham Research Archive

e-theses repository

This unpublished thesis/dissertation is copyright of the author and/or third parties. The intellectual property rights of the author or third parties in respect of this work are as defined by The Copyright Designs and Patents Act 1988 or as modified by any successor legislation.

Any use made of information contained in this thesis/dissertation must be in accordance with that legislation and must be properly acknowledged. Further distribution or reproduction in any format is prohibited without the permission of the copyright holder.

ABSTRACT

This research explores the utilisation of softwood Kraft lignin as an alternative precursor for the production of fibrous preforms for the subsequent production of carbonised fibres. Currently, only 1-2% of lignin is used for low valued-added applications and the rest is burned as a fuel for energy generation. Electro-spinning was used to transform lignin solutions into fibrous preforms. Acetone-soluble softwood Kraft lignin was electro-spun successfully using a non-toxic binary solvent and without the use of polymer blends. Prior to electro-spinning, the impurities from lignin were removed to aid electro-spinning and carbonisation. Initially, the as-received lignin was characterised, including determining the inorganic content, lignin content and the molecular weight distribution. The inorganic content in the as-received lignin was $1.195 \pm 0.021\%$ and the two major elements present in the ash were sulphur and sodium.

As-received lignin was purified using the following methods: (i) treatment with acidified water; and (ii) fractionation using acetone. The experimental matrix for the treatment of lignin with acidified water was optimised using Taguchi analysis. The inorganic content of as-received lignin was reduced to $0.354 \pm 0.020\%$ after treatment with acidified water. Whereas the acetone-soluble lignin obtained from fractionation with acetone had an ash content of $0.055 \pm 0.021\%$. Hence, due to the lower inorganic content in the acetone-soluble lignin fraction, it was used for fibre formation studies using electro-spinning.

A novel approach for electro-spinning of acetone-soluble softwood Kraft lignin without polymer blending was carried out. The acetone-soluble lignin was dissolved in a 2/1 (v/v) mixture of acetone and dimethyl sulfoxide. Bead-free and electro-spun lignin fibres with a circular cross-section were produced when a concentration of the acetone-soluble lignin was 53 wt%. The average fibre diameter was $1.16 \pm 0.21 \mu\text{m}$. Subsequent to electro-spinning, procedures for (i) removing the residual solvent, (ii) thermo-stabilisation and (iii) carbonisation were undertaken to enable the production of carbonised lignin fibres. In each procedure, properties of the resultant fibres were characterised using range of analytical techniques. Randomly orientated and short-

lengths of axially-aligned carbonised fibres from 100% acetone-soluble lignin were demonstrated for the first time.

ACKNOWLEDGEMENTS

I would like to take this opportunity to express my sincere gratitude to my supervisor Professor Gerard Fernando for his invaluable supervision and support during my PhD programme. His support provided me with effective tools and equipment to undertake my research. The weekly meeting with him and his guidance helped to undertake me for the research design, experimentation and analysis required to complete this thesis.

I would also like to thank to my co-supervisors Dr. Surya Pandita and Dr. Stephen Kukureka for their advice and support of. My sincere thanks go to Frank Biddlestone for his patience for training me to use all the analytical equipment in the laboratory. I am grateful to Dr. Raj Machavaram for all his helps. I would like to thank, Inam Khan, all over three and half years we have worked together. Thank you to be more than my colleague. I would also like to thank to the staff at the School of Metallurgy and Materials, University of Birmingham.

In addition, I would also like to thank the National Science and Technology Development Agency (NSTDA) for giving me the opportunity to gain more knowledge and experience. Financial support was received from the Royal Thai Government Scholarship.

Finally, I am extremely grateful to my family for all their love and continuing support in accomplishing my dream; thank you for standing by me.

CONTENTS

1. INTRODUCTION	1
2. LITERATURE REVIEW AND RESEARCH GAPS	5
2.1 Carbon Fibres.....	5
2.1.1 An Overview of Carbon Fibres	5
2.1.2 Production of Carbon Fibres from Polyacrylonitrile	8
2.1.2.1 Wet-spinning of PAN	10
2.1.2.2 Thermo-stabilisation of PAN.....	10
2.1.2.3 Carbonisation of PAN.....	11
2.1.3 Properties of Carbon Fibres Derived from Polyacrylonitrile.....	13
2.2 Lignocellulosic as an Alternative Precursor for the Production of Carbon Fibres	14
2.2.1 Lignin	16
2.2.2 Extraction of Lignin	22
2.2.3 LignoBoost and LignoForce Process	24
2.2.4 Properties of Commercially Available Lignin	26
2.2.5 Treatments for Lignin	28
2.3 Fibre Formation using Lignin	35
2.3.1 Melt-spinning of Lignin	35
2.3.2 Electro-spinning Lignin.....	43
2.3.3 Dry-spinning Lignin	54
2.3.4 Wet-spinning Lignin.....	58
2.4 Heat Treatment of Lignin	62
2.4.1 Thermo-stabilisation of Lignin	62
2.4.2 Carbonisation of Lignin Precursor	63

2.5	Mechanical Properties of Carbon Fibres from Lignin.....	65
2.6	Research Gaps.....	72
2.7	Aim and Objectives.....	72
2.8	Overview of the Research	73
2.9	Structure of the Thesis	75
3.	EXPERIMENTAL.....	76
3.1	Materials.....	76
3.2	Treating Lignin with Acidified Water and Fractionation using Acetone	76
3.2.1	Treatment of Lignin with Acidified Water.....	76
3.2.2	Molecular Weight Fractionation of Lignin using Acetone.....	79
3.2.3	Determination of the Lignin Content and Composition	82
3.2.3.1	Determination of the Moisture Content.....	84
3.2.3.2	Determination of the Ash Content	84
3.2.3.3	Klason or Acid-insoluble Lignin	85
3.2.3.4	Acid-soluble Lignin	86
3.3	Electro-spinning of Acetone-soluble Lignin.....	87
3.3.1	Preparation of Acetone-soluble Lignin Solutions.....	87
3.3.2	Electro-spinning of Acetone-soluble Lignin Fibres	88
3.3.2.1	Electro-spinning of Randomly Aligned Acetone-soluble Lignin Fibres	88
3.3.2.2	Electro-spinning of Aligned Acetone-soluble Lignin Fibres..	90
3.3.3	Heating of Electro-spun Acetone-soluble Lignin Fibres to Remove Acetone and DMSO	91
3.3.4	Thermo-stabilisation of Electro-spun Acetone-soluble Lignin Fibres	94
3.3.5	Carbonisation of Electro-spun Acetone-soluble Lignin Fibres.....	96
3.3.6	Electro-spinning of Acetone-soluble Lignin with Processing Aids ..	101
3.4	Characterisation Techniques.....	102

3.4.1 Helium Gas Pycnometer	102
3.4.2 Laser Particle Size Analysis.....	103
3.4.3 Scanning Electron Microscopy	103
3.4.4 Fourier Transform Infrared Spectroscopy	103
3.4.5 Differential Scanning Calorimetry.....	104
3.4.6 Thermo-gravimetric Analysis.....	104
3.4.7 Gel Permeation Chromatography	105
3.4.8 Viscometry	105
3.4.9 Electrical Conductivity	106
3.4.10 X-ray Photoelectron Spectroscopy.....	106
3.4.11 Raman Spectroscopy.....	106
3.4.12 Atomic Force Microscope	107
4. TREATMENT OF LIGNIN USING ACIDIFIED WATER AND MOLECULAR WEIGHT FRACTIONATION OF LIGNIN	108
4.1 Introduction.....	108
4.2 Characterisation of As-received BioChoice®Lignin.....	109
4.2.1 Physical Properties of As-received BioChoice®Lignin.....	109
4.2.2 Molecular Weight Distribution of As-received BioChoice®Lignin	113
4.2.3 Determination of the Ash Content in As-received BioChoice®Lignin and Its Elemental Compositions.....	114
4.2.4 Lignin Content of As-received BioChoice®Lignin	115
4.2.5 Thermal Properties of As-received BioChoice®Lignin.....	118
4.2.5.1 Thermo-gravimetric Analysis of As-received BioChoice®Lignin.....	118
4.2.5.2 Differential Scanning Calorimetry of As-received BioChoice®Lignin.....	120

4.2.6	Functional Group Analysis of As-received BioChoice® Lignin by Fourier Transform Infrared Spectroscopy	123
4.3	Treatment of As-received BioChoice® Lignin with Acidified Water	128
4.3.1	Taguchi Design of Experiments	129
4.3.2	Analysis of Variance.....	134
4.3.2.1	P-value and F-ratio.....	134
4.3.2.2	Fisher Pairwise Plot.....	137
4.3.2.3	Percentage Contribution.....	139
4.3.3	Effect of pH on Specified Properties of Acid-treated Lignins.....	142
4.3.3.1	Ash Content of Acid-treated Lignins	142
4.3.3.2	Differential Scanning Calorimetry of Acid-treated Lignins .	143
4.3.3.3	Functional Group Analysis of Acid-treated Lignins by Fourier Transform Infrared Spectroscopy	147
4.4	Molecular Weight Fractionation of As-received BioChoice® Lignin Using Acetone	149
4.4.1	Fractionation Yield	150
4.4.2	Characterisation of Lignins Obtained from Fractionation Using Acetone.....	150
4.4.2.1	Physical Characteristics of Acetone-soluble and Acetone- insoluble Lignins.....	150
4.4.2.2	Molecular Weight Distribution of Acetone-soluble and Acetone-insoluble Lignins.....	151
4.4.2.3	Determination of the Ash Content in Acetone-soluble and Acetone-insoluble Lignins and Their Elemental Compositions	156
4.4.2.4	Lignin Content of Acetone-soluble and Acetone-insoluble Lignins.....	161
4.4.2.5	Thermo-gravimetric Analysis of Acetone-soluble and Acetone-insoluble Lignins.....	163

4.4.2.6	Differential Scanning Calorimetry of Acetone-soluble and Acetone-insoluble Lignins.....	170
4.4.2.7	Functional Group Analysis of Acetone-soluble and Acetone-insoluble Lignins by Fourier Transform Infrared Spectroscopy	174
4.5	Treating Acetone-insoluble Lignin with Acidified Water	177
4.6	Summary	180
5.	ELECTRO-SPINNING OF ACETONE-SOLUBLE LIGNIN	182
5.1	Introduction.....	182
5.2	Criteria for Selecting the Solvent for Electro-spinning of Acetone-soluble lignin	183
5.3	Influence of the Concentration of Acetone-soluble Lignin on the Solution Properties and Morphology of Electro-spun Fibres.....	185
5.3.1	Viscosity and Electrical Conductivity of Acetone-soluble Lignin Solutions	185
5.3.2	Morphology of Electro-spun Acetone-soluble Lignin Fibres	187
5.4	Randomly Aligned Electro-spun Acetone-soluble Lignin Fibres and Their Properties	192
5.4.1	Scanning Electron Microscopy of Electro-spun Acetone-soluble Lignin Fibres	192
5.4.2	Differential Scanning Calorimetry of Electro-spun Acetone-soluble Lignin Fibres	195
5.4.3	Thermo-gravimetric Analysis of Electro-spun Acetone-soluble Lignin Fibres	199
5.5	Heating of Electro-spun Acetone-soluble Lignin Fibres to Remove Acetone and DMSO.....	201
5.5.1	Scanning Electron Microscopy of Heated Electro-spun Acetone-soluble Lignin Fibres	202

5.5.2	Differential Scanning Calorimetry of Heated Electro-spun Acetone-soluble Lignin Fibres	205
5.5.3	Thermo-gravimetric Analysis of Heated Electro-spun Acetone-soluble Lignin Fibres	208
5.5.4	Fourier Transform Infrared Spectroscopy of Heated Electro-spun Acetone-soluble Lignin Fibres	210
5.6	Thermo-stabilisation of Electro-spun Acetone-soluble Lignin Fibres	212
5.6.1	Scanning Electron Microscopy of Thermo-stabilised Electro-spun Acetone-soluble Lignin Fibres	213
5.6.2	Differential Scanning Calorimetry of Thermo-stabilised Electro-spun Acetone-soluble Lignin Fibres	215
5.6.3	Fourier Transform Infrared Spectroscopy of Thermo-stabilised Electro-spun Acetone-soluble Lignin Fibres	219
5.6.4	X-ray Photoelectron Spectroscopy of Thermo-stabilised Electro-spun Acetone-soluble Lignin Fibres	223
5.7	Carbonisation of Electro-spun Acetone-soluble Lignin Fibres	231
5.7.1	Taguchi Analysis on the Effect of Carbonisation Condition on Fibre Diameter	232
5.7.2	Taguchi Analysis on the Effect of Carbonisation Condition on Graphitic Structure of Lignin Analysed using Raman Spectroscopy	237
5.7.3	Scanning Electron Microscopy Carbonised Electro-spun Acetone-soluble Lignin Fibres	244
5.7.4	Raman Spectroscopy Carbonised Electro-spun Acetone-soluble Lignin Fibres	247
5.7.5	X-ray Photoelectron Spectroscopy of Carbonised Electro-spun Acetone-soluble Lignin Fibres	248

5.8	Production of Aligned Electro-spun Acetone-soluble Lignin Fibres and their Properties	250
5.9	Summary	254
6.	CONCLUSION AND RECCOMENDATION FOR FUTURE RESEARCH	257
6.1	Conclusion and Contribution to Knowledge	257
6.2	Other Research Outcomes	258
6.3	Recommendation for Future Research.....	258
	APPENDICES	259
	Appendix A: Alternative Solvent for Electro-spinning of Lignin.	260
	Appendix B: Surface Roughness of Electro-spun Acetone-soluble Lignin Fibres	261
	Appendix C: FTIR Spectra of Lignin Fibres Heated in a Vacuum Oven, Nitrogen and Air.	264
	Appendix E: Response table of Analysis of Varian (ANOVA)	268
	Appendix F: Interaction Plot of Carbonisation Parameters	270
	Appendix G: Processing Aid for Electro-spinning of Acetone-soluble Lignin ..	272
	LIST OF REFERENCES	278

LIST OF FIGURES

Figure 2.1 (a) Schematic illustration of the ABA packing sequence of the hexagonal graphitic crystal structure and (b) sp^2 hybridisation showing the sigma and pi-bonds [2,39].	6
Figure 2.2 The production of carbon fibres from PAN, rayon and mesophase pitch [7,19].	6
Figure 2.3 Repeat unit chemical structure of cellulose with a 1-4 glycosidic linkage.	7
Figure 2.4 Typical structure of mesophase pitch for the production of carbon fibres [19].	8
Figure 2.5 Chemical structure of acrylonitrile monomer and PAN.	9
Figure 2.6 Production of carbon fibres from PAN-based precursor [2,45].	9
Figure 2.7 Chemical reaction during thermo-stabilisation in air of the PAN homopolymer; adapted from [17,46,48].	11
Figure 2.8 Schematic illustration of graphite formation adapted from [17,53].	12
Figure 2.9 Schematic illustration of a typical plant cell wall and associated macro and micro-structural components [20,58,59].	15
Figure 2.10 Common monomers of lignin and the respective lignin units [20,26].	17
Figure 2.11 Common linkages in lignin [60].	18
Figure 2.12 The branched molecular structure of softwood lignin according to Adler, 1977 [67].	20
Figure 2.13 The linear structure of softwood lignin as proposed by Crestini <i>et al.</i> , 2011 [69].	21
Figure 2.14 Different extraction processes to separate lignin from lignocellulosic biomass [71].	22
Figure 2.15 (a) LignoBoost process and (b) LignoForce process to isolate Kraft lignin [73].	25

Figure 2.16 A plot showing the change in T_g and PDI of lignin from fractionation using organic solvent with respect to weight average molecular weight (M_w). Data compiled from different lignin sources of Indulin AT [124], BioChoice® Lignin [98], softwood Kraft lignin from USA and Sweden [29].	31
Figure 2.17 A plot of glass transition temperatures of parent lignin and the permeated lignin fraction from ceramic membrane filtration [134,135].	34
Figure 2.18 SEM micrographs of the cross-sectional area of melt-spun carbon fibres from a butylated-lignin/PLA blend [155,156].	37
Figure 2.19 SEM micrographs of carbon fibres from 50% yellow poplar lignin and 50% grass lignin [164].	37
Figure 2.20 (a) Typical set-up for electro-spinning and key components of the electro-spinner and (b) fibre formation by electro-spinning.	43
Figure 2.21 Filament cross-sectional morphology dependence on the ratio of evaporation rate to diffusion rate [194].	54
Figure 2.22 SEM micrographs of as-spun fibres from dry-spinning of acetylated softwood Kraft lignin. The solution was spun at room temperature at two different concentrations: (a) 2.15 g·ml ⁻¹ and (b) 2.00 g·ml ⁻¹ [196,197].	55
Figure 2.23 Schematic illustration of the continuous flow of the Aqueous Lignin Purification using the Hot Acids (ALPHA) process [199–201].	56
Figure 2.24 SEM micrographs of carbon fibres derived from: (a) medium; (b) higher; and (c) highest M_w lignins from the ALPHA process [201].	56
Figure 2.25 The PAN/sulfonate lignin fibres obtained from the air thermo-stabilisation step with finger-like macrovoids [142].	59
Figure 2.26 Schematic of the overview of this research.	74
Figure 3.1 Flow diagrams of the methods used in this study for treating lignin with acidified water.	79
Figure 3.2 Flow diagrams of fractionation lignin using acetone.	80

Figure 3.3 Schematic illustration of the set-up for the fractionation of lignin using acetone.....	81
Figure 3.4 Photographs showing the apparatus used for the evaporation of acetone: (a) vacuum pump with dry ice condenser; and (b) rotary evaporator.	82
Figure 3.5 Flow diagram presenting the steps for determining the lignin content and composition.....	83
Figure 3.6 Schematic set-up of reflux unit for lignin dissolving.	88
Figure 3.7 Schematic illustration of the custom-built electro-spinner.....	89
Figure 3.8 Schematic illustration of the modified parallel electrodes for producing highly-aligned electro-spun lignin fibres: (a) modified-graphite U-shaped electrode; (b) components of the modified U-shaped graphite and insulating polystyrene strip-PS; (c) the assembled electrode assembly with the insulating strip; and (d) orientation of the aligned electro-spun lignin fibres.....	91
Figure 3.9 A flow diagram indicating the heating environments for the electro-spun acetone-soluble lignin fibres prior to oxidative thermo-stabilisation.	92
Figure 3.10 Schematic illustration of the experimental set up for heat treatment of electro-spun acetone-soluble lignin fibres.....	93
Figure 3.11 Illustration of the heating rate and dwell periods that were used for the thermo-stabilisation experiments. The red circles represent the time when samples were removed for characterisation.	94
Figure 3.12 Schematic illustration of the experimental set up for the thermo-stabilisation of electro-spun acetone-soluble lignin fibres.	95
Figure 3.13 Photograph of PYRO THERM furnaces used in this study.....	96
Figure 3.14 Schematic illustration of the experimental set up for measuring the temperature gradient in the PYRO THERM furnace.	97
Figure 3.15 Temperature profile of the tube furnace used for thermo-stabilisation and carbonisation experiments.	98

Figure 3.16 Calibration curves for the PYRO THERM tube furnace at the centre of the furnace using heating rates of: (a) 2; (b) 5; and (c) 10 K·minute ⁻¹	99
Figure 4.1 The visual appearance of as-received softwood Kraft lignin (BioChoice®lignin).....	109
Figure 4.2 SEM micrographs of as-received lignin at a range of magnifications.	111
Figure 4.3 Particle size distribution of as-received lignin obtained using a laser particle size analyser.	112
Figure 4.4 Molecular weight distribution curves for pre-dried as-received lignin samples as determined by GPC.	114
Figure 4.5 UV/Visible spectra of pre-dried as-received lignin.....	116
Figure 4.6 TGA and DTG curves for pre-dried as-received lignin: (a) the thermal decomposition range from 25 °C to 900 °C divided into four main stages and (b) enlarged view of the first stage region.	119
Figure 4.7 DSC thermograms for pre-dried as-received lignin: (a) first heating; (b) second heating; and (c) third heating. The insert in (a) shows an expanded view between 170 and 250 °C.....	122
Figure 4.8 FTIR spectra of as-received lignin: (a) whole spectral range; and (b) enlarged view from 1,800-600 cm ⁻¹	125
Figure 4.9 Effect of acidified water treatment conditions on the average S/N values for ash content.	133
Figure 4.10 Effect of acidified water treatment conditions on the average mean value of ash content.	133
Figure 4.11 Fisher pairwise comparison for the effect of treating lignin with acidified water: (a) pH, (b) acidified water-to-lignin ratio, (c) washing time and (d) number of cycles.....	138
Figure 4.12 Percentage contribution of controllable factors influencing the ash content of lignin.....	139
Figure 4.13 Interaction effect plot for means of ash content.....	140

Figure 4.14 The effect of treating lignin for the ash content.	141
Figure 4.15 The ash content versus the elemental compositions.....	143
Figure 4.16 DSC traces for: (a) pre-dried as-received lignin; and (b), (c) and (d) are as-received lignin treated with acidified water at pH 2, pH 4 and pH 6, respectively.....	144
Figure 4.17 Glass transition temperatures analysed from as-received lignin and acid treated lignin samples.....	146
Figure 4.18 FTIR spectra for as-received and acid-treated lignins: (a) whole spectral range; (b) enlarged view from 1800- 600 cm ⁻¹	148
Figure 4.19 A mechanism for the reaction between HCl and two lignin units [121,122].....	149
Figure 4.20 SEM micrographs of acetone-soluble lignin ((a) and (b)) and acetone- insoluble lignin ((c) and (d)).	151
Figure 4.21 Molecular weight distribution curves for as-received, acetone-soluble and acetone-insoluble lignins determined using GPC.....	152
Figure 4.22 Ash or inorganic content calculated based on the as-received lignin. ...	157
Figure 4.23 Inorganic elements found in the ash from: as-received lignin; acetone- soluble lignin; and acetone-insoluble lignin.....	158
Figure 4.24 Elements and their contents detected in lignin samples used in this current study: (a) full view of the ash content from 0 to 1.2% and (b) enlarged view of a maximum ash content of 0.3%.....	159
Figure 4.25 Ash content in the lignin samples determined in this current study in accordance with the TAPPI T211 om-02 standard.....	160
Figure 4.26 TGA and DTG curves for acetone-soluble lignin: (a) the thermal decomposition range from 25 °C to 900 °C divided into four main stages; and (b) enlarged view of the first stage.	165
Figure 4.27 TGA and DTG curves for acetone-insoluble lignin: (a) the thermal decomposition range from 25 °C to 900 °C divided into four main stages; and (b) enlarged view of the first stage region.	166

Figure 4.28 Overlaid TGA and DTG curves for pre-dried as-received lignin, acetone-soluble lignin and acetone-insoluble lignin: (a) and (b) the thermal decomposition range from 25 °C to 900 °C divided into four main stages.	167
Figure 4.29 DSC thermograms for; (a) as-received lignin and lignins from fractionation using acetone; (b) acetone-soluble and (c) acetone-insoluble lignins.....	171
Figure 4.30 Glass transition temperatures analysed from as-received lignin and lignins obtained from fractionation using acetone.	172
Figure 4.31 A plot of T_{gs} versus weight average molecular weight (M_w). The results from the current work are plotted as red circle and fitted with a linear regression line. The data and the data from the literature have also been plotted [29,83,124].	173
Figure 4.32 FTIR spectra of as-received, acetone-soluble and acetone-insoluble lignins: (a) whole spectral range; and (b) enlarged view from 1800- 600 cm^{-1}	176
Figure 4.33 Inorganic elements found in the ash content from acid-treated acetone-insoluble lignin compared with other lignin samples produced in this work.	178
Figure 4.34 Flowchart showing the steps used for obtaining acetone-soluble lignin and acid-treated acetone-insoluble lignin.....	181
Figure 5.1 Observed relationship between the viscosity and shear rate for acetone-soluble lignin solutions at specified concentrations.	186
Figure 5.2 SEM micrographs showing the effect of the lignin concentrations on the fibre morphology: 45 wt% (a and a*) , 48 wt% (b and b*), 53 wt% (c and c*) and 58 wt% (d and d*).	189
Figure 5.3 Histograms and normal distributions for the fibre diameters for electro-spun acetone-soluble lignin fibres at different lignin concentrations of: (a) 48 wt%, (b) 53 wt% and 58 wt%.	190

Figure 5.4 SEM micrographs of the surface of electro-spun acetone-soluble lignin.	193
Figure 5.5 Histogram and normal distribution of the fibre diameter for the as-spun acetone-soluble lignin fibres.	193
Figure 5.6 SEM micrographs of a cross-sectional views of electro-spun acetone-soluble lignin fibres.	194
Figure 5.7 DSC thermograms; (a) showing three successive heating scans for electro-spun acetone-soluble lignin fibres where the thermal analysis was carried out in nitrogen and (b) expanded view of the first heating scan from 60-180 °C.....	196
Figure 5.8 DSC thermograms where the thermal analysis was carried out in nitrogen from 25-250 °C: (a) showing three successive heating scans for electro- spun acetone-soluble lignin; and (b) expanded view of the first heating scan from 60-180 °C.	198
Figure 5.9 TGA and DTG curves for electro-spun acetone-soluble lignin fibres.....	200
Figure 5.10 Overlaid TGA and DTG curves of electro-spun acetone-soluble lignin fibres plotted in solid line and acetone-soluble lignin powder plotted in dotted line.	201
Figure 5.11 Fibre morphology as a function of temperatures and environments.....	203
Figure 5.12 Relationship between boiling point and external pressure for DMSO, water and acetone [296].	205
Figure 5.13 DSC thermograms illustrating three successive heating scans for electro- spun acetone-soluble lignin fibres heated in a vacuum oven at 140 °C for six hours.	207
Figure 5.14 An overlaid the first heating scan thermogram of electro-spun acetone- soluble lignin (dotted line) and the electro-spun fibres heated in a vacuum oven at 140 °C for six hours (solid line).	208
Figure 5.15 TGA and DTG curves for electro-spun lignin acetone-soluble lignin fibres heated on a vacuum oven at 140 °C for six hours.	209

Figure 5.16 DTG and TGA and curves: a- acetone-soluble lignin powder, b- electro-spun acetone-soluble lignin fibres, c- electro-spun acetone-soluble lignin fibres heated in a vacuum oven at 140 °C for six hours. Sample code with an asterisk represents the mass-loss data.....	210
Figure 5.17 Overlaid FTIR spectra for lignin fibres dried in an air-circulating and nitrogen-circulating and a vacuum oven at 140 °C.....	211
Figure 5.18 Photographs of the electro-spun acetone-soluble lignin fibres showing the colour after thermo-stabilisation in air.	212
Figure 5.19 Fibres morphologies of the electro-spun acetone-soluble lignin fibres thermo-stabilised in: nitrogen (a-e) and air (f-j) at 150 to 250 °C with a dwell time of one hour.....	214
Figure 5.20 DSC thermograms of lignin fibres thermo-stabilised in nitrogen (a) first heating scan and (b) second heating scan. (*) DSC traces of the electro-spun acetone-soluble lignin fibres heated in a vacuum oven at 140 °C for six hours.	216
Figure 5.21 DSC thermograms for electro-spun acetone-soluble lignin fibres thermo-stabilised in nitrogen: (a) first heating scan and (b) second heating scan. (*) DSC traces for the electro-spun acetone-soluble lignin fibres heated in a vacuum oven at 140 °C for six hours.	217
Figure 5.22 FTIR spectra of lignin thermo-stabilised in nitrogen (50 ml·minute ⁻¹) at 150, 180, 200, 220 and 250 °C. (*)FTIR spectra of the electro-spun fibres heated in a vacuum oven at 140 °C for six hours.	221
Figure 5.23 FTIR spectra of lignin thermo-stabilised in air (50 ml·minute ⁻¹) at 150, 180, 200, 220 and 250 °C. (*) FTIR spectra of the electro-spun fibres heated in a vacuum oven at 140 °C for six hours.	222
Figure 5.24 XPS spectra of electro-spun acetone-soluble lignin heated in: (a) nitrogen and (b) air. (*) XPS spectra of the electro-spun acetone-soluble lignin fibres heated in a vacuum oven at 140 °C for six hours. ...	224

Figure 5.25 XPS spectra of electro-spun acetone-soluble lignin fibres thermo-stabilised at 250 °C in (a) nitrogen and (b) air. XPS spectra of the electro-spun fibres heated in a vacuum oven at 140 °C for six hours coded in (*).	227
Figure 5.26 Overlaid high-resolution XPS spectra of the electro-spun acetone-soluble lignin fibres thermo-stabilised in: (a) nitrogen; and (b) air. (*) XPS spectra of the electro-spun fibres heated in a vacuum oven at 140 °C for six hours.	228
Figure 5.27 Relative concentration of C1- C4 under specified thermo-stabilisation conditions: (a) thermo-stabilised in nitrogen and (b) thermo-stabilised in air.....	230
Figure 5.28 SEM micrographs of carbonised electro-spun acetone-soluble lignin fibres. The labels from (a) to (i) represent the fibre morphology obtained from experiment 1-9 detailed in Table 5.8.....	233
Figure 5.29 The distribution of measured fibres diameters from the carbonised lignin fibres obtained from nine experiments (see Table 5.8).	234
Figure 5.30 Main effect and signal-to-noise ratio plots for the diameters of carbonised lignin fibres.....	235
Figure 5.31 Interaction plots for the fibre diameter of carbonised electro-spun lignin fibres.	236
Figure 5.32 Main effect and signal-to-noise ratio plots for the distribution of fibre diameter of carbonised electro-spun lignin fibres.....	236
Figure 5.33 Deconvolution of typical Raman spectra for electro-spun acetone-soluble lignin fibres carbonised at 1,500 °C.	238
Figure 5.34 Main effect and S/N ratio plots for the I_D/I_G ratio for the carbonised electro-spun lignin fibres.	240
Figure 5.35 Main effect and S/N ratio plots for the FWHM for the D-band for the carbonised electro-spun lignin fibres.....	241

Figure 5.36 Main effects and S/N ratio plots for the FWHM for the G-band for the carbonised electro-spun lignin fibres.....	241
Figure 5.37 Main effects and S/N ratio plots for the A_D/A_G ratio for the carbonised electro-spun lignin fibres.	242
Figure 5.38 Percentage contribution of main effect on interested properties.	244
Figure 5.39 SEM micrographs of the surface morphology and cross-sectional view of electro-spun acetone-soluble lignin fibres. Fibres carbonised at 1,000 °C ((a) and (d)), 1,200 °C ((b) and (e)) and 1,500 °C ((c) and (f)).	245
Figure 5.40 Average fibre diameter and distribution of electro-spun acetone-soluble lignin fibres carbonised at (a) 1,000 °C, (b) 1,200 °C and (c) 1,500 °C..	246
Figure 5.41 An overlaid plot of Raman spectra for electro-spun acetone-soluble lignin fibres carbonised at 1,000 °C, 1,200 °C and 1,500 °C.....	248
Figure 5.42 XPS spectra of carbonised electro-spun acetone-soluble lignin fibres which are carbonised at 1,000 °C, 1,200 °C and 1,500 °C.	249
Figure 5.43 Photographs of electro-spun acetone-soluble lignin fibres collected on: (a) an unmodified parallel-plated graphite ground electrode and (b) modified parallel-plate graphite ground electrode. The ruler is in centimetre scale.....	251
Figure 5.44 SEM micrographs of aligned electro-spun acetone-soluble lignin fibres: fibre surface morphology ((a) and (b)) and cross-sectional view ((c) and (d)).	252
Figure 5.45 SEM micrographs of aligned electro-spun fibres carbonised at: (a) 1,000 °C, (b) 1,200 °C and (c) 1,500 °C.	253
Figure 5.46 Fibre diameter and distribution of fibre diameter of as-spun aligned fibres and carbonised fibres at various carbonisation temperatures.	254
Figure 5.47 Illustration of the procedure for the production of carbon fibres from electro-spun acetone-soluble lignin fibres.	256

LIST OF TABLES

Table 1.1	Physical and mechanical of carbon fibres and other selected reinforcing fibres materials	1
Table 1.2	Volume of available lignin and the extracted lignin volume in 2015.....	3
Table 2.1	Classification of carbon fibres.....	14
Table 2.2	Lignocellulosic compositions from different plant sources.	16
Table 2.3	Mono-lignol composition of softwood, hardwood and grasses.	17
Table 2.4	Approximate percentage of the inter-monolignolic linkages of lignin found in nature	19
Table 2.5	Compiled properties of selected commercially available lignins.	27
Table 2.6	A compiled list of the literature on lignin fibres via melt-spinning.....	39
Table 2.7	A summary of the key processing parameter for electro-spinning.....	45
Table 2.8	A compilation of selected papers on the electro-spinning of lignin fibres.	48
Table 2.9	A compiled list of the literature on lignin fibres via dry-spinning.	57
Table 2.10	A compiled list from the literature on lignin fibres manufactured by wet-spinning.	60
Table 2.11	Compiled list of mechanical values of carbon fibres from lignin-based precursor via melt-spinning, dry-spinning and wet-spinning.....	67
Table 2.12	Mechanical values of nano-carbon fibres from lignin-based precursor via electro-spinning.	70
Table 3.1	The parameters for washing lignin using acidified water and their levels.	77
Table 3.2	Taguchi design of experiment used in this study to determine the optimum parameters for acid-washing lignin.	77

Table 3.3	Taguchi design of experiments for the carbonisation of electro-spun acetone-soluble lignin fibres.	100
Table 4.1	Compiled properties of selected commercially available lignins.	110
Table 4.2	A summary of the ash content and the elements present in as-received lignin after combustion at 525°C.	115
Table 4.3	Compiled data for as-received lignin and relevant properties of selected commercially available lignins.	117
Table 4.4	Band assignments for pre-dried as-received lignin.	126
Table 4.5	Summary of the characteristic properties of pre-dried as-received lignin.	127
Table 4.6	The parameters that were used for treating BioChoice® Lignin with acidified water and their levels with regard to the Taguchi DoE.	129
Table 4.7	The combinations of L9 Taguchi orthogonal array, the results of the ash content and S/N ratios.	131
Table 4.8	Response table for S/N values for obtaining the minimum ash content.	132
Table 4.9	Response table for means of obtaining the lowest ash content.	132
Table 4.10	Results of the ANOVA for ash content and grouping using Fisher pairwise comparison.	136
Table 4.11	Compilation of enthalpy, peak of endothermic and T _g data for as-received lignin and as-received lignin treated with acidified water. .	145
Table 4.12	Normalised absorbance for specified hydroxyl groups for as-received and acid-treated lignin.	147
Table 4.13	Summary of the molecular weight distributions and the T _g for as-received, acetone-soluble and -insoluble lignins and compiled molecular weight results.	154
Table 4.14	A summary of the lignin content in as-received, acetone-soluble and acetone-insoluble lignins.	162

Table 4.15	Compiled TGA results for as-received lignin and lignin from acetone fractionation. The TGA experiment conducted from 25 to 900 °C and heating rate 10 K·minute ⁻¹ under an argon with a flow rate of 50 ml·minute ⁻¹	168
Table 4.16	Relative intensities of FTIR absorbance band for hydroxyl groups and condensation index for as-received, acetone-soluble and acetone-insoluble lignins.	175
Table 4.17	Compiled properties of lignins produced and used for fibre fabrication.....	179
Table 5.1	A compilation of solvents used for electro-spinning of lignin and their properties	184
Table 5.2	Viscosity and electrical conductivity of lignin solutions at specified concentrations. The measurements were obtained at 25 °C.....	187
Table 5.3	Selected papers on electro-spinning of lignin with the relevant information on the solution, fibre morphology and fibre diameter.	191
Table 5.4	Compiled DSC results of thermo-stabilised samples.....	218
Table 5.5	Carbon, oxygen and sulphur contents for as-spun lignin fibres heated in a vacuum oven and in nitrogen or oxygen at specified temperatures.	225
Table 5.6	Chemical state of carbons and their binding energy and function groups between carbon and oxygen.	226
Table 5.7	The parameters investigated and their levels for the carbonisation of electro-spun lignin fibres.....	231
Table 5.8	Combination factors of nine experiments and measured fibre diameter of the carbonised fibres.	232
Table 5.9	The combinations of L9 Taguchi orthogonal array, the results of the analysed data from Raman spectra.	239
Table 5.10	A summary of the Taguchi analysis for the carbonisation parameters for acetone-soluble electro-spun lignin fibres.	243

Table 5.11 Carbon and oxygen contents in the electro-spun acetone-soluble lignin fibres carbonised at 1,000 °C, 1,200 °C and 1,500 °C.....	250
--	-----

LIST OF ABBREVIATIONS

AFM	Atomic Force Microscope
ALPHA	Aqueous Lignin Purification with Hot Acids
ANOVA	Analysis of variance
CI	Condensation index
DTG	Derivative thermogravimetry
DSC	Differential Scanning Calorimetry
DMSO	Dimethyl sulfoxide
DMF	Dimethylformamide
DMAc	Dimethylacetamide
FTIRS	Fourier Transform Infrared Spectroscopy
GPC	Gel Permeation Chromatography
M_w	Weight-average molecular weight
M_n	Number-average molecular weight
PAN	Polyacrylonitrile
PDI	Polydispersity Index
PE	Polyethylene
PEG	Polyethylene glycol
PEO	Polyethylene oxide
PET	Polyethylene terephthalate
PP	Polypropylene
PS	Polystyrene
PTFE	Polytetrafluoroethylene
SEM	Scanning Electron Microscopy

TGA	Thermo-gravimetric Analysis
T _g	Glass transition temperature
XPS	X-ray Photoelectron Spectroscopy

1. INTRODUCTION

Carbon fibres are used extensively in applications where the overall weight of the structure is important, for example in industrial sector such as aerospace [1], automotive [2], civil infrastructure [3,4], marine vehicles [5] and sports equipment [6]. A summary of selected properties for three common classes of carbon fibres is presented in Table 1.1; the data for E-glass, S-glass and Kevlar fibres have also been included for comparison purposes. It can be seen that carbon fibres have higher specific modulus and strength than the other type of fibre reinforcements.

Table 1.1 Physical and mechanical of carbon fibres and other selected reinforcing fibres materials [7–9].

Materials	Density 10³ kg·m⁻³	Specific modulus GPa/(kg·m⁻³)	Specific strength GPa/(kg·m⁻³)
Carbon fibres (Toray T700s) /High strength carbon fibres (HS)	1.8	127.8	2.7
High modulus carbon fibres (HM)	1.8	217.1	1.3
Ultra-high modulus carbon fibres (UHM)	2.2	336.7	1.0
S-glass fibres	2.5	34.9	1.8
E-glass fibres	2.6	27.9	1.3
Kevlar fibres (Kevlar 29)	1.4	40.3	2.5

The production capacity of carbon fibres globally was 104,000 tonnes in 2018 [10], which was contributed by three leading manufacturers: Toray & Zoltek, SGL and Toho,

are comprised nearly 70% of the overall carbon fibre market [11]. The global demand for carbon fibres is estimated to reach 117-120,000 tonnes by 2022 [12]. One of the key driving forces stimulating the demand for carbon fibres is the need to reduce the fuel consumption of transportation-based application. The development and use of lightweight carbon fibre-reinforced composites is perceived as a promising way to achieve this target [13,14].

96% of the carbon fibres are produced from polyacrylonitrile (PAN), a petroleum-based polymer, and for example, it cost around £42 per kilogram (5,000 metres of Torayca 12K, T700SC) [15]; however the cost of carbon fibres depends on their grade. The cost of carbon fibres is dominated by the cost of the PAN-precursor which contributes up to 50% of the total cost [16]. Moreover, during carbonisation, PAN generates toxic gases such as hydrogen cyanide (HCN), nitric oxide (NO) and nitrous oxide (N₂O) [7,17]. Therefore, low-cost and bio-renewable materials have been studied extensively in the search for a sustainable alternative precursor [18,19].

Lignin is an aromatic polymer and it is the second most abundant renewable biomaterial on Earth, after cellulose [20]. An estimated 300 billion tonnes of lignin is available in the biosphere and it increases annually by 20 billion tonnes [21] in the form of wood. Annually, about 141 million tonnes of lignin is generated globally from two major segments: the pulping and biorefinery industries (see Table 1.2). About 81 million tonnes of lignin is generated annually as a co-product from the paper and pulping-industries [22].

With reference to the available volume of lignin compiled in Table 1.2, ~78,000 thousand tonnes of lignin is available from Kraft pulping, which contributes nearly 96% of the overall lignin from the Kraft pulping industry. However, only about 75,000 tonnes of Kraft lignin is extracted and used for commercial applications, such as an additive for concrete [23], adhesives [24] and dyestuff dispersants [25]. It is said that less than 1% of the lignin is used as a value-added material, whereas the rest is burnt off for power generation [26].

Table 1.2 Volume of available lignin and the extracted lignin volume in 2015 [27].

Segment	Production volume 10 ³ tonnes	Available volume 10 ³ tonnes
Lignosulfonate	1,100	3,000
Kraft lignin	75	78,000
Soda lignin	5	20
Biorefinery	3	60,000
Total		141,020

It has been reported that the properties of lignin are highly variable and this is caused by a number of factors, including its biomass source [28], geographic origin [29], growing condition, extraction method [30,31] and purification method used [32–34]. Therefore, this variability in the properties has to be addressed if commercially relevant products are to be manufactured, to the required quality and performance, on a repeatable basis.

The abundance of sustainable and low-cost Kraft lignin along with its aromatic composition makes it a leading candidate as an alternative precursor with great potential for the production of carbonised fibres. In this thesis, softwood Kraft lignin (BioChoice lignin) was selected and used as the main raw material for the formation of lignin fibre preforms. However, in literature, which is discussed in Chapter 2, it is reported that the softwood Kraft lignin could only be spun with chemical treatment and/or polymer blending. However, when lignin is blended with polymers to aid processing, it is known to cause the formation of defects and voids in the resultant carbonised fibres [35–37]. Therefore, there is a significant need to develop new methods to spin a sustainable material such as softwood Kraft lignin, with a view to producing carbon fibres in the future.

In this thesis, characterisation of the as-received softwood Kraft lignin is addressed and it is used as a reference point for the subsequent treatments. Two methods were used for treating as-received lignin: (i) treatment with acidified water; and (ii) molecular weight fractionation using acetone. These treatment methods were used to reduce the inorganic content in as-received lignin. DMSO and lignin were selected as the secondary solvent and precursor respectively in order to consider the green and sustainability requirement for fibre formation. Acetone was selected as the primary solvent because of the high boiling point of DMSO and a volatile solvent was required to enable fibre formation during electro-spinning. A mixture of DMSO and acetone was identified and optimised for electro-spinning lignin, and the key processing conditions for producing lignin fibre preforms is reported. It was necessary for the electro-spun lignin fibres to maintain their circular cross-section, without fusing, during thermo-stabilisation and carbonisation to produce carbonised lignin fibres.

2. LITERATURE REVIEW AND RESEARCH GAPS

2.1 Carbon Fibres

2.1.1 An Overview of Carbon Fibres

Carbon fibres by definition must constitute at least 92 wt% of carbon [2] whilst those made up to 99 wt% are called graphite fibres [38]. Carbon fibres can be crystalline, amorphous or semi-crystalline. Crystalline carbon contains a graphitic crystal structure consisting of six carbon atoms arranged in a two-dimensional hexagonal ring in the x-y plane, as illustrated in Figure 2.1 (a). The distance between one carbon atom and the other three nearest neighbours is 0.142 nm. In the plane (Figure 2.1 (b)), each carbon atom is bonded to three others via sigma (σ)-bonds which represent the overlap of sp^2 hybrid orbitals. The unpaired hybridised p_z orbitals overlap to form pi (π)-bonds. These π -bonds are presented above and below the σ -bonded ring and the electrons are said to be delocalised (Figure 2.1 (b)). This delocalisation of the π electrons leads to good electrical and thermal conductivity in the x-y plane. Figure 2.1(a) shows that the stacking of the hexagonal graphitic layers corresponds to an ABA-packing sequence. The distance between the A and B layers is 0.335 nm. The bonding between the graphitic layers is weak van der Waals bonding. Due to the difference between the in-plane and out-of-plane bond strength, the in-plane bond strength is more than that of the out-of-plane and hence the higher modulus in a direction parallel to the plane [39].

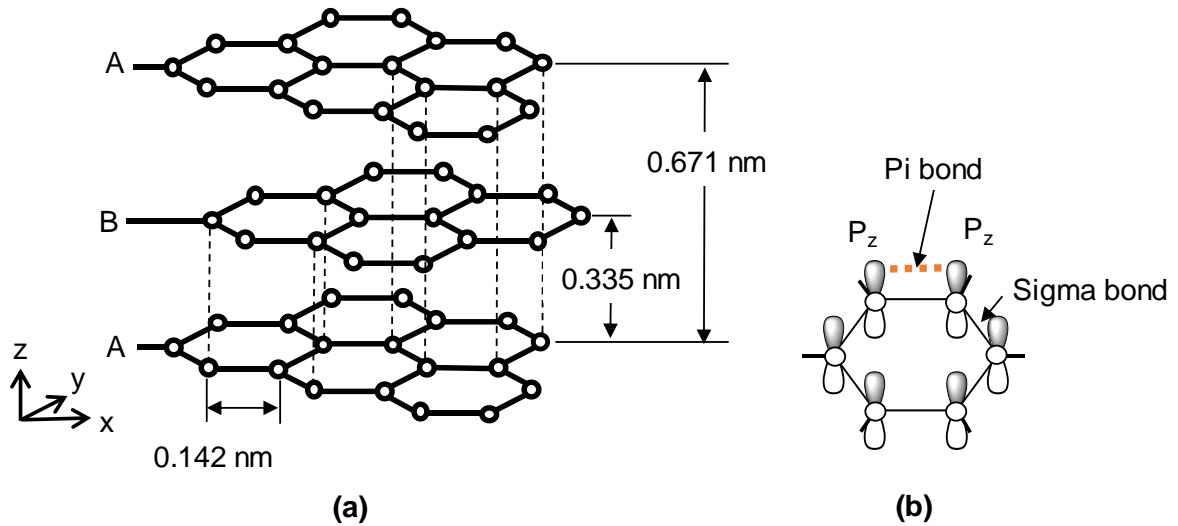


Figure 2.1 (a) Schematic illustration of the ABA packing sequence of the hexagonal graphitic crystal structure and (b) sp^2 hybridisation showing the sigma and pi-bonds [2,39].

The three main precursors used for the production of carbon fibres are rayon, pitch and polyacrylonitrile (PAN). Each precursor requires different processing techniques and conversion procedures for the production of carbon fibres, as shown in Figure 2.2.

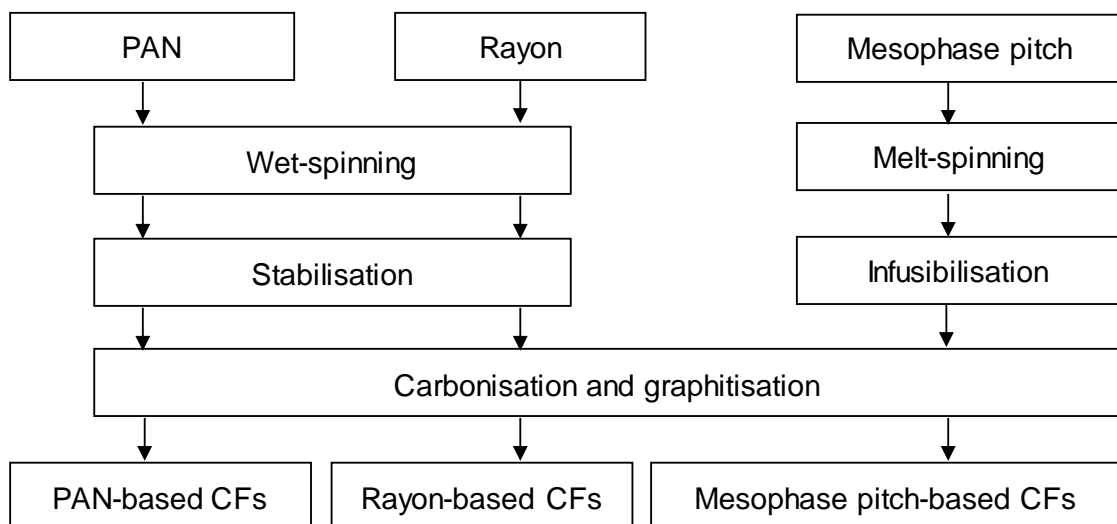


Figure 2.2 The production of carbon fibres from PAN, rayon and mesophase pitch [7,19].

Rayon-based carbon fibres are made from cellulose, consisting of D-glucose monomer units connected by 1-4 glycosidic linkages (see Figure 2.3) [9,19]. The viscose rayon precursor is extracted from cellulose pulping and wet-spun through spinnerets to form fibres. The cellulose is dissolved and treated with carbon disulphide to form cellulose xanthate. The xanthate is dissolved in sodium hydroxide prior to extrusion into a coagulation bath containing 10-15% sulphuric acid; then it is hydrolysed and solidified into cellulose filaments. The filaments are air thermo-stabilised at 400 °C. The stabilised fibres are carbonised between 900-2,000 °C and graphited between 2,800-2,900 °C in an inert atmosphere. During graphitisation, the filaments are stretched to enhance the modulus of the carbon fibres [40].

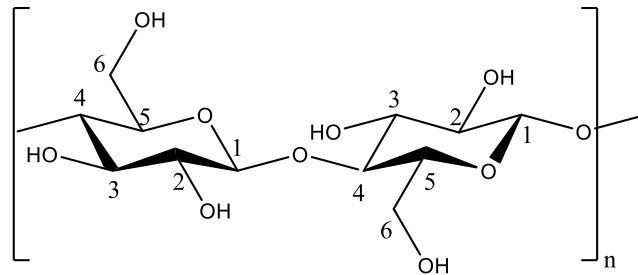


Figure 2.3 Repeat unit chemical structure of cellulose with a 1-4 glycosidic linkage.

Pitch is a tarry substance that is a solid or highly viscous liquid at room temperature and consists of aromatic hydrocarbons comprising three to eight aromatic rings, with an average molecular weight of 300-400 g·mol⁻¹ [2]. Pitch can be obtained from petroleum fraction, coal tar or by the pyrolysis of polyaromatic polymers [41]. Isotropic pitches from coal tar and petroleum pitch are promising precursor materials due to their low cost [17,42]. Heating isotropic pitch between 400-500 °C leads to the condensation of the aromatic unit and it is transformed into a multi-ring structure with an anisotropic character, as presented in Figure 2.4. The anisotropic pitch, or mesophase pitch, is able to form filaments via melt-spinning [19].

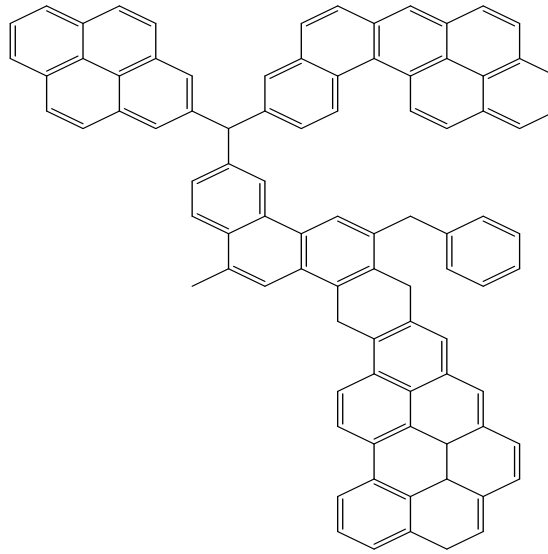


Figure 2.4 Typical structure of mesophase pitch for the production of carbon fibres [19].

The filaments from mesophase pitch are thermo-stabilised in air between 250-350 °C; this step is known as infusibilisation [43]. Carbonisation is performed between 1,500-1,800 °C. Then, the carbonised fibres are graphitised at 3000 °C in an inert atmosphere and this leads to an enhancement of Young's modulus [17].

2.1.2 Production of Carbon Fibres from Polyacrylonitrile

Approximately 90-96% of high performance carbon fibres are derived from PAN-based precursors [14]. Figure 2.5 shows the chemical structure of acrylonitrile and PAN.

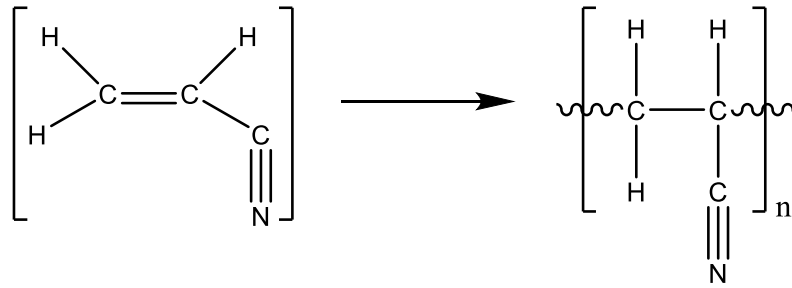


Figure 2.5 Chemical structure of acrylonitrile monomer and PAN.

A common manufacturing method for the production of carbon fibres from PAN co-polymers is summarised in Figure 2.6. Usually in co-polymerisation, acrylonitrile monomers are co-polymerised with a 5 mol% of other monomers, such as acrylic acid, methacrylic acid, methyl methacrylate and itaconic acid [38,44]. The monomers are copolymerised in polar solvents such as dimethylacetamide (DMA_c), dimethylformamide (DMF), dimethyl sulfoxide (DMSO), or aqueous sodium thiocyanate solutions to prepare the “dopes” for spinning. Typically, the weight-average molecular weight (M_w) and polydispersity index (PDI) of the PAN copolymers are between 70,000-260,000 g·mol⁻¹ and 1.5-3.5, respectively [19,38].

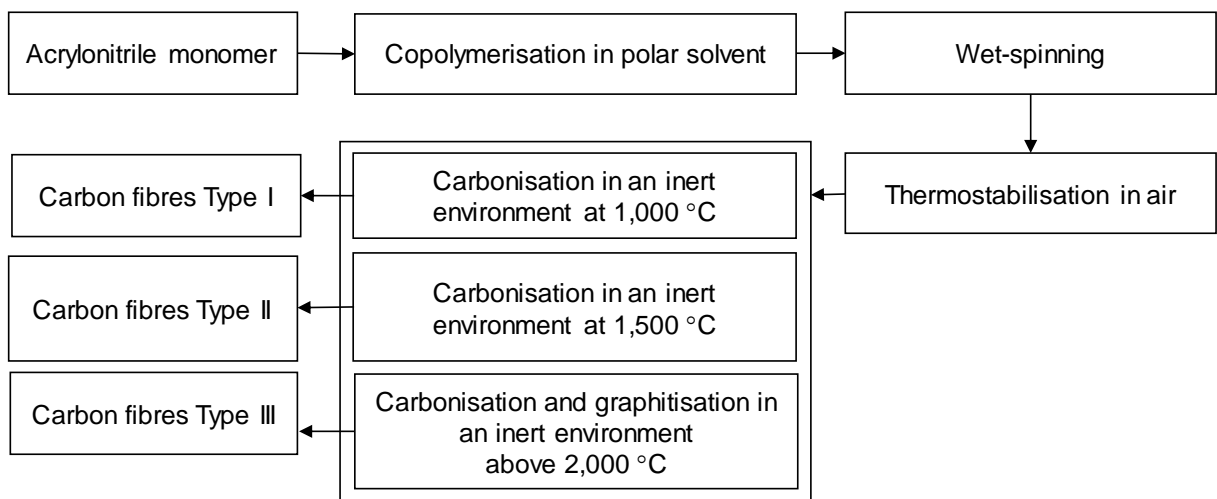


Figure 2.6 Production of carbon fibres from PAN-based precursor [2,45].

2.1.2.1 Wet-spinning of PAN

The PAN copolymer is dissolved in polar solvents such as DMAc, DMF or DMSO for the preparation of dopes with concentrations in the range of 15-25 wt% and corresponding viscosities between 10-200 Pa·s [19]. Wet-spinning is a common technique that used for fibre formation. Stretching during spinning is required to enhance the molecular orientation of the filaments. The fibres are solidified by solvent extraction from the filament into the bath. Washing is carried out to remove the excess solvent and the fibres are drawn through and stretched in a bath of ethylene glycol or glycerol between 120-180 °C to further improve the molecular orientation. Drying and stress relaxation steps are used to remove water and reduce the residual stress, respectively [2,17].

2.1.2.2 Thermo-stabilisation of PAN

During thermo-stabilisation, the PAN copolymer is stabilised between 200-300 °C in air to avoid the fusion of individual fibres. During this heat treatment, PAN undergoes a cyclisation reaction. Different models of cyclisation can be found in the literature [17,19]. One of the mechanisms, described by Houtz [46,47], is dehydration and cyclisation reactions (see Figure 2.7).

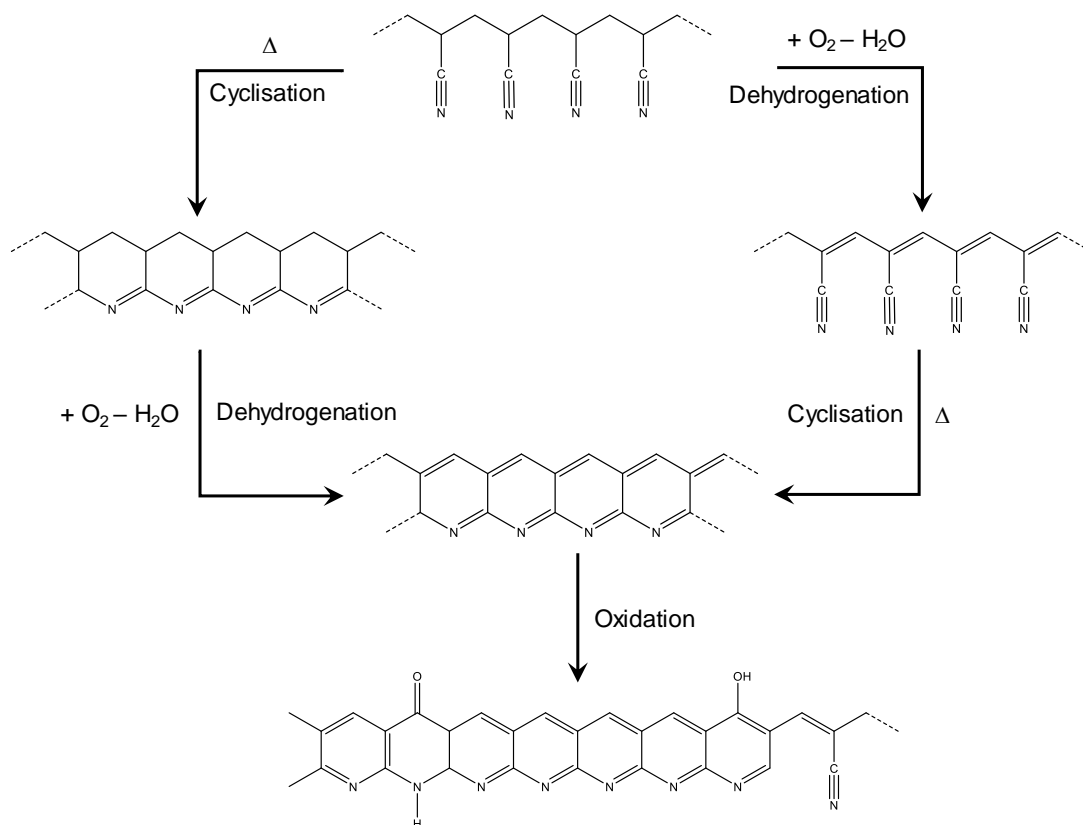


Figure 2.7 Chemical reaction during thermo-stabilisation in air of the PAN homopolymer; adapted from [17,46,48].

Thermo-stabilisation, which includes cyclisation and oxidation, is an exothermic reaction, therefore the chemical composition of the resulting polymer depends on the heating programme [49]. Fitzer *et al.* [47,50] reported that the cyclisation of PAN is initiated by ions and free-radicals. Therefore, incorporation of acids such as methacrylate and itaconic acid could reduce the onset temperature for cyclisation [51].

2.1.2.3 Carbonisation of PAN

During carbonisation, the thermo-stabilised fibres are heated to between 800-1600 °C under an inert atmosphere and tension is applied to the fibres in order to induced molecular orientation [52]. In the early stages of heating, a low heating rate is employed so that the formation of decomposing gases does not create voids in

the fibre structure. Goodhew *et al.* [53] found that the intermolecular dehydrogenation reaction of cyclised structures occurs around 400-600 °C. Between 600-1,300 °C, denitrogenating was said to take place along with the development of graphite-like ribbons that are oriented along the fibre axis. A general reaction scheme for the dehydrogenation and denitrogenating of the thermo-stabilised PAN is presented in Figure 2.8.

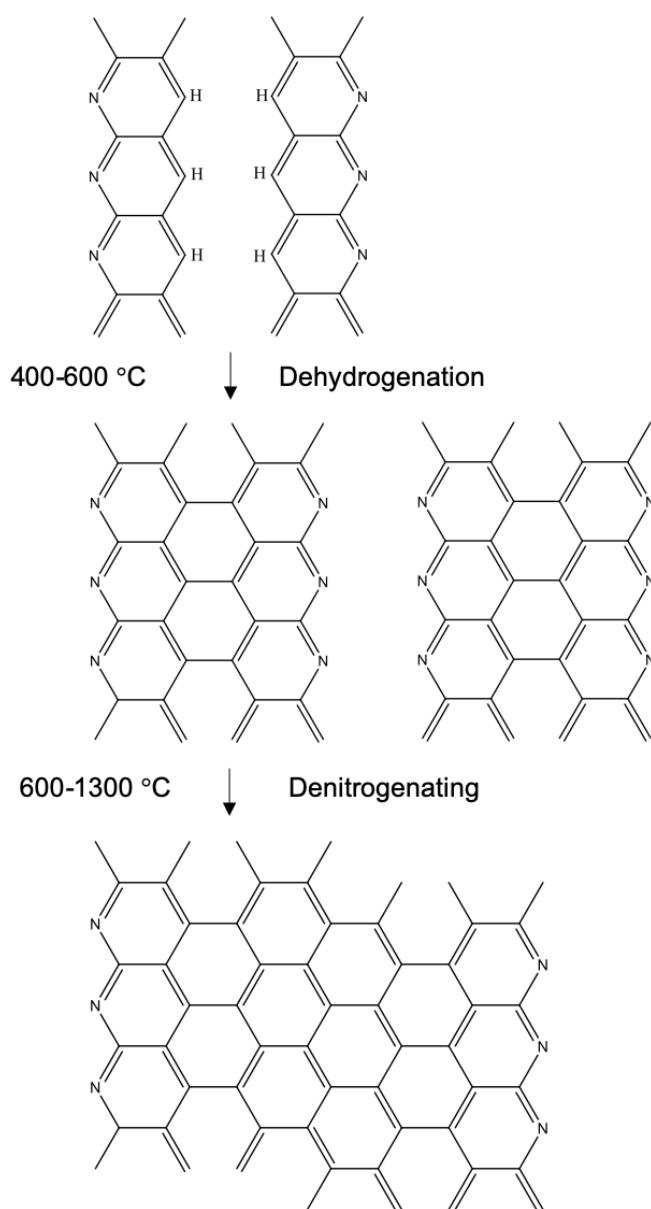


Figure 2.8 Schematic illustration of graphite formation adapted from [17,53].

High-strength carbon fibres are obtained by carbonisation between 1,500-1,600 °C. Further increases in the carbonisation temperature lead to the production of higher modulus fibres at the cost of a lower failure strain [54]. The carbonisation and graphitisation temperatures depend on the desired properties of the final carbon fibres [55]. Graphitisation up to 3,000 °C is required to achieve moduli above 350 GPa. However, above 2,000 °C, nitrogen is replaced by argon due to the fact that it can react with carbon and form cyanogen [17]. During carbonisation further evolved gases such as HCN, H₂O, O₂, H₂, CO, NH₃, CH₄, are found in the temperature range 200-1,000 °C [19]. Alternative stabilisation methods such as plasma electron beam-assisted cyclisation [56,57] and microwave-assisted processing [16] have been investigated to minimise stabilisation time and energy consumption.

2.1.3 Properties of Carbon Fibres Derived from Polyacrylonitrile

With reference to Figure 2.6, the carbon fibres can be classified based on the heat treatment (carbonisation and graphitisation) temperatures into three types: Type I, Type II and Types III, where the final heat treatment temperatures are above 2,000 °C, around 1,500 °C and below 1,000 °C, respectively [2]. Table 2.1 shows the classifications of carbon fibres, which include ultra-high modulus (UHM), high modulus (HM), intermediate modulus (IM), low modulus and high-tensile (HT) and super high tensile (SHT) fibres with their tensile modulus values.

Table 2.1 Classification of carbon fibres [45].

Carbon fibres type	Heat treatment temperature	Final mechanical properties	
Type I	>2,000 °C	UHM	Modulus > 450 GPa
		HM	Modulus 350-450 GPa
		IM	Modulus 200-350 GPa
Type II	≈1,500 °C	HT	Modulus <100 GPa Tensile strength >3.0 GPa
		SHT	Tensile strength >4.5 GPa
Type III	<1,000 °C	SHT	Tensile strength >4.5 GPa

Carbon fibres can be alternatively classified by their commercial availability into general-purpose (GP) type, which are amorphous and isotropic with low tensile strength and modulus. The high-performance (HP) type has a high proportion of graphite structure with high tensile strength and modulus. Activated carbon fibres (ACFs), having a large number of open pores, act as adsorption fibres [39].

2.2 Lignocellulosic as an Alternative Precursor for the Production of Carbon Fibres

Lignocellulosic biomass refers to non-edible plants or non-edible parts of a plant and comprises three main polymers, i.e. cellulose, hemicellulose and lignin, all of which are present in a plant cell wall [20]. The plant cell wall is usually divided into two categories: (i) primary cell wall and (ii) secondary cell wall. A primary cell wall is a wall surrounding growing cells. The structure of a primary cell wall is composed of cellulose fibrils, while the matrix contains hemicellulose, pectin and wax [58].

Once the growth stops, the secondary cell wall is deposited interior to the primary cell wall. A secondary cell wall is much thicker than a primary cell wall and it contains

cellulose, hemicellulose and lignin [20]. The cellulose chains are present as a parallel array and arranged into bundles, and they form the framework of the plant cell wall. The bundles of cellulose are bonded with hemicellulose and lignin as illustrated in Figure 2.9. In between two adjacent cells, a middle lamellar layer is formed to bind them to each other.

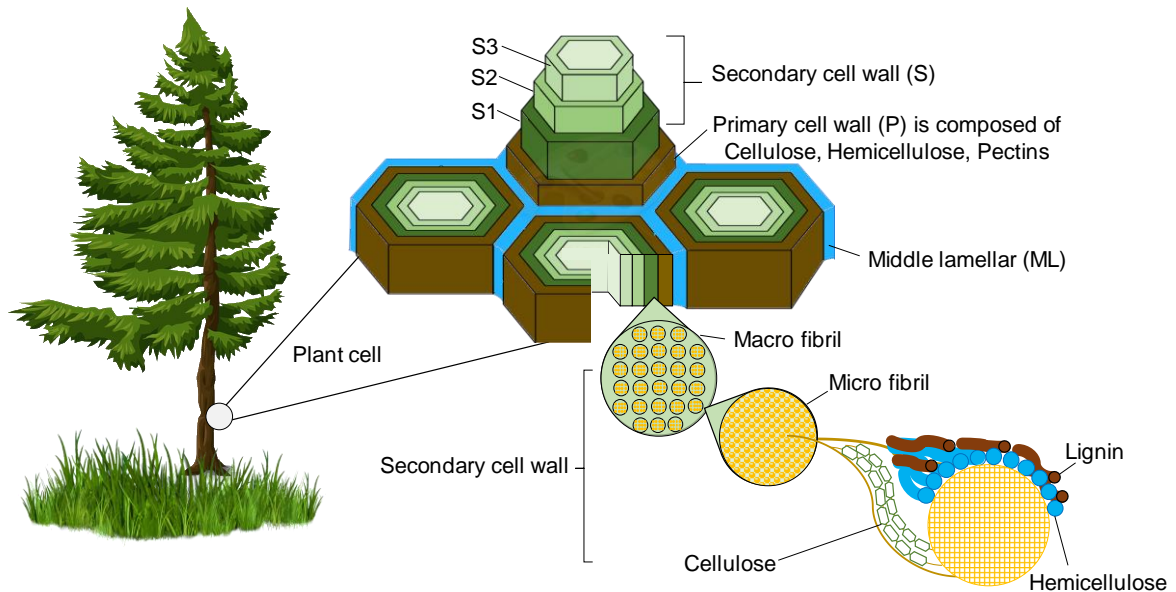


Figure 2.9 Schematic illustration of a typical plant cell wall and associated macro and micro-structural components [20,58,59].

Generally, lignocellulosic biomass consists of 35-50% cellulose, 20-35% hemicellulose and 10-25% lignin, as shown in Table 2.2. Apart from these three major components, small amounts of protein, fat and inorganic elements such as silica, magnesium and potassium can also be found. The components can vary with the plant species [20,28], location and age [29].

Table 2.2 Lignocellulosic compositions from different plant sources [20,59,60].

Type of biomass		Cellulose (%)	Hemicellulose (%)	Lignin (%)
Softwood	Pine	42-50	24-27	20
	Spruce	45	23	22
Hardwood	Poplar	50-53	26-28	15-16
	Eucalyptus	54	18	21
	Oak	40	36	24
Grasses	Grasses	25-40	25-50	10-30
	Switchgrass	35-40	25-30	15-20

2.2.1 Lignin

Lignin is an amorphous bio-polymer with one of the highest aromatic content and the second most abundant bio-polymer in the world after cellulose [20]. At least 300 billion tonnes of lignin is available and increases annually by 20 billion tonnes [21]. About 81 million tonnes of lignin is generated annually as a by-product of the paper and pulping industries [22].

Lignin is one of the most promising bio-based precursors for the production of carbon fibres [61–64]. Lignin is composed of three primary monomeric units, namely, p-coumaryl, coniferyl and sinapyl alcohols. These mono-lignols form lignin units such as p-hydroxyphenyl (H), guaiacyl (G) and syringyl (S), respectively (see Figure 2.10). Table 2.3 shows the combination of H, G and S units depending on the plant species, which are mainly categorised into wood including softwood and hardwood, and non-wood as grass. For example, softwood is mainly composed of G units; hardwood is

made up of S and G units and traces of H units. Grasses are made up of all three mono-lignols [20].

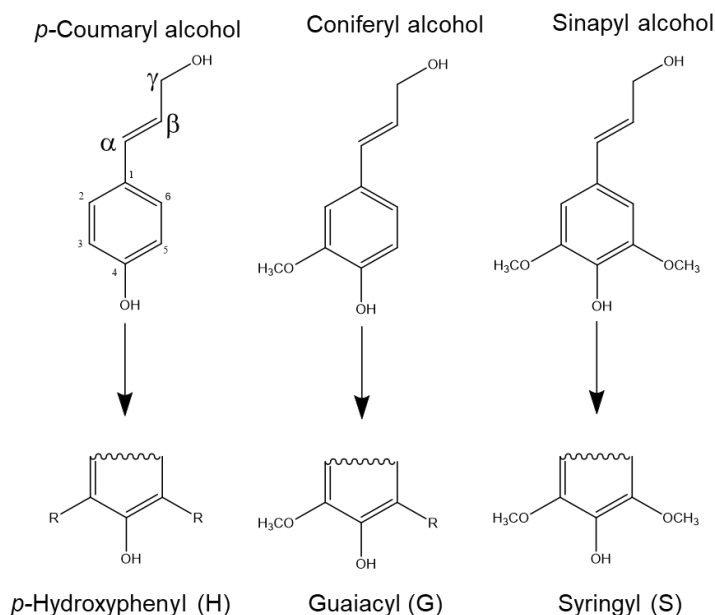


Figure 2.10 Common monomers of lignin and the respective lignin units [20,26].

Table 2.3 Mono-lignol composition of softwood, hardwood and grasses [20,60].

Type of biomass	Mono-lignol distribution in lignin (%)		
	H	G	S
Softwood	<5	>95	0
Hardwood	0-8	25-50	45-75
Grasses	5-35	35-80	20-55

The H, G and S units are bonded by different linkages of which the most common linkage is β -O-4' contributing about 50% [60,65] of the total linkages. Some common linkages and their relative contributions are shown in Figure 2.11 and Table 2.4.

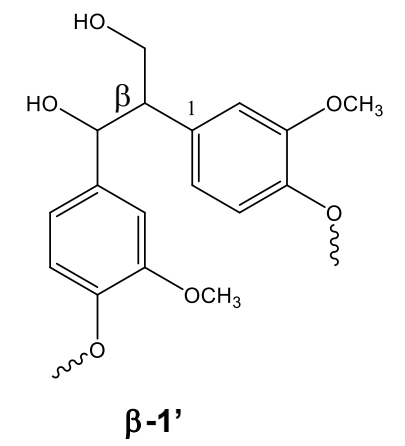
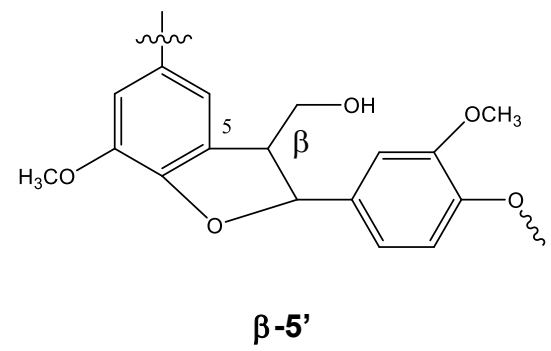
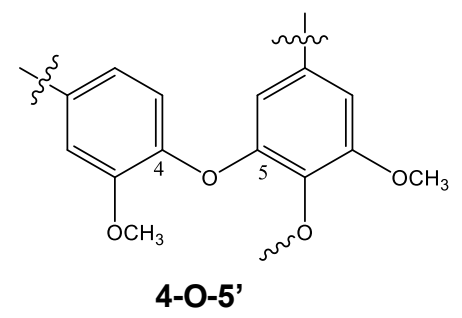
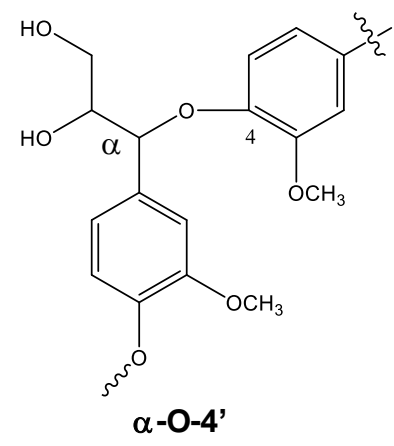
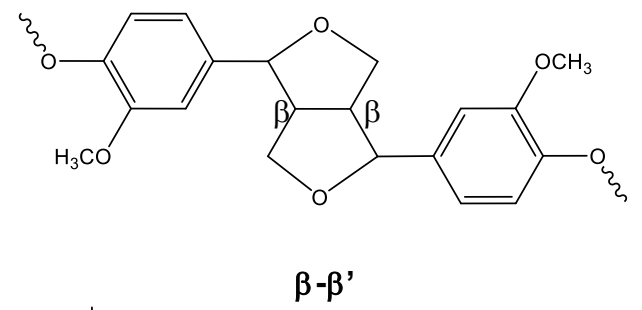
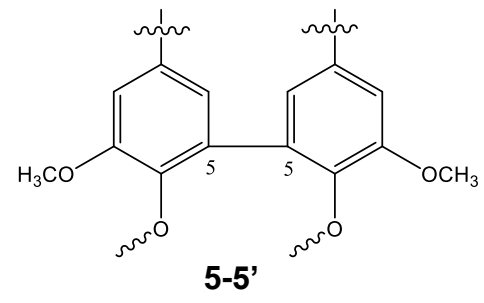
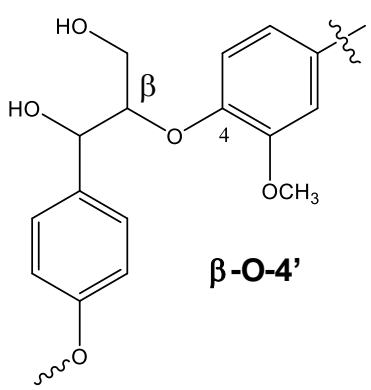


Figure 2.11 Common linkages in lignin [60].

Table 2.4 Approximate percentage of the inter-monomeric linkages of lignin found in nature [20,60,66].

Linkages		Percentage of total linkages (%)		
		Softwood	Hardwood	Grass
1	β -Aryl ether (β -O-4')	45-50	60	82
2	α -Aryl ether (α -O-4')	6-8	8	2
3	Biphenyl (5-5')	18-25	10	-
4	Resinol (β - β')	3	2	2-5
5	Biphenyl ether (4-O-5')	4-8	5	-
6	Pheylcoumaran (β -5')	9-12	6	7-8
7	1,2-Diaryl propane (β -1')	7-10	7	2

A linked-model for softwood lignin, as shown in Figure 2.12, was proposed by Adler in 1977 [67]. In 2003, a linearity model of lignin from wheat straw was proposed by Banoub and Delmas [68]. A linear model for softwood lignin was also proposed by Crestini *et al.*, in 2011 [69]; this is illustrated in Figure 2.13. In Crestini *et al.*'s model, lignin was suggested as being a linear helical structure and β -O-4' linkage was claimed likely to be linear linkage. However, consensus has not been reached on the actual structure of lignin [70].

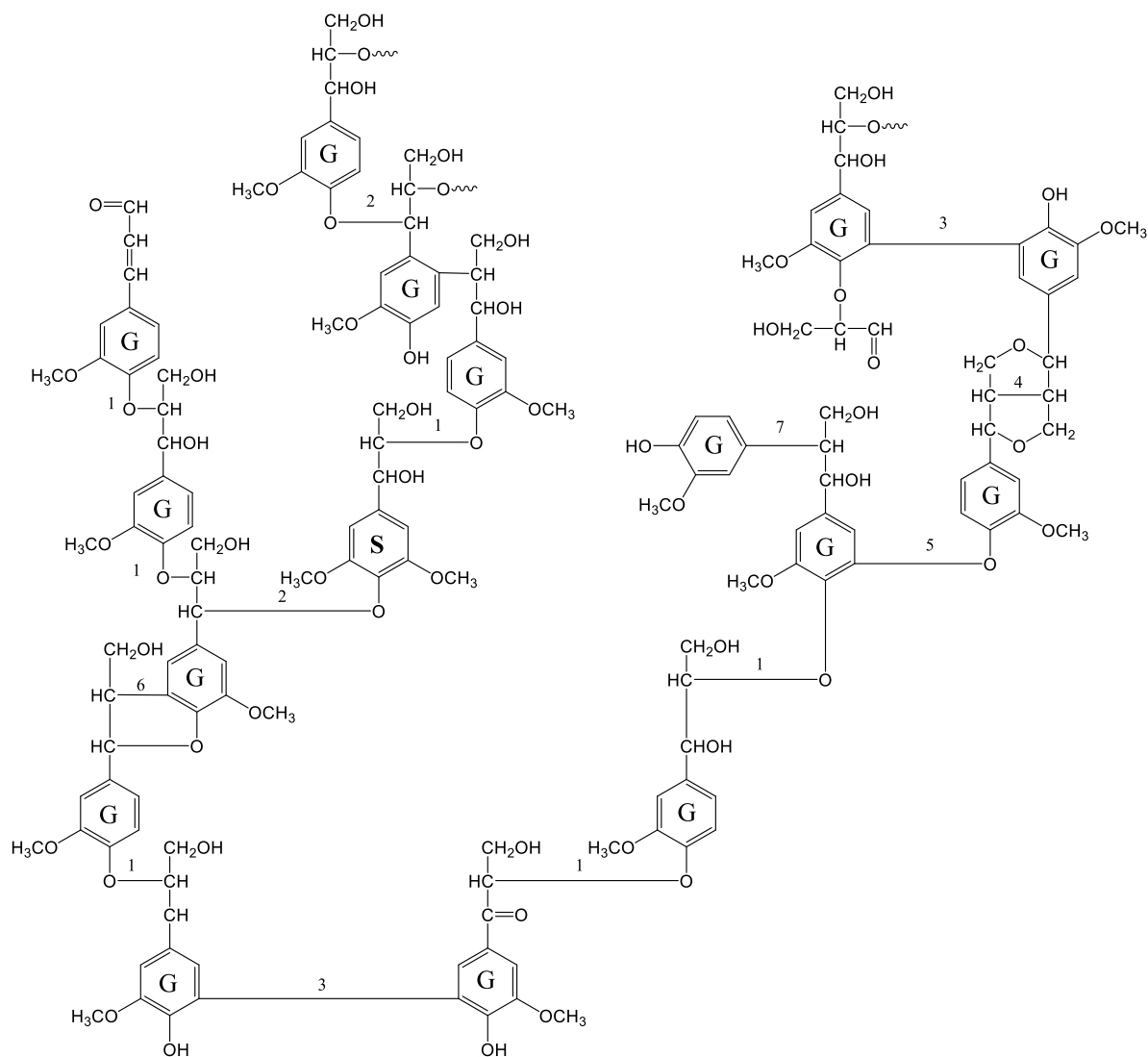


Figure 2.12 The branched molecular structure of softwood lignin according to Adler, 1977 [67].

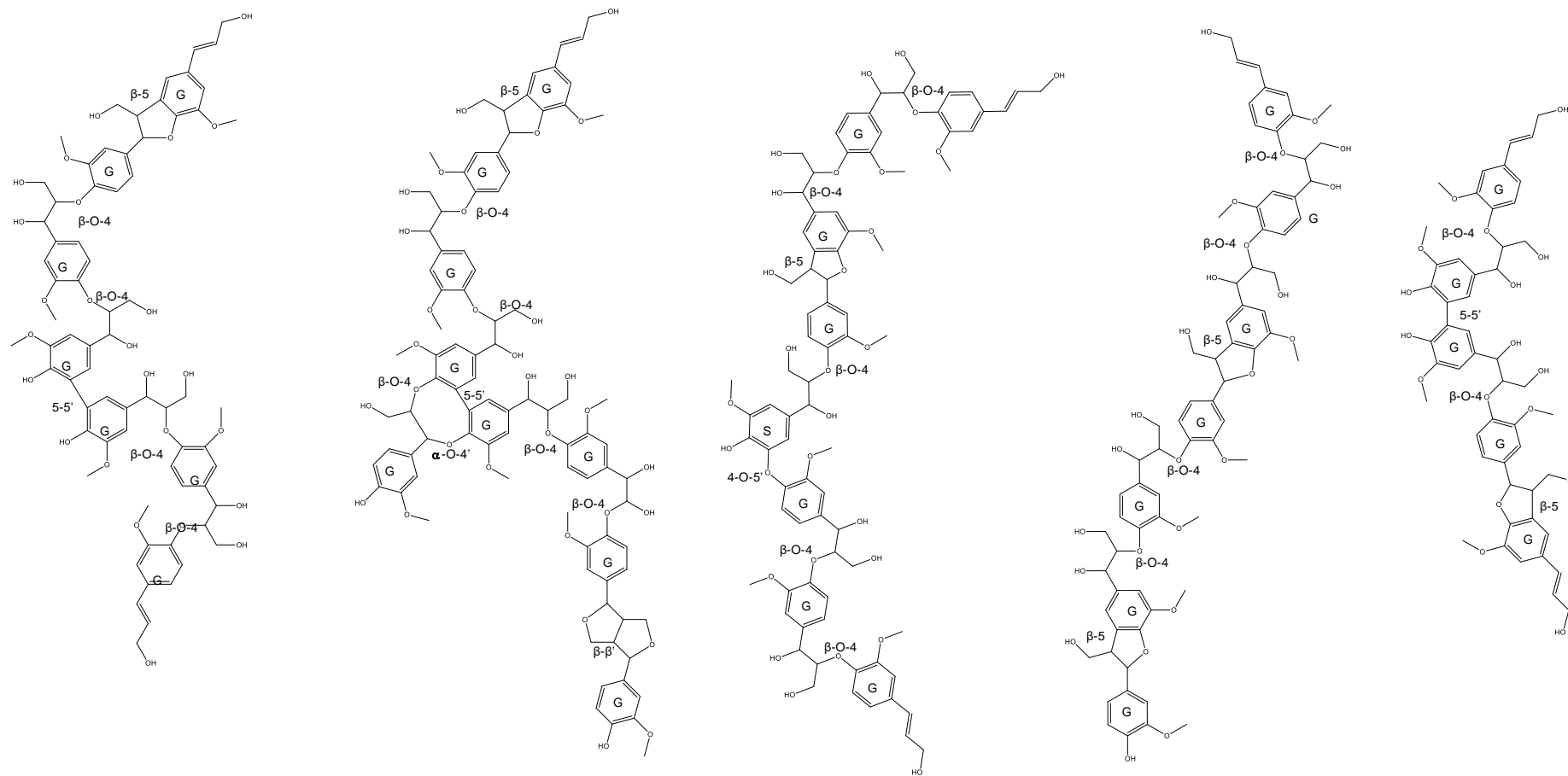


Figure 2.13 The linear structure of softwood lignin as proposed by Crestini *et al.*, 2011 [69].

The source of the lignin contributes to the lignin structure; moreover, the extraction method of lignin was reported to heavily influence the final lignin structure [30,31]. The extraction and isolation of lignin is explained in the following section.

2.2.2 Extraction of Lignin

Lignin can be extracted using several processes such as Kraft pulping, Organosolv, sulphite pulping and soda pulping. The extraction process can be categorised into sulphur-based or sulphur-free processes as presented in Figure 2.14 [26,71]. The detail of each process will be described in the following sections.

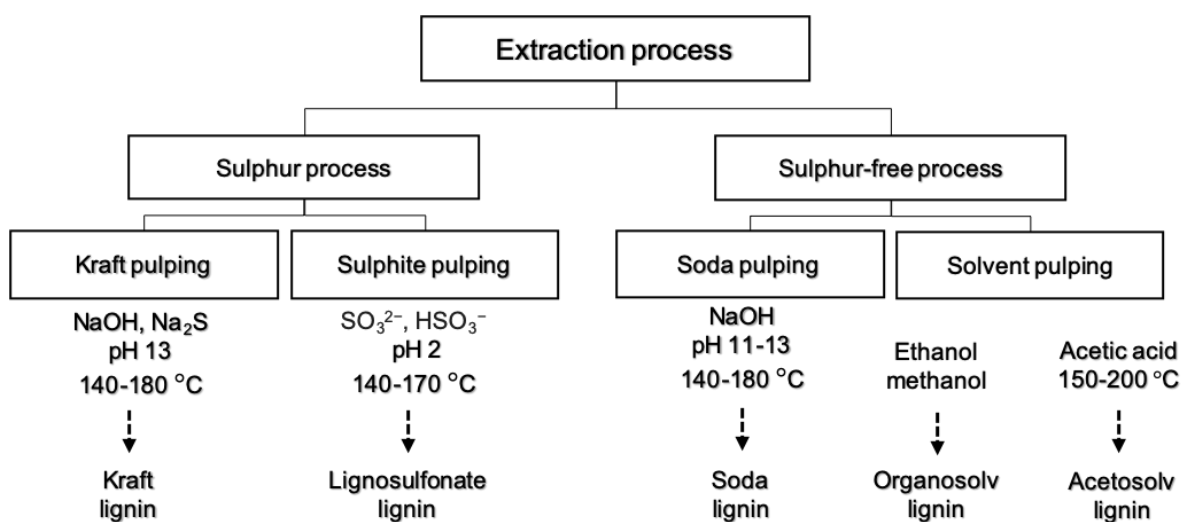


Figure 2.14 Different extraction processes to separate lignin from lignocellulosic biomass [71].

2.2.2.1 Kraft Pulping

In Kraft pulping, the biomass is treated with a high alkaline mixture (pH 13) of sodium hydroxide (NaOH) and sodium sulphide (Na₂S), known as white liquor. It is heated to between 140-180 °C for 2-4 hours. The soluble fraction is referred to as black liquor.

The lignin is isolated from the black liquor by acid precipitation using sulphuric acid followed by separation by filtration. The precipitated lignin is washed with distilled water and dried. Typically, a residual sulphur content in lignin is between 2-3% [26,71].

2.2.2.2 Sulphite Pulping

In sulphite pulping, the biomass is reacted in an aqueous solution of sulphite (SO_3^{2-}) or bisulphite (HSO_3^-) salt of sodium, ammonium, magnesium, or calcium at temperatures around 140-170 °C [72,73]. This reaction can progress relatively rapidly at low pH [74]. Sulfonated groups are introduced onto lignin, leading the resultant lignin to be soluble in water. The sulphur content of lignosulfonate is about 5-6% [26].

The presence of sulphur in lignin extracted from Kraft pulping and Sulphite pulping is reported as being attributable to the chemical agent used in lignin extraction. Sulphur found in Kraft lignin is ascribed as due to sodium sulphide used in delignification and sulphuric acid as an acidified agent used for lignin precipitation [75,76]. Lignosulfonates have generally more sulfonated group and anionic charges compared to Kraft lignin [72], thus lignosulfonates are water-soluble. There are many reports that have attempted to explain the localisation of the sulphur in lignin, however the subject has been controversial [77]. For example, sulphur in Kraft lignin is believed to be in the lignin in many forms, such as ions, elemental sulphur, as adsorbed polysulphide and as organically bound sulphur [78,79].

The sulphur element found in lignin is reported as contributing to void formation during the heat treatment step of the lignin fibres. At temperatures starting from 300 °C, the releasing of sulphur containing gases, mainly SO_2 and H_2S , occurs [80,81]. With an increase in heat treatment temperature, i.e. to 1,400-2,200 °C, irreversible voids are created. The formation of voids can diminish the mechanical properties of the resultant carbon fibres.

2.2.2.3 Soda Pulping

The soda lignin is free from sulphur, therefore soda pulping is used to treat non-wood biomass such as wheat straw [31], sugarcane bagasse [26] and flax [82]. The biomass is reacted in a sodium hydroxide aqueous solution at a temperature around 160 °C. Lignin is recovered by acidifying it to pH 2 with sulphuric acid.

2.2.2.4 Solvent Pulping

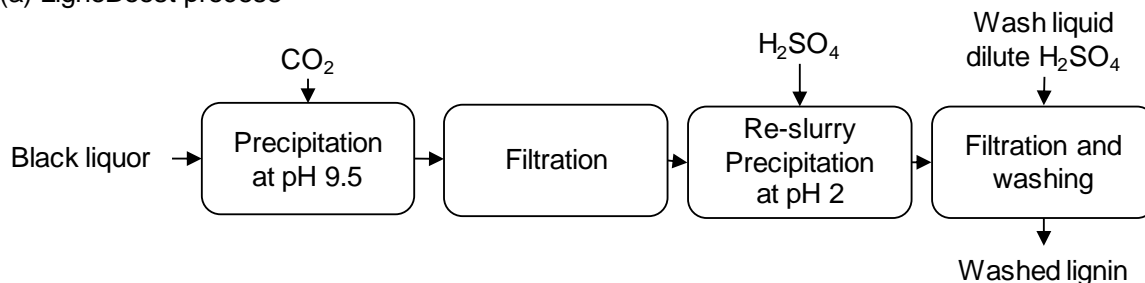
Organic solvents such as methanol [83,84], ethanol [85] and acetic acid [86] are used to extract lignin selectively between 110-185 °C, without the solubilisation of cellulose and hemicellulose. Organosolv lignin is obtained after removing the solvent. The most common Organosolv processes are based on ethanol/water pulping. There are two commercially available Organosolv lignins; Lignol[®] from Canada [87] and Alcell[®]lignin–USA [88]. The reported ash content in Alcell[®]lignin is 0.1% [82,88–90]. If acetic acid is used for lignin extraction, the obtained lignin is known as acetosolv lignin [91] and it is recovered by evaporation of the solvent.

2.2.3 LignoBoost and LignoForce Process

New approaches to precipitate Kraft lignin from black liquor are known as the LignoBoost and LignoForce process; a flowchart showing the procedures is illustrated in Figure 2.15. LignoBoost was introduced in 2002 and the patent was granted in 2006 [92,93]. In this process, the black liquor is acidified by carbon dioxide between 60-80 °C and a pH of 9.5. The filtrated lignin is re-dispersed in water and re-precipitated with H₂SO₄ of pH 2 prior to washing with dilute H₂SO₄. This is a two-stage process. The final lignin (LignoBoost[®]Lignin or BioChoice[®]Lignin) has 1% ash content and 2.5% sulphur content, which are lower when compared to the one-stage precipitation process which has normally a 2-3% ash and 3% sulphur [94].

The LignoBoost®Lignin was also reported to have a higher lignin yield and a lower operational cost of H₂SO₄ [73,94].

(a) LignoBoost process



(b) LignoForce process

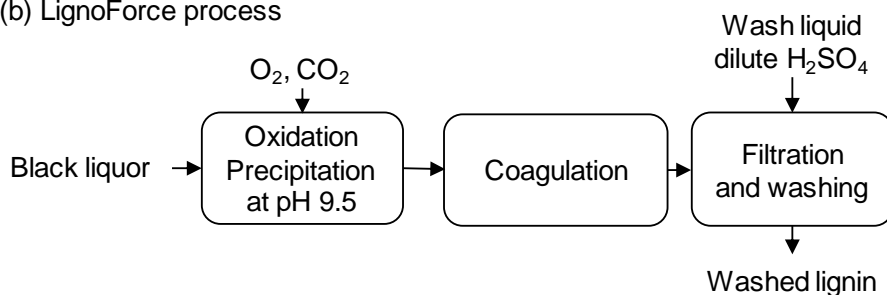


Figure 2.15 (a) LignoBoost process and (b) LignoForce process to isolate Kraft lignin [73].

In 2011, the LignoForce process was developed where the oxidation of black liquor is carried out using oxygen at 75-80 °C until the sulphide content is reduced, prior to precipitation by carbon dioxide, and until the pH drops to 9.5. Then the slurry containing the precipitated lignin is coagulated by mixing at the lower temperature between 60-65 °C. The coagulated lignin is filtrated and washed with dilute sulphuric acid acidified water. Kouisni *et al.*, have reported the properties of lignin isolated from several black liquors (e.g. softwood, hardwood and eucalyptus) using the LignoForce process [95]. They found the ash content and sulphur content of lignins obtained from those three black liquors are in the range of 0.04-1.5% and 1.3-2.6%, respectively. Reference lignin was isolated from the same black liquors, but it was not oxidised. They have reported that the emission of sulphur compound from LignoForce®Lignin is

lower than that from lignin without oxidation. In summary, the benefits of this process are lower sulphur compound emission, reduction in chemical consumption and high lignin purity [96].

2.2.4 Properties of Commercially Available Lignin

Table 2.5 presents a compiled summary of the characteristics of selected commercially available lignins. The ash content of softwood Kraft Lignin (Indulin AT) is between 2-4%, which is higher than that of softwood Kraft lignin obtained from the LignoBoost (BioChoice®Lignin) and the LignoForce processes which range from 0.1-1.5%. Alcell®lignin which is an Organosolv lignin has an ash content of 0.1%. Alkaline lignin extracted from wheat straw (Protobind 2400) was reported to have an ash content of 1-1.6%. The lignin content of wood-based lignins is over 96% whilst that of non-wood lignins has a lower lignin content of 86%.

Gel permeation chromatography (GPC) is a common characterisation technique for determining the number average molecular weight (M_n) and weight average molecular weight (M_w) of polymer. The polydispersity index (PDI) is calculated from M_w/M_n . The M_w of softwood Kraft lignin is reported in the range of 5,000-8,000 $\text{g}\cdot\text{mol}^{-1}$ and the reported PDI is in the range of 3-9. The M_w and PDI of Organosolv hardwood lignin are lower than those of the softwood Kraft lignin, and a low ash content of 0.1% is obtained.

The glass transition temperature (T_g) of lignin is measured using differential scanning calorimetry (DSC). The T_g obtained from softwood Kraft lignin ranges from 130-160 °C, while lignin from hardwood is reported to be between 70-108 °C. The reported T_g is related to its M_w . The lowest T_g is found in the lignin from wheat straw which is 59 °C.

The mass-loss characteristics of materials are obtained by Thermo-gravimetric Analysis (TGA). The degradation temperature is taken from the maximum of the first derivative of the TGA curve which is coded as T_{DTG} . The T_{DTG} is presented varying in the range from 350-390 °C.

Table 2.5 Compiled properties of selected commercially available lignins.

Samples	Origin	Extraction process	Ash content (%)	Klason lignin (%)	Acid-soluble lignin (%)	Lignin content (%)	Mw (g·mol ⁻¹)	PDI	T _g (°C)	T _{DTG} (°C)	Reference
Indulin AT	Softwood	Kraft	2-4	88.8	4.1	92.9	6,000-8,000	4-9	132	378	[32,97]
BioChoice®lignin	Softwood	Kraft and LignoBoost	1.36	91.1	5.4	96.5	5,200-6,700	3-7	147	390	[32,98]
InnoForce®lignin	Softwood	Kraft and LignoForce	0.1-1.5	N/A	N/A	N/A	6,000	3-4	160	350	[96,99,100]
Alcell®lignin	Hardwood	Organosolv	0.1	96.1	0.4	96.5	1,300-3,900	2	70-108	350	[82,89,90,101-103]
Protobind 2400	Wheat straw	Alkaline	1-1.6	79	9	86	2,000-5,000	3-4	59	372	[97]

2.2.5 Treatments for Lignin

According to the ash content of commercial softwood Kraft lignin compiled in Table 2.5, it has been reported as in the range between 0.1-4.0 wt% [32,94,96–100,104,105]. The major inorganic minerals found in the residual ash are sulphur, sodium, potassium and magnesium [94,105–107]. The amount of inorganic elements found in lignin has been mentioned as it may cause defects in the resultant carbon fibres thus damage the mechanical properties [18,64].

Furthermore, alkali and alkaline earth metals found in lignin have been reported to be a catalyst during pyrolysis, and the affects the product yield [106,108,109]. Major inorganics found in lignin are sodium and potassium [94,96,110,111]. The influence of alkali and alkaline earth metals has been studied and it has been reported that demineralisation by washing lignin with acidified water (H_2SO_4) can increase the gaseous content and liquid products, whereas the char yield decreased [106,109]. The reduced char content was explained by a lower inorganic content. Sodium is known as a carbon gasification catalyst [107,112], which is described as promoting demethoxylation and demethylation [113,114]. Moreover, the infusion of alkali and alkaline earth metals into lignin prior to pyrolysis was reported to increase the char yield and volatile aromatic products [108], and the char yield was correlated with the electropositive metal cation. This is similar to other publications [115,116] which presented the effect of alkali and alkaline earth metals in the following order of sodium > potassium > calcium > magnesium with regard to their catalytic activity.

The production of carbon fibres from lignin is influenced by the purity of the lignin and its inorganic elements including sulphur, alkaline and alkaline earth metals. Therefore, the pre-treatment of lignin becomes a necessary step. Several methods have been adopted to manipulate the properties of lignin.

2.2.5.1 Acid Washing

In order to remove inorganic impurities, washing lignin with acidified water has been reported as a simple purification method and been used by many researchers [94,117–120]. Acids such as hydrochloric acid and sulphuric acid have been used. Washing the lignin with distilled water is the simplest way to remove water-soluble impurities. An efficient way to remove the inorganic is washing with acidified water. This involves washing with diluted hydrochloric acid or sulphuric acid which can reduce the ash content to 0.5 wt% [77].

Moreover, acid washing contributes to the reduction of aliphatic-OH. The ratio of aliphatic-OH to methoxy group measured by ^1H NMR, is decreased significantly by 70% when the lignin is treated with 0.15 M hydrochloric acid [121,122].

Zhang [119] reported that acidified water at pH 2; 10 ml of acidified water per gram of softwood Kraft lignin; 15 minutes of mixing time; and 25 washing cycles was the best procedure for washing lignin. However, the optimum washing condition was not accomplished by statistical analysis.

2.2.5.2 Molecular Weight Fractionation

Organic solvents such as methanol [34], acetone [31], ethanol [123], tetrahydrofuran and 2-butanone [124] have been used for the fractionation of lignin. Lignin from different sources (Indulin AT Kraft softwood, Protobind 1000 and corn stover) were fractionated using methanol [34]. A similar trend was reported for all these three lignins where the methanol-soluble fraction presented lower T_g than the parent lignins, whereas the highest T_g was detected for the methanol-insoluble fraction. For example, the parent softwood Kraft lignin (Indulin AT) had a T_g of 147 °C, while the T_g of methanol-soluble and methanol-insoluble fractions were 117 °C and 200 °C, respectively. Furthermore, the parent lignin and methanol-insoluble fractions possessed a higher thermal degradation temperature relative to the methanol-soluble lignin.

The commercial Indulin AT lignin has been fractionated using organic solvents such as tetrahydrofuran, methanol and 2-butanone [124]. The highest fractionation yield was reported when using tetrahydrofuran which was 62%. The fractional yields were correlated to their solubility [124]. Compared to the parent lignin, all soluble fractions had a decrease in the M_w and PDI, whereas a higher value was found in the insoluble fraction. Figure 2.16 shows a plot of M_w versus T_g and PDI for lignin fractionated using different organic solvents. The data are compiled from different lignin sources of Indulin AT [124], BioChoice®Lignin [98], softwood Kraft lignin from USA and Sweden [29]. It can be concluded that an increase in the M_w tended to increase the T_g and PDI of lignin.

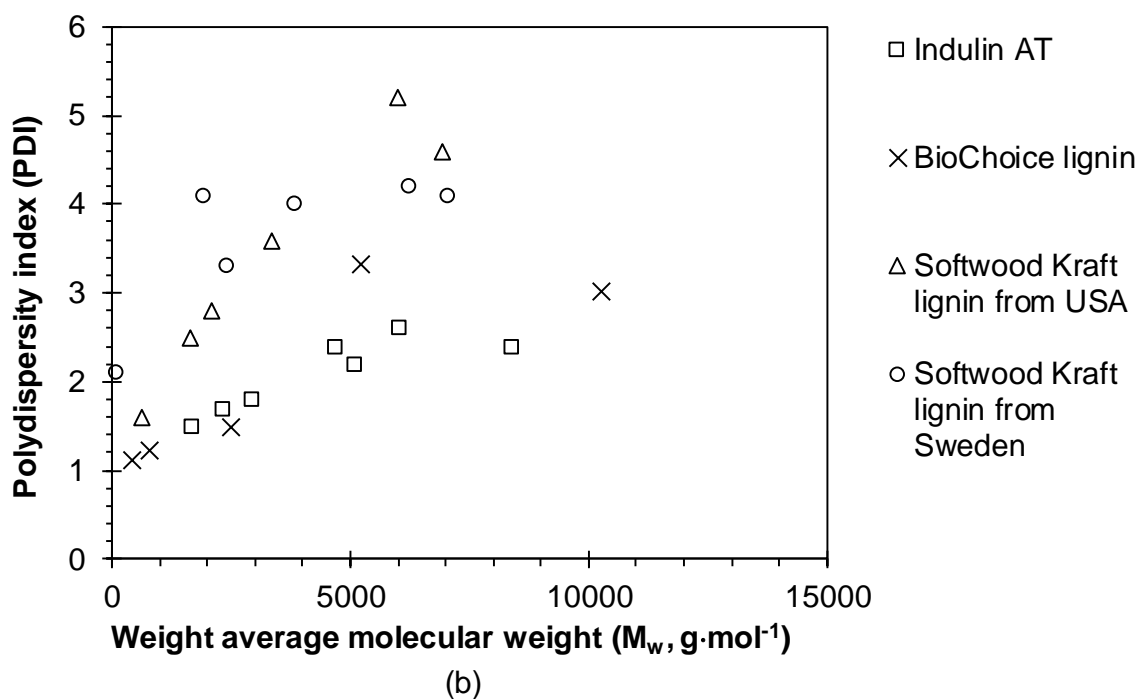
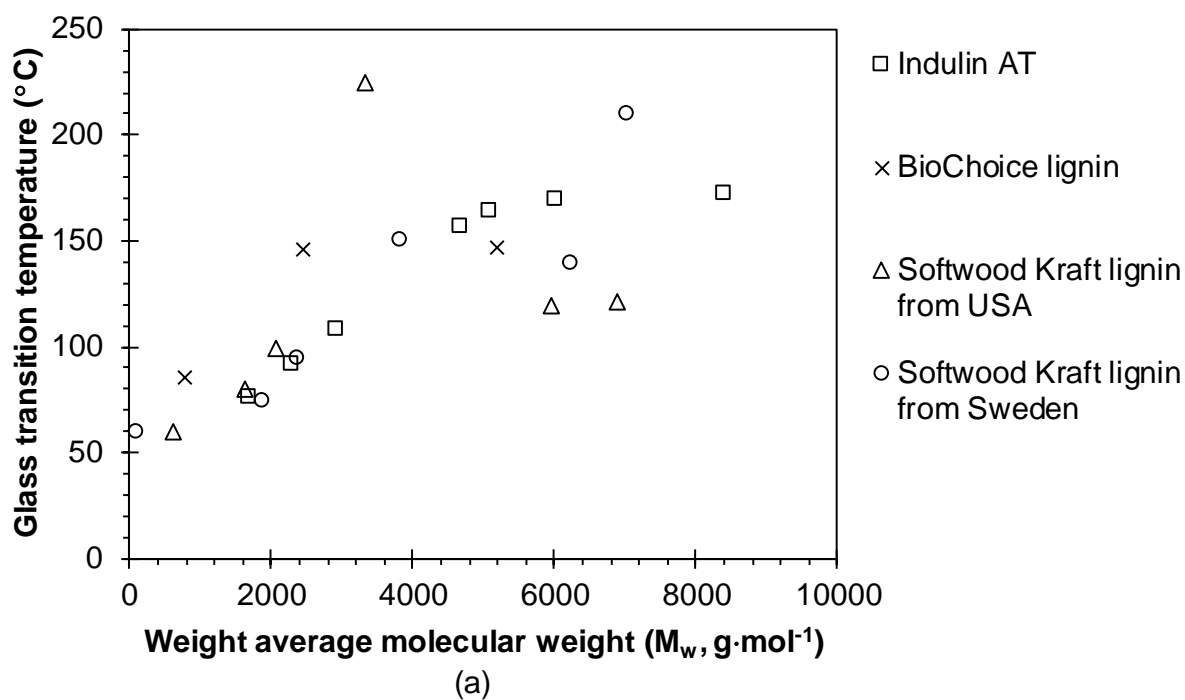


Figure 2.16 A plot showing the change in T_g and PDI of lignin from fractionation using organic solvent with respect to weight average molecular weight (M_w).

Data compiled from different lignin sources of Indulin AT [124], BioChoice®Lignin [98], softwood Kraft lignin from USA and Sweden [29].

The use of binary solvents and aqueous solvents for the fractionation of lignin has been reported. A soluble fraction lignin obtained using a 9:1 volume ratio of binary solvent of ethanol and acetone had a M_w of $2,890 \text{ g}\cdot\text{mol}^{-1}$, a PDI of 2.3 and a T_g of $128 \text{ }^\circ\text{C}$ [123]. Aqueous solvent such as aqueous acetone [31] and aqueous ethanol [85], have been exploited. It was reported that the solubility of lignin was decreased with an increasing concentration of water. The highest solubility was found when the water concentration was around 20-40% by volume [31,125]. Lower M_w and PDI with an increasing water concentration was reported when using both aqueous acetone and aqueous ethanol [85].

Single-step solvent fractionation and sequential-step fractionation with solvents were carried out by many researchers [29,98,126]. Softwood Kraft lignin from different locations (USA, Sweden) was used for solvent fractionation in a sequential manner using dichloromethane, n-propanol, methanol and a binary solvent of dichloromethane and methanol. The lowest M_w , i.e. $611 \text{ g}\cdot\text{mol}^{-1}$ was produced from soluble fraction using dichloromethane [29]. The M_w and PDI of soluble fraction were increased with the sequence of solvent used in the order ethyl acetate, ethanol, methanol and acetone. The lowest M_w was obtained from ethyl acetate which was $740 \text{ g}\cdot\text{mol}^{-1}$ [126].

2.2.5.3 Precipitation

Precipitation of black liquor in different acidic and basic solutions can also be used to obtain specific molecular weight distributions of lignin. Wheat straw black liquor was precipitated stepwise by adding 0.1 M HCl until the pH of the black liquor dropped to 10.5, 9.0 and 2.0. Lignin isolated from pH 2 had a lower ash content and a higher lignin content when compared to lignin isolated using a basic solution (pH 10.5 and pH 9.0) [127].

Using acidic levels from pH 7 to pH 2 had no significant effect on the M_w and PDI of the isolated lignin [128–130]. For example, the lignin from oil palm trunk which was isolated at acidic levels from pH 7 to pH 2, showed M_w in the range between $2,100\text{-}2,200 \text{ g}\cdot\text{mol}^{-1}$ and PDI of 1.41-1.46 [128]. Apart from lignin from oil palm trunk,

lignin from black liquor obtained from pulping showed M_w of 1,300-1,400 $\text{g}\cdot\text{mol}^{-1}$ [130]. On the other hand, the significant effect of the acidic level was reported on precipitation yield, when the precipitation of lignin from brewers' spent grain black liquor was studied. At pH 2.15, the highest lignin yield was recovered, and the concentration of soluble-lignin fraction was reduced from 12.44 $\text{g}\cdot\text{l}^{-1}$ to 2.31 $\text{g}\cdot\text{l}^{-1}$ [131].

2.2.5.4 Physical Fractionation

Physical fractionation, also known as membrane filtration, is a separation process where a ceramic or polymer membrane is used to separate different molecular weight fractions. For example, black liquor is forced through the membrane at pressures in the range of 1-10 bar [132]. The smaller molecules pass through, whereas large molecules are retained on the membrane surface. Different types of lignins (Kraft, soda and Organosolv lignins) were filtrated through 5kDa polyethersulfone, and the permeated lignins showed lower M_w and lower PDI compared to the parent lignins [133]. The same result was reported, when black liquor from softwood and hardwood Kraft lignin was filtrated through a 15kDa ceramic membrane [134,135]. The original softwood lignin and permeated softwood lignin had M_w of 6,400 $\text{g}\cdot\text{mol}^{-1}$ and 3,300 $\text{g}\cdot\text{mol}^{-1}$, respectively. The PDI of softwood lignin was 5.0; after filtration the PDI of permeated softwood lignin was reduced to 2.6 [135]. Moreover, the reported T_g of permeated softwood lignin was lower than that of the parent lignin.

Figure 2.17 shows a plot of M_w versus T_g and PDI. The plotted data for the T_g and molecular characteristics are compiled from parent lignin and permeated lignin from ceramic filtration [133–135]. Lignin with a higher M_w possessed a higher T_g and PDI. This trend is similar to the lignin fractionated using different organic solvents, as presented previously in Figure 2.16.

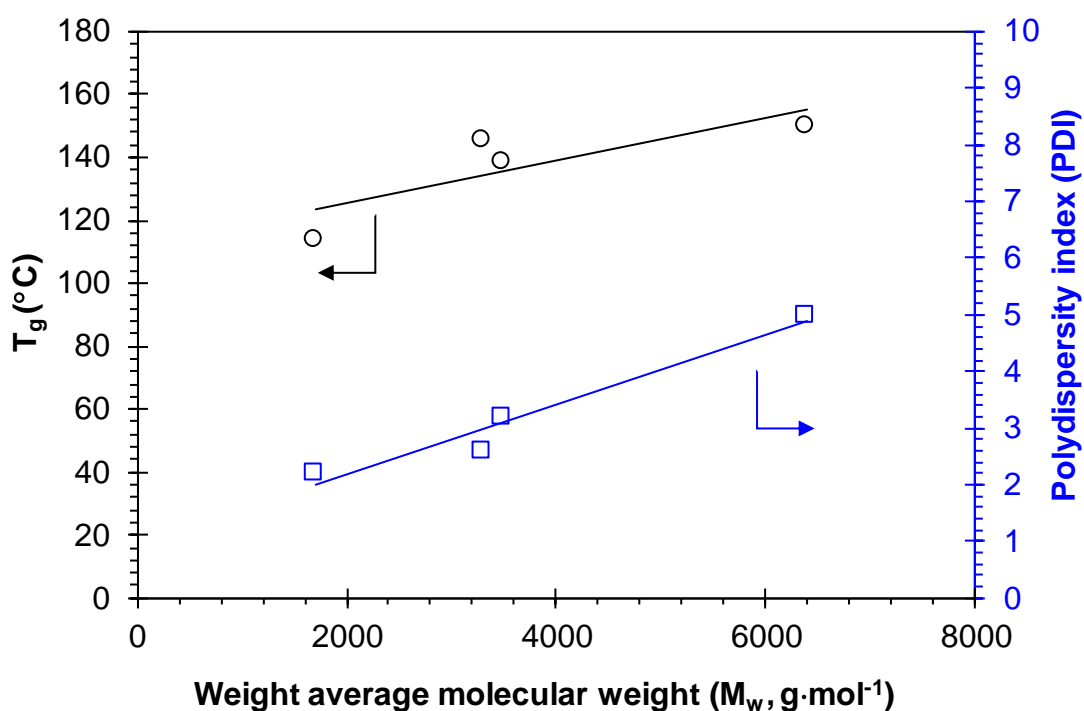


Figure 2.17 A plot of glass transition temperatures of parent lignin and the permeated lignin fraction from ceramic membrane filtration [134,135].

2.2.5.5 Blending Lignin with a Polymer

Polymers, such as polyethylene (PE) [63,136], polypropylene (PP) [137], polyethylene oxide (PEO) [138] and polyethylene terephthalate (PET) [139] have been blended with lignin at the processing temperature range from 130 to 260 °C, prior to melt-spinning. For other spinning techniques such as wet-spinning, dry-spinning and electro-spinning, polymer blends have been introduced to lignin solutions prior to spinning. For example, PAN blended lignin, up to 50 wt%, has been wet-spun [44,140–142]. For electro-spinning polymers such as PEO [35,36,143–146], PAN [147,148] and PVA [149–151] have been blended with lignin,

Miscibility between lignin and polymers has been studied extensively. Generally, the miscibility of a polymer blend can be classified into three terms; fully miscible, partially miscible and completely immiscible. Determination of the T_g is one of

the methods used to investigate miscibility [152]. If a single T_g is observed in between that of the neat constituents, it is indicative of a fully miscible system on a scale of 5 to 15 nm. An immiscible blend possesses the two composition-independent T_g s that are close to those of the neat constituents. A partially miscible blend has two composition-independent T_g s located in between those of neat constituents. The T_g has been used extensively to study the miscibility between lignin and other polymers [137–139,153,154]. For example, PEO [138,153] and PET [139] were miscible with lignin, whereas PP is immiscible with lignin [137]. Apart from synthetic polymers that may limit sustainable development in the future, a bio-renewable polymer, PLA has been blended with chemically modified lignin for the production of carbon fibres [155,156].

2.3 Fibre Formation using Lignin

Spinning techniques for producing fibres from lignin are presented in this section. The production techniques considered include melt-spinning, electro-spinning, wet-spinning and dry-spinning. In each spinning technique, a summary of the literature on the production of lignin fibres is included.

2.3.1 Melt-spinning of Lignin

Melt-spinning starts with polymer pellets or powders being heated above their T_g and/or T_m followed by extrusion through a spinneret. The extruded filaments are drawn before being directed into a chamber where they are quenched to form solid filaments. Melt-spinning is claimed to be a rapid, convenient and commonly used technique for the formation of polymer fibres [157,158].

Several types of lignin without involving polymer blending with other polymers have been melt-spun. Sudo *et al.*, [61,159,160] and Uraki *et al.*, [161] utilised acetosolv lignin, obtained from birch hardwood, and subjected it to chemical modification via acetylation in order to improve the melt-spinnability. They found its spinnability was improved by increasing the degree of substitution acetyl groups. Kubo *et al.* [162]

investigated acetosolv lignins extracted from hardwood and softwood for the production of carbon fibres. Sequential extraction steps, using aqueous acetic acid, were performed to remove the infusible fraction. The acetosolv hardwood lignin was melt-spun and converted into carbon fibres, whereas the acetosolv lignin from commercial softwood Kraft lignin could not be spun, even though the infusible fraction was removed.

Table 2.6 represents a compiled list from the selected literature on the production of lignin-based carbon fibres via melt-spinning. This includes key properties for melt-spinning such as M_w , T_g and spinning temperature. This table is divided into two parts: spinning of lignin without and with a polymer blend. Hardwood lignin could be proceeded into fibres without a secondary polymer. Here the processing temperature used was 70-80 °C higher than the T_g of hardwood lignin [117,162]. On the other hand, it has been reported that softwood Kraft lignin needs to be modified chemically prior to melt-spinning [155,156,163]

With reference to Table 2.6, Kubo *et al.*, [162], were of the opinion that softwood Kraft lignin required pre-treatments (molecular fractionation, chemical modification) in order for it to be melt-spun. Lignin has been blended with polymers such as PE [63,136], PP [137,139], PEO [64], PET [139], PVA [154] and PLA [155,156] to enable melt-spinning. However, fibre fusion during the thermo-stabilisation step was highlighted as a concern when the concentration of the polymer was greater than 5 wt% [64]. Moreover, voids were found in the resultant carbon fibres derived from a butylated-lignin/PLA blend, 90/10 [155,156]; this is shown in Figure 2.18.

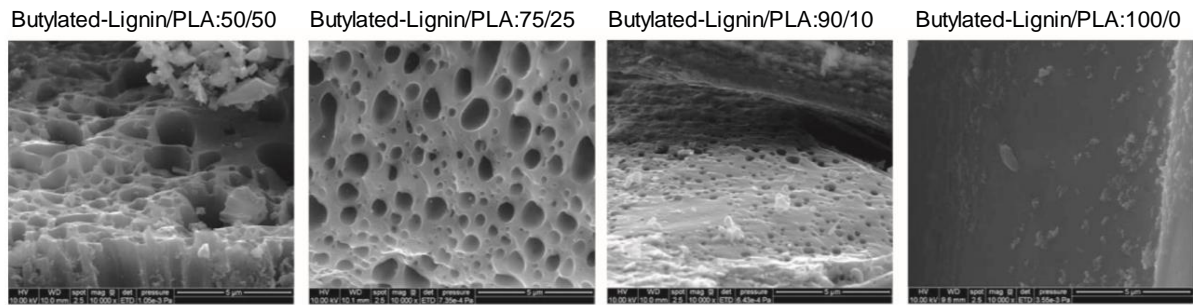


Figure 2.18 SEM micrographs of the cross-sectional area of melt-spun carbon fibres from a butylated-lignin/PLA blend [155,156].

In order to avoid the formation of voids caused by the high concentration of the second polymer, the blending of two types of lignin was explored. Organosolv hardwood lignin from yellow poplar wood was blended with soda switchgrass lignin prior to melt-spinning [164,165]. The morphology of the resultant carbon fibres from hardwood lignin/grass lignin is shown in Figure 2.19 where defect-free surfaces are observed. Molecular weight fractionation was controlled using ceramic membrane fractionation; the permeated fraction of softwood Kraft lignin was blended with 5 wt% of the permeated fraction obtained from hardwood Kraft lignin [134,135].

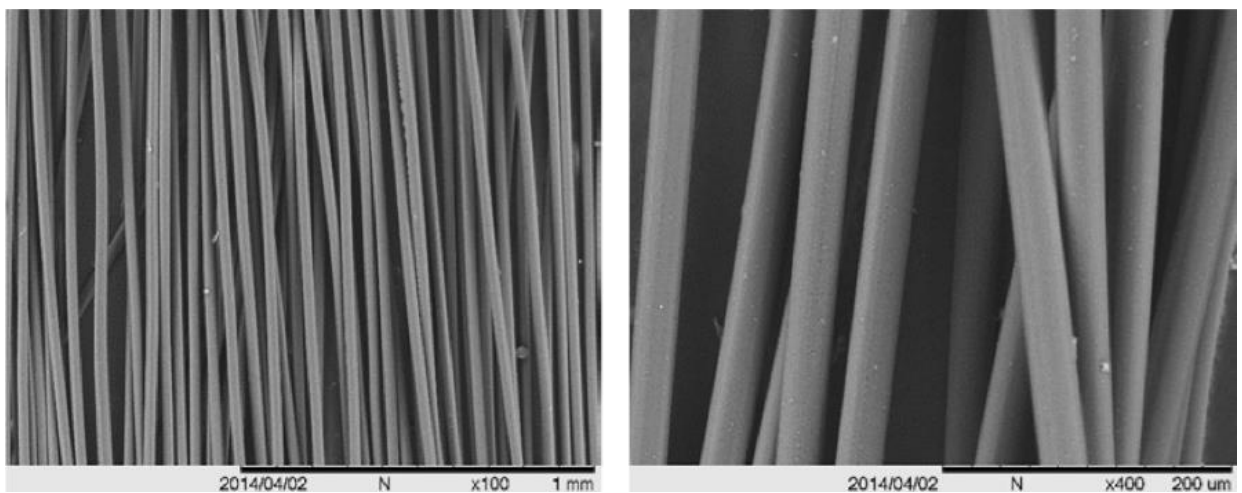


Figure 2.19 SEM micrographs of carbon fibres from 50% yellow poplar lignin and 50% grass lignin [164].

With reference to Table 2.6, there are many key parameters that have to be considered for the melt-spinning of lignin. For example, the presence of carbohydrate and inorganic element is known to have an adverse effect during the pyrolysis of lignin. Hence, the concentration of these impurities has to be reduced before manufacturing lignin fibres. The molecular weight distribution is another key parameter with synthetic polymers. In general, molecular weight in the range 20,000-60,000 g·mol⁻¹ is required for fibre formation [157,166]. It is seen in Table 2.6 that the weight average molecular weight is significantly lower for lignin. Therefore, this is one reason why it is blended with synthetic or bio-polymers with a higher molecular weight and lower molecular weight distribution, the so-called polydispersity index (PDI), is normally between 1.5 -2.0 for synthetic polymer [167].

Therefore, it is surprising to note a larger PDI for lignin, this leads to a suggestion about the heterogeneity of lignin with the added complication of it being able to cross-link about approximately 140 °C. This has implications for the processing of lignin and its blends because lignin can accumulate in the processing equipment and cross-link. The consequences for this can be detrimental for most processing fibre fusion and is often cited as a problem with the fibre formation for lignin. This can be avoided with vertical extrusion when the lignin leaving the spinneret is quenching rapidly to solidify the fibres. Heating lignin above its T_g can also have another consequence in that, if heated in air, it can oxidise, giving rise to the formation of polar functional groups. These functional groups can lead to the re-absorption of moisture in the fibres during storage. Absorbed moisture can lead to void formation. Since the desired intention is to ultimately manufacture carbon fibres, it is the mechanical properties of the as-spun, oxidised and carbonised fibres that take on a significant prominence. However, this literature review and data presented in Table 2.6 suggest that standardisation is required with regard to quality control of the starting materials, the removal of impurities and developing an understanding of the starting materials and the chemical and physical changes that occur during thermal processing. The next section of this review will consider electro-spinning.

Table 2.6 A compiled list of the literature on the production of lignin fibres via melt-spinning.

Lignin	M _w of lignin (g·mol ⁻¹) [PDI]	Treatment of lignin	M _w of treated lignin (g·mol ⁻¹) [PDI]	Polymer blend/ M _w (g·mol ⁻¹)	Blend ratio of lignin/ polymer blend (w/w)	T _g (°C)	Processing temperature (°C)	Fibre diameter (µm)	Reference
Lignin without polymer blend									
Hardwood acetosolv	4,800 [2.7 PDI]	Fractionation using aqueous acetic acid	N/A	N/A	N/A	47	Could not be spun	N/A	[162]
Softwood acetosolv	6,400 [3.0 PDI]		4,400 [2.4 PDI]			128	210	10-45	
Softwood Kraft	5,400 [2.8 PDI]		500 [1.5 PDI]			127	Could not be spun	N/A	
Hardwood Kraft	N/A	N/A	N/A	N/A	N/A	130	200	12-20	[117]
Hardwood Organosolv						88			
Softwood Kraft (Indulin AT)	N/A	Chemical modification: butylating	N/A	N/A	100/0	159	180	100-200	[155,156]

Lignin	M _w of lignin (g·mol ⁻¹) [PDI]	Treatment of lignin	M _w of treated lignin (g·mol ⁻¹) [PDI]	Polymer blend/ M _w (g·mol ⁻¹)	Blend ratio of lignin/ polymer blend (w/w)	T _g (°C)	Processing temperature (°C)	Fibre diameter (µm)	Reference
Softwood Kraft	1,690 [1.3 PDI]	Chemical modification: peracylation	3,000-8,000 [7-9 PDI]	N/A	N/A	160	180	12	[163]
Switchgrass Organosolv Yellow poplar Organosolv	N/A	Fractionation Methyl isobutyl ketone, ethanol and water	N/A	N/A	N/A	128 115	180-190	N/A	[164,165]
Softwood Kraft Hardwood Kraft	6,400 [5.0 PDI] 3,500 [3.2 PDI]	Membrane filtration	3,300 [2.6 PDI] 1,700 [2.2 PDI]	N/A	N/A	150 114	 180	N/A	[134,135]

Lignin	M _w of lignin (g·mol ⁻¹) [PDI]	Treatment of lignin	M _w of treated lignin (g·mol ⁻¹) [PDI]	Polymer blend/ M _w (g·mol ⁻¹)	Blend ratio of lignin/polymer blend (w/w)	T _g (°C)	Processing temperature (°C)	Fibre diameter (µm)	Reference
Permeated softwood Kraft/ permeated hardwood Kraft									
Lignin with polymer blend									
Hardwood Kraft	N/A	N/A	N/A	PP/127,000	75/25	N/A	220	N/A	[137]
Hardwood Kraft	N/A	N/A	N/A	PET/18,000 PP/127,000	95/5	N/A	200-300 200-230	31 47	[139]
Hardwood Kraft	2,400 [1.9 PDI]	N/A	N/A	PVA/93,400 PVA/23,000	N/A	N/A	210-250	N/A	[154]
Hardwood Kraft	N/A	N/A	N/A	PLA/177,000	80/20	N/A	220-240	N/A	[168]
Hardwood Kraft	N/A	N/A	N/A	PEO/100,000	97/3	N/A	N/A	34	[64]
Softwood Kraft	N/A	N/A	N/A	PP, PE, PET,	N/A	N/A	130-260	N/A	[63,136]

Lignin	M _w of lignin (g·mol ⁻¹) [PDI]	Treatment of lignin	M _w of treated lignin (g·mol ⁻¹) [PDI]	Polymer blend/ M _w (g·mol ⁻¹)	Blend ratio of lignin/polymer blend (w/w)	T _g (°C)	Processing temperature (°C)	Fibre diameter (µm)	Reference
				PEO					
Softwood Kraft (Indulin AT)	N/A	Chemical modification: butylating	N/A	PLA	95/5	159	180	100-200	[155,156]

2.3.2 Electro-spinning Lignin

Electro-spinning is a fibre fabrication process which employs electrostatic charging to draw polymer jets into thin filaments or spin fibres with a diameter of a few tens of nanometres to a few micrometres. Electro-spinning can be classified into (i) solution electro-spinning and (ii) melt electro-spinning, based on the state of the polymer used.

The set-up for electro-spinning consists of three major components: (i) a feeding unit, (ii) a high-voltage power supply and (iii) a collector electrode (see Figure 2.20 (a)) [169,170].

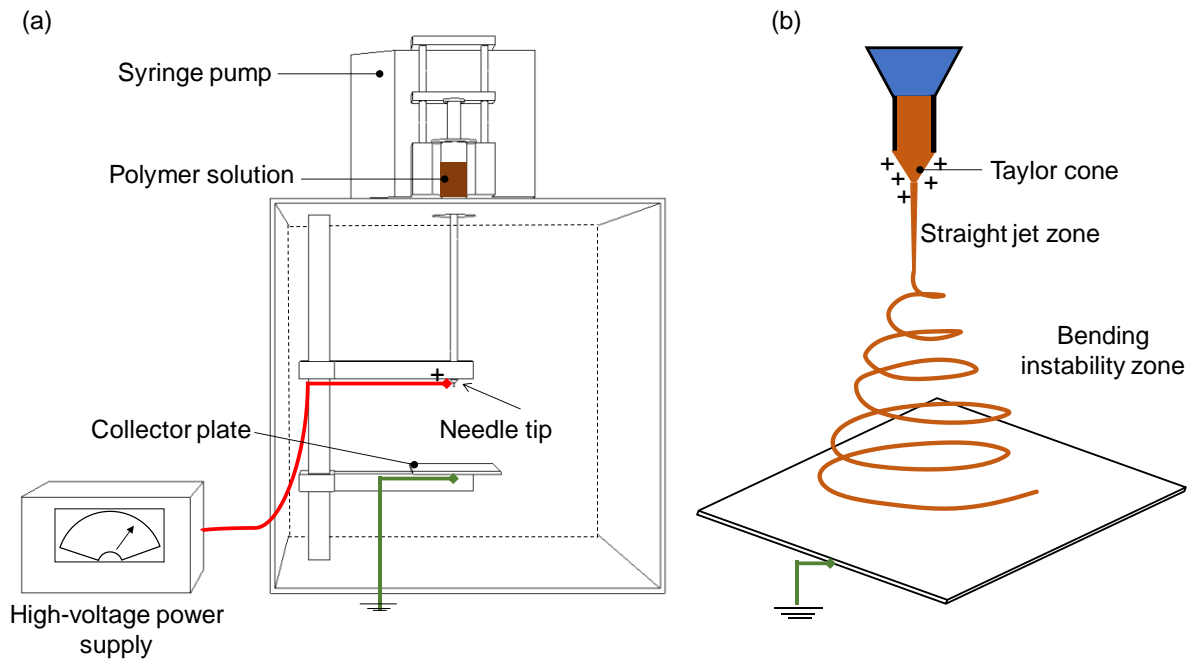


Figure 2.20 (a) Typical set-up for electro-spinning and key components of the electro-spinner and (b) fibre formation by electro-spinning.

In general, a polymer solution or polymer melt is fed into a syringe and the liquid is driven by a dispensing unit or syringe pump. More than one solution can also be fed in if a core and cladding structure are desired in the output fibre. Such liquids are generally subjected to a spinning motion to enable phase separation and/or uniformity

in viscosity. The needle of the syringe is connected to a high-voltage supply to induce charges into the polymer solution. With increasing voltage, the charge density on the surface of the droplet at the tip of the needle also increases. The repulsion between the accumulated like-charges tends to oppose the surface tension, which maintains the spherical shape of the droplet. The droplet is also subjected to an attractive force from the grounded collector electrode. At a critical voltage, the droplet that has deformed into a cone (the Taylor cone) stretches out into a thin fibre-like structure. Eventually a polymer jet ejects outward from the vicinity of the needle tip in the form of a jet that proceeds in a random or sometimes spiral trajectory over some distance before it is collected in the form of fibre on the grounded electrode [169,170].

In the aforesaid process, the thinning of the droplet into a fibre, followed by further stretching and whipping forces, aids in reducing the fibre diameter and accelerates solvent evaporation. The separation between the tip of the needle and the ground electrode in conjunction with the ambient temperature and relative humidity determine the state of the fibres produced. Incomplete solvent evaporation can lead to fibre fusion and non-uniform fibre diameters. Therefore, optimal control of the process parameters is essential to achieve consistent electro-spun fibres [169].

Table 2.7 presents a summary of the selected parameters that are considered to have a significant influence on the characteristics of fibres manufactured via electro-spinning.

Table 2.7 A summary of the key processing parameters for electro-spinning.

Variable parameter	Parameter	Effect on electro-spun fibres	References
Polymer solution	Concentration and viscosity	<ul style="list-style-type: none"> • Bead type defects can be eliminated by increasing the concentration. • Increasing concentration leads to an increase in the viscosity and fibre diameter. 	[171–173]
	Surface tension	<ul style="list-style-type: none"> • Increasing the surface tension leads to bead formation. 	[169]
	Conductivity	<ul style="list-style-type: none"> • Increasing in conductivity of polymer solution, the critical voltage for electro-spinning is reduced. 	[169]
	Dielectric constant	<ul style="list-style-type: none"> • Bead formation can be reduced by using solvent with a high dielectric constant. 	[174]
	Solvent evaporation rate	<ul style="list-style-type: none"> • Lower evaporation rate leads to the formation of flat and porous fibres. 	[175]
Processing condition	Applied voltage	<ul style="list-style-type: none"> • The fibre diameter is reduced by increasing the voltage. 	[176]
	Temperature	<ul style="list-style-type: none"> • Increasing the solution temperature enhances polymer chain mobility and lowers the viscosity leading to a reduction in fibre diameter. 	[177]
	Working	<ul style="list-style-type: none"> • Increasing the distance between the 	[178,179]

Variable parameter	Parameter	Effect on electro-spun fibres	References
	distance	tip of the needle and collector leads to a reduction in fibre diameter and the fusion of fibres.	
	Solution Feed rate	<ul style="list-style-type: none"> Increasing the feed rate tends to increase fibres diameter. 	[180,181]
Ambient	Humidity	<ul style="list-style-type: none"> Decreasing the humidity accelerates the evaporation rate of the solvent. 	[177,182]

Table 2.8 shows a compilation of previous literature where the electro-spinning of lignin fibres has been demonstrated. Fibres from lignin without blending have been reported rarely except for hardwood Organosolv lignin dissolved in ethanol using a coaxial needle [103,183]. Ethanol was used in the outer skin which allowed for encapsulating the lignin in the core. On the other hand, softwood lignin required pre-treatments such as molecular weight fractionation [36,145,146], chemical modification [184,185] and blending with a polymers such as PEO [35,36,143–146], PAN [147,148] and PVA [149–151] for the fibre formation via electro-spinning. It was claimed that softwood lignin alone did not have sufficient viscoelasticity for electro-spinning [35,139,143]. This was explained by Dallmeyer *et al.* [35] who reported the Newtonian behaviour for neat softwood Kraft lignin solution and this was converted into a non-Newtonian characteristic by adding PEO. Moreover, they claimed that the Newtonian solution could not create a stable electro-spinning jet. Increasing the molecular weight, with the addition of PEO, increased the viscosity of the lignin solution; however, the excessive solution viscosity was found to be unsuitable for spinning.

With reference to Table 2.8, there are many key parameters that have to be considered for the electro-spinning of lignin, such as the solvent used for dissolving of lignin and/or the polymer blend and the total polymer concentration affecting

the solution viscosity. Solubility is one of the criteria for solvent selection. Ethanol [103,183], acetone/DMA_c [186] and DMF [187,188] have been used for dissolving Organosolv lignin. DMF, DMSO and chloroform were used for Kraft lignin according to the data compiled in Table 2.8.

Several researchers have studied the blending of PAN with lignin and DMF as the solvent. The use of PAN carries a cost concern, moreover it is unsustainable. DMF is a toxic solvent with environmental and health concerns [143,144,149]. For these reasons, lignin blended with water-soluble polymers such as PEO and PVA were explored as an alternative choice to replace the use of PAN [143,150,151,189,190].

It shown in Table 2.8 that polymers in the range 0.2 wt% to 70 wt% have been added to lignin. For example, a small amount of PEO (0.2-5 wt%) [36,143–145] was added to the lignin solution, whereas 25 wt% to 75 wt% of PAN [147,148], PVA [149–151] and PCL [191] ranging from 25 wt% to 75 wt% were required for electro-spinning lignin. The concentration of the polymers used with lignin is dictated by the miscibility between the two polymers. PEO and lignin have been reported as being miscible with lignin [138,153], hence only a small concentration of PEO is required. On the other hand, PAN [185] and PVA [154] are immiscible with lignin, therefore, higher amounts of PAN and PVA are required for blending. In addition to blending, solvent fractionation and/or chemical modification have been used to treat lignin, in order to improve the miscibility between lignin and other specified polymers [36,145,146,184,185,191].

Table 2.8 A compilation of selected papers on the electro-spinning of lignin fibres.

Lignin	M _w of lignin (g·mol ⁻¹) [PDI]	Treatment of lignin	M _w of treated lignin (g·mol ⁻¹) [PDI]	Solvent	Polymer blend/ M _w (g·mol ⁻¹)	Blend ratio of lignin/ polymer blend (w/w)	Total polymer concentration	Solution viscosity (Pa·s)	Fibre diameter (nm)	Reference
Hardwood Organosolv (Alcell®)	2,300 [7.9 PDI]	N/A	N/A	Ethanol	N/A	N/A	50 wt%	3.5-4.0	800-3,000	[103,183]
Hardwood Organosolv (Alcell®)	2,300 [7.9 PDI]	N/A	N/A	DMF	PEO/ 600,000	90/10	35-20 wt%	N/A	500	[187]
Hardwood Organosolv	1,900 [2.1 PDI]	N/A	N/A	DMF	PAN	40/60	25 wt%	0.988	2,277	[188]
Hardwood Organosolv	N/A	N/A	N/A	Acetone and DMA _c 2/1 (v/v)	CA/ M _n ~30,000	84/16	20 wt%	N/A	450	[186]
Softwood Kraft	2,700	N/A	N/A	NaOH	PEO/	95/5	11 wt%	N/A	500-	[143,144]

Lignin	M _w of lignin (g·mol ⁻¹) [PDI]	Treatment of lignin	M _w of treated lignin (g·mol ⁻¹) [PDI]	Solvent	Polymer blend/ M _w (g·mol ⁻¹)	Blend ratio of lignin/ polymer blend (w/w)	Total polymer concentration	Solution viscosity (Pa·s)	Fibre diameter (nm)	Reference
(Indulin AT)				aqueous	5,000,000				10,000	
Softwood Kraft (Indulin AT)	3,700 [8.4 PDI]	N/A	N/A	DMF	PEO/ 600,000	99/1	40 wt%	0.15	700-1,500	[118]
Hardwood Kraft	2,500 [7.6 PDI]						40 wt%	0.05		
Sulfonate lignin (Kraftsperser 25M)	2,200 [6.6 PDI]						30 wt%	N/A		
Hardwood Organosolv (Alcell®lignin)	2,300 [7.9 PDI]						40 wt%	0.03		
Pyrolytic lignin	2,600 [7.5 PDI]						40 wt%	0.02		
Softwood Kraft	3,700	N/A	N/A	DMF	PEO/	99.6/0.4	45 wt%	N/A	N/A	[35]

Lignin	M _w of lignin (g·mol ⁻¹) [PDI]	Treatment of lignin	M _w of treated lignin (g·mol ⁻¹) [PDI]	Solvent	Polymer blend/ M _w (g·mol ⁻¹)	Blend ratio of lignin/ polymer blend (w/w)	Total polymer concentration	Solution viscosity (Pa·s)	Fibre diameter (nm)	Reference
(Indulin AT)	[7.9 PDI]				1,000,000					
Softwood Kraft (Indulin AT) blend with fractionated softwood lignin	3,700 [7.9 PDI]	Methanol fractionation (F ₁₋₃) Methanol/ methylene chloride fractionation (F ₄)	71,00 38,000	DMF	PEO/ 1,000,000	99.8/0.2 Blend ratio of F ₄ /F ₁₋₃ is 30/70	32 (w/v)	N/A	N/A	[36]
Softwood Kraft (Indulin AT) blend with fractionated softwood lignin and incorporate		Methanol fractionation and Methanol/ methylene	6,800 35,000	DMF	PEO/ 600,000	99/1 Blend ratio of F ₄ /F ₁₋₃ is 30/70 MWNTs	25 wt%	N/A	900-1,200	[145]

Lignin	M _w of lignin (g·mol ⁻¹) [PDI]	Treatment of lignin	M _w of treated lignin (g·mol ⁻¹) [PDI]	Solvent	Polymer blend/ M _w (g·mol ⁻¹)	Blend ratio of lignin/ polymer blend (w/w)	Total polymer concentration	Solution viscosity (Pa·s)	Fibre diameter (nm)	Reference
multiwalled carbon nanotubes (MWNTs)		chloride fractionation				contents 1, 4, 6 wt%				
Softwood Kraft (Indulin AT) blend with fractionated softwood lignin	3,700 [7.9 PDI]	Methanol fractionation and Methanol/ methylene chloride fractionation	6,800 35,000	DMF	PEO/ 1,000,000	99.8/0.2	30 wt%	N/A	N/A	[146]
Softwood Kraft (Indulin AT)	3,700 [7.9 PDI]	Methanol/ methylene chloride fractionation	N/A	DMF	PEO/ 1,000,000	99/1	30 wt%	N/A	500-900	[192,193]
Softwood Kraft	3,700	N/A	N/A	DMSO	PVA/	50/50	30 wt%	N/A	750	[149]

Lignin	M _w of lignin (g·mol ⁻¹) [PDI]	Treatment of lignin	M _w of treated lignin (g·mol ⁻¹) [PDI]	Solvent	Polymer blend/ M _w (g·mol ⁻¹)	Blend ratio of lignin/ polymer blend (w/w)	Total polymer concentration	Solution viscosity (Pa·s)	Fibre diameter (nm)	Reference
(Indulin AT)	[7.9 PDI]				1,300,000					
Softwood Kraft (Sigma-Aldrich)	10,000	N/A	N/A	Water	PVA/ 125,000	75/25	5-8 wt%	N/A	148 ± 4	[150]
Softwood Kraft (Sigma-Aldrich)	10,000	N/A	N/A	Water	PVA/ 85,000- 124,000	30/70 50/50 70/30	9 to 12 wt%	N/A	150-300	[151]
Softwood Kraft (Sigma-Aldrich)	10,000	N/A	N/A	DMF	PAN	50/50	17 wt%	N/A	1,100 ± 340	[147]
Softwood Kraft (Sigma-Aldrich, low sulfonated)	60,000	N/A	N/A	Water	PEO/ 600,000	74/26 86/14 90/10	10 wt%	N/A	100–500	[189]
Softwood Kraft	60,000	N/A	N/A	DMF	PAN/	50/50	50 wt%	320	300	[148]

Lignin	M _w of lignin (g·mol ⁻¹) [PDI]	Treatment of lignin	M _w of treated lignin (g·mol ⁻¹) [PDI]	Solvent	Polymer blend/ M _w (g·mol ⁻¹)	Blend ratio of lignin/ polymer blend (w/w)	Total polymer concentration	Solution viscosity (Pa·s)	Fibre diameter (nm)	Reference
(Sigma-Aldrich, low sulfonated)					150,000					
Softwood Kraft (Sigma-Aldrich)	28,000	Lignin-co-PMMA and Blending with PCL	20,000-100,000 [1.2-1.3 PDI]	Chloroform/ methanol	PCL	25/75	14 wt%	N/A	300-600	[191]
Hardwood Kraft Moorim Pulp & Paper Co. (South Korea)	16,100	Methanol fractionation and graft with PAN	256,000	DMF	N/A	N/A	17 wt%	N/A	900-1,200	[184]
Corn stover Organosolv	4,000 [1.3 PDI]	Chemical modification: butylating	N/A	DMF	PAN/ 150,000	50/50	20 wt%	1.48	1,690	[185]

2.3.3 Dry-spinning Lignin

Dry-spinning is one of the solution-spinning techniques where the solidification of the filament is achieved by heat-induced evaporation. Typically, the solidification rate in dry-spinning is slower than that of melt-spinning [158,194]. This is explained by their solidification mechanisms. In dry-spinning, preparation of a polymer solution or dope is the first step. The criteria for solvent selection are dissolving ability and solvent volatility. However, the solvent's flammability, risk of explosion and toxicity are causes for concern. After the full dissolution of the polymer, the solution is filtered and deaerated in order to avoid void formation. Key process parameters are polymer concentration and thermal diffusion coefficient.

The cross-sectional morphology of a dry-spinning filament is dependent on the ratio of the solvent evaporation rate to solvent diffusion rate (γ) – see Figure 2.21. If this ratio is close to 1, a near-circular cross-section can be formed. If the ratio is higher than 1, a thicker, hard skin can be formed. However, if the solvent evaporation rate is much greater than the solvent diffusion rate, the solvent remains inside the filament, causes longitudinal distortion of the skin and forms a flat or peanut-shaped cross-section.

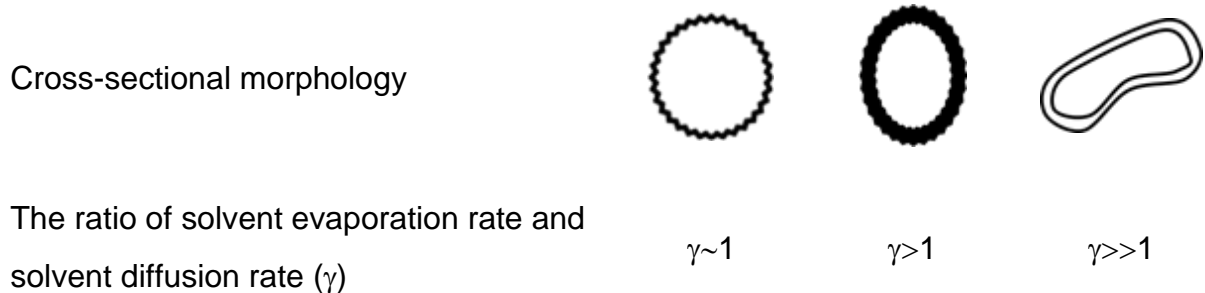


Figure 2.21 Filament cross-sectional morphology dependence on the ratio of evaporation rate to diffusion rate [194].

Dry-spun lignin was demonstrated by Otani *et al.* [195] in 1965. They used alkaline solution to dissolve lignin and the solution was extruded and dried. After carbonisation,

the fibres showed the presence of voids due to residual NaOH.

Table 2.9 shows a compiled list from the literature on lignin-based carbon fibres produced by dry-spinning. Acetylated softwood Kraft lignin was successfully manufactured by Zhang and Ogale [196–198]. The acetylated lignin was fully dissolved in acetone. A high concentration of lignin solution ($2.15 \text{ g}\cdot\text{ml}^{-1}$) provided a lignin precursor without crevice patterns, while an increased spinning temperature created more crevice patterns, as shown in Figure 2.22 [197].

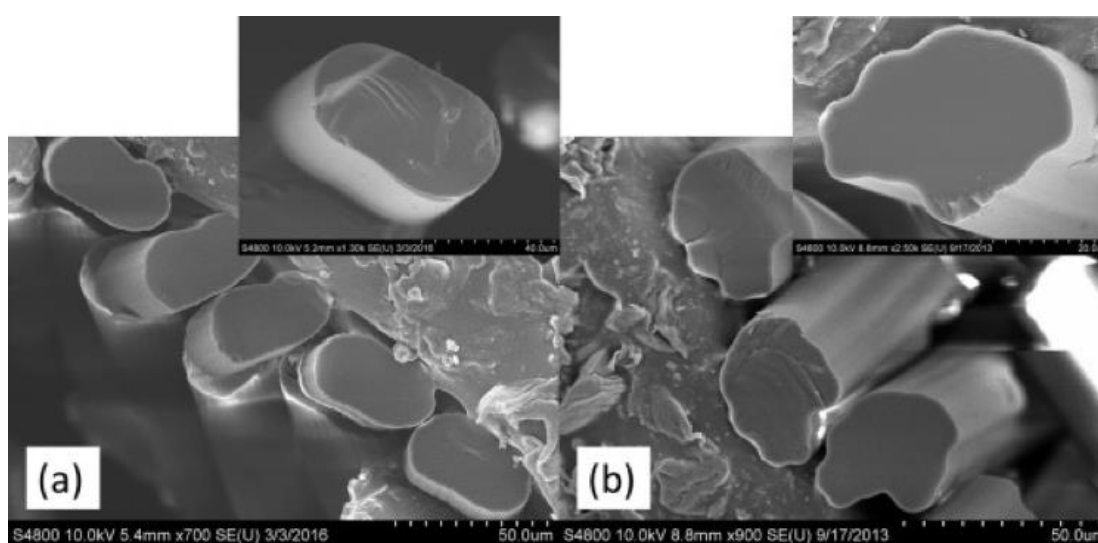


Figure 2.22 SEM micrographs of as-spun fibres from dry-spinning of acetylated softwood Kraft lignin. The solution was spun at room temperature at two different concentrations: (a) $2.15 \text{ g}\cdot\text{ml}^{-1}$ and (b) $2.00 \text{ g}\cdot\text{ml}^{-1}$ [196,197].

In a recent report, dry-spun softwood lignin without chemical modification was produced successfully [199,200]. Prior to dry-spinning, softwood Kraft lignin was purified and fractionated via a continuous and simultaneous system called Aqueous Lignin Purification with Hot Acids (ALPHA) as shown in Figure 2.23. A hot acetic acid-water mixture was used in the ALPHA to fractionate and solvate softwood lignin. A low ash content of 0.06-0.08 wt% was extracted and an increase in molecular weight was found when the acetic acid to water ratio was increased. Lignins with different molecular weights from the ALPHA process were dry-spun at 30-40 °C and carbonised at 1,000 °C. The resultant carbon fibres from the highest molecular weight

(28,600 g·mol⁻¹) showed a tensile modulus of 98 GPa and tensile strength of 1.39 GPa. The cross-sectional morphologies of carbon fibres produced from ALPHA are shown in Figure 2.24 [201].

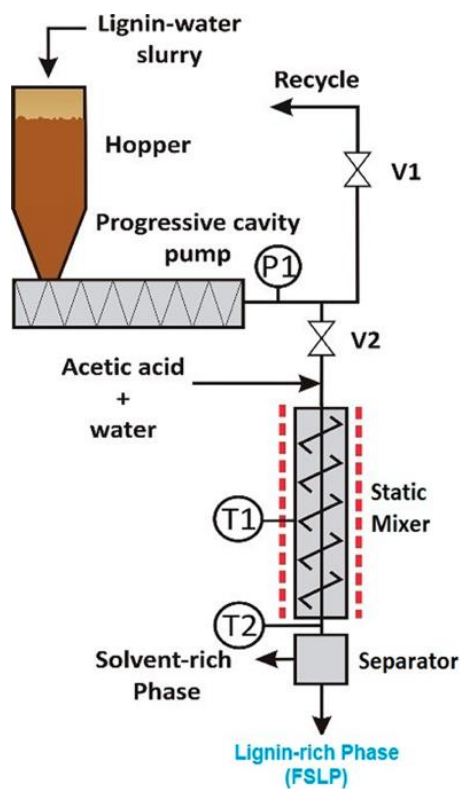


Figure 2.23 Schematic illustration of the continuous flow of the Aqueous Lignin Purification using the Hot Acids (ALPHA) process [199–201].

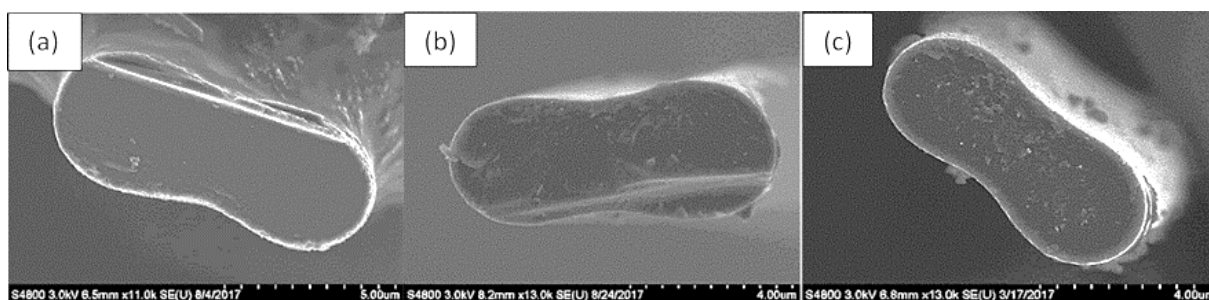


Figure 2.24 SEM micrographs of carbon fibres derived from: (a) medium; (b) higher; and (c) highest M_w lignins from the ALPHA process [201].

Table 2.9 A compiled list from the literature on the production of lignin fibres via dry-spinning.

Lignin	M _w of lignin (g·mol ⁻¹) [PDI]	Purification method	M _w of purified lignin (g·mol ⁻¹)	Solvent	Total polymer concentrations	Fibre diameter (μm)	Reference
Softwood Kraft (Indulin AT)	3,700 [7.9 PDI]	Partial acetylation	N/A	Acetone	75 wt%	5.9	[119,196– 198]
Softwood Kraft	5,270 [6.6 PDI]	Aqueous Lignin Purification with Hot acids	7,200- 28,000	Acetic acid/water	85 wt%	5.6-6.2	[201]

2.3.4 Wet-spinning Lignin

Wet-spinning is a solution spinning process where the filaments are extruded into a liquid coagulation bath and solidified to form fibres. The polymer is dissolved in an appropriate solvent and the solution is degassed prior to being pressurised through a metering pump to a spinneret. The spinneret is submerged in a coagulation liquid which is a non-solvent; this is known as wet-spinning. The counter diffusion occurs between the solvent in the solution filament and the non-solvent in the coagulation bath [202,203]. At this stage, the extruded gel-like filament is transformed into a rubber-like solid [204]. Another method of wet-spinning is dry-jet wet-spinning, where the polymer solution is extruded into air prior to being submerged in a liquid bath [205]. The air gap allows the extruded gel-like filament to be stretched before entering a coagulation liquid.

Table 2.10 shows a compiled list from the literature on lignin-based carbon fibres manufactured by wet-spinning [44,142,206–208]. The wet-spinning of lignin without a second polymer has not been reported in the literature. PAN is the most used polymer blend used for wet-spinning lignin; lignin without any treatments was added into PAN spinning dope containing an organic solvent such as DMSO, DMF and DMAc. The lignin loading was in the range 30-50 wt%. For dopes with 15 wt% of PAN, sulfonate lignin was added where the concentration of the lignin was between 15-47 wt%. The blended dopes were extruded to a water coagulation bath at room temperature. The blend fibres showed finger-like macrovoids with a radial orientation [142]. These finger-like features have been reported by many researchers. The formation of these structures were said to be due to the counter diffusion of solvent/non-solvent and phase separation during coagulation [142,209–211]. The tensile strength and modulus decreased with an increasing concentration of lignin. Moreover, after air thermo-stabilisation at 230 °C with a dwell time of two hours, the stabilised-fibres still showed the finger-like macrovoids and a rough surface, as shown in Figure 2.25.

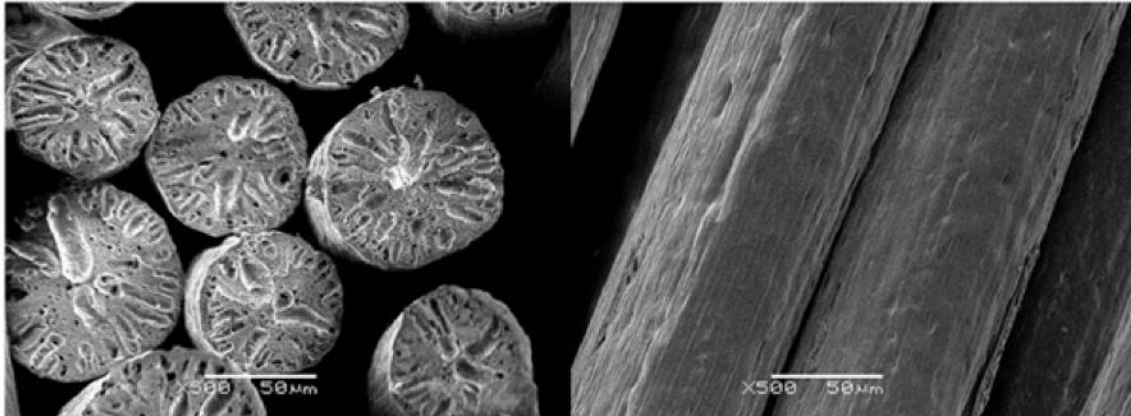


Figure 2.25 The PAN/sulfonate lignin fibres obtained from the air thermo-stabilisation step with finger-like macrovoids [142].

Void-free carbon fibres derived from lignin/PAN blends were demonstrated by Fitzer and Miller [44] where gel-spinning was used. The blend dope was extruded into a methanol bath at $-50\text{ }^{\circ}\text{C}$ and then stored in a methanol bath at $-30\text{ }^{\circ}\text{C}$ for 12 hours. The significant reduction in the fraction was said to be due to the decreased counter-diffusion rate and reduced rate of leaching for the lignin. Adding lignin into a water coagulation bath to eliminate void formation has been reported by Jin and Ogale [207], who reported that the addition of 0.1 - 0.2 wt% of lignin into a coagulant bath in order to control of lignin diffuses from the fibre surface. They found that the concentration of lignin in the coagulant was constant when 0.2 wt% of lignin was incorporated in the bath. Void-free carbon fibres with a tensile strength of $1.20 \pm 0.10\text{ GPa}$ and modulus of $130 \pm 3\text{ GPa}$ were claimed by these authors.

With reference to Table 2.10, carbon fibres obtained from a co-polymer of PAN and lignin was demonstrated [141,212] where the ratio of acrylonitrile to lignin of 8:2 was recommended. Other blends such as PVA [213] and cellulose [214] have been blended with lignin and subjected to wet-spinning.

Table 2.10 A compiled list from the literature for lignin fibres manufactured by wet-spinning.

Lignin	M _w of lignin (g·mol ⁻¹)	Treatment of lignin	Solvent	Polymer blend/ M _w (g·mol ⁻¹)	Blend ratio of lignin/ Polymer blend (w/w)	Total polymer concentration	Reference
Unspecified sulfonate	N/A	N/A	DMSO	PAN	47/53	28 wt%	[142]
Softwood Kraft	2,700	N/A	DMSO	PAN/ 12,000	50/50	20 wt%	[206]
Softwood Kraft (Indulin AT)	N/A	N/A	DMSO	PAN/ 233,000	50/50	16 wt%	[207]
Grass soda (Protobind)	N/A	N/A	DMAc	PAN/ 250,000	30/70	20 wt%	[44]
Hardwood (Lignol Innovation)	1,900	N/A	DMF	PAN/ 150,000	40/60	25 wt%	[208]
Hardwood	N/A	Copolymerisation with PAN	DMSO	PAN	50/50	16 wt%	[212]
Unspecified lignin	N/A	Copolymerisation	DMSO	PAN	45/55	N/A	[141]

Lignin	M _w of lignin (g·mol ⁻¹)	Treatment of lignin	Solvent	Polymer blend/ M _w (g·mol ⁻¹)	Blend ratio of lignin/ Polymer blend (w/w)	Total polymer concentration	Reference
		with PAN					
Unspecified Kraft	N/A	N/A	DMSO/water	PVA/ 140,000	50/50	10 w/v	[213]
Hardwood Organosolv Beech wood	N/A	N/A	[DBNH]OAc*	cellulose	20/80	15 wt%	[214]

*[DBNH]OAc refers to 1,5-Diazabicyclo[4.3.0]non-5-enium acetate

2.4 Heat Treatment of Lignin

2.4.1 Thermo-stabilisation of Lignin

Thermo-stabilisation is a processing step subsequent to fibre formation, intended to prevent the fusion of the spun fibres during heat treatment. Fibre fusion can occur for a number of reasons during thermo-stabilisation. For example: (i) the presence of solvent-rich filaments in intimate contact; and (ii) the T_g of lignin (70-160°C), with reference to the data compiled in Table 2.5, being lower than the processing temperature which can vary from 200-300 °C [117,135,196,215–217]. Thermo-stabilisation of lignin filaments is reported to minimise fibre fusion by oxidation and cross-linking [217,218]. There are few studies reporting the effect of the conditions used in thermo-stabilisation of lignin [217–221]. Most of the studies [217–219] reported the properties of the stabilised lignin which was ground into a powder prior to characterisation. The effect of thermo-stabilisation on lignin with nanoscale fibres has been investigated [220]. A number of papers have reported on the increase in the oxygen concentration and a decrease in that of hydrogen. The loss of hydrogen is explained by the cleavage of C-H or O-H bonds [217,219,220]. The decrease in the hydrogen content is supported by the functional group characterised by Fourier-transform infrared spectroscopy (FTIRS). The absorbance bands for C-H and O-H decreased with an increase in thermo-stabilisation temperature. Moreover, the signal at 1700 cm^{-1} , representing the carbonyl group, increases rapidly when the stabilisation is above 250 °C [218,220,221]. Similar results have been reported from solid state ^{13}C NMR [219] and X-ray photoelectron spectroscopy (XPS) [217]. An increase in the T_g was found with decreasing heating rate [218]. Some authors have reported that the T_g cannot be detected when lignin is stabilised over 250 °C at 0.2 $\text{K}\cdot\text{minute}^{-1}$ [217,218]. The increased T_g is attributed to cross-link reactions. The thermo-stabilisation conditions, including temperature, heating rate and dwell time, have been said to have a minor effect on the mechanical properties of carbon fibres derived from lignin [219,220]. The tensile strength and modulus of lignin fibre carbonised at 1,000 °C were said to be in the range 35-48 MPa

for the tensile strength and 6-11 GPa for the tensile modulus [220].

From these reports, it can be concluded that the main purpose of thermo-stabilisation is to prevent the fibre fusion during carbonisation. Therefore, the key parameters in thermo-stabilisation for the lignin have to be considered. The fibre morphology of the stabilised fibres has to be investigated prior to proceeding with carbonisation.

The structural development during the oxidative thermo-stabilisation of lignin is not conclusive as several reaction mechanisms have been proposed but universal agreement has not been reached [217,218,221,222]. The mechanism is said to involve many stages: (i) the cleavage of the C-O bond at the β -O-4' position, which is the major constituent in the lignin structure. (ii) Both the C-O cleavages produce free-radicals in the phenoxy rings. Hydrogen abstraction followed by the formation of formaldehyde, are the reactions that take place on the phenoxy free-radical. (iii) Once the free-radicals are formed, the rearrangement of a free-radical can occur. The free-radical favours locating at the α -position; however, it can relocate to the β -position. Once the free-radical moves to the β -position, then the cleavage at the β position is again progressed.

In the presence of oxygen, auto-oxidation can take place leading to the formation of carbonyl and carboxyl groups [218,223]. In an oxygen atmosphere, a cross-link is possible, leading to a more thermo-stable structure. Following the cross-linking reaction, the oxidised lignin fibre acquires a higher T_g and this aids in retainment of its geometry during carbonisation.

2.4.2 Carbonisation of Lignin Precursor

After thermo-stabilisation, carbonisation and graphitisation are carried out. The stabilised fibres are heat-treated in an inert atmosphere at specified temperatures to obtain the desired properties. For lignin, the reported carbonisation temperature is between 600 °C-1,400 °C [144,184,185,219,224]. During carbonisation, mass-loss is significant and the total yield obtained is around 30%–50% [13,64,103]. Carbon is

the main component on the fibre surface and its concentration increases with increasing carbonisation temperature [37,103,225].

Raman spectroscopy is a technique that is used for characterising various forms of carbon (crystalline and amorphous). It is employed to analyse the ordered graphitic structure through the ratio between the D-band and G-band which is defined as the R-value. The D and G-bands are located at around $1,310\text{ cm}^{-1}$ and $1,580\text{ cm}^{-1}$, respectively. The D-band represents the breathing mode of a 6-carbon atom in an aromatic ring and this band is attributed to a disordered structure. The G-band corresponds to the in-plane stretching mode of the sp^2 carbon in the aromatic ring and aliphatic chain [226–228]. The R-value is used to indicate the graphitic-like structure in carbon fibres obtained from lignin [36,103,145,215,229]. The R-value for carbon powder derived from lignin decreases from 3.5 to 2.1 when the carbonisation temperature is increased from $800\text{ }^\circ\text{C}$ to $1,400\text{ }^\circ\text{C}$ [219]. The same decrease in the R-value has been reported in carbon fibres obtained from lignin [144], fibres from copolymer of lignin and PAN [184] and PAN fibres [36]. A statistical design of experiment, a two-level factorial, was explored to investigate the effect of the carbonisation conditions, including the heating rate ($2.0, 4.5$ and $7.0\text{ K}\cdot\text{minute}^{-1}$), carbonisation temperature ($800, 950$ and $1,100\text{ }^\circ\text{C}$) and dwell time ($3.0, 6.5$ and 10.0 hours) by Poursorkhabi *et al.* [144]. They found that the R-value decreased when the carbonisation temperature and heating rate were increased, whereas the R-value was increased from 2.2 to 2.5 when the dwell time was increased from three hours to 10 hours. In terms of the mechanical property, an improvement in tensile strength and modulus was found with decreasing R-value [184] and increasing carbonisation temperature [225].

With reference to the aforesaid review, the carbonisation condition is the key to obtaining the desired mechanical properties for lignin-based carbon fibres. Therefore, the key parameters in carbonisation have to be taken into account for the production of carbon fibres from the lignin.

2.5 Mechanical Properties of Carbon Fibres from Lignin

The mechanical properties of a single filament of carbon fibre produced from lignin by different spinning techniques, such as melt-spinning, dry-spinning and wet-spinning are compiled in Table 2.11. The single filaments were evaluated according to the ASTM test method D-3379-75 or ASTM C1557-20.

With reference to Table 2.11, carbon fibres derived from lignin without a blended polymer exhibited tensile strengths in the range from 10 to 1,000 MPa and a tensile modulus between 1-100 GPa. Carbon fibres obtained from PAN/lignin via wet-spinning showed better results in both the tensile strength and modulus, which were 1,200-1,400 MPa and 100-200 GPa, respectively. These properties depended on many factors, such as extraction method [215], conditions during thermo-stabilisation [220] and carbonisation [144,225]. However, these properties are far from those of standard grade carbon fibres (T700), having 4900 MPa and 230 GPa in tensile strength and tensile modulus, respectively.

The mechanical properties of carbon fibres produced by electro-spinning are measured generally in the form of a randomly-aligned mat. The electro-spun mat is cut into a rectangular shape and the dimensions are measured. The specific stress is calculated using Equation 2.1 [230], which has been used by many researchers [146,184,185,231,232].

$$\text{Tensile stress (N} \cdot \text{Tex}^{-1}) = \frac{[\text{Force(N)} / \text{sample width(mm)}]}{\text{areal density (g/m}^2\text{)}} \quad \text{Equation 2.1}$$

Tex represents the mass of one kilometre of the fibres. The areal density is calculated from the sample mass per square metre (m^2). The tensile stress ($\text{N} \cdot \text{Tex}^{-1}$) is converted to the stress units of GPa multiplying by the bulk density; in the case of lignin

$1.35 \times 10^3 \text{ kg}\cdot\text{m}^{-3}$ is used for the bulk density [146,184]. The mechanical testing of single nano-fibres has been investigated using a sensitivity tensile tester [233], atomic force microscope (AFM) [234,235], nano-indentation [224,229] and *in situ* SEM tensile tester [236]. However, a few publications have reported the mechanical properties of single nano-carbon fibres from lignin. The reported mechanical values of carbon fibre mats and nano-carbon fibres from lignin-based precursor are presented in Table 2.12.

Table 2.11 Compiled list of mechanical values of carbon fibres from lignin-based precursor via melt-spinning, dry-spinning and wet-spinning.

Materials	Chemical or thermal modifications	Polymer blend	Carbonisation temperature (°C)	Tensile strength (MPa)	Tensile modulus (GPa)	Strain to failure (%)	Reference
Carbon fibres from melt-spinning							
Hardwood lignin	Steam explosion Blending of chloroform-soluble and carbon disulphide-insoluble fraction	N/A	1,000	660 ± 230	40.7 ± 6.3	-	[61]
Hardwood lignin	Acetosolv	N/A	1,000	355 ± 53	39.1 ± 13.3	0.98 ± 0.25	[161]
Softwood lignin	Acetosolv	N/A	1,000	26.4 ± 3.1	3.59 ± 0.43	0.71	[162]
Hardwood lignin	Acetosolv	N/A	1,000	5.8 ± 1.7	0.84 ± 0.29	0.75	[162]
Hardwood lignin	-	N/A	1,000	388	40	1.0	[64]
Hardwood Kraft lignin	Solvent fractionation	N/A	1,000	520 ± 182	28.6 ± 3.2	N/A	[117]
Softwood Kraft lignin with 10% Hardwood Kraft	Blending of lignin	N/A	1,000	300	30	0.7-1.2	[135]

Materials	Chemical or thermal modifications	Polymer blend	Carbonisation temperature (°C)	Tensile strength (MPa)	Tensile modulus (GPa)	Strain to failure (%)	Reference
lignin prepared by ultrafiltration							
Softwood from conventional cooking process	Thermal treatment at 140 °C for eight hours	N/A	1,200	465 ± 85	32.3±1.5	1.5	[216]
Softwood Kraft lignin	Chemical modification: peracylation	N/A	2,200	750	41.1	-	[163]
Hardwood lignin	N/A	PEO	1,000	339 ± 53	33 ± 2	1.25 ± 0.26	[64]
Hardwood Kraft lignin	N/A	PET	1,000	703	94	1.06	[139]
Hardwood Kraft lignin	N/A	PP	1,000	437	54	0.85	[139]
Softwood Kraft lignin	N/A	PLA	1,000	10	0.02	0.4	[155,156]
Yellow poplar	Solvent fractionation	N/A	1,000	550 ± 96	36.5 ± 2.81	1.3 ± 0.12	[165]
Alamo switchgrass lignin	Organosolv fractionation	N/A	1,000	370 ± 74	34.7 ± 3.03	1.01 ± 0.17	[165]

Materials	Chemical or thermal modifications	Polymer blend	Carbonisation temperature (°C)	Tensile strength (MPa)	Tensile modulus (GPa)	Strain to failure (%)	Reference
Organosolv lignin from Alamo switchgrass (<i>Panicum virgatum</i>) and yellow poplar	Organosolv fractionation and blending of lignin	N/A	1,000	750	42	N/A	[164]
Carbon fibres from dry-spinning							
Softwood Kraft lignin	Acetylation	N/A	1,000	1,040 ± 100	52 ± 2	2.0 ± 0.2	[196–198]
Softwood lignin	Aqueous Lignin Purification with hot acids (ALPHA)	N/A	1,000	1,000-1,300	98 ± 5	1.2-1.4	[201]
Carbon fibres from wet-spinning							
Softwood Kraft lignin	N/A	PAN	1,200	1,200 ± 0.1	105.7 ± 3.1	1.1 ± 0.1	[207]
Grass soda lignin (Protobind)	N/A	PAN	1,000	1,370 ± 200	194 ± 8	0.72 ± 0.1	[44]

Table 2.12 Mechanical values of nano-carbon fibres from lignin-based precursor via electro-spinning.

Materials	Treatment of lignin	Polymer blend	Testing form /carbonisation temperature (°C)	Tensile strength (MPa)	modulus (GPa)	Strain to failure (%)	Reference
Hardwood lignin	Methanol fractionation and co-polymerised with polyacrylonitrile	PAN	Random mat /1,400	89.4 ± 25.5	2.5 ± 0.6	N/A	[184]
Unspecified Organosolv lignin	Chemical modification: butylation	PAN	Random mat /1,000	83 ± 17	6.1 ± 0.6	1.4 ± 0.2	[185]
Softwood lignin	Methanol fractionation and methanol/methylene chloride fractionation	PEO	Random mat /1,000	74.1±14.6	4.1 ± 1.4	3.0 ± 1.1	[146]
Alkaline lignin	Acid precipitation	PAN	Random mat /1,000	N/A	22	N/A	[229]
Lignin from corn	Ethanol fractionation And iodine treatment	PAN	Random mat /1,400	89 ± 3	5.3 ± 0.3	1.14 ± 0.03	[231]

Materials	Treatment of lignin	Polymer blend	Testing form /carbonisation temperature (°C)	Tensile strength (MPa)	modulus (GPa)	Strain to failure (%)	Reference
Softwood lignin	Methanol fractionation and Methanol/methylene chloride fractionation	PEO with nanocrystalline cellulose	Random mat /1,000	40	8.0	0.5	[192]
Softwood lignin	Methanol fractionation and Methanol/methylene chloride fractionation	PEO with multiwalled carbon nanotube	Random mat /1,000	N/A	4.6 ± 0.75	0.97 ± 0.21	[145]
Seed coats of V.planifolia	Alkaline extraction	N/A	Single fibre/900	Modulus in transverse axis: 15.51 GPa. Modulus in axial axis: 34.52 GPa.			[224]

2.6 Research Gaps

In this section, a critical assessment of the research gap is summarised from the author's perspective of the literature.

- Softwood Kraft lignin has a great potential to serve as the precursor for the production of carbonised fibres. It has the potential to facilitate the production of carbon fibres in the future.
- Softwood lignin itself has not been spun without blending it with a polymer and/or chemical modification; these procedures are generally required for producing softwood lignin fibres.
- Blending lignin with polymers can lead to the formation of defects and voids when the fibres are thermo-stabilised and carbonised.
- The majority of the publications with regard to the production of lignin fibres use solvents that are toxic.
- The effect of the oxidation environment during the thermo-stabilisation of fibrous lignin preform has not been investigated in detail.
- Previous studies have not considered the use of a grounded electrode assembly during electro-spinning where the fibres can be heat-treated without the need for removing the fibres from the collector.

2.7 Aim and Objectives

The overall aim of this project was to identify and develop the sample preparation methods to enable lignin to be electro-spun to produce fibrous preforms that could be thermo-stabilised and carbonised. The specific aim of this project are as follows:

- To characterise the properties of as-received softwood Kraft lignin, (BioChoice®Lignin).
- To select and optimise a method to remove the inorganic content from as-received lignin.

- To develop a protocol to fractionate as-received lignin using acetone.
- To identify a primary non-toxic solvent and to optimise the electro-spinning of lignin without using a polymer blend.
- To develop and optimise procedures to enable thermo-stabilisation and the carbonisation of electro-spun randomly-oriented and aligned lignin fibres.
- To characterise the physical, thermal and spectral properties of the electro-spun, thermo-stabilised and carbonised lignin fibres.

2.8 Overview of the Research

The overview of this research is presented in Figure 2.26. Inorganic content of as-received lignin was removed by treating with acidified water. The key parameters involved in the experiments were optimised and analysed using the Taguchi design of experiment (DoE). Fractionation of lignin was explored using acetone. The acetone-soluble and acetone-insoluble fractions obtained from the fractionation were characterised and compared with the as-received lignin.

Fibre formation using lignin without a polymer blend was studied using 100% acetone-soluble lignin. This was demonstrated successfully using electro-spinning. The electro-spun lignin fibres were heated under different conditions prior to thermo-stabilisation in order to remove the residual solvent. During thermo-stabilisation, the effects of nitrogen flow and air flow on the fibre morphology, development of chemical structure and the thermal properties were investigated. The Taguchi method was used to optimise the carbonisation conditions for the production of carbon fibres. Finally, the key properties of the carbon fibres produced from the lignin precursor were characterised.

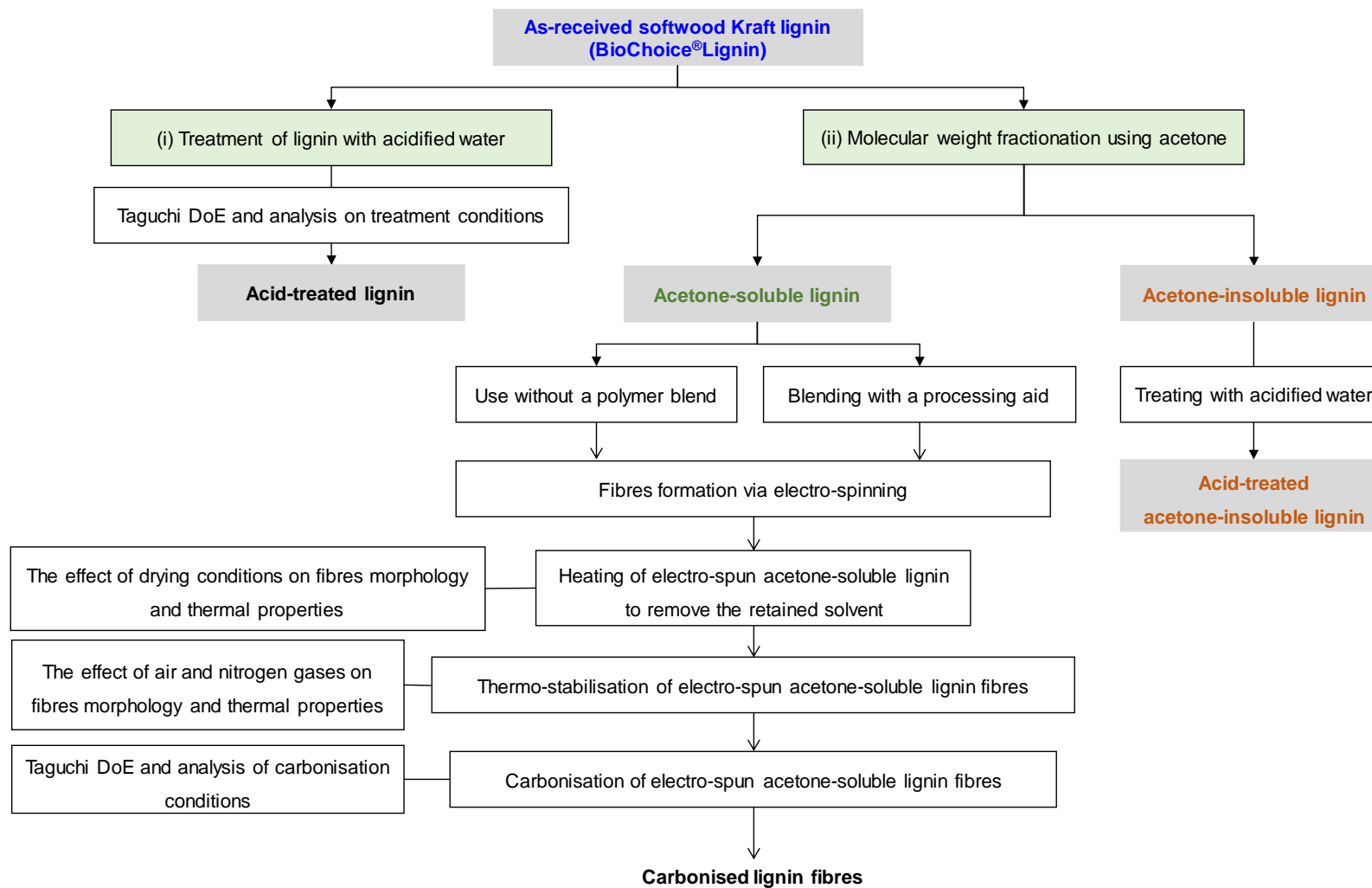


Figure 2.26 Schematic of the overview of this research.

2.9 Structure of the Thesis

This thesis has six chapters; the main details in each chapter are described below.

- Chapter 1: Introduction, aim and objectives of this study are explained and an overview of this work is summarised.
- Chapter 2: Literature review on carbon fibre and its manufacturing are presented. Lignin structure, types of lignin and their extraction methods are reviewed. Previous reports on the use of a lignin precursor for the production of carbonised fibres are compiled and discussed.
- Chapter 3: Materials, experimental methodologies and characterisation techniques are detailed.
- Chapter 4: Result and discussion – treatment of lignin using acidified water and molecular weight fractionation of lignin. In this chapter the key characteristics of as-received lignin are analysed. Treating as-received lignin with acidified water and fractionation using acetone are carried out. The treated lignins with acidified water and fractionated lignins are characterised and compared with the as-received lignin prior to electro-spinning to produce fibres.
- Chapter 5: Result and discussion – electro-spinning of acetone-soluble lignin. In this chapter, 100% acetone-soluble lignin without polymer blend is used for electro-spinning. Electro-spun fibres are heated prior to thermo-stabilisation and carbonisation. The effect of thermo-stabilisation conditions on the fibre morphology, thermal properties and chemical composition on the fibre surface are studied. The carbonisation condition is optimised with the Taguchi methodology. The properties of the carbonised lignin fibres are investigated.
- Chapter 6: This chapter contains the conclusions of this research and suggestions for future work.

3. EXPERIMENTAL

3.1 Materials

Softwood Kraft lignin (BioChoice®Lignin) used in this study was purchased from Domtar Corporation, USA. AR-certified acetone was purchased from Fisher Scientific, UK. 72% sulfuric acid (Product number: 45596) was supplied from Alfa Aesar. AR-certified hydrochloric acid, and dimethyl sulfoxide (anhydrous, $\geq 99.9\%$), vanillin (ReagentPlus®, 99%), polyethylene glycol 400 and potassium bromide (FTIR grade, $\geq 99\%$ trace metals basis) were obtained from Sigma-Aldrich, UK. Sodium chloride solution (HI7033), a calibration solution for electrical conductivity measurements was purchased from HANNA instruments, UK.

3.2 Treating Lignin with Acidified Water and Fractionation using Acetone

In this study, the treatment methods used for as-received lignin were: (i) treating with acidified water; and (ii) fractionation using acetone. These treatment methods were studied to remove inorganic content in the as-received lignin. The experimental methods are described in the following sections.

3.2.1 Treatment of Lignin with Acidified Water

The Taguchi orthogonal array experimental design was implemented to investigate the key parameters that were known to affect the purity of the resultant lignin. The lowest residual ash content attainable was set as the target. Four key parameters were studied, namely (i) acidic level, (ii) the acidified water-to-lignin ratio, (iii) washing time and (iv) the number of cycles. For each parameter, three levels are set and the details of each parameter are shown in Table 3.1.

Table 3.1 The parameters for washing lignin using acidified water and their levels.

Parameters	pH	Acidified water-to-lignin ratio (cm ³ :g)	Washing time (minutes)	Number of cycles
Level 1	2	5	15	1
Level 2	4	50	30	3
Level 3	6	100	60	5

A L9 orthogonal array, representing 3⁴ full factorial experiments was carried out. The experimental combinations involving nine experiments are presented in Table 3.2.

Table 3.2 Taguchi design of experiment used in this study to determine the optimum parameters for acid-washing lignin.

Experimental number	pH	Acidified water-to-lignin ratio (cm ³ :g)	Washing times (minutes)	No. of cycles
Exp. 1	2	5	15	1
Exp. 2	2	50	30	3
Exp. 3	2	100	60	5
Exp. 4	4	5	30	5
Exp. 5	4	50	60	1
Exp. 6	4	100	15	3
Exp. 7	6	5	60	3
Exp. 8	6	50	15	5
Exp. 9	6	100	30	1

As-received lignin was sieved through a 40-mesh (model woven wire mesh sieves, Retsch (UK) Ltd., UK) to obtain particle sizes smaller than 400 μm . The sieved-lignin was pre-dried in a vacuum oven (Model OVA031, Fistreem Vacuum Oven, UK) at 80 °C for six hours prior to treating using acidified water in accordance with the conditions specified in Table 3.2. Properties of the pre-dried as-received sample such as density, particle size, particle shape, thermal properties and molecular weight were characterised. Experimental details for these analytical techniques are described in Sections 3.4.1 to 3.4.7.

The acidified water and lignin were stirred using an overhead stirrer (Pro40 Digital Overhead Stirrer, SciQuip, UK). The overhead stirrer consisting of a variable-speed motor that was attached to a polytetrafluoroethylene (PTFE) shaft with a PTFE-coated paddle. The stirrer was operated at 200 rpm. After treating with the acidified water, the lignin suspension was filtrated using 1 μm glass filter (Whatman[®] glass microfibre, Grade GF/B, Sigma-Aldrich, UK) and washed several times with deionised water until the lignin dispersion reached pH7. The pH neutral lignin from each experiment was dried in a vacuum oven at 80 °C for six hours and stored in an airtight container until required. A summary of the procedures used for washing the lignin with acidified water is showed in Figure 3.1.

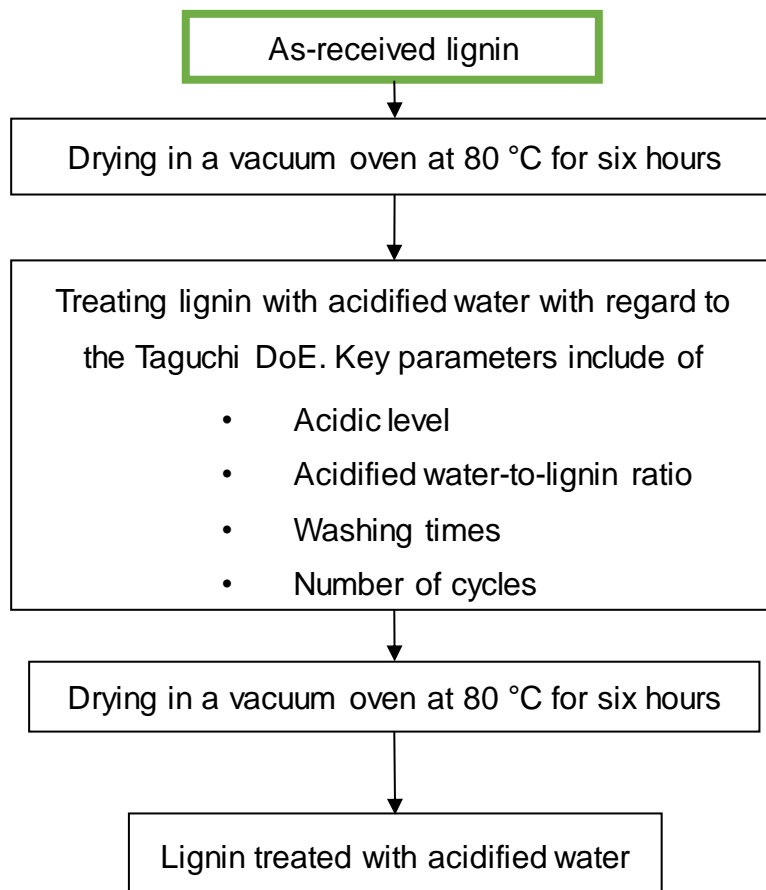
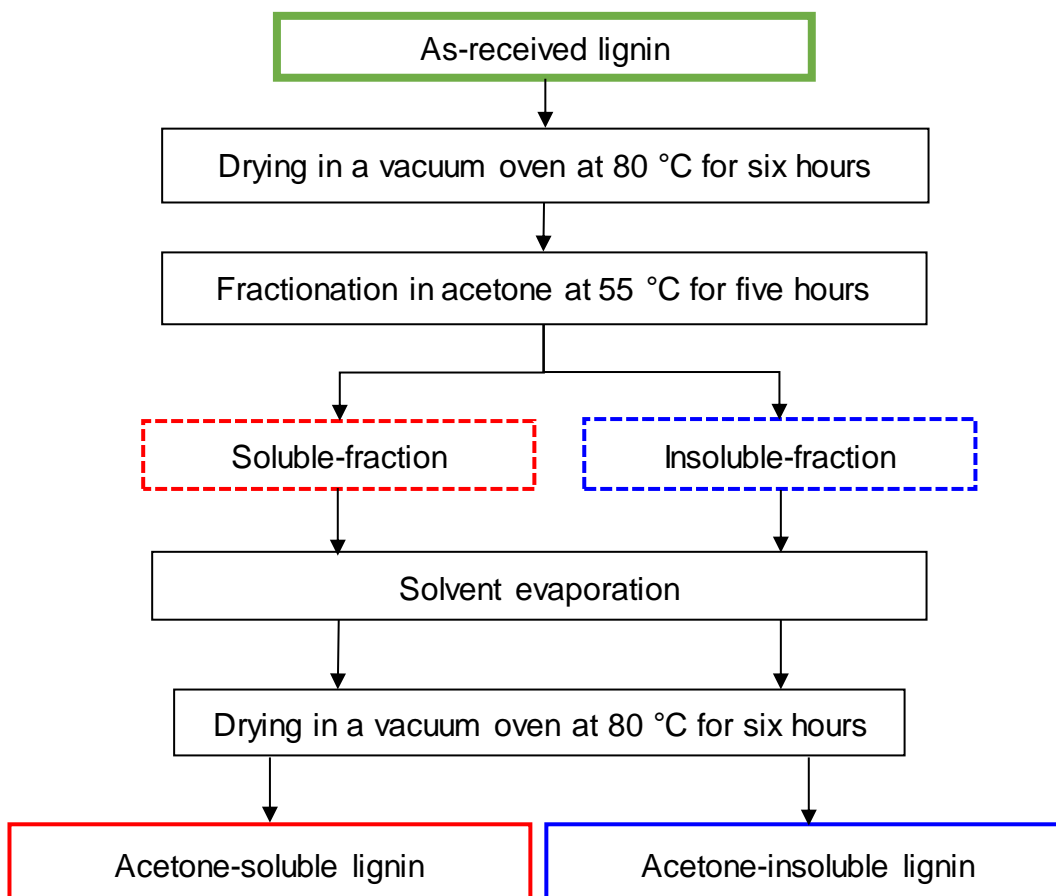


Figure 3.1 Flow diagrams of the methods used in this study for treating lignin with acidified water.

3.2.2 Molecular Weight Fractionation of Lignin using Acetone

Figure 3.2 shows a flow diagram of the procedures used for the fractionation of lignin using acetone. Prior to refluxing, the as-received lignin was dried at 80 °C in a vacuum oven for six hours. 100 g of the pre-dried lignin sample was introduced to a three-neck round-bottom flask along with 1,500 ml of acetone. The lignin to acetone ratio was 1 g:15 cm³.



(b)

Figure 3.2 Flow diagrams of fractionation lignin using acetone.

The round-bottom flask was positioned and secured in a temperature-regulated water bath (Techne TE-10D Heater Circulator, UK). The experimental set-up for refluxing the lignin is illustrated in Figure 3.3. The refluxing was performed at 55 °C for five hours and agitation was provided by bubbling argon gas at 50 ml·minute⁻¹.

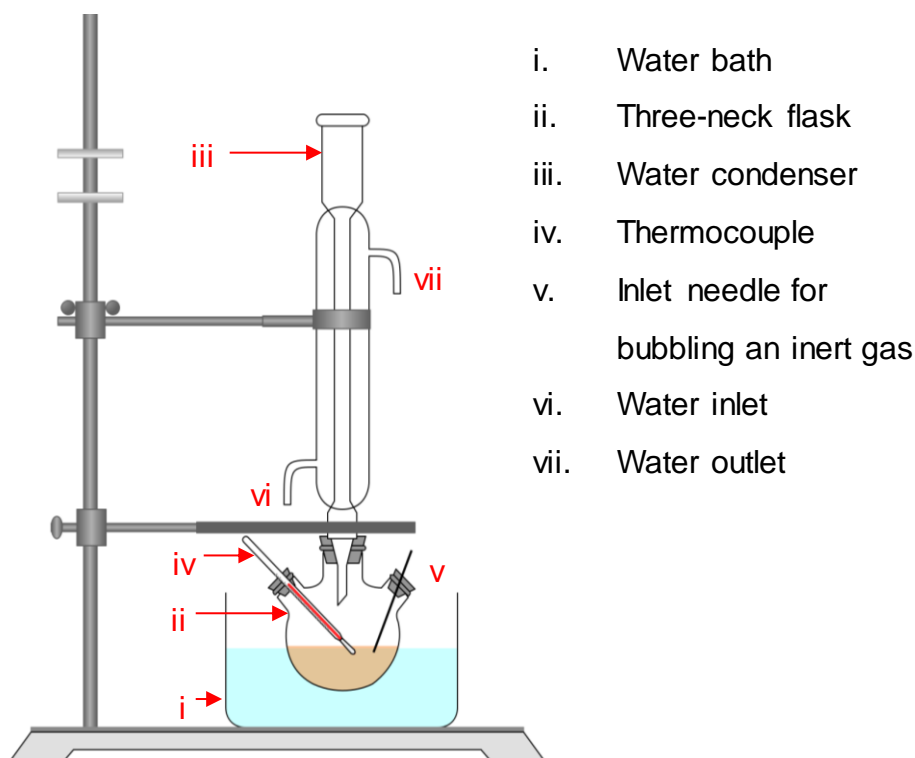


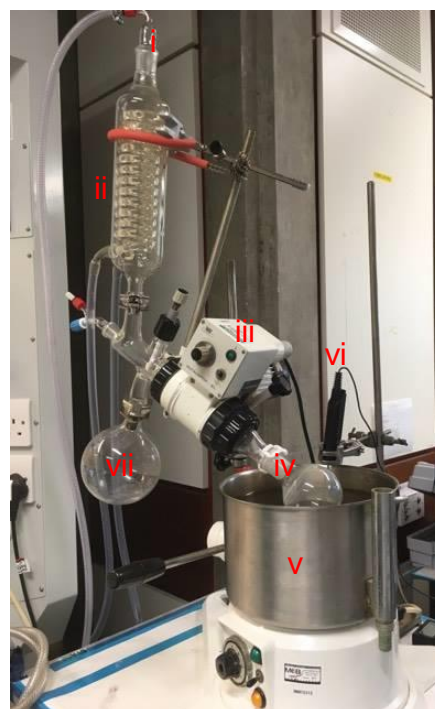
Figure 3.3 Schematic illustration of the set-up for the fractionation of lignin using acetone.

The lignin-soluble fraction was filtrated using a glass filter paper with 1 μm pore diameter (Whatman[®] glass microfibre, Grade GF/B, Sigma-Aldrich, UK). The filtrate was processed to remove the acetone using a rotary evaporator (Buchi Rotavapor[®]-R, Brinkman, Switzerland) equipped with a vacuum pump (Vacuubrand MD 1C VARIO with CVC3000 vacuum controller, Germany) and a dry ice solvent trap. Photographs of the apparatus are showed in Figure 3.4. During the evaporation of acetone, the water bath of the rotary evaporator was maintained at 53 ± 2 °C and at a vacuum level of 300 mbar. The soluble-lignin fraction obtained was dried in a vacuum oven at 80 °C for six hours and transferred to a silica gel-loaded desiccator to cool to room temperature. The mass of acetone-soluble lignin was recorded and the yield was calculated. The same procedure was applied to the acetone-insoluble fraction. After weighing, the lignins obtained from fractionation were stored in airtight sample vials for further characterisations and experiments.



(a)

- i. Vacuum port inlet
- ii. Water condenser
- iii. Rotating controller
- iv. 250 ml single neck round bottom flask
- v. Water bath with temperature controller
- vi. Thermocouple
- vii. Solvent collection flask
- viii. Solvent trap with dry ice condenser
- ix. Solvent safe vacuum pump



(b)

Figure 3.4 Photographs showing the apparatus used for the evaporation of acetone: (a) vacuum pump with dry ice condenser; and (b) rotary evaporator.

3.2.3 Determination of the Lignin Content and Composition

The lignin content can indicate the purity of the lignin. In the current study, a key aspect was to identify and determine the effectiveness of specified methods for treating lignin. The lignin samples used in this study were: (i) as-received lignin; (ii) acetone-soluble lignin; (iii) acetone-insoluble lignin; and (iv) lignins treated with acidified water. These samples were analysed using the procedures outlined in Figure 3.5. Sample preparation was in accordance with the TAPPI method T257 cm-02 [237]. The lignin was ground and sieved using a 40-mesh screen in order to obtain particle size smaller than 400 μm .

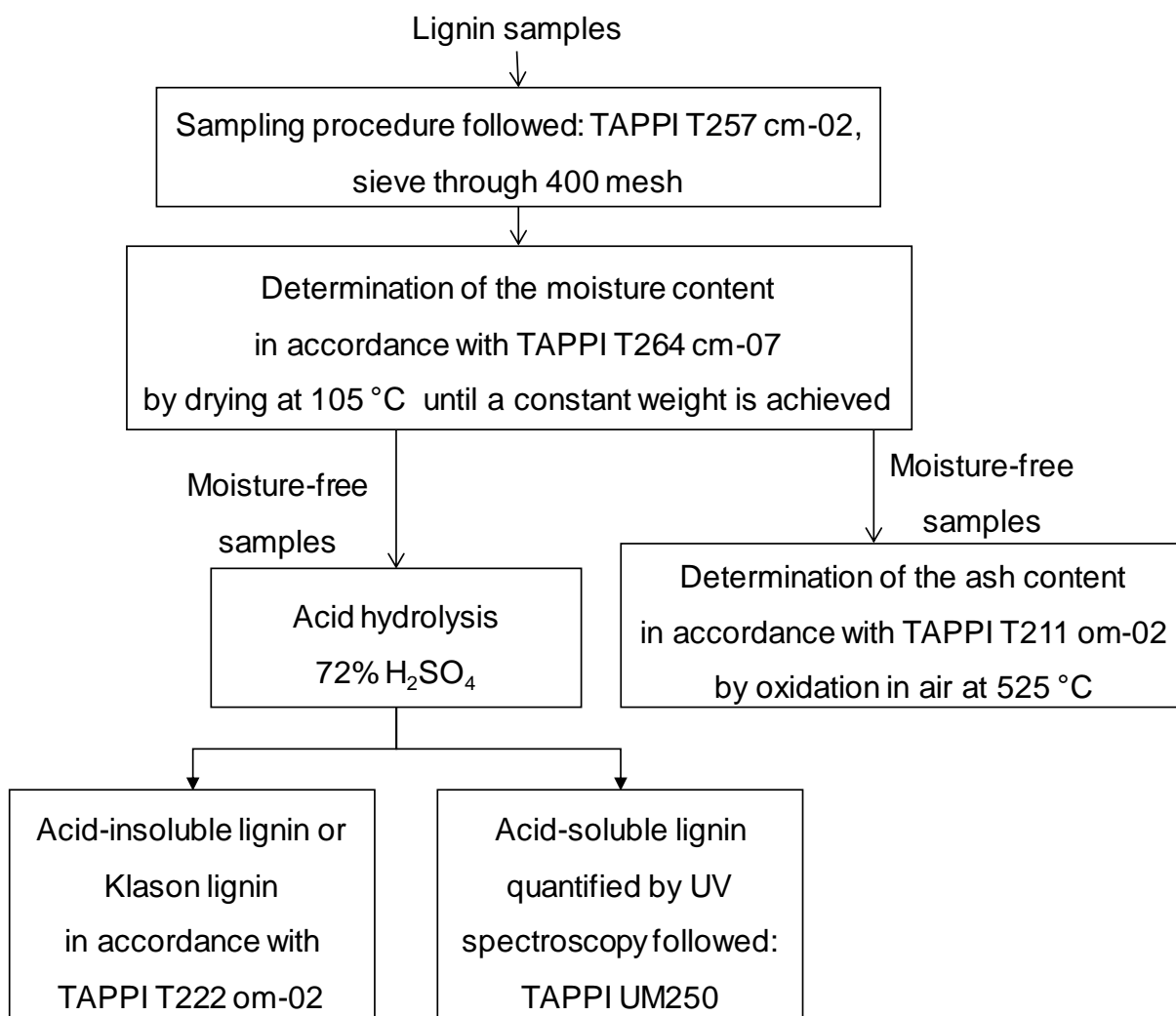


Figure 3.5 Flow diagram presenting the steps for determining the lignin content and composition.

The protocol used for determining the moisture content, ash content, fractions of acid-soluble and acid-insoluble lignins are explained in the following sections.

3.2.3.1 Determination of the Moisture Content

The measurement of moisture content was carried out by following the method specified in TAPPI T264 cm-07 [238]. Sieved-lignin sample mass (2 g) was weighed to the nearest milligram and stored in a tared sample vial prior to drying in an oven at 105 ± 3 °C for two hours. After two hours of drying, the sample vial was taken from the oven and capped with a stopper. The airtight vial was cooled in a desiccator. Before weighing the sample, the stopper was opened momentarily to equalise the air pressure. The sample vial was replaced in the oven for one hour followed by cooling to room temperature and re-weighing. When the weights did not change by more than 0.002 g, the moisture content (%) was calculated using Equation 3.1 [238]:

$$\text{Moisture content (\%)} = \frac{\text{Initial mass} - \text{Constant dried mass}}{\text{Initial mass}} \times 100 \quad \text{Equation 3.1}$$

3.2.3.2 Determination of the Ash Content

The ash content was determined in accordance with TAPPI T211 om-02 standard via combustion at 525 °C [239]. Empty porcelain crucibles with lids were placed in a muffle furnace (Carbolite RHF16, UK) at 525 ± 25 °C for four hours. The crucibles were allowed to cool in the furnace to 100 °C and placed in a desiccator where they were cooled to room temperature to minimise moisture absorption. The heat-treated crucibles were then weighed on an analytical balance with a precision of 0.1 mg. Approximately 1.0 g of moisture-free samples of lignin were placed in each of the aforesaid crucibles. These crucibles without lids were replaced in the muffle furnace and pre-heated to 100 °C for one hour. The lids were then put over the crucibles and the temperature was raised to 525 °C, so that the samples were subjected to combustion without flaming. The lids were removed from the crucibles when the temperature was 525 ± 25 °C. When the lignin samples were completely combusted, as indicated by the disappearance of black particles, the crucibles were

removed from the furnace and allowed to cool to room temperature in a desiccator. The crucibles with the ash were weighed and the ash content was determined using Equation 3.2 [239]:

$$\text{Ash content (\%)} = \frac{\text{Mass of ash}}{\text{Mass of moisture-free sample}} \times 100 \quad \text{Equation 3.2}$$

3.2.3.3 Klason or Acid-insoluble Lignin

The Klason lignin content was determined in accordance with TAPPI T222 om-02 standard [240]. Lignin samples (1 ± 0.1 g) were weighed and placed in a 100 cm^3 beaker. The beaker containing the samples was kept in a water bath which maintained the temperature at $2 \text{ }^\circ\text{C} \pm 1^\circ\text{C}$. 15 cm^3 of 72% sulphuric acid was dispensed gradually into the beaker. The lignin powder was dispersed in the sulphuric acid by stirring with a glass rod.

Then the beaker containing this mixture was kept in a water bath at $20 \pm 1 \text{ }^\circ\text{C}$ and covered with a watch glass for two hours. During this step, the dispersed sample was stirred frequently. Subsequently, the dispersed sample was transferred to a 1L flask. The sample was diluted with 560 ml deionised water to obtain a total volume of 575 cm^3 or 3% concentration of sulphuric acid. Then the solution was refluxed for four hours at $100 \text{ }^\circ\text{C}$. The solution was cooled, allowing the acid-insoluble component to settle overnight. The acid-insoluble lignin was filtered using a Buchner funnel through a $1 \text{ }\mu\text{m}$ pore glass filter. The soluble component (supernatant) was collected to quantify the amount of acid-soluble lignin as described in Section 3.2.3.4.

The acid-insoluble lignin was neutralised by washing with hot deionised water. The samples were dried at $105 \pm 3 \text{ }^\circ\text{C}$ in an air-circulating oven (Gallenkamp Oven, UK) until the sample weight attained a constant value. The acid-insoluble lignin content was calculated using Equation 3.3 [240]:

$$\text{Acid-insoluble lignin (\%)} = \frac{\text{Mass of acid-insoluble lignin}}{\text{Initial mass}} \times 100 \quad \text{Equation 3.3}$$

3.2.3.4 Acid-soluble Lignin

UV/Visible spectrophotometer A M550 (Chemspec Ltd., UK) was used to analyse the acid-soluble lignin. The filtrated soluble lignin from the acid-insoluble experiment was placed in a quartz cuvette (type 1/Q/10, Starna Scientific, UK) with 10 mm path length. A 3% solution of H₂SO₄ was used as the background. The absorbance at 205 nm was used for quantifying the lignin content. The acceptable band intensity was in the range of 0.2–0.7 AU. In instances where the absorbance was higher than 0.7, the solution was diluted with 3% H₂SO₄. The acid-soluble content was calculated according to TAPPI UM250 using Equation 3.4 [241]:

$$\text{Acid-soluble lignin (mg}\cdot\text{g}^{-1}\text{)} = \frac{A \times D \times V}{a \times b \times M} \times 1000 \quad \text{Equation 3.4}$$

where,

A = Absorbance at 205 nm,

D = Dilution factor,

V = Volume of the lignin solution (l),

a = Extinction coefficient of lignin, 110 g·l⁻¹·cm⁻¹,

b = Cuvette path length (cm), here it is 1 cm,

M = Sample weight used in the acid-soluble experiment (g).

3.3 Electro-spinning of Acetone-soluble Lignin

Electro-spinning was employed to fabricate lignin fibres where their diameter was on the sub-micrometre scale. Acetone-soluble lignin was used as the main raw material for the production of electro-spun lignin fibres. The following sub-section details the step that were developed to produce carbonised lignin fibres.

3.3.1 Preparation of Acetone-soluble Lignin Solutions

Acetone-soluble lignin was dissolved in a binary solvent of acetone and DMSO. The binary solvent was prepared using a volume-to-volume (v/v) ratio of 2:1 of acetone and DMSO. The criteria for the selection of these two solvents will be discussed in Chapter 5. The following lignin concentrations were used: 45 wt%, 48 wt%, 53 wt% and 58 wt%. A reflux unit was used for dissolving lignin. A schematic of the reflux set-up is given in Figure 3.6. A 250 cm³ three-neck round bottom flask was used. The top centre neck was attached to a water condenser; one neck was used for bubbling the inert gas at a flow rate of 20 ml-minute⁻¹; and the other neck served as the insert for the thermocouple. A magnetic stirrer was employed for stirring the solution at room temperature for five hours. The solutions were stored in an airtight container prior to the measuring the viscosity and conductivity. The details of the measurements of viscosity and conductivity of the solution are described in Section 3.4.8 and 3.4.9. A fresh solution was used for electro-spinning.

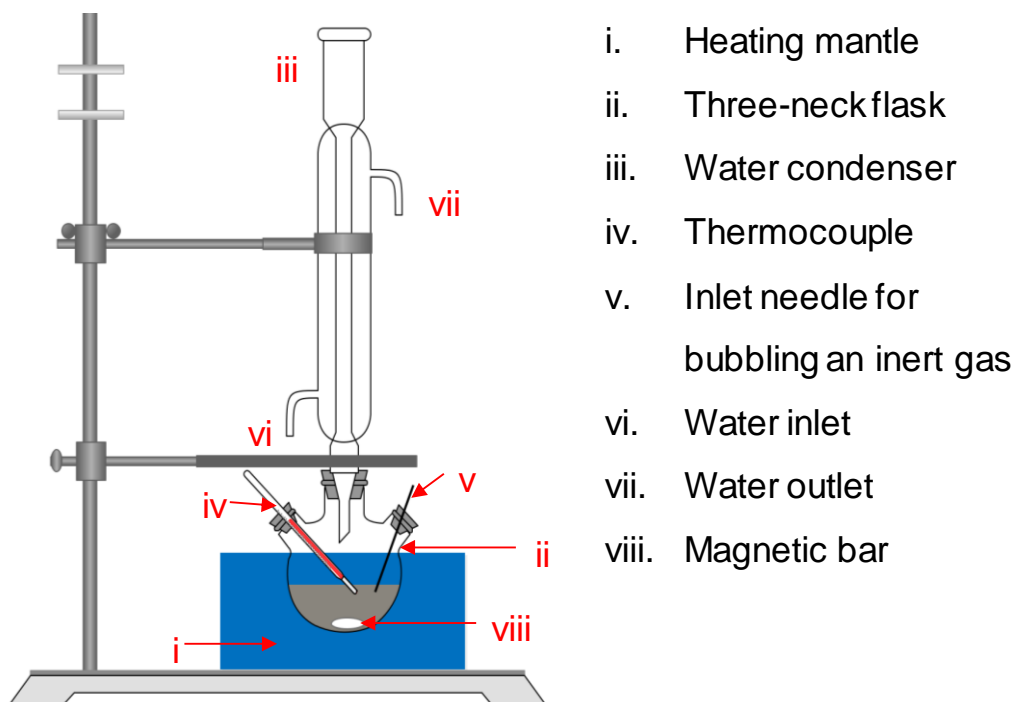


Figure 3.6 Schematic set-up of reflux unit for lignin dissolving.

3.3.2 Electro-spinning of Acetone-soluble Lignin Fibres

3.3.2.1 Electro-spinning of Randomly Aligned Acetone-soluble Lignin Fibres

Figure 3.7 shows the custom-built electro-spinner and the main components are defined. A copper plate of dimensions 10 cm x 10 cm was grounded and used to collect the randomly oriented fibres, otherwise referred to as a random mat. The vertical distance between the needle tip to the surface of the collector plate was 12 cm. A controlled solution feed rate of $0.1 \mu\text{l}\cdot\text{minute}^{-1}$ was maintained using a liquid dispensing unit (model 941-371-1003, World Precision Instruments, UK). The dispenser was connected to a 5 cm^3 disposable plastic syringe (Terumo®, UK) and needle a flat-tip 25 G (0.254 mm inner diameter) stainless steel needle (Part number AD 725050, Adhesive Dispensing Ltd, UK) via a PTFE tubing (Masterflex transfer tubing, Cole-Parmer, UK) of 20 cm length was connected to the positive

terminal of a high-voltage power supply (Variable High Voltage DC Power Supply, 73030, Genvolt Ltd., UK). An operating voltage of 12 kV was applied between the needle and the grounded collector plate. During electro-spinning the air temperature within the chamber was maintained between 30 and 35 °C. The electro-spun fibres were collected for three minutes.

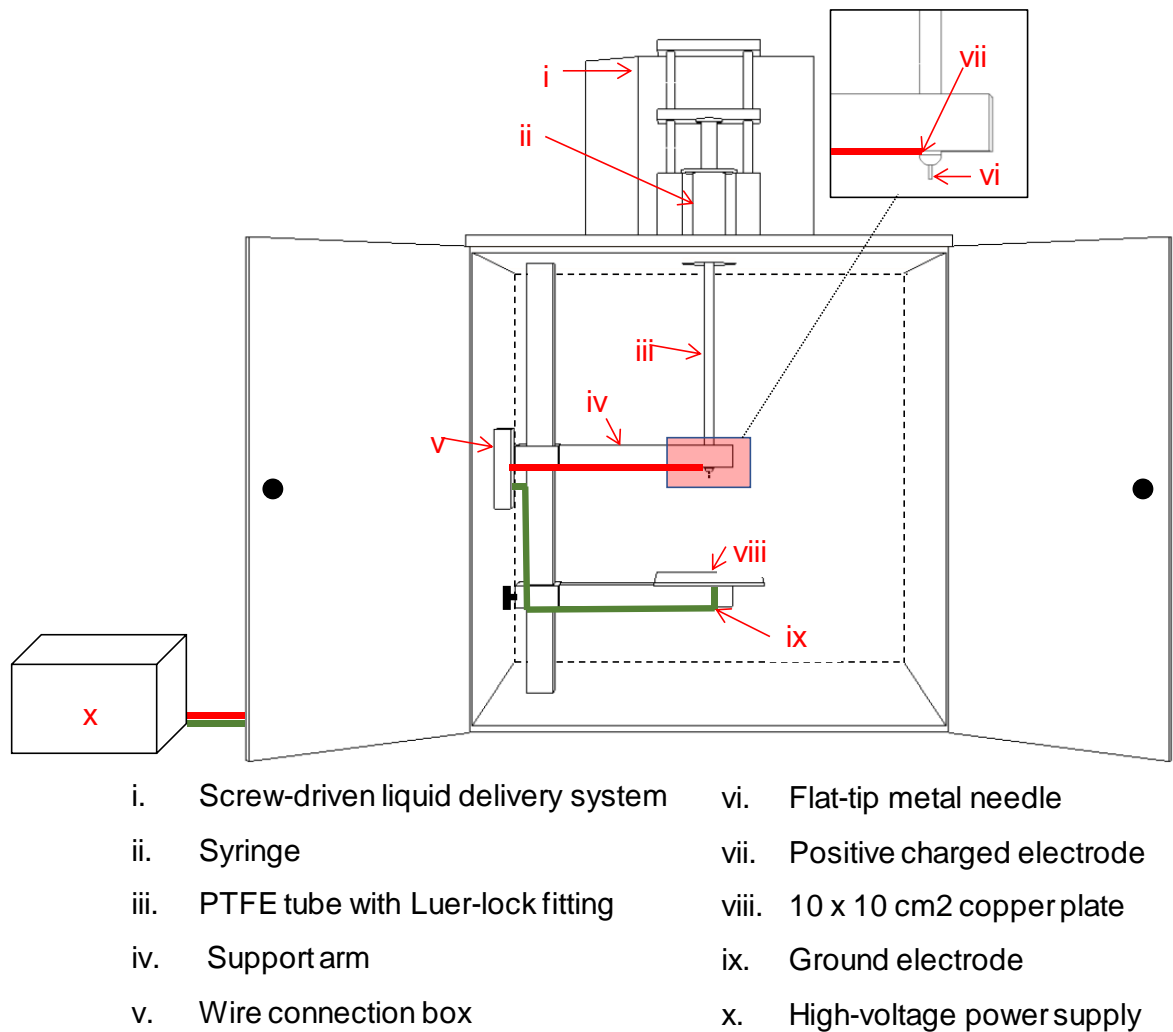


Figure 3.7 Schematic illustration of the custom-built electro-spinner.

3.3.2.2 Electro-spinning of Aligned Acetone-soluble Lignin Fibres

Figure 3.8 shows a schematic illustration of a modified collector electrode to enable the production of aligned fibres, relatively parallel to each other. The electrode was comprised of a U-shaped graphite structure. The graphite was covered with an adhesive-backed PTFE insulation sheet except along the top inner edges on the left and right sides and the bottom side. The two exposed edges acted as a pair of parallel electrodes and the gap (3.6 cm) in between was where the fibres were collected parallel to each other but perpendicular to the edges. The graphite was assembled with 3 mm thick polystyrene (PS) plate with a rectangular slot and another PS strip was placed in between parallel electrodes (see Figure 3.8 (a) and (b)). The assembled graphite electrode was placed on the copper plate position shown in Figure 3.8 (c), so the bottom side of the modified U-shaped electrode with exposed parallel edges was kept in electrical contact with the grounded copper plate. The vertical distance from the needle tip to the level of the two parallel edges was 12 cm. A solution feed rate of $0.1 \mu\text{l}\cdot\text{minute}^{-1}$ was maintained and the operating voltage between the needle and the grounded plate was 12 kV. During electro-spinning the air chamber was maintained between 30 and 35 °C. Figure 3.8 (d) shows the orientation of the electro-spun aligned fibres.

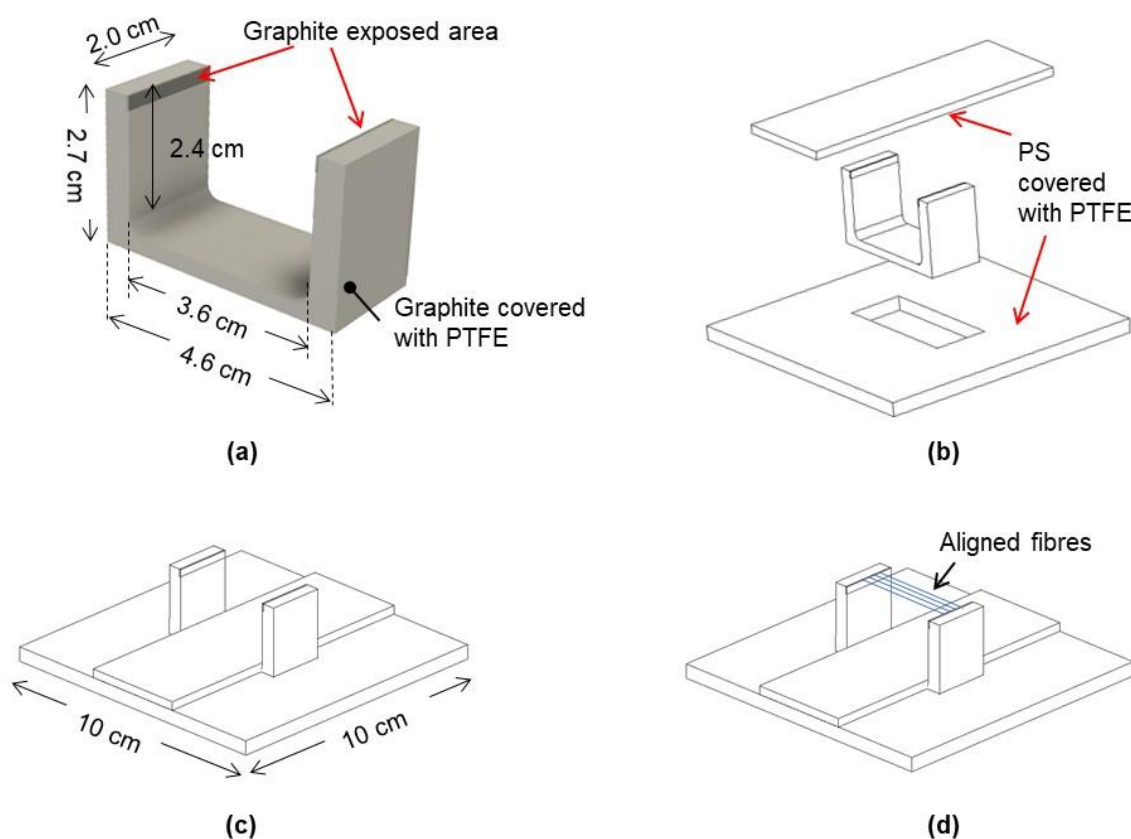


Figure 3.8 Schematic illustration of the modified parallel electrodes for producing highly-aligned electro-spun lignin fibres: (a) modified-graphite U-shaped electrode; (b) components of the modified U-shaped graphite and insulating polystyrene strip-PS; (c) the assembled electrode assembly with the insulating strip; and (d) orientation of the aligned electro-spun lignin fibres.

3.3.3 Heating of Electro-spun Acetone-soluble Lignin Fibres to Remove Acetone and DMSO

After electro-spinning, the electro-spun fibres were subjected to a drying regime to remove any residual solvent prior to thermo-stabilisation and carbonisation. A flow diagram showing the heating experimental procedures is given in Figure 3.9. The heating methods investigated were as follows: (i) heating in an air-circulating oven; (ii) heating in a nitrogen flow oven; and (iii) heating in a vacuum oven. The electro-spun fibres were placed in an oven where the desired gas flows through via inlet and

outlet ports with a controlled flow of 50 ml·minute⁻¹. Figure 3.10 illustrates the experiment set up for heat treatment of electro-spun acetone-soluble lignin fibres. The dried-air (UN 1002, BOC, UK) and purified nitrogen (oxygen-free, pure (99.999%) nitrogen, BOC, UK) were used. The drying temperatures used were 100 °C, 140 °C, 180 °C and 200 °C for six hours.

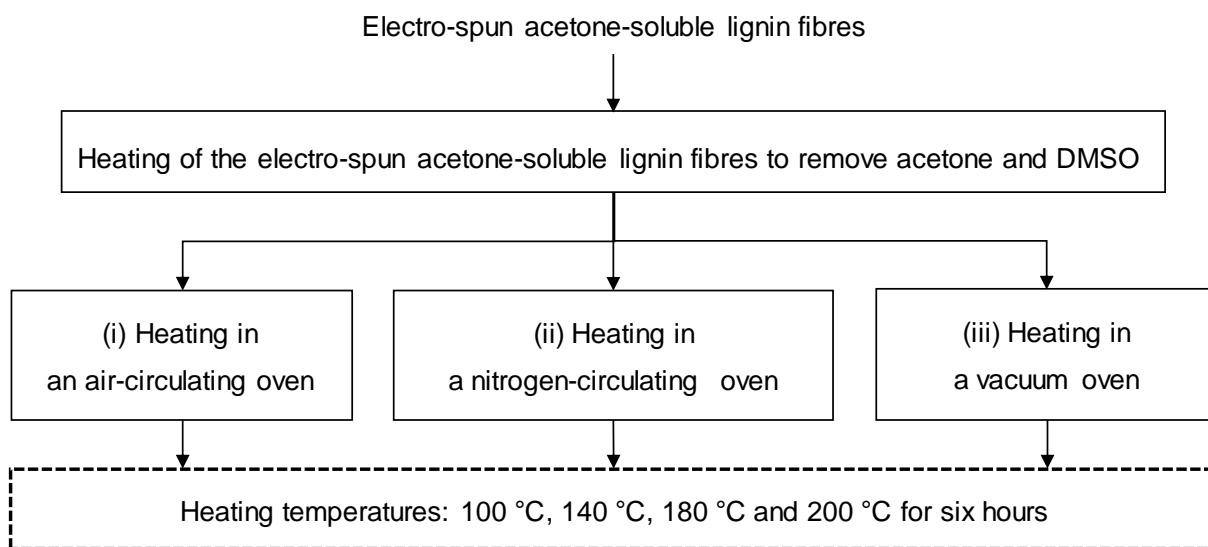


Figure 3.9 A flow diagram indicating the heating environments for the electro-spun acetone-soluble lignin fibres prior to oxidative thermo-stabilisation.

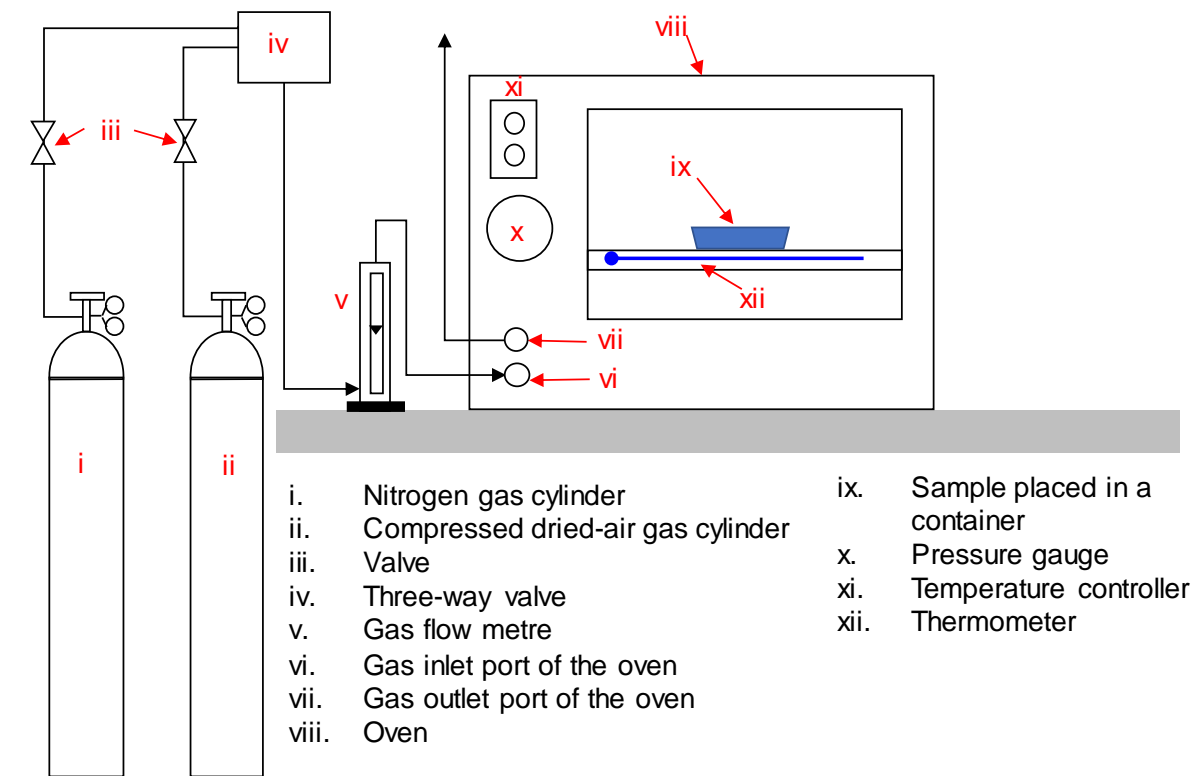


Figure 3.10 Schematic illustration of the experimental set up for heat treatment of electro-spun acetone-soluble lignin fibres.

The morphology of the resultant fibres was studied using a scanning electron microscope (SEM, Hitachi 3030, Japan). Prior to undertaking inspecting the samples, they were sputter-coated with a gold as described in Section 3.4.3. Fibre diameter distribution was measured using ImageJ software (version 1.52p). The comparison of fibre diameters was conducted by ANOVA using Minitab18 at a significance level, p-value, of 0.05.

Fourier Transform Infrared (FTIR) spectroscopy was used to characterise the heated electro-spun acetone-soluble lignin fibres collected from different heating condition. The experimental procedures for FTIR analytical techniques are detailed in Section 3.4.4.

3.3.4 Thermo-stabilisation of Electro-spun Acetone-soluble Lignin Fibres

Thermo-stabilisation experiments were conducted in an alumina tube furnace (PYRO THERM Furnaces, UK). A sacrificial alumina tube (ALM4638, Almath Crucibles Ltd., UK) with inner and outer diameters of 38 and 46 mm, respectively and length of 1,500 mm was inserted into the tube furnace. The electro-spun fibres heated in a vacuum oven at 140°C for six hours were placed on a graphite crucible and heated from room temperature to dwell isothermally at 100 °C, 150 °C and 250 °C for one hour at each temperature. The heating rate was 0.5 K·minute⁻¹. A schematic illustration of the heating and dwell regimes is shown in Figure 3.11.

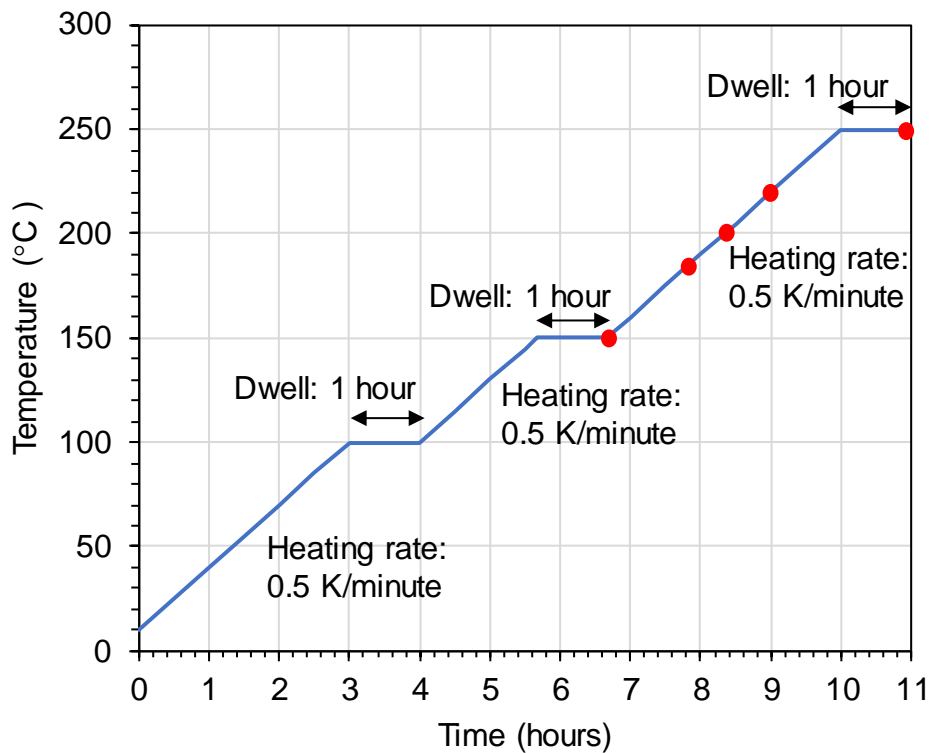


Figure 3.11 Illustration of the heating rate and dwell periods that were used for the thermo-stabilisation experiments. The red circles represent the time when samples were removed for characterisation.

Flow rate of compressed dried-air or purified nitrogen was maintained at 50 ml·minute⁻¹ to study their effect of the gaseous atmosphere during thermo-stabilisation on the fibre morphology, thermal properties and chemical structure. The effluent gases were bubbled through a sodium carbonate solution prior to release to atmosphere through a local extract and ventilation system. A schematic illustration of the experimental set up is illustrated in Figure 3.12 and a photograph of PYRO THERM furnaces assembly with metal flanges is presented in Figure 3.13 .

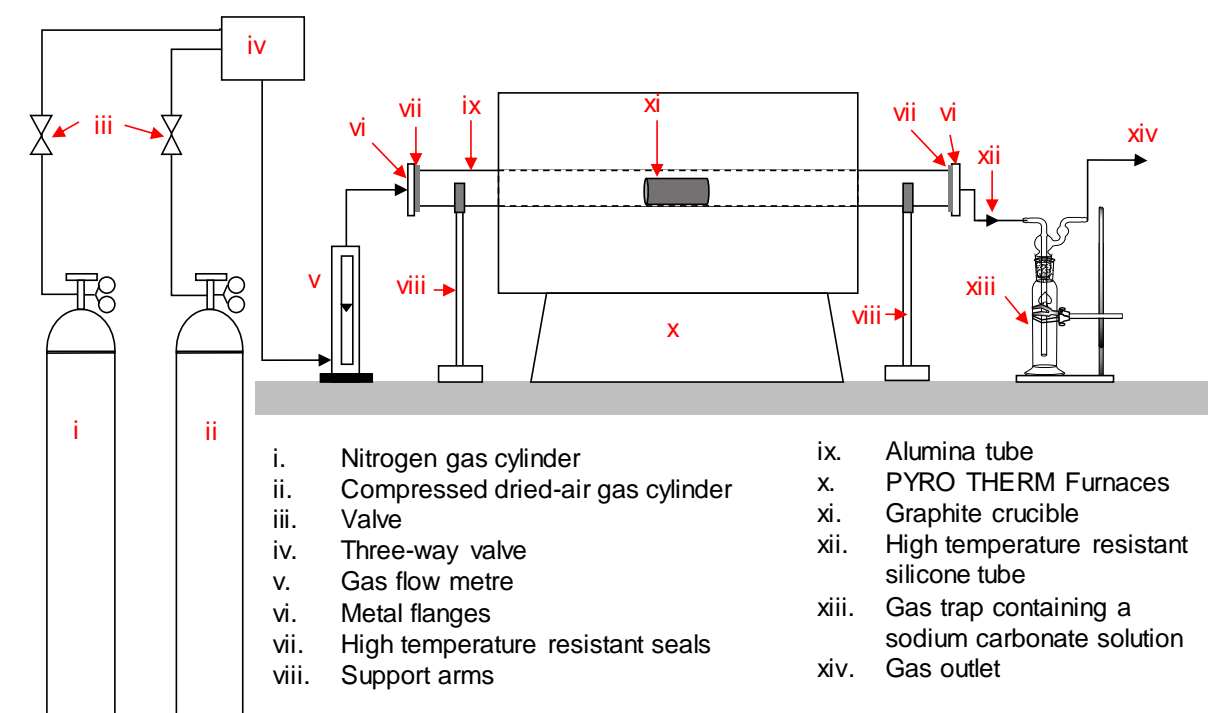


Figure 3.12 Schematic illustration of the experimental set up for the thermo-stabilisation of electro-spun acetone-soluble lignin fibres.



Figure 3.13 Photograph of PYRO THERM furnaces used in this study.

The samples were removed from the furnace at 150 °C, 180 °C, 200 °C, 220 °C and 250 °C, as indicated by the red circle in Figure 3.11. Change in the fibre morphology was observed using SEM. The effects of the thermo-stabilisation conditions on thermal properties and the surface chemical composition were studied using, FTIR spectroscopy, differential scanning calorimetry (DSC) and X-ray photoelectron spectroscopy (XPS). Experimental details for these analytical techniques are described in Sections 3.4.4, 3.4.5 and 3.4.10, respectively.

3.3.5 Carbonisation of Electro-spun Acetone-soluble Lignin Fibres

The temperature gradient in the PYRO THERM furnace was assessed prior to undertaking the carbonisation studies. The temperature was measured by platinum rhodium thermocouples (R Type) and recorded using Pico TC-08 and Picolog Data Logging Software (Pico Technology, UK). The centre of the furnace tube, the distance was defined as the reference position "0". The temperature gradient was measured from the centre in 10 cm increments. A schematic illustration of the experimental set up is illustrated in Figure 3.14.

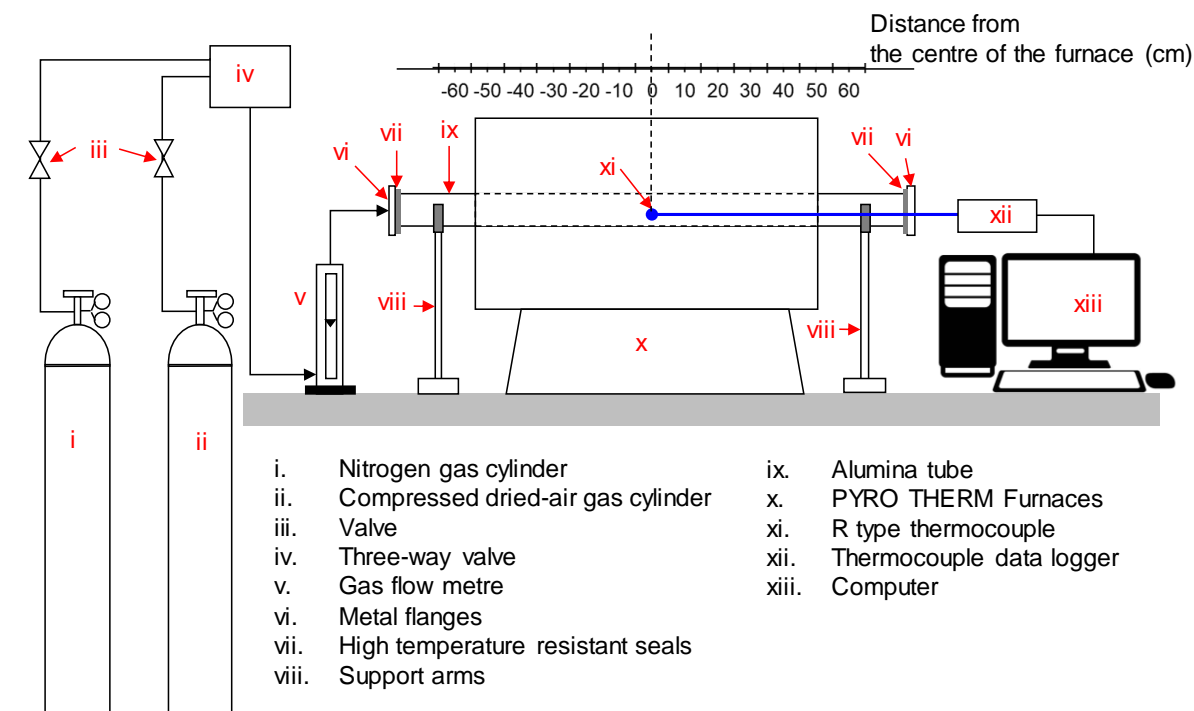


Figure 3.14 Schematic illustration of the experimental set up for measuring the temperature gradient in the PYRO THERM furnace.

The flow purified nitrogen gas through the furnace was set as $50 \text{ ml}\cdot\text{minute}^{-1}$. The temperature controller was programmed to heat from room temperature to $1,500^\circ\text{C}$ at $5 \text{ K}\cdot\text{minute}^{-1}$. Once the temperature was reached, the thermocouple was withdrawn by 10 cm from the centre of the furnace. A dwell time at each measuring position was five minutes for the temperature to equilibrate before collecting data. This procedure was recorded until the thermocouple was withdrawn by 60 cm from the centre of the furnace. The measured temperature gradient of the furnace at the programmed temperature of $1,500^\circ\text{C}$ is displayed in Figure 3.15.

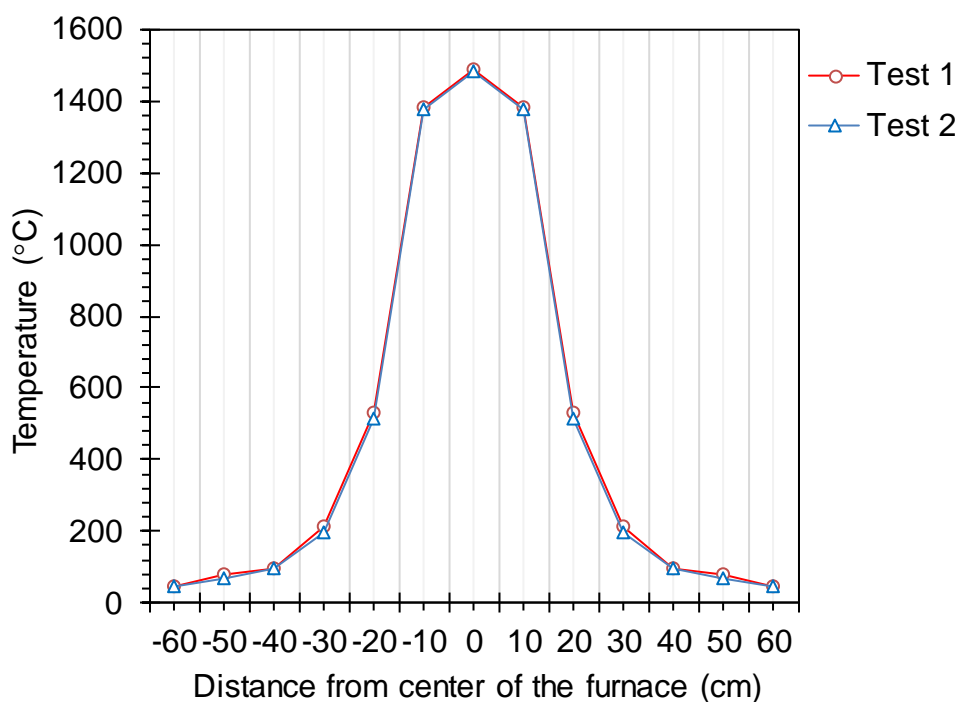


Figure 3.15 Temperature profile of the tube furnace used for thermo-stabilisation and carbonisation experiments.

The experimental set up for the temperature measurement at different heating rates used ($2, 5$ and $10 \text{ K}\cdot\text{minute}^{-1}$) was the same as the set up for the temperature gradient measurement (see Figure 3.14). The thermocouple was placed at the centre of the furnace tube, the temperature was recorded with a function of time. A plot of the heating time versus temperature at $2, 5$ and $10 \text{ K}\cdot\text{minute}^{-1}$ are presented in Figure 3.16 (a), (b) and (c), respectively. The discontinuous red line represents the linear regression line.

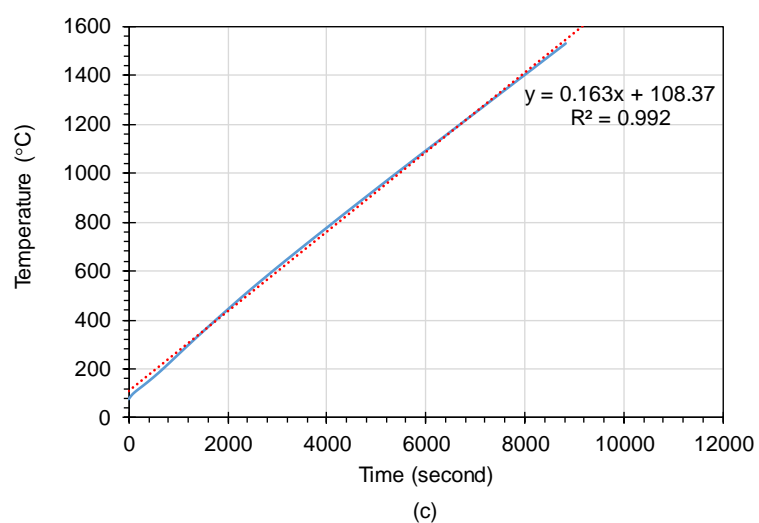
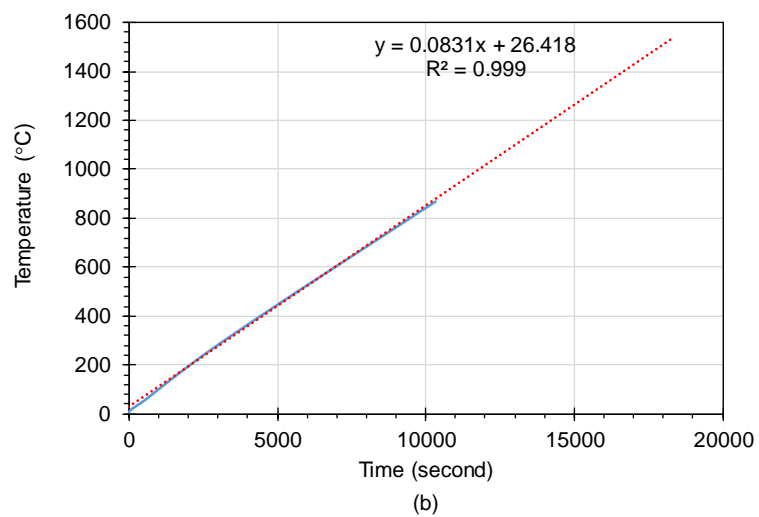
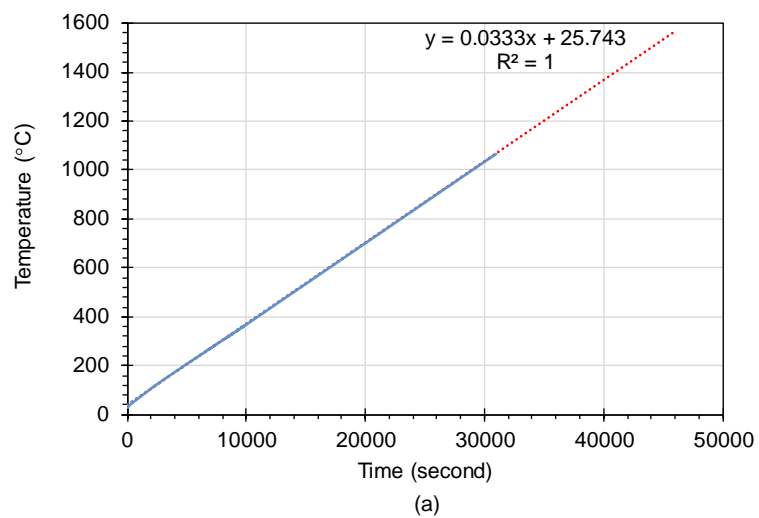


Figure 3.16 Calibration curves for the PYRO THERM tube furnace at the centre of the furnace using heating rates of: (a) 2; (b) 5; and (c) 10 K·minute⁻¹.

With reference to the carbonisation experiment, the electro-spun acetone-soluble lignin fibres heated in vacuum oven at 140 °C for six hours were transferred to a graphite crucible and placed at the centre of the furnace. The samples were heated from room temperature to dwell isothermally at 100 °C, 150 °C and 250 °C for one hour at each temperature. The heating rate was constant at 0.5 K·minute⁻¹ under an air flow of 50 ml·minute⁻¹. After thermo-stabilisation, the gas was switched from the compressed dried-air to purified nitrogen. The nitrogen flow was maintained for 15 minutes before turning on the heater in order to remove air from the furnace tube. The carbonisation experiments were conducted with a nitrogen flow rate of 50 ml·minute⁻¹.

The operating for the carbonisation experiments were derived using the Taguchi experimental design method. The key parameters assumed to affect the resultant carbon fibres were: (i) the heating rate; (ii) carbonisation temperature; and (iii) the dwell times. The details of these experiments and the nine experiments are detailed in Table 3.3.

Table 3.3 Taguchi design of experiments for the carbonisation of electro-spun acetone-soluble lignin fibres.

Experimental No.	Heating rate (K·minute⁻¹)	Carbonisation temperature (°C)	Dwell time (hour)
Exp. 1	2.5	1,000	0
Exp. 2	2.5	1,200	1
Exp. 3	2.5	1,500	3
Exp. 4	5.0	1,000	1
Exp. 5	5.0	1,200	3
Exp. 6	5.0	1,500	0
Exp. 7	10.0	1,000	3
Exp. 8	10.0	1,200	0
Exp. 9	10.0	1,500	1

The morphology and composition of the resultant carbon fibres were determined by using SEM and Raman spectroscopy, respectively. The graphitic structure formed during carbonisation was studied using the latter technique. The optimum conditions for the carbonisation of electro-spun lignin fibres was derived using Taguchi analyses and an analysis of Variance (ANOVA).

The effect of carbonisation temperatures (1,000 °C, 1,200 °C and 1,500 °C) was studied at the constant heating rate at 2.5 K·minute⁻¹ and a dwell time one hour. After carbonisation, the morphology of the carbonised fibres was observed using SEM. The chemical composition on the fibre surface was characterised using XPS. The crystalline structures of the carbonised fibres were observed by X-ray diffraction (XRD). Raman spectroscopy was used to investigate the graphitic structure of the carbonised fibres. Atomic force microscope (AFM) was employed to measure the surface roughness of the fibres. Details of these analytical techniques are described in Section 3.4.3, 3.4.10, 3.4.11, 3.4.12 and 3.4.13, respectively.

3.3.6 Electro-spinning of Acetone-soluble Lignin with Processing Aids

In the previous sections, the acetone-soluble lignin was electro-spun without any processing aids. In the current study, the feasibility of using vanillin and polyethylene glycol (PEG) as a processing aid was investigated in order to improve the uniformity of the electro-spun fibres. The effects of the processing aid content on the glass transition temperature (T_g) of acetone-soluble lignin were studied. 53 wt% of acetone-soluble lignin was dissolved in a binary solvent of acetone and DMSO with a volume to volume (v/v) ratio of 2:1 of acetone and DMSO prior to the adding of the processing aid. A procedure for the preparation of the lignin solution was described in Section 3.3.1.

Vanillin was added to acetone-soluble lignin in the range from 0 to 2.0 g per 100 g of lignin (parts per hundred parts, phr). In the case of PEG, different concentrations (2.5, 5.0, 7.5 and 10.0 phr) were studied. For example, at the 2.0 phr of vanillin, 0.06 g of vanillin was added into was added into the lignin solution containing 3 g of lignin after the lignin was fully dissolved. A magnetic stirrer was used for stirring the solution

at room temperature for five hours. The lignin solution with the processing aid was transferred into an airtight vial and stored until required for electro-spinning. The viscosity and conductivity of the lignin solutions were measured as described in Section 3.4.8 and 3.4.9, respectively.

Random mats of the electro-spun fibres were produced using the procedure described in Section 3.3.2. The fibre morphology of the electro-spun fibres was obtained using SEM. The fibre diameter was analysed using the ImageJ software. The fibres were thermostabilised and carbonised following the procedure detailed in Sections 3.3.4 and 3.3.5.

3.4 Characterisation Techniques

3.4.1 Helium Gas Pycnometer

The densities of the as-received lignin and fibres were determined using a gas pycnometer (AccuPyc II 1340) from Micromeritics Instrument Corporation, USA. Approximately 0.5 g of the pre-dried sample was placed in an aluminium crucible of known volume of 1.3345 cm³, which is defined as V_{cell} in Equation 3.5 and weighed using a four-digit analytical balance. The crucible containing the sample was placed in a cell of the measurement chamber. The chamber was closed, and helium gas was introduced to the sample chamber with a flow rate of 137.9 Pa·minute⁻¹ until it rose to 19.5 MPa (P_1). After it equilibrated at the 0.13 MPa, the gas was released to an expansion cell (V_{exp}) with a known volume of 0.9161 cm³; this resulted in the pressure decreasing. The drop-in pressure was recorded as P_2 . Three samples of lignin were measured, and five cycles were conducted for each sample. The volume of the sample (V_{sample}) was calculated using Equation 3.5 and the density of the sample was calculated by dividing the mass of the sample by its volume. Three samples of lignin were measured, and three cycles were conducted for each sample.

$$V_{\text{sample}} = V_{\text{cell}} - \frac{V_{\text{exp}}}{\left(\frac{P_1}{P_2} - 1\right)} \quad \text{Equation 3.5}$$

3.4.2 Laser Particle Size Analysis

The particle size distribution of lignin was studied using a laser diffractometer (Mastersizer 2000, Malvern Instruments Ltd, UK) that was attached to a liquid dispersion unit, which consists of a pump and stirrer. The speed of the stirrer was maintained at 1,700 rpm. 2.5% (w/v) of the lignin sample was dispersed in distilled water and sonicated for three minutes using a 60 W ultrasonic homogeniser before being loaded into the liquid dispersion unit. The value of “obscurance” was set between 10 to 30% and the refractive indices of the lignin and water were 1.6 and 1.33, respectively. Three samples of lignin were measured, and five cycles were conducted for each sample.

3.4.3 Scanning Electron Microscopy

A scanning electron microscope (SEM, Hitachi 3030, Japan) was used to characterise the fibre morphology. In order to observe the cross-sectional views of the fibres, they were fractured under liquid nitrogen. The samples were gold-coated for three minutes and observed at an accelerating voltage of 15 kV. Philips XL-30 FEG Environmental SEM with Oxford Inca EDS was used for observation of cross-sectional view of electro-spun fibres. 10 kV accelerated voltage was used.

3.4.4 Fourier Transform Infrared Spectroscopy

Fourier Transform Infrared Spectroscopy (FTIR) was used to identify and analyse the functional groups present in as-received lignin and treated lignins. Changes in the

functional groups in lignin after thermo-stabilisation was also investigated. FTIR spectroscopy of the lignin samples was carried out using a Thermo Scientific Nicolet 870 spectrometer. 200 mg of pre-dried potassium bromide (KBr) and 1 mg of pre-dried lignin samples were ground and pressed into a disc with a diameter of 13 mm and a thickness of 0.6 mm. All the samples were measured in the transmission mode. The FTIR spectra were acquired using an average of 100 scans at a resolution of 4 cm^{-1} in the wavelength range of 4,000 to 400 cm^{-1} . Omnic 8.1 software was used to analyse the spectra.

3.4.5 Differential Scanning Calorimetry

The thermal properties of lignin used in this current work were analysed using differential scanning calorimetry. Moreover, changes in thermal characteristics of the lignins after thermo-stabilisation was studied. The thermograms for lignin were obtained using a Mettler Toledo differential scanning calorimeter (DSC-1, METTLER TOLEDO Ltd., UK) and DSC 7 (PerkinElmer Inc, UK). Approximately 5.0 ± 0.5 mg of the as-received lignin and the lignin produced in this study were placed in 40 μl aluminium pans. In the first scan, the lignin samples were heated from 25 $^{\circ}\text{C}$ to 250 $^{\circ}\text{C}$ at a heating rate of 10 $\text{K}\cdot\text{minute}^{-1}$ and kept isothermal for three minutes. Then, the samples were cooled to 25 $^{\circ}\text{C}$ at the cooling rate of 10 $\text{K}\cdot\text{minute}^{-1}$ and held for three minutes. The second and third scans were performed in the same step as the first scan. During all the scans, the samples were maintained under nitrogen atmosphere at a flow rate of 20 $\text{ml}\cdot\text{minute}^{-1}$. Prior to conducting the experiments, the instruments were calibrated using pure indium and tin. At least two samples of lignin were measured per type of lignin.

3.4.6 Thermo-gravimetric Analysis

Thermo-gravimetric Analysis (TGA) was performed using a NETZSCH STA 449C (Germany) equipment. 10 mg samples were used in each experiment.

The thermograms were collected as the sample was ramped from 25 °C to 900 °C at 10 K·minute⁻¹ in an argon atmosphere, maintained at a flow rate of 50 ml·minute⁻¹. Two samples of lignin were evaluated for each type of lignin. The residual char was determined from the TGA thermogram; this gives an indication of the carbon and inorganic content after pyrolysing the lignin fibres at 900 °C in an inert atmosphere.

3.4.7 Gel Permeation Chromatography

The molecular weight and polydispersity index of the as-received and acetone-soluble lignin samples were determined by using a gel permeation chromatography (GPC) (Agilent 1260 Infinity II Multi-Detector). This was undertaken in order to determine the molecular weight distribution in fractionated as-received lignin using acetone. This was carried out at Science City Research Alliance, The University of Warwick by S. S. Lawton and D. W. Lester. This system was equipped with PLgel 5 µm mixed D columns (300 x 7.5 mm) and a PLgel 5 µm guard column. The lignins were dissolved in DMF at a concentration of 0.1 mg·ml⁻¹ and filtered through 0.22 µm nylon filter. The injected volume was 80 µl.

3.4.8 Viscometry

The viscosity of the solutions was determined using a parallel-plate rheometer (Discovery Hybrid Rheometer, model HR-1, UK). 40 mm diameter plates were employed in this study. The viscosity was measured by subjecting the sample to a shear rate in the range 0.1 to 100 s⁻¹ at 30 °C. A solvent trap was used for minimising the evaporation of acetone during the measurements. Three samples were measured per type of lignin.

3.4.9 Electrical Conductivity

The conductivity of the solutions was measured using a Jenway 4510 Conductivity Meter (UK). Prior to obtaining the measurements, the equipment was calibrated at 25 °C using a standard solution of sodium chloride (HI7033) supplied by HANNA Instruments. A glass vial containing the polymer solution was immersed in a temperature controllable water bath (Grant Instruments GD100, UK) in order to measure the conductivity at $25 \pm 1^\circ\text{C}$.

3.4.10 X-ray Photoelectron Spectroscopy

X-ray Photoelectron Spectroscopy (XPS) analyses were performed on a Kratos Axis Supra™, (Shimadzu Group Company, Kratos Analytical Ltd, UK), which was equipped with a monochromator Al K α X-ray source ($h\nu = 1486.6$ eV). The analysis of XPS spectra was undertaken to study the changes in chemical structure of lignin after thermo-stabilisation. The sample was placed on a double-sided carbon tape before being inserted into a multi-specimen holder; the pressure in the analysis chamber was 10^{-6} Pa. The energy used for the wide survey scan was 160 eV and 40 eV for the narrow or high-resolution scan, which was used for the spectra of C1s and O1s.

Spectral deconvolution was performed with the CasaXPS program. C1s spectrum was deconvoluted using a Shirley type background and curve fitted using a mixed function of Gaussian/Lorentzian (70/30). The full width at half maximum (FWHM) of the deconvoluted components was consistent. The C-C component of the C1s spectrum of carbon (at 285.0 eV) was used to set the binding energy scale. Atomic fraction was calculated based on the peak area of each components.

3.4.11 Raman Spectroscopy

Inelastic scattering in the carbonised lignin fibres was measured using a Raman spectrometer (Renishaw RE-04, UK), equipped with a 488 nm diode laser. The

analysed area was observed through a microscope at a magnification of 50x. A total of 10 accumulation per sample were collected at 10% laser power in the range of 320-3,200 cm^{-1} over an exposure time of 10 seconds. A 2,400 $\text{lines}\cdot\text{mm}^{-1}$ grating was used as a filter. Two tests were carried out for each carbonised sample.

3.4.12 Atomic Force Microscope

The fibre topology and surface roughness of the carbonised lignin fibres were determined using an atomic force microscope (AFM), BRUKER Innova[®], USA. The topological images were obtained using the tapping mode in air, at room temperature. A BRUKER[®] RTESPA-300 silicon probe with an 8 nm tip radius was used; the resonant frequency and spring constant of the cantilever were 300 kHz and 40 $\text{N}\cdot\text{m}^{-1}$, respectively. High-magnification topological images were obtained over an area of 20 $\mu\text{m} \times 20 \mu\text{m}$. The digital resolution of the images was 256 \times 256 points. The average roughness (R_a) data were analysed by Gwyddion software [242]. The R_a data were acquired by randomly applying a linear line with 8 μm length along the fibre surface and the average value of R_a was obtained by three repeated measurements.

4. TREATMENT OF LIGNIN USING ACIDIFIED WATER AND MOLECULAR WEIGHT FRACTIONATION OF LIGNIN

4.1 Introduction

Amongst the variety of lignins that are available, softwood Kraft lignin was chosen as the raw material due to its abundance and low-cost (£68/kg) as compared to with other commercially available types of lignin such as Sigma-Aldrich lignin, CAS Number 8068-05-1, (£304/kg) [243–245]. This chapter provides a comparison between two methods that were used for removing the inorganic content from as-received lignin. The method with the lowest inorganic content was used for fibre-spinning without the need for polymer blending or chemical modification.

As-received lignin (BioChoice®lignin) was characterised and used as the reference point or benchmark for subsequent treatments and characterisation studies. The techniques used for treating the lignin are: (a) treatment with acidified water; and (b) molecular weight fractionation using acetone. Treating lignin with aqueous hydrochloric acid has been reported as a method for removing inorganics [77], whilst fractionation using organic solvents has been used to obtain different molecular weight fractions [124,246]. With reference to acid-treatment, a Taguchi-based design of experiments (DoE) was used to define the optimum combination of parameters in order to reduce the ash content after pyrolysis [247]. The four key parameters chosen are: (i) the pH; (ii) the ratio of the lignin-to-acid concentration; (iii) washing time; and (iv) the number of washing cycles. These parameters were set as the controllable variables. The optimal combination of parameters was defined as the one that resulted in a reduced ash content.

The fractionation of lignin using acetone was carried out to obtain a specific molecular weight distribution. The acetone-soluble and acetone-insoluble lignins were characterised. The results are presented and discussed in this chapter.

4.2 Characterisation of As-received BioChoice®Lignin

4.2.1 Physical Properties of As-received BioChoice®Lignin

Figure 4.1 shows the visual appearance of the as-received lignin, BioChoice®lignin, purchased from the Domtar Corporation. The moisture content in the lignin was determined using the TAPPI T264-cm-07 standard by drying it in an air-circulating oven at 105 ± 3 °C for two hours. The moisture content was found to be $28.4 \pm 0.8\%$. Tomani, (2010) reported the moisture content of softwood Kraft lignin obtained by LignoBoost as being 32.3% [94] which was close to the results obtained in this work. The moisture content in specified classes of lignin from the literature is summarised in Table 4.1.



Figure 4.1 The visual appearance of as-received softwood Kraft lignin (BioChoice®lignin).

Table 4.1 Compiled properties of selected commercially available lignins.

Lignin samples	Resources	Extraction process	Moisture content (%)	Ash content (%)	M _w (g·mol ⁻¹)	PDI	References
Indulin AT	Softwood	Kraft	4.5	2-4	6,000-8,000	4-9	[32,97,104,111]
BioChoice [®]	Softwood	Kraft and LignoBoost	32	1.36	5,200-6,700	3-7	[32,94,98,105]
InnoForce [®]	Softwood	Kraft and LignoForce	5	0.1-1.5	6,000	3-4	[96,99,100]
Alcell [®]	Hardwood	Organosolv	2	0.1	1,300-3,900	2	[73,82,89,90,101–103]
Protobind	Wheat straw	Alkaline	6.5	1-1.6	2,000-5,000	3-4	[97,111,244,248]

SEM micrographs of the as-received lignin are showed in Figure 4.2 where the particles are seen to be irregular, agglomerated and inhomogeneous with regard to the particle size distribution. Figure 4.2 (a), shows that the agglomerate varied from a few microns up to 50 μm . The agglomerates consist of spherical granules combining to form particle with irregular shape. The surface of the spherical particle are smooth as shown in Figure 4.2 (b) and Figure 4.2 (c).

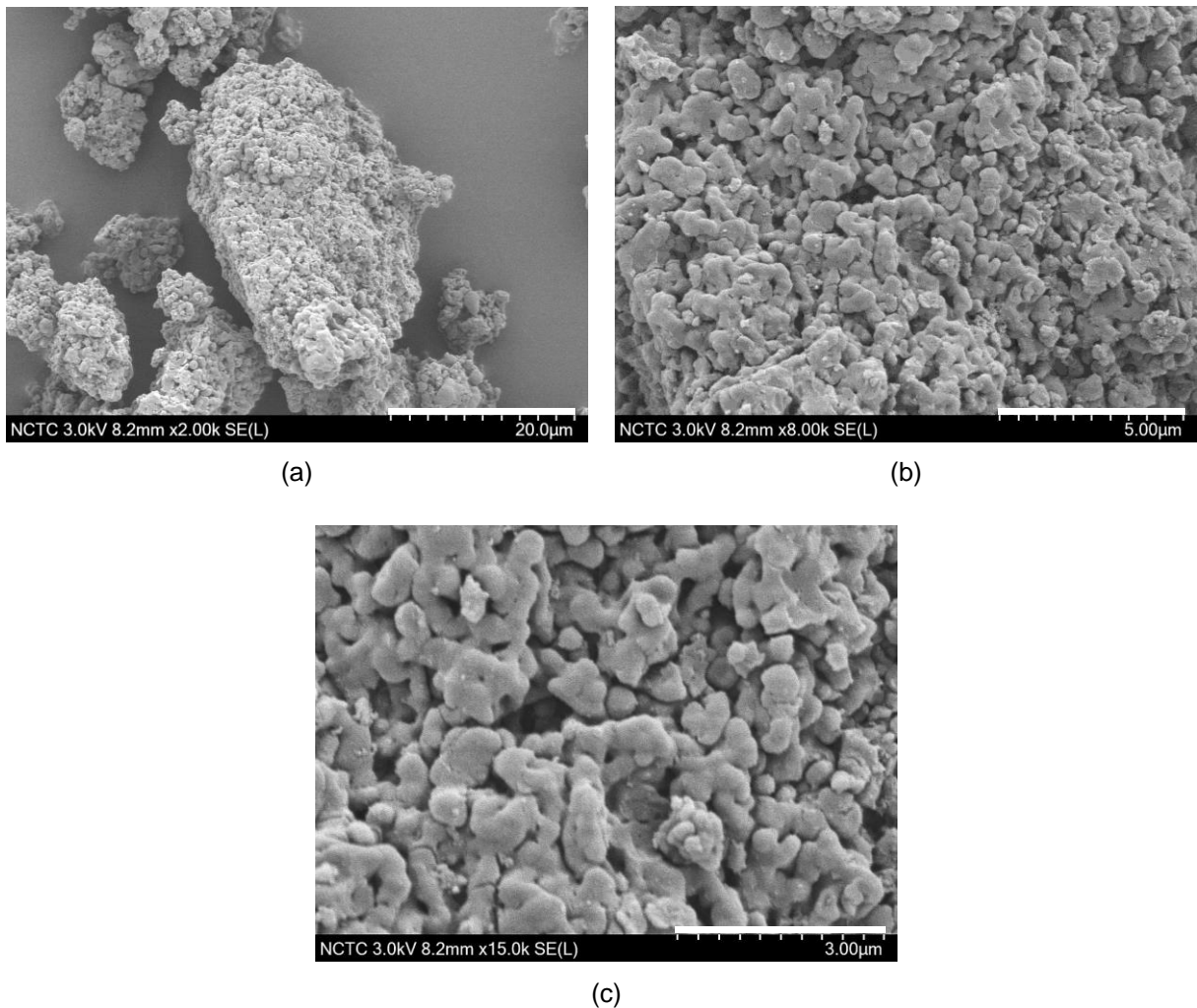


Figure 4.2 SEM micrographs of as-received lignin at a range of magnifications.

The particle size distribution of the pre-dried as-received lignin was determined following the procedure described in Section 3.4.2. Figure 4.3 displays a bi-modal distribution with the peaks centred at 8.9 μm and 44.6 μm . D-values of $d(0.1)$, $d(0.5)$

and $d(0.9)$ are commonly used to describe the particle size [249]. In this current study, they are $2.5 \pm 0.0 \mu\text{m}$, $13.2 \pm 0.2 \mu\text{m}$ and $57.5 \pm 0.3 \mu\text{m}$, respectively. For example, $d(0.5)$ indicates that 50% of the sample comprises particles with a diameter smaller than $13.2 \mu\text{m}$. The obtained $d(0.9)$ value shows a good correlation with the morphology observed by SEM. The particle size distribution as defined by Equation 4.1[250] is 4.16:

$$\text{Particle size distribution} = \frac{d(0.9) - d(0.1)}{d(0.5)} \quad \text{Equation 4.1}$$

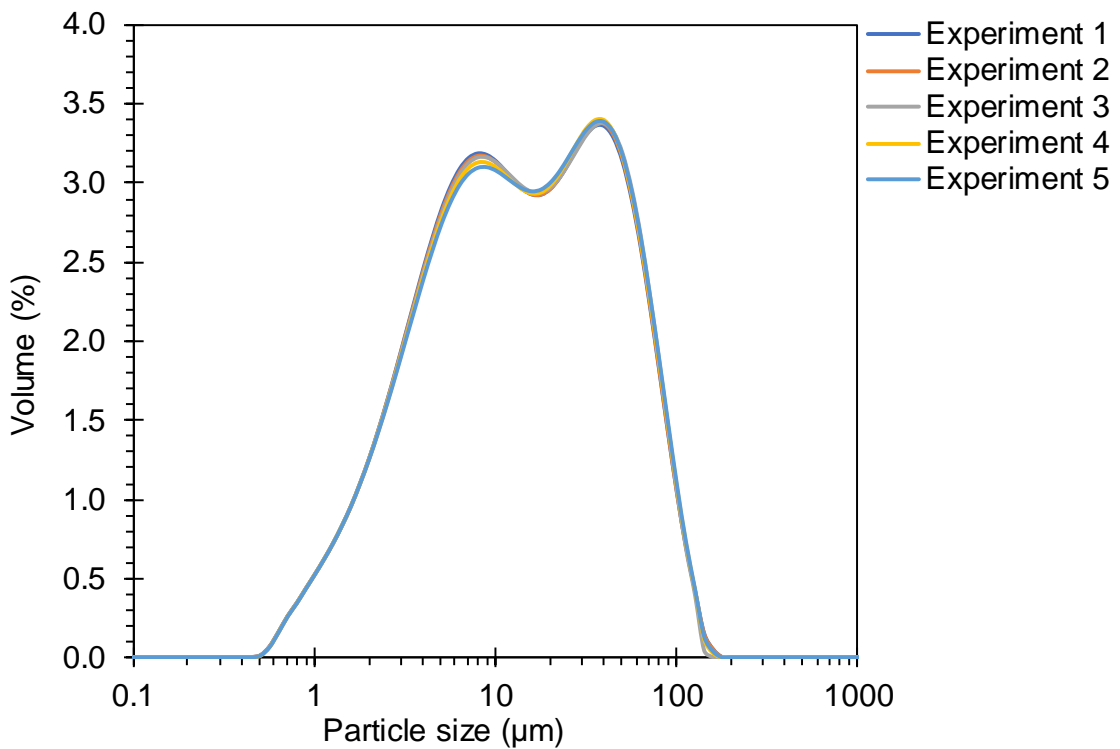


Figure 4.3 Particle size distribution of as-received lignin obtained using a laser particle size analyser.

The average density of the as-received lignin particles was measured using a gas pycnometer and the measurement protocol is described in Section 3.4.1. The average

density of as-received lignin is $1.39 \pm 0.01 \times 10^3 \text{ kg}\cdot\text{m}^{-3}$ and is close to the data reported in the literature, which is 1.350 to $1.397 \times 10^3 \text{ kg}\cdot\text{m}^{-3}$ [251,252].

4.2.2 Molecular Weight Distribution of As-received BioChoice®Lignin

Gel permeation chromatography (GPC) analysis of the lignin was carried out by Science City Research Alliance, The University of Warwick. The pre-dried as-received lignin was dissolved in dimethylformamide (DMF). A broad distribution profile of molecular weight with an additional high molecular weight shoulder is seen in Figure 4.4. The weight-average molecular weight (M_w) and number-average molecular weight (M_n) were determined based on using polymethyl methacrylate (PMMA) as the calibration polymer. The M_w and M_n are $6,000 \pm 283 \text{ g}\cdot\text{mol}^{-1}$ and $2,700 \pm 141 \text{ g}\cdot\text{mol}^{-1}$, respectively. The polydispersity index (PDI) from the relationship of M_w/M_n for the as-received lignin is 2.22. With reference to Table 4.1, the M_w and M_n obtained in this current work show a good correlation with those reported in the literature where BioChoice®lignin was determined by GPC [32,98,105].

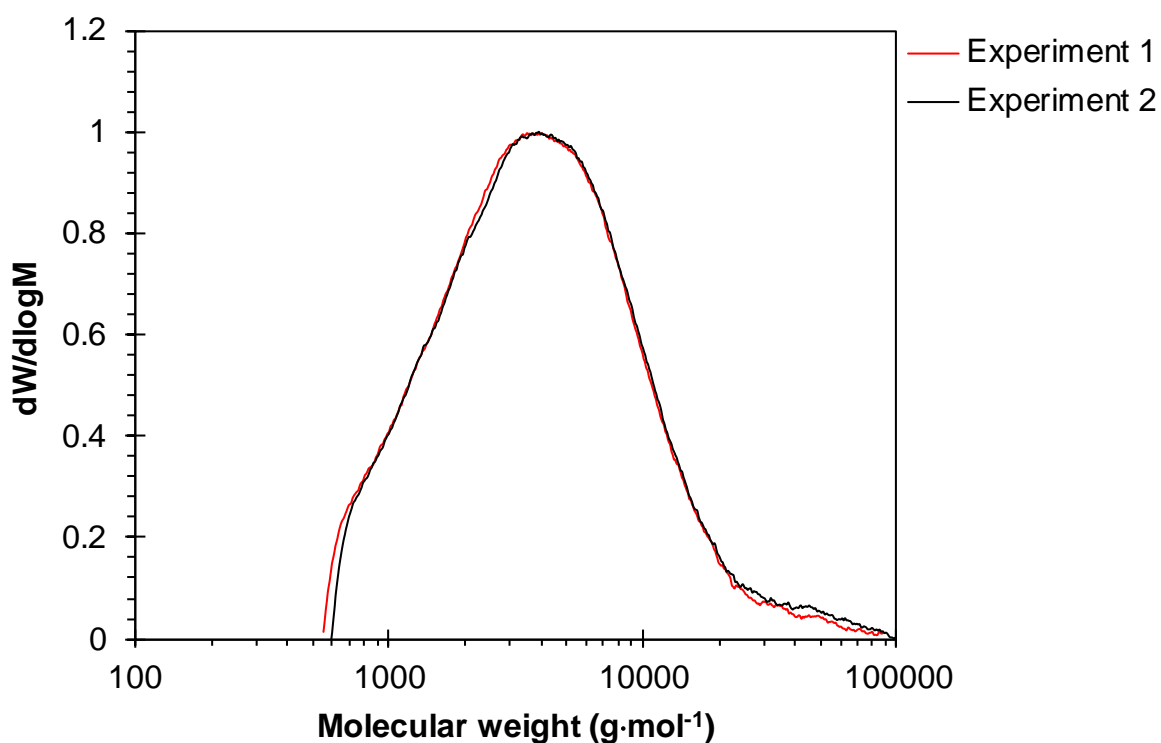


Figure 4.4 Molecular weight distribution curves for pre-dried as-received lignin samples as determined by GPC.

4.2.3 Determination of the Ash Content in As-received BioChoice® Lignin and Its Elemental Compositions

The ash content in the BioChoice® lignin was determined in accordance with the TAPPI T211 om-02 standard. The lignin samples were heated in an air-circulating furnace at 525 °C for four hours. The elemental composition of the ash was determined via energy dispersive X-ray spectroscopy (EDX) attached to the SEM. The ash content of the as-received lignin is $1.195 \pm 0.021\%$. The ash content in types of lignin reported by other researchers is summarised in Table 4.1. Overall, the ash content reported here is similar to that reported in Table 4.1, where softwood Kraft lignin generally shows an ash content between 0.1 and 4% [32,94,96–100,104,105].

The elemental composition was calculated by using the initial weight of lignin and a summary of the data are presented in Table 4.2. Sulphur and sodium are the two

major components present in the ash at 46% and 42%, respectively. The presence of sulphur in the ash can be attributed to the extraction procedures for Kraft pulping involving sodium hydroxide (NaOH) and sodium sulphide (Na₂S) and the use of sulphuric acid for isolation of lignin [14,26,71,253]. Silicon, magnesium and potassium are presented in relatively smaller concentrations of 2% to 5% in the ash.

Table 4.2 A summary of the ash content and the elements present in as-received lignin after combustion at 525°C.

Sample	Ash content (%)	Element in the ash	Elemental composition (%)	
			Average	SD.
As-received lignin	1.195 ± 0.021	Sulphur	0.555	0.066
		Sodium	0.501	0.022
		Silicon	0.068	0.033
		Potassium	0.048	0.002
		Magnesium	0.027	0.009

4.2.4 Lignin Content of As-received BioChoice®Lignin

The lignin content was determined using the methods recommended by the Technical Association of the Pulp and Paper Industry (TAPPI). The relevant standards for determining the lignin content in biomass are TAPPI T222 and TAPPI UM 250 and the procedure is described in Section 3.2.3. Lignin content represents the purity of lignin which is defined as the sum of the Klason lignin or acid-insoluble lignin and acid-soluble lignin. An UV/Visible spectrophotometer was used to determine the acid-soluble lignin concentration where the absorbance at 200-205 nm is said to be characteristic of an aromatic lignin unit, as defined in the TAPPI UM 250

[86,241,254–256]. Figure 4.5 shows the absorption band for acid-soluble lignin of pre-dried as-received lignin. The absorbance at approximately 205 nm was used to quantify the acid-soluble lignin content using Equation 3.4 [241] described in Section 3.2.3.

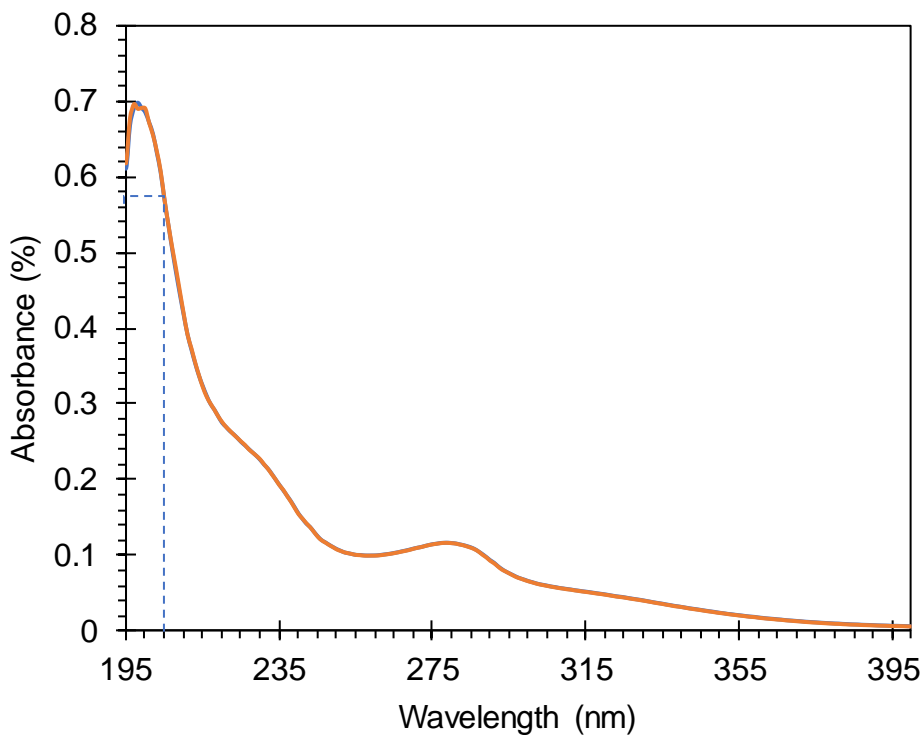


Figure 4.5 UV/Visible spectra of pre-dried as-received lignin.

The acid-insoluble lignin and acid-soluble lignin content in the as-received lignin are $92.7 \pm 0.9\%$ and $4.45 \pm 0.01\%$, respectively and the total lignin content is $97.2 \pm 0.9\%$. The Klason lignin and acid-soluble lignin from previously publications are compiled in Table 4.3.

Table 4.3 Compiled data for as-received lignin and relevant properties of selected commercially available lignins.

Lignin samples	Klason lignin (%)	Acid-soluble lignin (%)	Total lignin (%)	T _{g2} (°C)	References
As-received lignin (BioChoice®)	92.7 ± 0.9	4.45 ± 0.01	97.2 ± 0.9	163.0 ± 1.5	Current work
Indulin AT	88.8	4.1	92.9	132	[32,97,111]
BioChoice®	91.1	5.4	96.5	147	[32,98]
InnoForce®	N/A	N/A	N/A	160	[96,99,100]
Alcell®	96.1	0.4	96.5	70-108	[82,89,90]
Protobind 2400	79	9	86	59	[97,111]

Total lignin content in BioChoice® lignin, which is the same lignin used in this current work have been reported as 96.5% [32,98]. The total lignin content of lignin reported in the current study is comparable to that reported previously. When compared to a similar softwood Kraft lignin product (Indulin AT), the total lignin content has been reported to be 93-99% [32,97]. Other types of lignins such as Organosolv lignin (Alcell® lignin) [82,89,90,101–103] and InnoForce® lignin [96,99,100] exhibit the similar range of total lignin content between 95-97%. The Protobind 2400 lignin extracted from wheat straw has the lowest total lignin content [97].

4.2.5 Thermal Properties of As-received BioChoice®Lignin

4.2.5.1 Thermo-gravimetric Analysis of As-received BioChoice®Lignin

Prior to characterising as-received lignin using thermogravimetric analysis (TGA), the sample was pre-dried in a vacuum oven at 80 °C for six hours in order to remove absorbed moisture. Figure 4.6 shows the mass-loss and the first derivative (DTG) curves of the as-received lignin as it was heated from 25 to 900 °C at 10 K·minute⁻¹ under an argon atmosphere at a flow rate of 50 ml·minute⁻¹.

The pre-dried as-received lignin samples exhibit distinct mass-loss characteristics as a function of temperature. The mass of the pre-dried as-received lignin after pyrolysis at 900 °C is 45.0 ± 1.2%; this is an average from two measurements. With reference to Figure 4.6 (a), the thermal decomposition of lignin can be divided into four main stages.

Figure 4.6 (b) shows an enlarged view of the first stage region; where a mass-loss of 1.9% was observed below 150 °C. The DTG curve displays a peak mass-loss at 66.2 °C with a mass-loss rate of 0.3 %/°C and an endset DTG at around 115 °C. The mass-loss found in this work shows a good correlation with the data reported in previous literature. The observed mass-loss in the range from 1 to 3% below 150 °C has been reported from the different lignins, such as LignoBoost®lignin [257], Alcell®lignin [258] alkaline lignin [259] and other lignin samples such as Klason lignins obtained from wheat straw and oak [257], maple lignin [260] and rice husk and rice straw lignins [261]. This loss is attributed to the evaporation of moisture from the sample [258–260]. A similar trend has been reported using a TGA coupled with FTIR spectroscopy and pyrolysis coupled with gas chromatography and mass spectrometry (Py-GC/MS). An evolution of water was the major volatile detected below 150 °C [257,262].

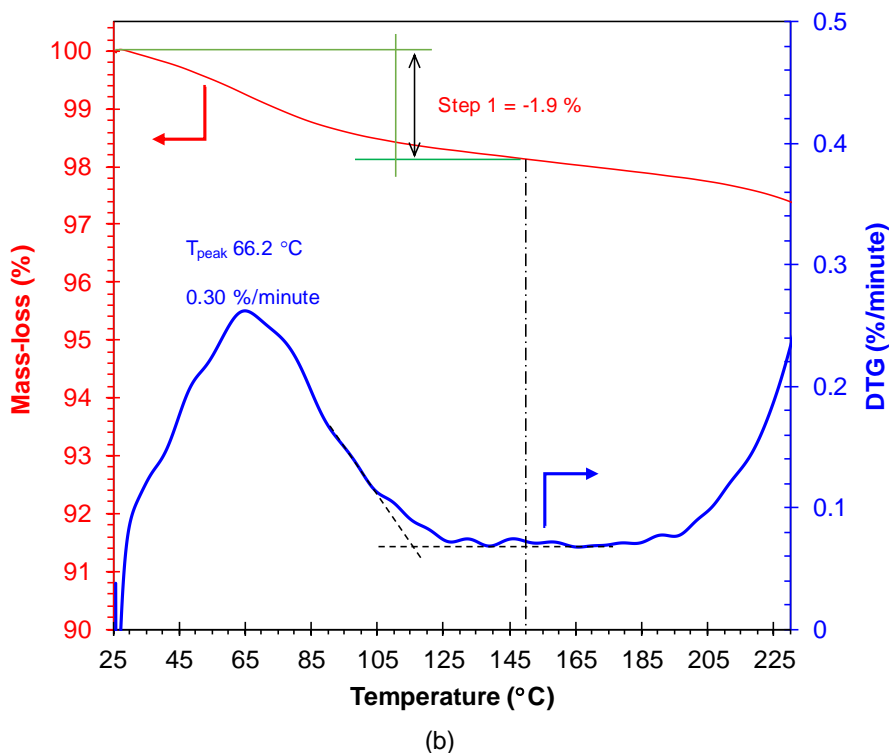
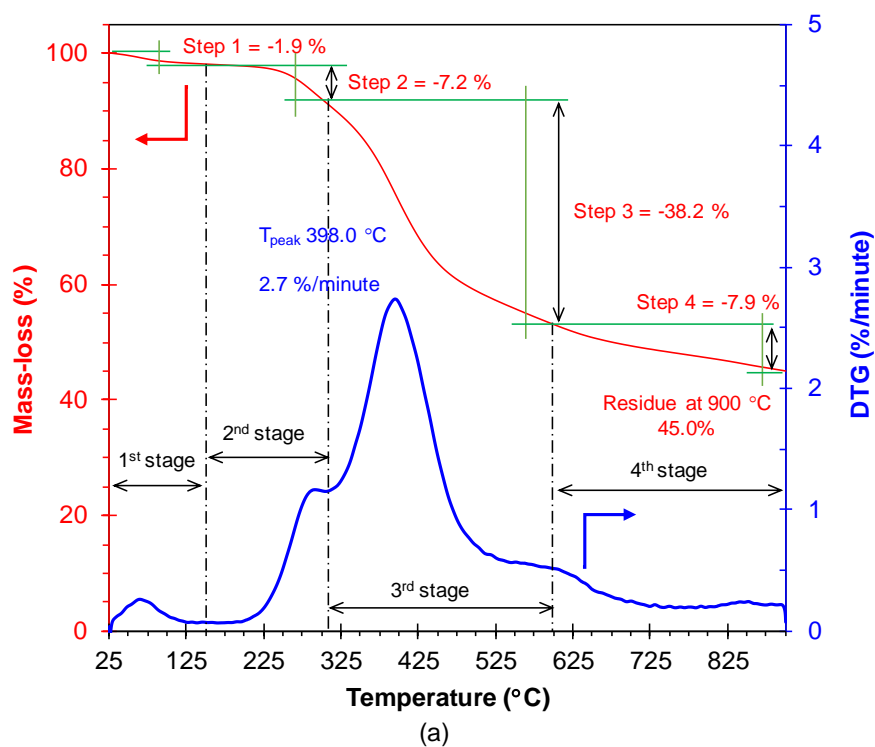


Figure 4.6 TGA and DTG curves for pre-dried as-received lignin: (a) the thermal decomposition ranged from 25 °C to 900 °C divided into four main stages and (b) enlarged view of the first stage region.

With, reference to Figure 4.6 (a), the second stage between 150 °C and 310 °C displays a DTG peak at 297 °C, with a mass-loss rate of 1.2 %/°C. In this stage, a mass loss of 7.2% is observed. This loss could be ascribed to the release of gases including CO, CO₂, CH₄ and H₂O as their characteristic bands were detected via TGA-FTIR spectroscopy [260,261,263] and fragments representing water and CO₂ [257].

The major mass-loss was found in the third stage, between 310 °C and 600 °C, where a fast degradation rate with a maximum mass-loss rate of 2.72 %/°C was shown. The maximum DTG was observed at 398 °C and approximately 38.2 % of the lignin was converted into volatiles. In this stage, the gases were reported to be the same as the observed in the second stage (e.g., CO, CO₂, CH₄, H₂O) [257,260,261,263]. Moreover, aromatic compounds such as phenols, alcohols, aldehydes, ketones, and acids are said to be emitted in this stage [257,259,262–264].

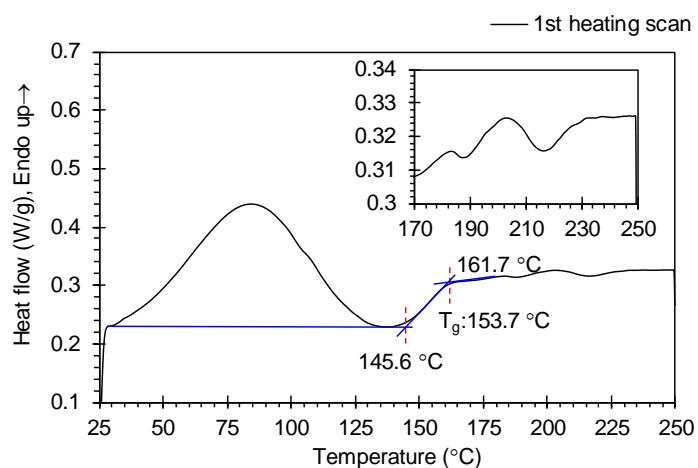
In the fourth stage, where the temperature is above 600 °C, the degradation rate decreased from 0.5 %/°C to a constant rate of 0.2 %/°C when the temperature reached 700 °C. In this slow degradation stage, the mass-loss was 7.9% and the emitted gases were reported to include of CO, CO₂ and aromatic compounds [262,263]. The residual mass at 900 °C is 45.1% and this is similar to that reported in the literature [32,98,255,257].

4.2.5.2 Differential Scanning Calorimetry of As-received BioChoice®Lignin

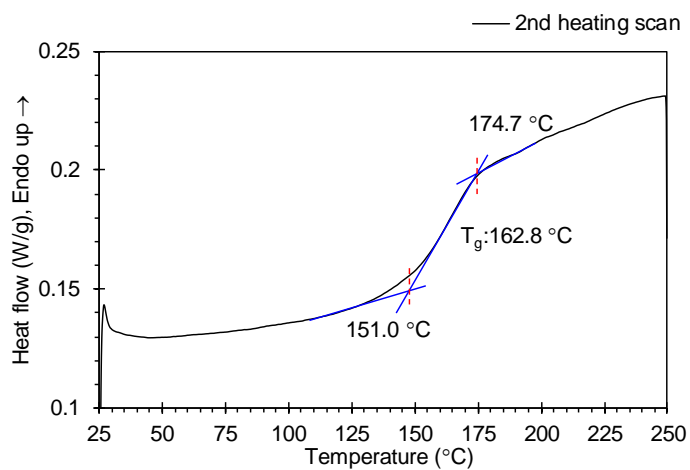
Thermal property of lignins such as the glass transition temperature (T_g) was determined using differential scanning calorimetry (DSC). The sample was heated at 10 K·minute⁻¹ from 25 to 250 °C under a nitrogen atmosphere. The measurement procedure is described in Section 3.4.5. It is important to establish and understand the thermal behaviour of lignin as it has significant implication for fibre formation. For example, in the first heating scan shown in Figure 4.7 (a), a pre-dried as-received lignin shows a broad endotherm between 39.2 and 123.7 °C with a peak at 86.5 °C and an enthalpy of 65.7 J·g⁻¹. The first endotherm peak in Figure 4.7 (a) is important because it suggests that pre-heating as-received lignin in a vacuum oven at 80 °C for

six hours is not sufficient to remove all absorbed moisture. Approximate 1.9 % (observed by TGA described in Section 4.2.5.1) of moisture retained or reabsorbed during storage. However, it is also known that lignin can cross-link during thermal treatment. Hence, the pre-drying temperature was set at 80 °C for six hours in a vacuum oven. This corresponds to the peak observed in the first endothermic peak in Figure 4.7 (a). The presence of the glass transition temperature obtained from the first heating scan (T_{g1}) around 153 °C is clearly seen. However, it accompanied by two successive exotherms at 190 °C and 210 °C (see the insert in Figure 4.7 (a)). These exotherms are most likely due to cross-linking reaction occurring in lignin which have been suggested from the previous literature [134,135,217,218,221]. Further evidence for this suggestion can be seen in the second and third scans where these exotherms are not detectable. Hence, the suggesting that cross-linking has occurred.

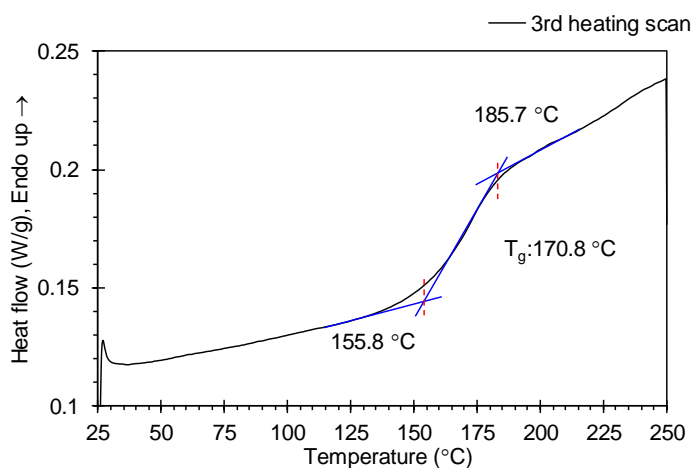
The DSC thermograms from the second and the third heating scans are shown in Figure 4.7 (b) and (c), respectively. The broad endotherm and thermal events below 150 °C disappear in the second and third heating scans. The glass transition temperature obtained from the second heating scan (T_{g2}) is 163.0 ± 1.5 °C. Table 4.3 presents a summary of the T_g of softwood Kraft lignin reported in the literature, which are in the range 130 °C to 160°C [34,83,97,98,124]. The T_{g2} of pre-dried as-received analysed in this work is comparable to the T_g compiled in Table 4.3. In the third heating scan, the glass transition temperature obtained from the third heating scan (T_{g3}) increased from 163 °C to 172.2 ± 1.4 °C. This increase may be attributed to further cross-linking in the lignin as it was heated twice previously to 250 °C.



(a)



(b)



(c)

Figure 4.7 DSC thermograms for pre-dried as-received lignin: (a) first heating; (b) second heating; and (c) third heating. The insert in (a) shows an expanded view between 170 and 250 °C.

The presence of moisture can be detrimental with regard to melt-processing of lignin as it can lead to the formation of voids. Moisture can also interact with polar solvents such as acetone and DMSO. This means that in fibre formation process such as electro-spinning, the presence of moisture can influence the electro-spinning parameter. Moreover, during subsequent heat treatment to remove the solvent, moisture can have an adverse effect of the properties of the fibres. The cross-linking in lignin is also important. For example, during melt-processing it can cross-link in the equipment.

The thermal properties of lignin are also important when defining the temperature regimes for heat treatment during and after fibres formation. During fibre formation, in addition to producing fibres with a uniform circular cross-section. It is essential to prevent the fusion of the individual filaments. This is generally, achieved by the evaporation of the solvent in solution-based fibres formation techniques. In these circumstances, a “skin” is formed on the fibres that helps to retain the circular cross-section. The morphology and nature of the skin is important when the fibres or preforms are heated to drive off the solvent. The temperature selection for this operation has to be below the T_g of lignin to prevent fibre fusion.

4.2.6 Functional Group Analysis of As-received BioChoice®Lignin by Fourier Transform Infrared Spectroscopy

Fourier transform infrared (FTIR) spectroscopy was used to identify the main functional groups present in the as-received lignin. A typical spectrum for a pre-dried as-received lignin is presented in Figure 4.8. A broad absorption band with a shoulder is observed in the hydroxyl (-OH) stretching region between 3,700-3,000 cm^{-1} . The broad absorbance band centred at 3,420 cm^{-1} and the shoulder at 3,620 cm^{-1} can be attributed to stretching vibrations of phenolic and aliphatic -OH groups. The absorbance bands found between 3,050-2,800 cm^{-1} correspond to the deformation of C-H in methyl and methylene groups. The stretching vibrations of the carbonyl group (C=O) are observed at 1,685 cm^{-1} . The peak at 1,591 cm^{-1} corresponds to the vibrations of aromatic skeleton and C=O stretching whilst

the strong peak at $1,514\text{ cm}^{-1}$ corresponds to the vibration of the aromatic skeleton. The three absorbance bands observed between $1,460\text{-}1,400\text{ cm}^{-1}$ can be assigned to C-H deformations. The vibrations of C-H associated with the phenolic O-H groups are observed at $1,365\text{ cm}^{-1}$.

The absorption band at $1,262\text{ cm}^{-1}$ represents the Guaiacyl ring (G-Unit) which is a predominant building block of softwood Kraft lignin. The vibrations of C-C, C-O and C=O stretching can be seen at $1,210\text{ cm}^{-1}$. The absorbance bands at $1,140$ and $1,120\text{ cm}^{-1}$ are assigned to aromatic C-H and C-O deformations in primary alcohols. The aliphatic secondary O-H associated with C-O deformation in secondary alcohol presents at $1,082\text{ cm}^{-1}$, and the absorption due to aliphatic primary O-H associated with aromatic C-H deformation and C-O in primary alcohol is presented at $1,035\text{ cm}^{-1}$. The two peaks at 855 and 815 cm^{-1} are assigned to out-of-plane C-H deformation in the G-units of lignin. The compiled peak assignments and characteristic absorbance bands for the G-units in lignin are shown in Table 4.4.

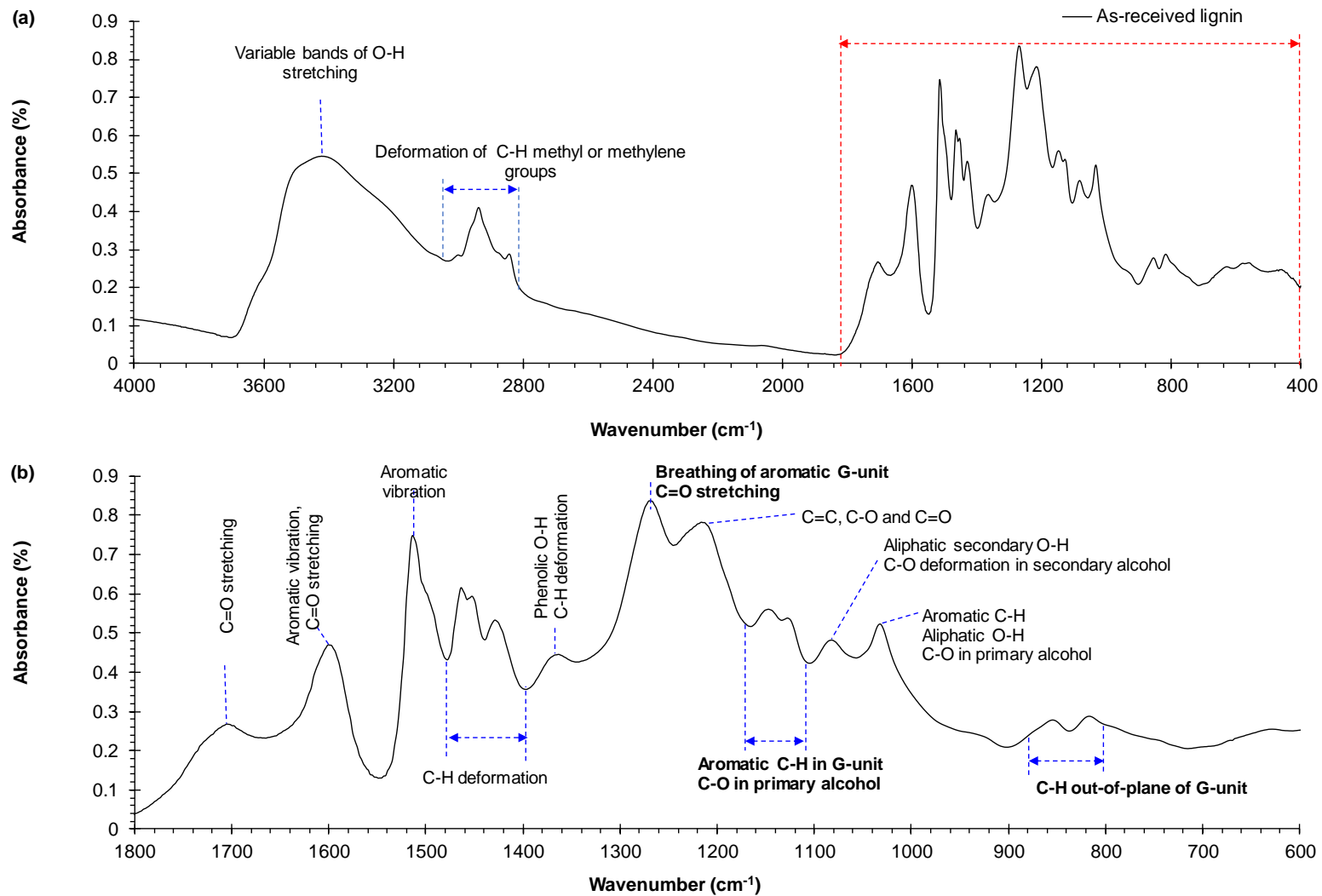


Figure 4.8 FTIR spectra of as-received lignin: (a) whole spectral range; and (b) enlarged view from 1,800-600 cm⁻¹.

Table 4.4 Band assignments for pre-dried as-received lignin [97,265,266]. The assignments in bold represent the characteristic band of softwood-wood lignin.

Wavenumber (cm⁻¹)		Absorbance peak assignments
Current observations	Previous reports	
3,408	3,440-3,430	O-H stretching in phenolic and aliphatic O-H group
2,940	2,940-2,930	C-H stretching in methyl and methylene group
2,850	2,689-2,880	C-H vibrations of methyl group or methoxy
1,685	1,727-1,690	C=O stretching (in conjugated aldehydes, ketone and carboxylic acids)
1,591	1,594	Aromatic vibration and C-O stretching
1,514	1,515-1,510	Aromatic skeleton vibration
1,460	1,465-1,450	C-H asymmetric bending of methyl and methylene group
1,422	1,428-1,420	C-H vibration of methyl group, aromatic skeleton vibration
1,365	1,370-1,365	C-H deformation in methyl, methoxy (O-CH ₃) group
1,365		Phenolic O-H C-H deformation in methyl, methoxy groups
1,270	1,270-1,260	Aromatic ring (Guaiacyl moieties) breathing with C=O stretch
1,210	1,200	C-C, C-O and C=O of ester stretching vibrations
1,140 and 1,120	1,160-1,140	Aromatic C-H in Guaiacyl unit C-O deformation in primary alcohol
1,082	1,085-1,080	Aliphatic secondary O-H C-O deformation in secondary alcohol
1,035	1,035-1,030	Aromatic C-H deformation C-O in primary alcohol Aliphatic primary O-H
855 and 815	855-852	C-H out-of-plane deformation in positions 2, 5 and 6 of Guaiacyl unit

The FTIR spectra characterisation of the pre-dried as-received lignin, BioChoice®Lignin, was used as a benchmark in subsequent treatments and heat treatment. The spectral assignment specified for the BioChoice®Lignin in Table 4.4 correlates well for softwood Kraft lignin reported in literature.

Primary motivation for using FTIR spectral analysis for lignin was to study if any changes was brought about by chemical treatment (treating lignin with acidified water, discussed in Section 4.3), molecular weight fractionation using acetone (Section 4.4) heating lignin fibres (Section 5.5) and thermo-stabilisation of lignin fibres (Section 5.6).

The presence of moisture was detected in the DSC and TGA and the results were presented in the two previous sections. Its presence is also clear in Figure 4.8 (a). The reason for selecting the pre-drying temperature of 80 °C in a vacuum oven for six hours was discussed previously. A compromise had to be made between desire to desorb the moisture from the lignin and to prevent it cross-linking prematurely.

A summary of the data generated for pre-dried as-received lignin is presented in Table 4.5. In general, the data in Table 4.5 agree with that reported in the literature. The data presented in Table 4.5 will be used as the benchmark in subsequent sections.

Table 4.5 Summary of the characteristic properties of pre-dried as-received lignin.

Characteristics		As-received lignin
Particle size, d(0.5) (µm)		13.2 ± 0.16
Density (kg·m ⁻³)		1.39 ± 0.01 x 10 ³
Ash content (%)		1.195 ± 0.021
Lignin content	Klason lignin (%)	92.7 ± 0.9
	Acid-soluble lignin (%)	4.45 ± 0.01
	Total lignin (%)	97.2 ± 0.9
Results from TGA	T _{DTG, onset} (°C)	251.9 ± 2.9
	T _{DTG, max} (°C)	391.5 ± 10.9
	Residue mass (%)	45.0 ± 1.2
	Char content (%)	43.8 ± 1.2

Characteristics		As-received lignin
Results from DSC		
First heating scan	Endothermic peak (°C)	87.0 ± 0.9
	Enthalpy (J·g ⁻¹)	65.7 ± 7.3
	T _{g1} (°C)	150.2 ± 6.8
Second heating scan	T _{g2} (°C)	163.0 ± 1.5
Third heating scan	T _{g3} (°C)	172.2 ± 0.4

4.3 Treatment of As-received BioChoice®Lignin with Acidified Water

Treating lignin with acidified water is a simple method to remove water-soluble and inorganic impurities; it has been used widely for Kraft lignin [79,118,120,145,196,197]. However, Organosolv lignin has been used in its as-received state [102,117,215,267]. This may be due to the high inorganic content in Kraft lignin as compared to Organosolv lignin, as seen in Table 4.1.

The as-received BioChoice®Lignin used in the current work has an ash content of 1.195 ± 0.021% and sulphur and sodium were found to be the two major elements at 46 wt% and 42 wt% of the ash, respectively. The as-received lignin was treated with acidified water in order to remove the inorganics. This was undertaken to enable a comparison of the properties of the lignin obtained from acid treatment and molecular weight fractionation with regard to the removal of contaminants.

Various acids have been used including hydrochloric acid [118,145], acetic acid [197] and sulfuric acid [120]. The processing conditions investigated in the literature include the pH and washing time. Zhang [119] studied different combinations of washing time, liquid-to-solid ratio and pH to identify the optimum processing conditions. Zhang reported that acidified water of pH 2; a ratio of acidified water to softwood Kraft lignin as 10 ml:1 g; a washing time of 15 minutes; and 25 treating cycles, were said to be optimal with regard to the removal of metal cations.

4.3.1 Taguchi Design of Experiments

In this work, the Taguchi design of experiments (DoE) methodology was performed with controllable factors in order to determine the optimum procedure for treating lignin with hydrochloric acid (HCl). This acid was chosen because it is a strong acid with a pKa of -9.3. The selected controllable factors and their levels are shown in Table 4.6. An L₉ (3⁴) orthogonal array was selected. The experimental combinations for nine experiments are given in Table 4.7.

Table 4.6 The parameters that were used for treating BioChoice®Lignin with acidified water and their levels with regard to the Taguchi DoE.

Parameters	pH	Acidified water-to-lignin ratio (cm ³ :g)	Washing time (minute)	Number of cycles
Level 1	2	5	15	1
Level 2	4	50	30	3
Level 3	6	100	60	5

In order to determine the best combination of test parameters, the ash content from each experiment were transformed to a signal-to-noise (S/N) ratio. Based on the Taguchi method, the term S/N ratio represents the ratio of the mean to its variation and it is used to evaluate the quality characteristics of a process. There are three types of quality characteristic definitions: (i) “lower is better”; (ii) “minimal is better”; and (iii) “higher is better” [268].

The ash content was determined in accordance with the TAPPI standard T211 om-02. The lowest value of ash content is the targeted response for this current work. Therefore the “lower is better” was selected for calculating the S/N ratio using Equation 4.2:

$$S/N = -10 \log \left[\frac{1}{n} \sum_{i=1}^n y_i^2 \right]$$

Equation 4.2

where y_i represents the experimental data. The average of experimental results (ash content) and the S/N ratio are shown in Table 4.7.

The effect of each controllable factor on the ash content was analysed and given an “S/N response”, as shown in Table 4.8. The optimal combination of treatment factors yields the highest value of the S/N ratio for each factor (see Figure 4.9), and the mean values are illustrated in Figure 4.10. According to this analysis, the levels and S/N ratios of the factors giving the lowest ash content correspond to a pH 4 (S/N response = 9.695); acidified water-to-lignin ratio of 100 (cm³:g) corresponds to an S/N of 8.952; treatment time of 30 minutes corresponds to a S/N of 8.770; and five washing cycles correspond to an S/N of 8.546. The ranking of the selected main factors, calculated based on the difference of maximum and minimum results is presented in Table 4.8 and Table 4.9.

Table 4.7 The combinations of L9 Taguchi orthogonal array, the results of the ash content and S/N ratios.

Experiment number	pH	Acidified water-to-lignin ratio (cm ³ :g)	Washing time (minute)	Number of cycles	Ash content (%)		S/N
					Average	SD	
Exp. 1	2	5	15	1	0.365	0.014	8.750
Exp. 2	2	50	30	3	0.353	0.02	9.034
Exp. 3	2	100	60	5	0.345	0.021	9.252
Exp. 4	4	5	30	5	0.326	0.065	9.727
Exp. 5	4	50	60	1	0.343	0.006	9.304
Exp. 6	4	100	15	3	0.314	0.048	10.054
Exp. 7	6	5	60	3	0.493	0.079	6.151
Exp. 8	6	50	15	5	0.465	0.086	6.659
Exp. 9	6	100	30	1	0.419	0.029	7.548

Table 4.8 Response table for S/N values for obtaining the minimum ash content.

Level	pH	Acidified water- to-lignin ratio (cm³:g)	Washing time (minute)	Number of cycles
1	9.012	8.210	8.488	8.534
2	9.695	8.332	8.770	8.413
3	6.786	8.952	8.236	8.546
Delta	2.909	0.742	0.534	0.133
Rank	1	2	3	4

Table 4.9 Response table for means of obtaining the lowest ash content.

Level	pH	Acidified water- to-lignin ratio (cm³:g)	Washing time (minute)	Number of cycles
1	0.354	0.395	0.381	0.376
2	0.328	0.387	0.366	0.387
3	0.459	0.359	0.393	0.379
Delta	0.131	0.035	0.027	0.011
Rank	1	2	3	4

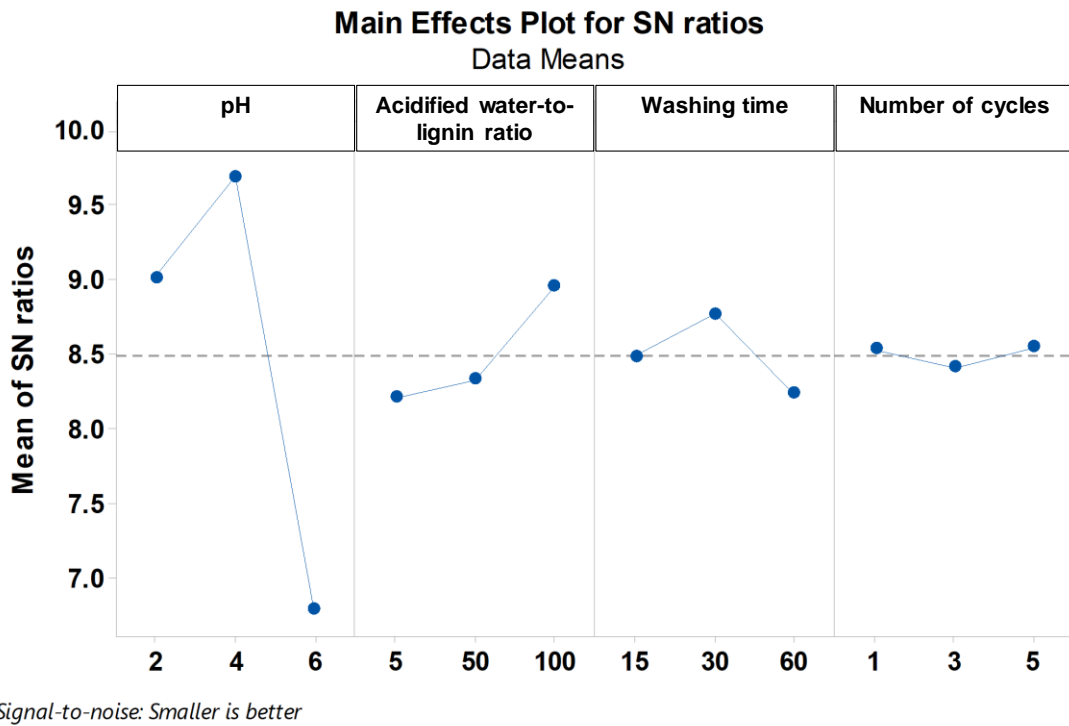


Figure 4.9 Effect of acidified water treatment conditions on the average S/N values for ash content.

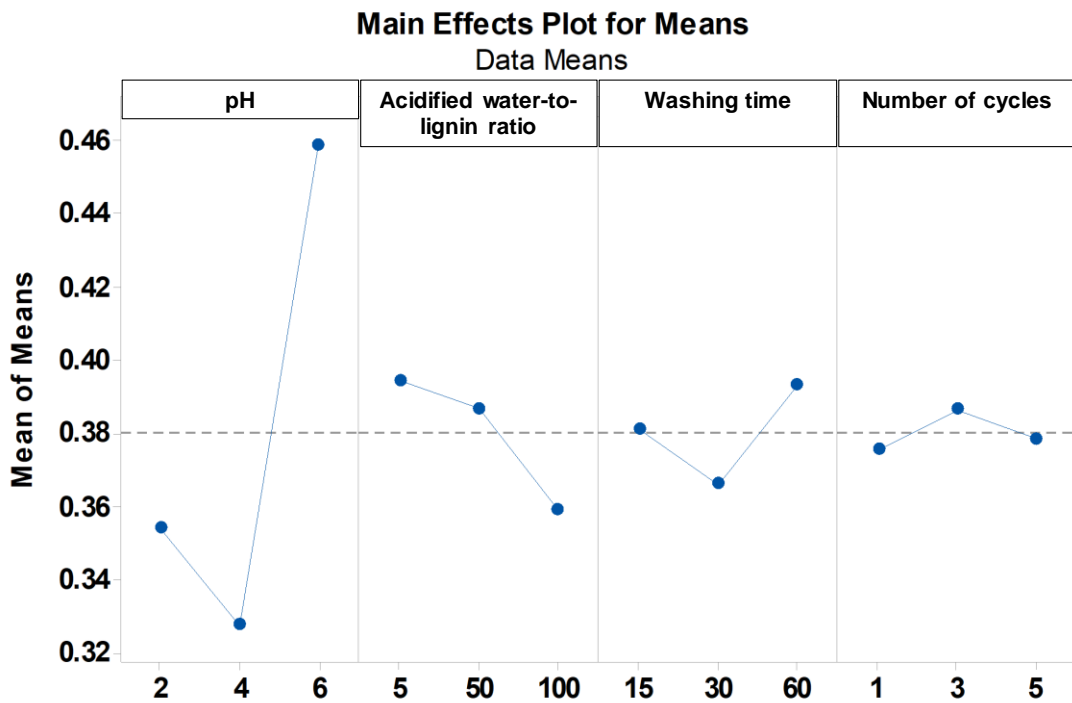


Figure 4.10 Effect of acidified water treatment conditions on the average mean value of ash content.

4.3.2 Analysis of Variance

4.3.2.1 P-value and F-ratio

The analysis of variance (ANOVA) is a statistical tool used for assessing the differences in datasets [269]. ANOVA can be used to assess the differences between the main factors by comparing their means and variance at specific confidence levels. In the current work, a 95% confidence level and 5% significance level (α 0.05) were used. According to Table 4.10, the P-value of three pHs (2, 4 and 6) is 0.03 which is lower than the α -value (0.05). It can be said that there is statistical significance with regard to the ash content at a reliability of 95%. The other factors have a P-value higher than 0.05, indicating that there are no statistically significant differences in their varied levels.

The F-ratio is commonly considered together with the P-value to determine the statistical significance at the desired confidence level (α 0.05). The F-ratio is the ratio of the total mean square (MS_T) to the residual error mean square (MS_E).

The total mean square (MS_T) can be evaluated from the total sum of the squares (SS_T) and its Degrees of Freedom (DOF) using Equations 4.3 and 4.4.

$$SS_T = \sum_{i=1}^n (y_i - \bar{y})^2 \quad \text{Equation 4.3}$$

$$MS_T = \frac{SS_T}{DOF(SS_T)} \quad \text{Equation 4.4}$$

where \bar{y} is an average of the observed values. The total sum of the squares (SS_T) refers to the deviation of the observed values (y_i) from their respective means. Degrees of Freedom (DOF) are equal to the number of levels minus 1.

The residual error mean square (MS_E) can be calculated using Equations 4.5 and 4.6. SS_E is the sum of the squares of error residual, which is the value that deviated from actual values of data and \hat{y} is the predicted mean from the estimation model.

$$SS_E = \sum_{i=1}^n (y_i - \hat{y})^2 \quad \text{Equation 4.5}$$

$$MS_E = \frac{SS_E}{DOF(SS_E)} \quad \text{Equation 4.6}$$

If the F-ratio is higher than the F-critical value, it can be concluded that there is statistical significance at the desired reliability level. In this current work, the F-critical value at the reliability level of 95% is 9.5521. From Table 4.10, the reported F-ratio of three pHs for pH 2, 4 and 6 is 11.74 which is larger than the F-critical value. This result is similar to that obtained via the analysis using the P-value. The difference levels in other controlled factors (acidified water-to-lignin ratio; washing time; and number of cycles) are not statistically significant because the P-value is higher than 0.05 and the F-ratio is lower than the F-critical value.

Table 4.10 Results of the ANOVA for ash content and grouping using Fisher pairwise comparison.

Factors	Degree of freedom	Adjusted Sum of square	Adjusted Mean of square	F-Ratio	Contribution (%)	P-Value
pH	2	0.057585	0.028792	11.74	66.7	0.003
Acidified water-to-lignin ratio	2	0.004113	0.002057	0.84	4.76	0.463
Washing time (minute)	2	0.002177	0.001088	0.44	2.52	0.655
Number of cycles	2	0.000393	0.000197	0.08	0.46	0.924
Error	9	0.022064	0.002452	-	25.56	
Total	17	0.086333				

4.3.2.2 Fisher Pairwise Plot

In order to analyse the difference of the mean values obtained from each level, one-way ANOVA was performed using Fisher pairwise comparison with a 95% confidence interval (CI) level [247]. Figure 4.11 shows a Fisher pairwise plot of the four controlled factors. In each plot, three pairs of levels are presented.

Considering pH 2 and pH 6, the 95% CI for the difference of these means ranges from -0.08 to 0.02. This range does not include zero, indicating that the difference between these mean values for the ash content obtained from pH 2 and pH 6 is statistically significant. Similar results of significant difference are found for pH 4 and pH 6, whereas there are no statistically significant differences between the mean values of pH 2 and pH 4.

For other factors, such as acidified water-to-lignin ratio, washing time and the number of cycles, the 95% CI of the differences for all their respective pairs of mean values include zero. It can therefore be concluded that the differences are not statistically significant.

According to the analysis of P-value, F-value and Fisher pairwise comparison, varying the pHs has a statistical significance in reducing the ash content. Moreover, the Fisher pairwise analysis showed that using pH 6 for the acidified water leads to a significant difference in the ash content when compared to using pH 2 or pH 4. The lignins treated with pH 2 and pH 4 did not have a statistically significant difference in their ash contents.

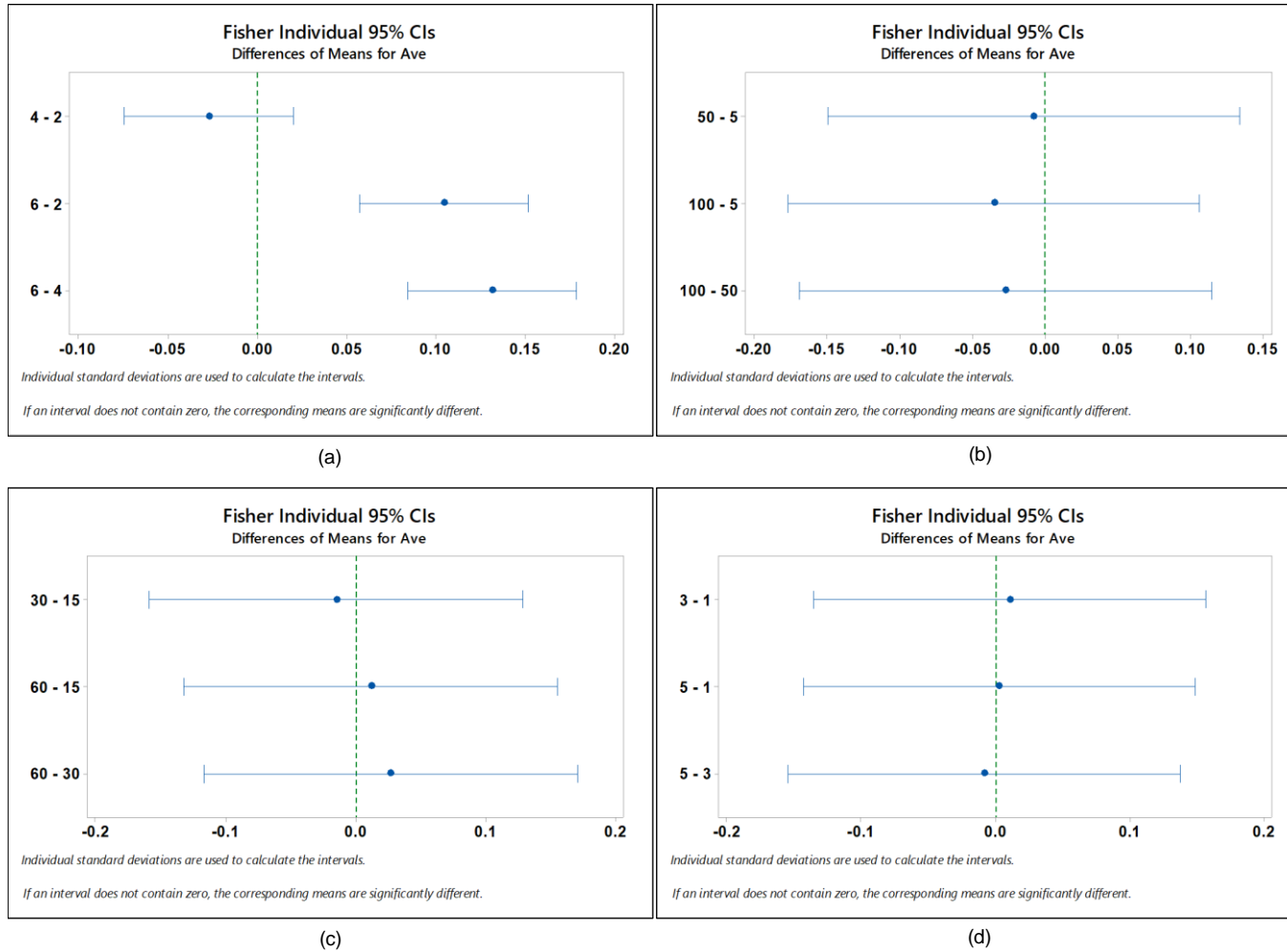


Figure 4.11 Fisher pairwise comparison for the effect of treating lignin with acidified water: (a) pH, (b) acidified water-to-lignin ratio, (c) washing time and (d) number of cycles.

4.3.2.3 Percentage Contribution

The percentage contribution of each factor in the ash content represents the degree of influence, and this is calculated from the ratio of the sum of squares to the total sum of squares; this is illustrated in Figure 4.12. The chart shows that the pH; acidified water-to-lignin ratio; washing time; and the number of cycles influenced the ash content by 66.70%; 4.76%; 2.52%; and 0.46%, respectively. Therefore, it can be concluded that the pH is the most influential factor in reducing the ash content at a reliability of 95% because its P-value is lower than 0.05 and the F-ratio is higher than the F-critical value. This result correlates with the rank analysis of the Taguchi method.

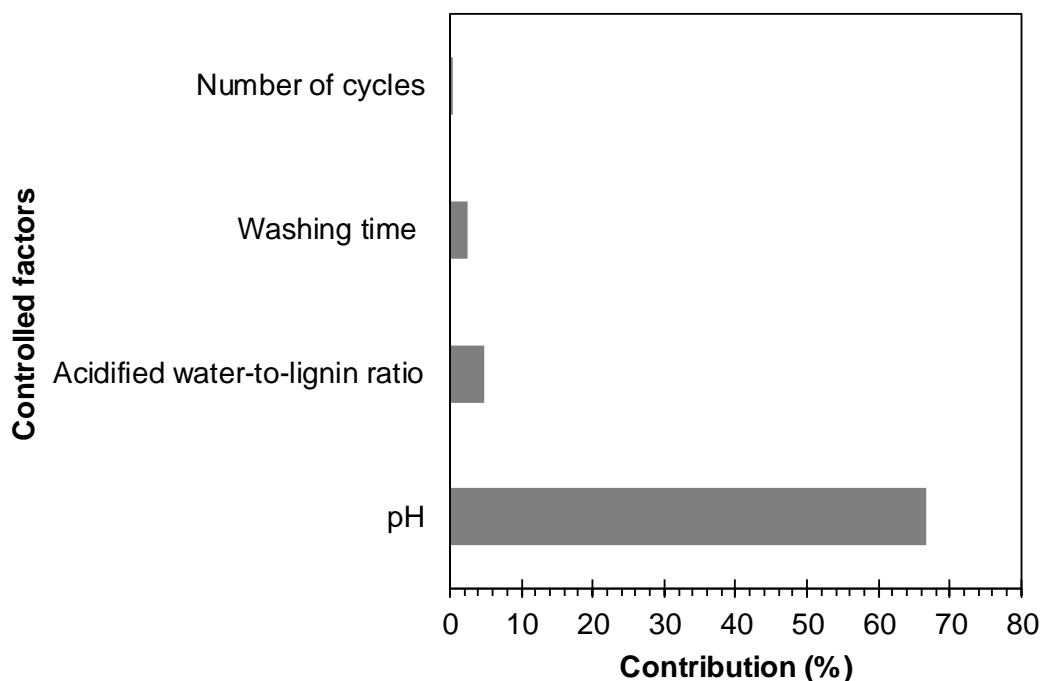


Figure 4.12 Percentage contribution of controllable factors influencing the ash content of lignin.

Figure 4.13 illustrates a matrix of the interaction effect of controlled factors used in this study. It clearly shows the dominant factor influencing the ash is pH whereas the other factors show an unclear influence on the ash content.

Interaction Plot for Ash content (%) Data Means

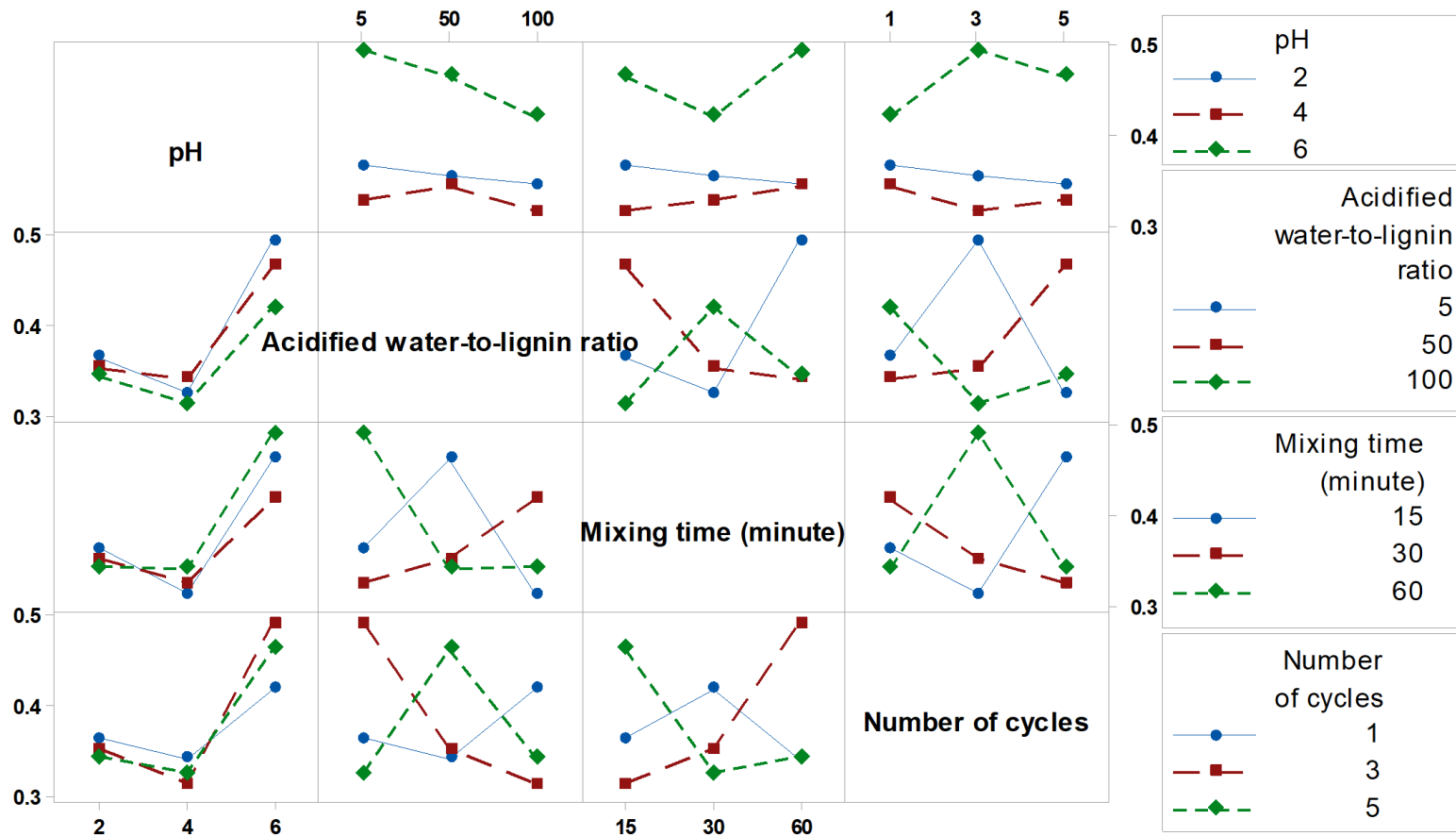
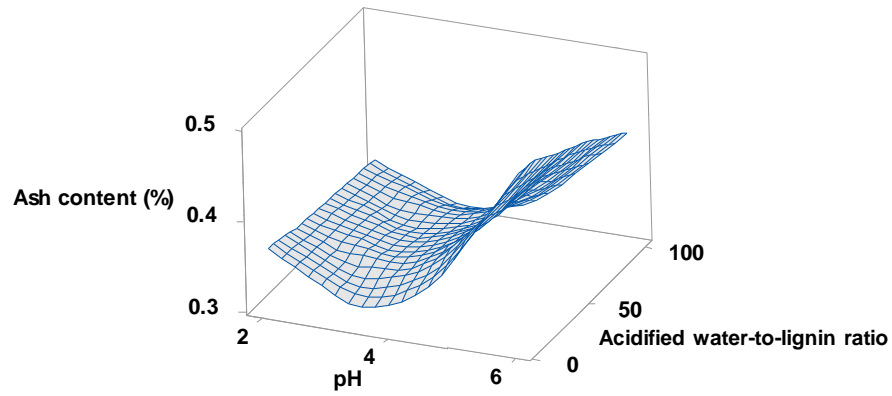
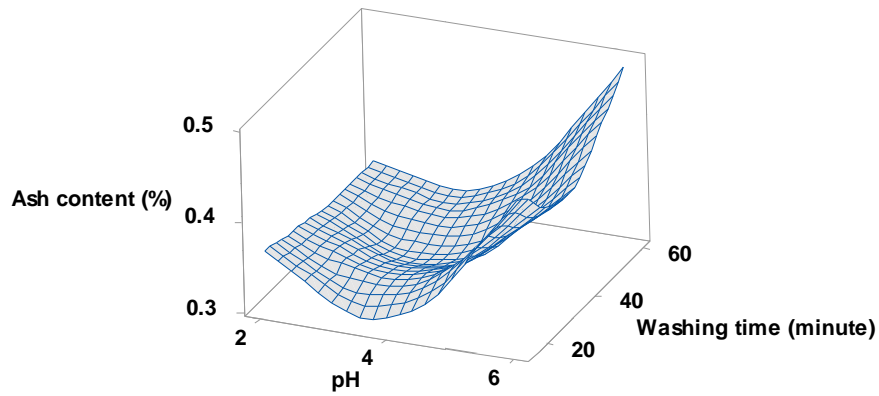


Figure 4.13 Interaction effect plot for means of ash content.

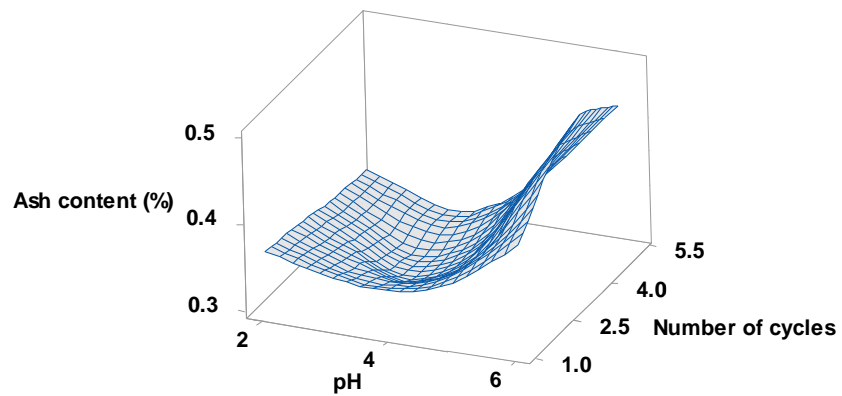
According to the ANOVA analysis, the controlled factor influencing the ash content is pH. Figure 4.14 presents the effect of the interaction between pH and other factors which was evaluated using 3D surface plots. This figure shows clearly that the ash content decreased with decreasing pH.



(a)



(b)



(c)

Figure 4.14 The effect of treating lignin for the ash content.

4.3.3 Effect of pH on Specified Properties of Acid-treated Lignins

According to the analysis from the Taguchi method and ANOVA, the predominant factor in the treatment condition affecting the ash content is the pH. Therefore, it was deemed important to investigate the influence of the pH on the ash content, the element composition of ash and the characteristics of acid-treated lignin.

4.3.3.1 Ash Content in Acid-treated Lignins

The lignin samples were heated in an air-circulating furnace at 525 °C for four hours. The ash content in the as-received lignin is $1.195 \pm 0.021\%$ which is used as the reference point. The ash content was reduced to $0.459 \pm 0.086\%$; $0.328 \pm 0.065\%$; and $0.354 \pm 0.020\%$ after treatment with acidified water of pH 6, pH 4 and pH 2, respectively. Figure 4.15 illustrates a bar chart of the ash content versus the elemental composition. Sulphur and sodium are the two main contributors which are 0.55 wt% and 0.50 wt% of the as-received lignin, respectively. After treating with pH 6 acidified water, the relative concentrations of sulphur and sodium decreased to 0.13 wt% and 0.14 wt%, respectively. The amount of magnesium and potassium obtained from treating lignin at pH 6 showed a similar range to those of the as-received lignin. Increasing the pH leads to a diminished sulphur content. The lowest sulphur content of 0.09 wt% was observed in the sample treated with acidified water at pH 2, which dropped by 82%, as compared to that contained in untreated lignin. The reduction in the sulphur content can be attributed to the removal of sulphate ions (SO_4^{2-}) via treating with acidified water [79]. The significant reduction of sodium has been described as due to the removal of alkaline ions by hydrolysis [270–272].

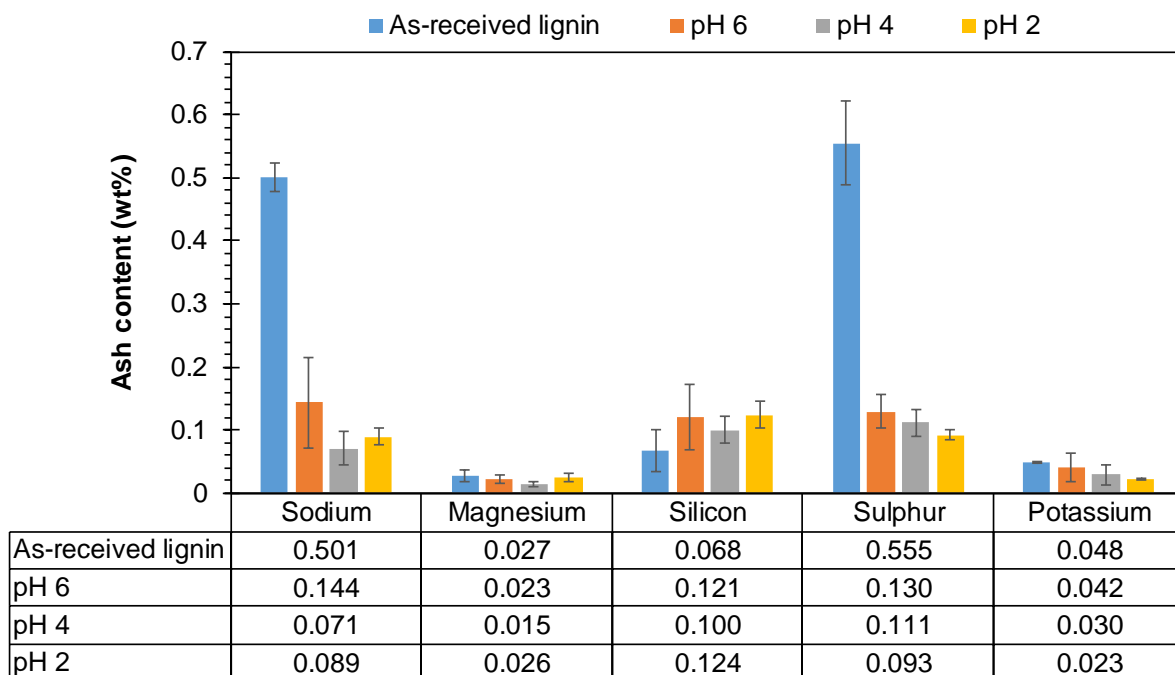


Figure 4.15 The ash content versus the elemental compositions.

4.3.3.2 Differential Scanning Calorimetry of Acid-treated Lignins

DSC thermograms of lignins treated with acidified water at pH 6, pH 4 and pH 2 compared with the as-received lignin sample are presented in Figure 4.16. In this experiment, all the lignin samples were pre-dried and tested under the same conditions in order to investigate the effect of pH of the acidified water on the thermal properties of the treated lignins. The DSC results were generated using the Perkin Elmer DSC-7. The cooling system on the equipment could only maintained the DSC sample/reference chamber at approximately 25 °C at the start of the scan. In the first scan, the lignin samples were heated from 25 °C to 200 °C at 10 K·minute⁻¹ and kept isothermal for three minutes. Then, the samples were cooled to 25 °C at 10 K·minute⁻¹ and held for three minutes. The second and third scans were performed using the same steps as the first scan. The DSC trace from the first heating scan is displayed as the black line and using the heat flow as the primary y-axis. The second and third heating DSC traces are shown as red and green lines and the heat flow values are on the secondary y-axis.

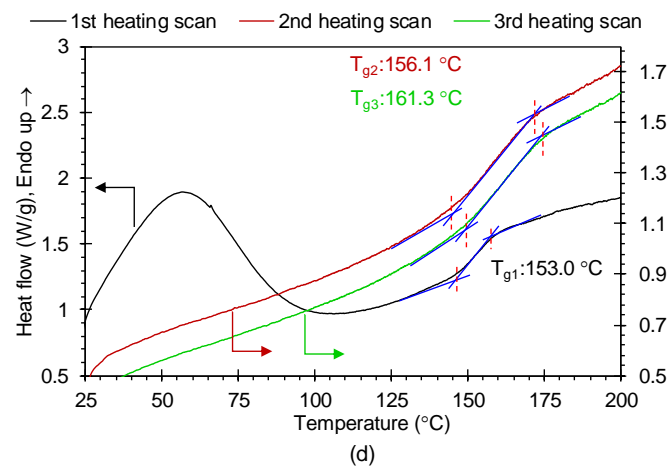
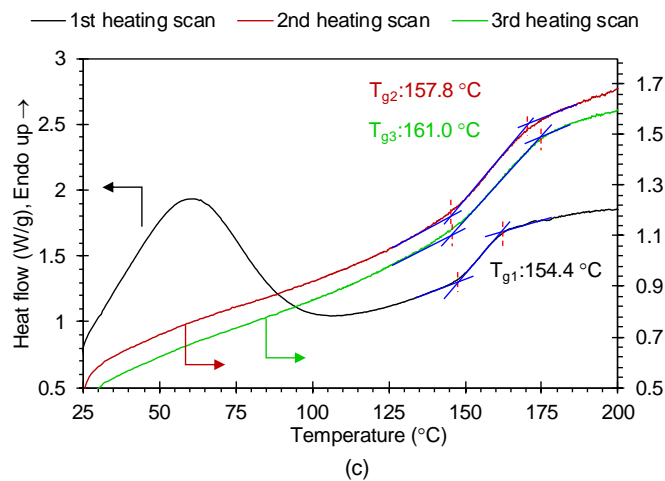
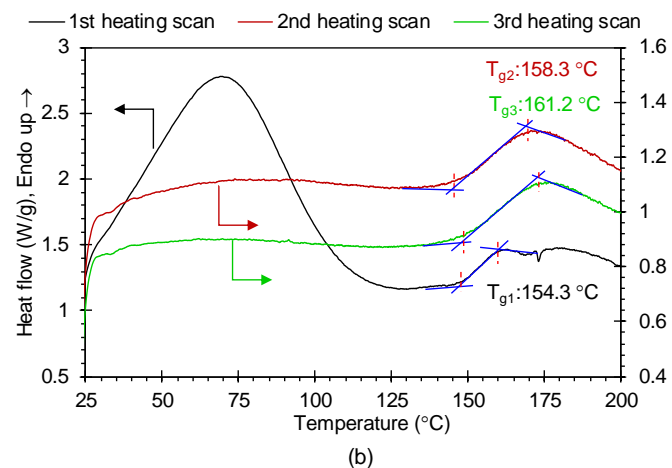
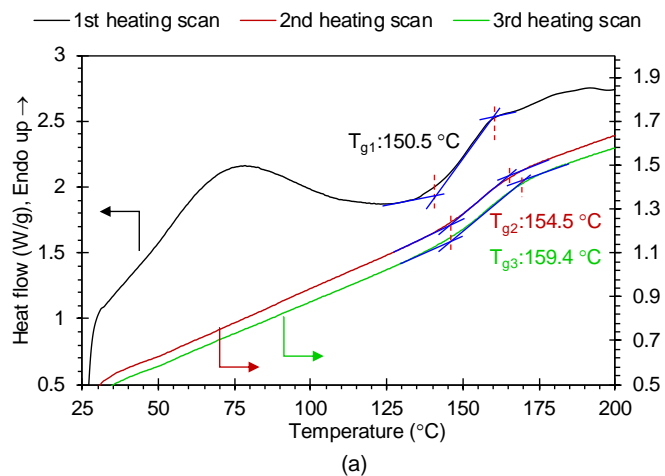


Figure 4.16 DSC traces for: (a) pre-dried as-received lignin; and (b), (c) and (d) are as-received lignin treated with acidified water at pH 2, pH 4 and pH 6, respectively.

As seen Figure 4.16, commencing the experiments at 25 °C meant that there was a significant error in the calculation of the enthalpy of fusion for the evaporation of moisture and any low-molecular weight component that may have been presented in the lignin. The term of “as-received lignin” refers to the lignin that was pre-dried in a vacuum oven at 80 °C for six hours. The enthalpy and peak for endothermic peak for as-received and the acid-treated lignins were calculated and the data are presented in Table 4.11. From the analysed results of peak temperatures and the enthalpy of the endothermic peak, it is difficult to draw any conclusion from this data set because of the difficulty in defining the position of baseline at start of the heating regime.

Table 4.11 Compilation of enthalpy , peak of endothermic and T_g data for as-received lignin and as-received lignin treated with acidified water.

Lignin types	Enthalpy (J·g ⁻¹)	Peak (°C)	T_{g1} (°C)	T_{g2} (°C)	T_{g3} (°C)
As-received lignin	34.1	76.9	150.5	154.5	159.4
As-received lignin treated at pH 2	41.5	69.0	154.3	158.3	161.0
As-received lignin treated at pH 4	30.1	59.6	154.4	157.8	161.0
As-received lignin treated at pH 6	25.1	56.4	153.0	156.1	161.3

In the first heating scan, a T_{g1} presented at the temperature above the endset of endothermic peak. In the second and third heating scans, the endothermic peak disappeared, and only a single T_g was observed. The T_g s analysed from all three heating scans of the lignin samples are compiled and plotted in Table 4.11 and Figure 4.17, respectively.

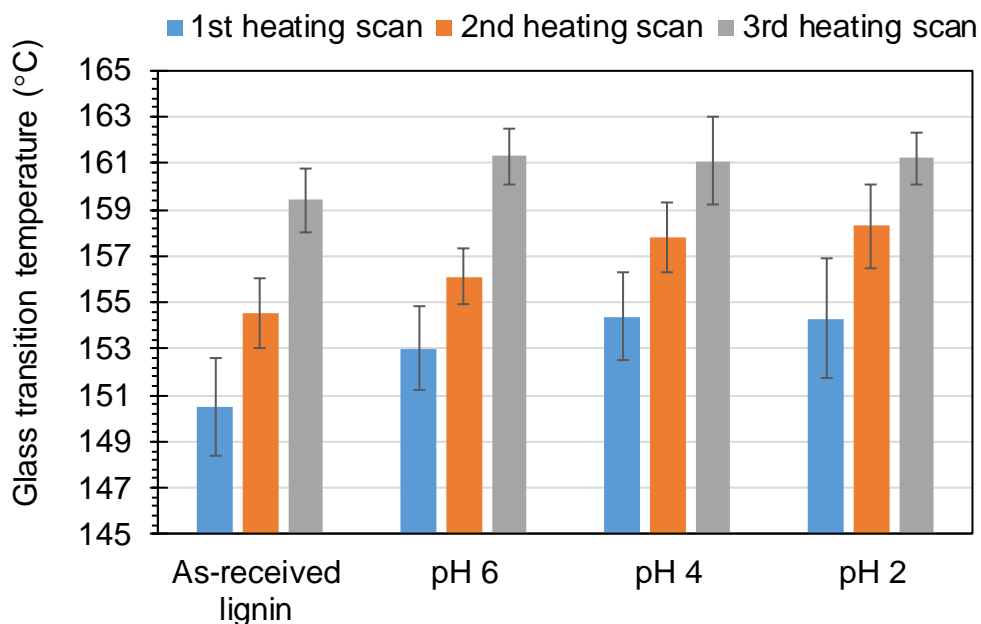


Figure 4.17 Glass transition temperatures analysed from as-received lignin and acid treated lignin samples.

From the plot, it can be seen that the use of acid treatment has an influence on the T_g . The as-received lignin treated with acidified water showed an increasing of T_g as compared to the as-received lignin. The T_g obtained from each scan increased as with the sequential of number of scans. The T_{g2} from the second heating scan was higher than that from the first heating scan, which increased by 4 °C. A similar increased trend was found in the T_{g3} from the third heating scan; T_{g3} increased by 3-5 °C from the second heating scan. The increase in T_g may be connected to the cross-linking occurring as the lignin was heated to 200 °C.

4.3.3.3 Functional Group Analysis of Acid-treated Lignins by Fourier Transform Infrared Spectroscopy

FTIR spectra of the as-received lignin and the as-received lignins treated with acidified water at pH 6, pH 4 and pH 2 are shown in Figure 4.18. The three acid-treated lignins show similar absorption spectra. The absorbance band centres deviate by about 2-3 cm^{-1} . Furthermore, there are no obvious absorbance band differences when compared to the as-received lignin. This means treating lignin with acidified water does not change the functional groups in lignin. In order to observe the effect of the pH on the total hydroxy content in the lignins, the FTIR spectra were normalised using the intensity of aromatic vibration band at 1,514 cm^{-1} . The relative intensity of the absorption bands of O-H stretching (3,390 cm^{-1}), phenolic O-H (1,365 cm^{-1}), aliphatic secondary O-H (1,081 cm^{-1}) and aliphatic primary O-H (1,030 cm^{-1}) were calculated in order to estimate the concentration of the hydroxyl groups; the data are presented in Table 4.12.

Table 4.12 Normalised absorbance for specified hydroxyl groups for as-received and acid-treated lignin.

Lignin samples	O-H (3,390 cm^{-1})	Phenolic O-H (1,365 cm^{-1})	Aliphatic secondary O-H (1,081 cm^{-1})	Aliphatic primary O-H (1,030 cm^{-1})	Total O-H content
As-received lignin	0.73	0.60	0.65	0.70	2.68
pH 6	0.62	0.58	0.63	0.75	2.58
pH 4	0.64	0.57	0.62	0.73	2.56
pH 2	0.65	0.56	0.59	0.71	2.50

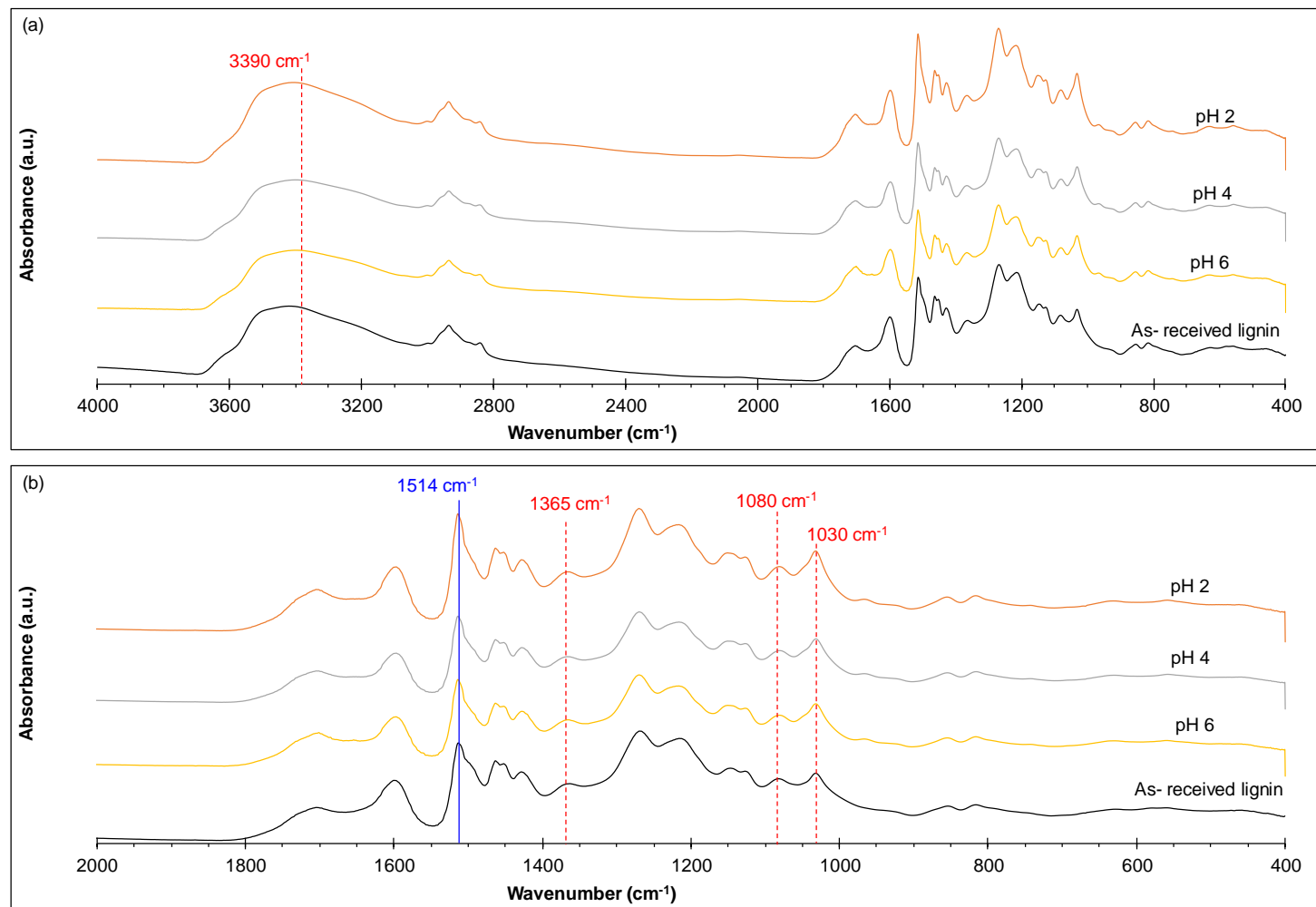


Figure 4.18 FTIR spectra for as-received and acid-treated lignins: (a) whole spectral range; (b) enlarged view from 1800- 600 cm^{-1} .

A drop in the total concentration of hydroxyl groups was found in the acid-treated samples. It is seen that the phenolic O-H and aliphatic secondary O-H concentration decreased with increasing acidic level. These results agree with that reported by Yasuda *et al.* [122,122] who stated that the acid treatment reduces the hydroxyl groups, especially in the aliphatic O-H. They proposed a reaction scheme to account for the reduction in the hydroxyl concentration after the acid treatment of lignin; see Figure 4.19.

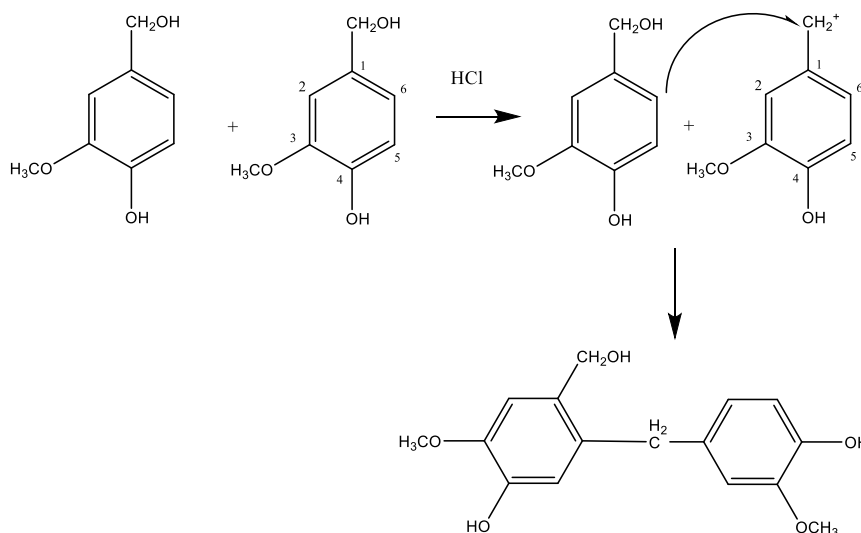


Figure 4.19 A mechanism for the reaction between HCl and two lignin units [121,122].

4.4 Molecular Weight Fractionation of As-received BioChoice® Lignin Using Acetone

The common processes that are used for molecular weight fractionation of lignin are ultra-filtration [130,132,245,273] and solvent fractionation [29,124,146,215]. In Section 4.3, a detailed account was presented on the consequences of treating lignin with acidified water to remove inorganic contaminants. In the current section, the merits of fractionating lignin with acetone was investigated as a means for removing the inorganic components. Since the fibre formation experiments undertaken in this study required a soluble solution, acetone was selected on the basis of cost, low toxicity and recoverability.

4.4.1 Fractionation Yield

The procedure for the fractionation of lignin using acetone is presented in Section 3.3.2. The yield after fractionation was calculated using the ratio of the dried mass of acetone-soluble lignin to the dried mass of as-received lignin. The yields for the soluble and insoluble acetone fractionated lignins are $57.4 \pm 0.6\%$ and $41.7 \pm 0.5\%$, respectively. The total recovered lignin ($99.1 \pm 0.6\%$) is below 100% due to the losses during the experiment. The yield of soluble fractionation correlates well to the solubility between lignin and solvent which have been reported [98,120,124,274,275]. For instance, the fractionation yields obtained from solvents such as tetrahydrofuran, methanol and 2-butanone are 62%, 40% and 21%, respectively [124]. These fractionation yields correlated with the Flory-Huggins polymer-solvent interaction parameter. The yields of soluble fraction from various organic solvents decreased with decreases solubility parameters [98].

4.4.2 Characterisation of Lignins Obtained from Fractionation Using Acetone

After fractionation, two types of lignins were obtained: acetone-soluble lignin and acetone-insoluble lignin. The characteristics of the two lignins are discussed in the following sections.

4.4.2.1 Physical Characteristics of Acetone-soluble and Acetone-insoluble Lignins

Figure 4.20 shows SEM micrographs of acetone-soluble lignin and acetone-insoluble lignin. Irregular shapes and sharp-edged lignin particles were observed. A smooth surface can be seen, and this differs from as-received lignin (see Figure 4.2) showing round granules on the surface. The smoother surface observed on the lignin

obtained from fractionation is attributed to the process used to obtain the lignins. In the solvent fractionation process, acetone was removed and recovered by solvent evaporation, therefore, the lignin had to be ground into powder, whereas the as-received lignin was separated by acid precipitation.

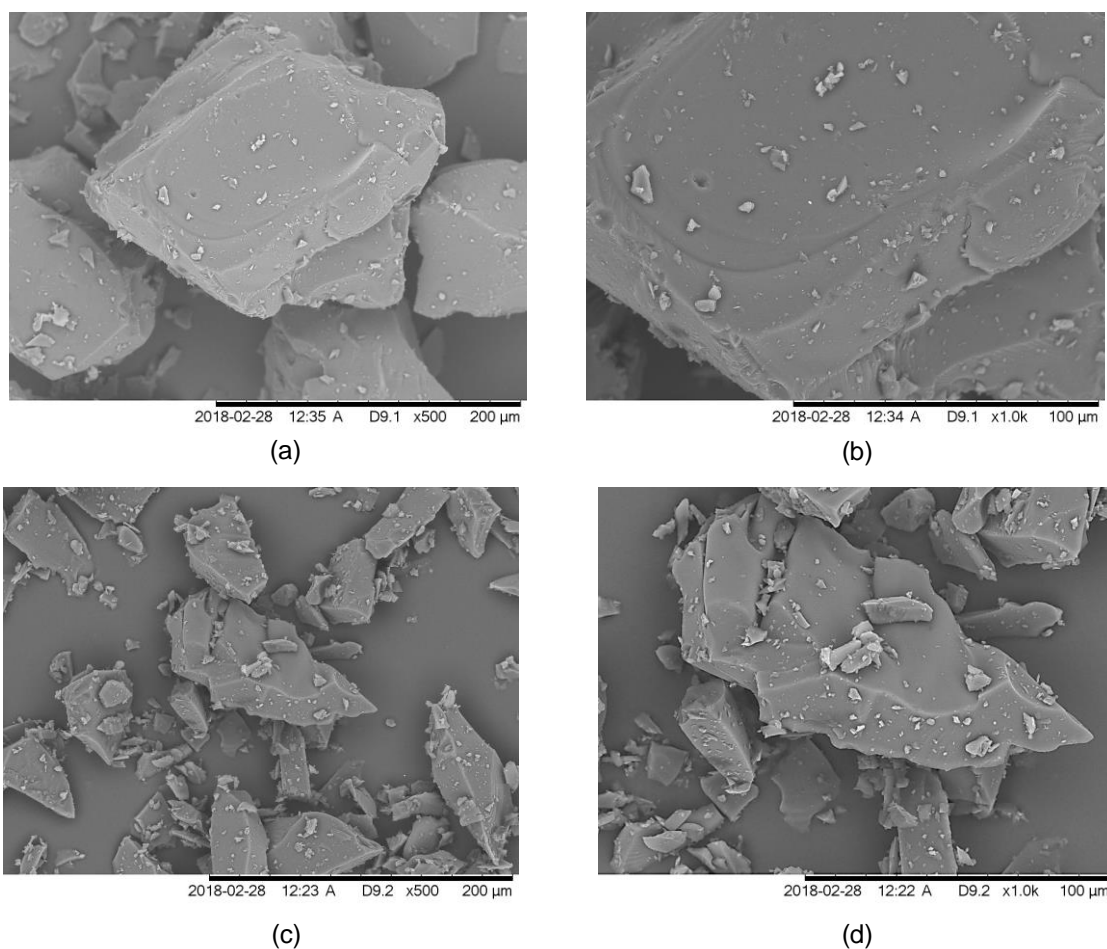


Figure 4.20 SEM micrographs of acetone-soluble lignin ((a) and (b)) and acetone-insoluble lignin ((c) and (d)).

4.4.2.2 Molecular Weight Distribution of Acetone-soluble and Acetone-insoluble Lignins

Figure 4.21 illustrates the molecular weight distributions for the as-received, acetone-soluble and acetone-insoluble lignins.

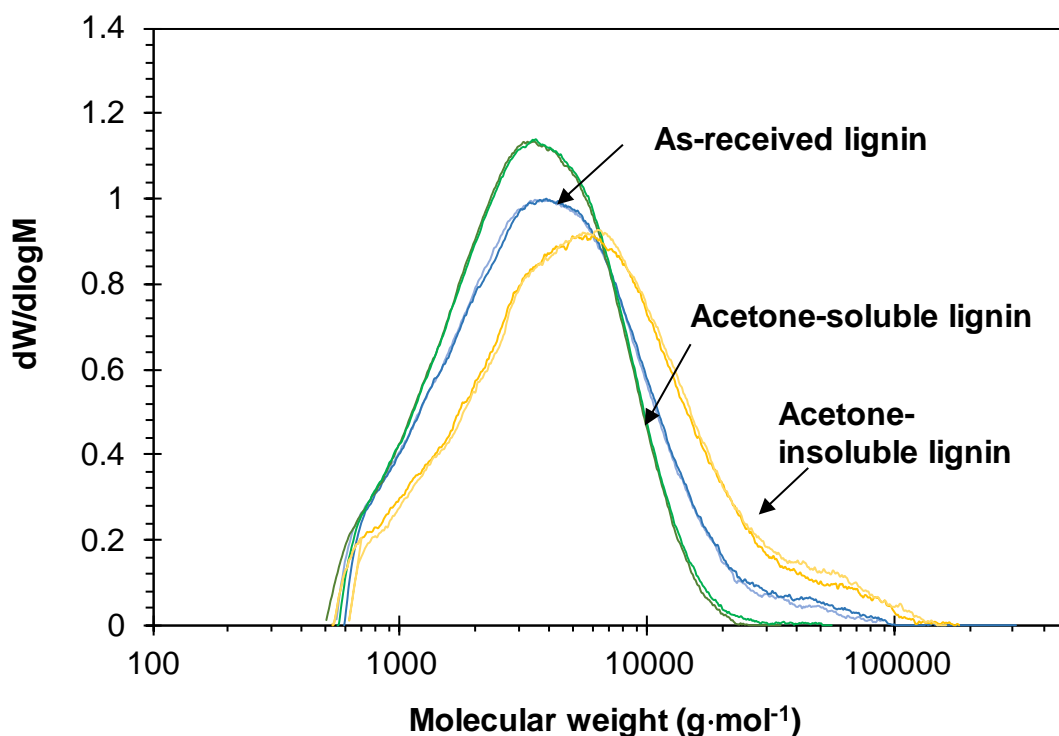


Figure 4.21 Molecular weight distribution curves for as-received, acetone-soluble and acetone-insoluble lignins determined using GPC.

The acetone-soluble fraction shows the narrowest molecular weight distribution, and the shoulder corresponding to the high molecular-weight component has diminished. The acetone-soluble lignin has a weight-average molecular weight (M_w) of $4,250 \text{ g}\cdot\text{mol}^{-1}$ which is 29% less than that of the as-received lignin ($6,000 \text{ g}\cdot\text{mol}^{-1}$), whereas acetone-insoluble lignin has the highest M_w of $9,600 \text{ g}\cdot\text{mol}^{-1}$. Similarly to other reports [31,83,85,98,124,276], the results of which are presented in Table 4.13, a lower molecular weight was expected from the solvent-soluble fraction. On the other hand, an increase in both M_w and M_n in acetone-insoluble lignin compared to the as-received lignin has been reported in the literature, as shown in Table 4.13. The increase in the M_w and M_n in the insoluble fraction was said to be due to aggregation occurring in the lignin solutions [31,83,85]. This may be the reason for the molecular weight distribution curves of the acetone-insoluble lignin shows a small

but a clear shoulder at the high-molecular weight region and a broad molecular weight distribution as shown in Figure 4.21.

The PDIs of acetone-soluble and acetone-insoluble lignins are presented in Table 4.13. The lowest and highest PDIs were found in the acetone-soluble lignin and acetone-insoluble lignin, respectively. The reduced PDI found in acetone-soluble lignin indicates a narrower molecular weight distribution; this implies an improvement in the homogeneity in molecular weight distribution [34,124]. On the other hand, an increase in PDI was observed for the acetone-insoluble lignin as compared to that of the as-received and acetone-soluble lignins. It can be said that the acetone-insoluble lignin has a heterogeneity in molecular weight distribution.

Table 4.13 Summary of the molecular weight distributions and the T_{g2} for as-received, acetone-soluble and -insoluble lignins and compiled molecular weight results.

Lignin samples	M_w (g·mol ⁻¹)	M_n (g·mol ⁻¹)	PDI	T_{g2} (°C)
Current work				
As-received lignin	6,000 ± 283	2,700 ± 141	2.22 ± 0.22	163.0 ± 1.5
Acetone-soluble lignin	4,250 ± 71	2,450 ± 71	1.73 ± 0.07	145.8 ± 0.3
Acetone-insoluble lignin	9,600 ± 566	3,400 ± 141	2.82 ± 0.28	189.1 ± 0.4
Data from the literature				
Indulin AT lignin [124]	4,680	1,980	2.4	157
Methanol-soluble Indulin AT lignin [124]	2,910	1,610	1.8	109
Methanol-insoluble Indulin AT lignin [124]	8,390	3,500	2.4	173
Softwood Kraft lignin [276]	6,000	1,500	4	153
Acetone-soluble softwood Kraft lignin [276]	3,500	1,000	3.5	114

Lignin samples	M_w (g·mol⁻¹)	M_n (g·mol⁻¹)	PDI	T_{g2} (°C)
Acetone-insoluble softwood Kraft lignin [276]	14,000	2,121	6.6	170
Softwood Kraft lignin [83]	7,190	2,360	3.05	153
Methanol-soluble softwood Kraft lignin [83]	3,000	1,590	1.90	117
Methanol-insoluble softwood Kraft lignin [83]	14,900	6,520	2.28	211
Softwood Kraft lignin [85]	4,100	2,100	2.0	N/A
Acetone-soluble softwood Kraft lignin [85]	1,100	1,600	1.4	N/A
Acetone-insoluble softwood Kraft lignin [85]	18,900	3,400	5.6	N/A
Softwood Kraft lignin [31]	4,130	2,080	2.0	N/A
Aqueous acetone-soluble softwood Kraft lignin [31]	2,260	1,390	1.6	N/A
Aqueous acetone-insoluble softwood Kraft lignin [31]	11,230	2,590	4.3	N/A

The molecular weight and polydispersity data obtained in the current study show a good correlation with those reported in the literature, as shown in Table 4.13. The soluble fraction is shown as a lower molecular weight distribution and polydispersity compared to the parent lignin. It is still unclear with regard to the correlations between lignin's chemical structure, its molecular weight, its "spinnability" and the properties of the resultant carbon fibres. However, recent reports, concerning fractionation technologies have reported that the lignin with a lower PDI and lower M_w can be used to produce the fibre. Moreover, the resultant carbon fibre shows an improvement in spinnability and mechanical properties [277–280]. For instance, carbon fibres produced from fractionated alkaline lignin with an uniform molecular weight distribution exhibited a two-fold increase in the tensile modulus [280]. A similar trend has been reported, where the elastic modulus of lignin/PAN carbon fibres increased from 16 GPa to 22 GPa when PDI decreased from 5 to 2 [278].

In the current work, acetone-soluble lignin was found to have lower PDI as compared to as-received lignin. It can be said that fractionation using acetone can be a potential procedure to improve the homogeneity of molecular weight distribution of softwood Kraft lignin. Moreover, using acetone-soluble lignin as a bio-material for the production of fibres will be discussed in Chapter 5.

4.4.2.3 Determination of the Ash Content in Acetone-soluble and Acetone-insoluble Lignins and Their Elemental Compositions

The ash content of the lignins was determined using the procedures described in Section 3.2.3.2 where the sample was oxidised in an air-circulating furnace at 525 °C for four hours. The ash content was calculated using Equation 3.2.

The ash contents in the as-received and acetone-soluble fraction are $1.195 \pm 0.021\%$ and $0.055 \pm 0.021\%$, respectively and in the acetone-insoluble fraction is $2.395 \pm 0.034\%$. The decrease in ash content of acetone-soluble lignin and the increase in ash content of acetone-insoluble lignin show a similar trend to the data from the literature [31,281,282]. The ash content from the soluble-fraction was reduced when compared to the parent lignins, whereas the ash content in

the insoluble-fraction was increased. The bar-graph presented in Figure 4.22 shows the ash content of acetone-soluble and acetone-insoluble lignins calculated based on the as-received lignin. It shows clearly that the inorganic compounds are retained in the acetone-insoluble lignin.

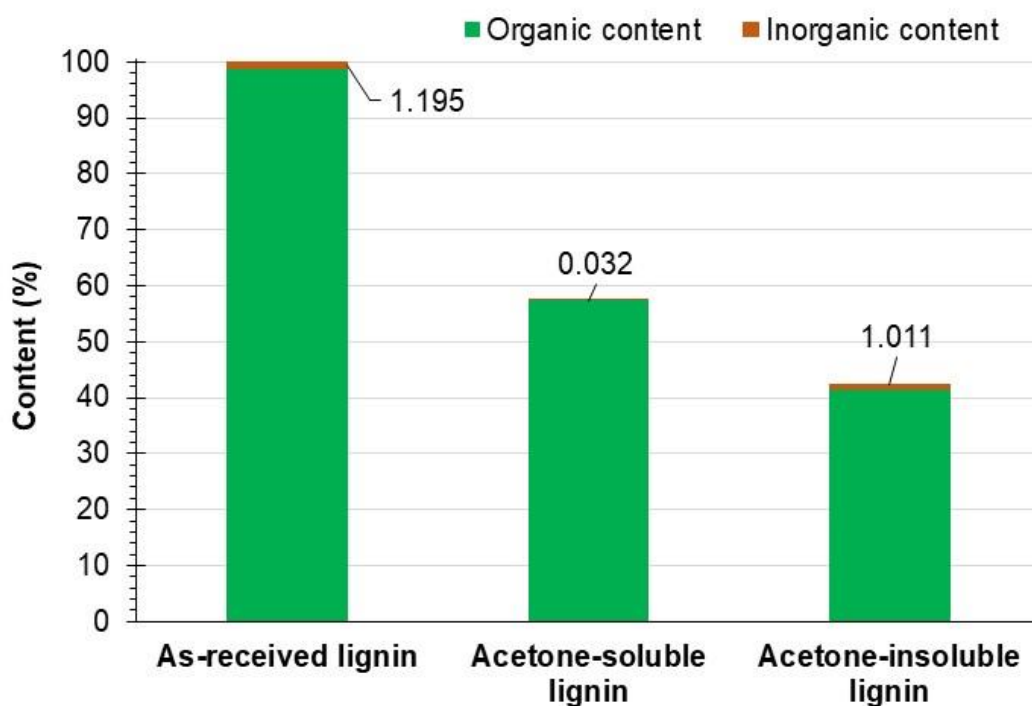


Figure 4.22 Ash or inorganic content calculated based on the as-received lignin.

The EDX facility on the SEM was used to determine the elemental composition of the ash from the acetone-soluble and acetone-insoluble lignins, and the data are presented in Figure 4.23. The acetone-soluble lignin, with an ash content of $0.055 \pm 0.021\%$, shows sulphur and sodium as the two main inorganic elements present at 0.024 wt% and 0.02 wt%, respectively. A similar trend was found in the acetone-insoluble lignin. Sulphur and sodium are the two major components which constitute 1.134 wt% and 1.015 wt%, respectively. The presence of silicon and potassium in acetone-soluble lignin is 0.008%. The highest amounts of magnesium, silicon and potassium were found in the acetone-insoluble lignin. It can be concluded that the inorganic impurities do not tend to dissolve in acetone.

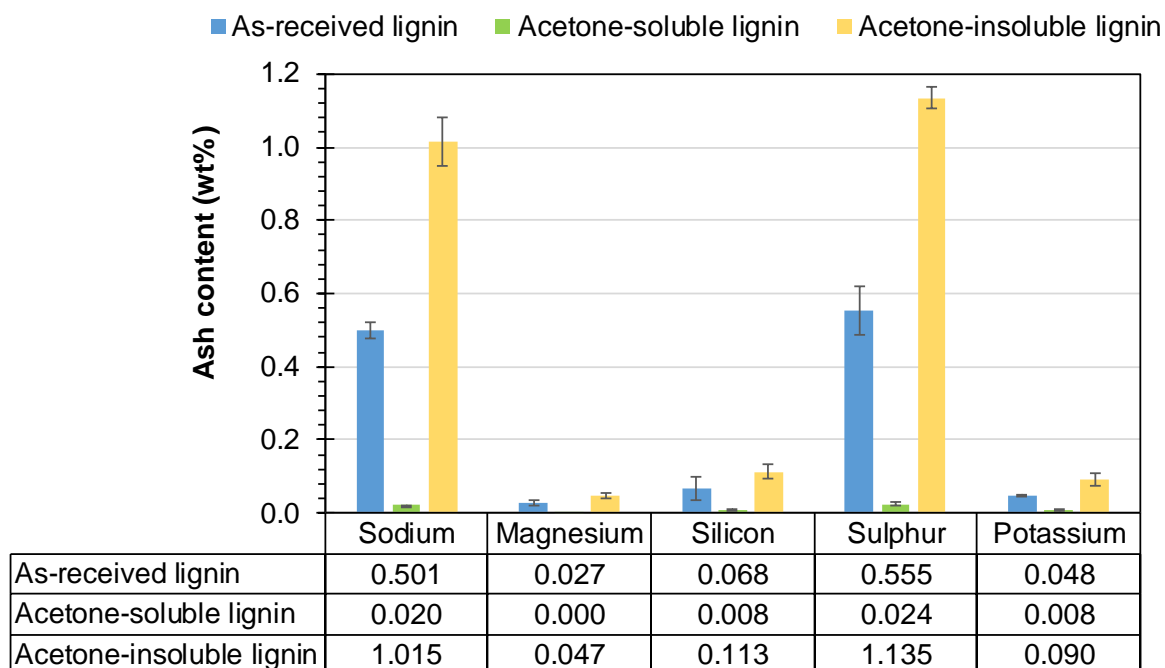
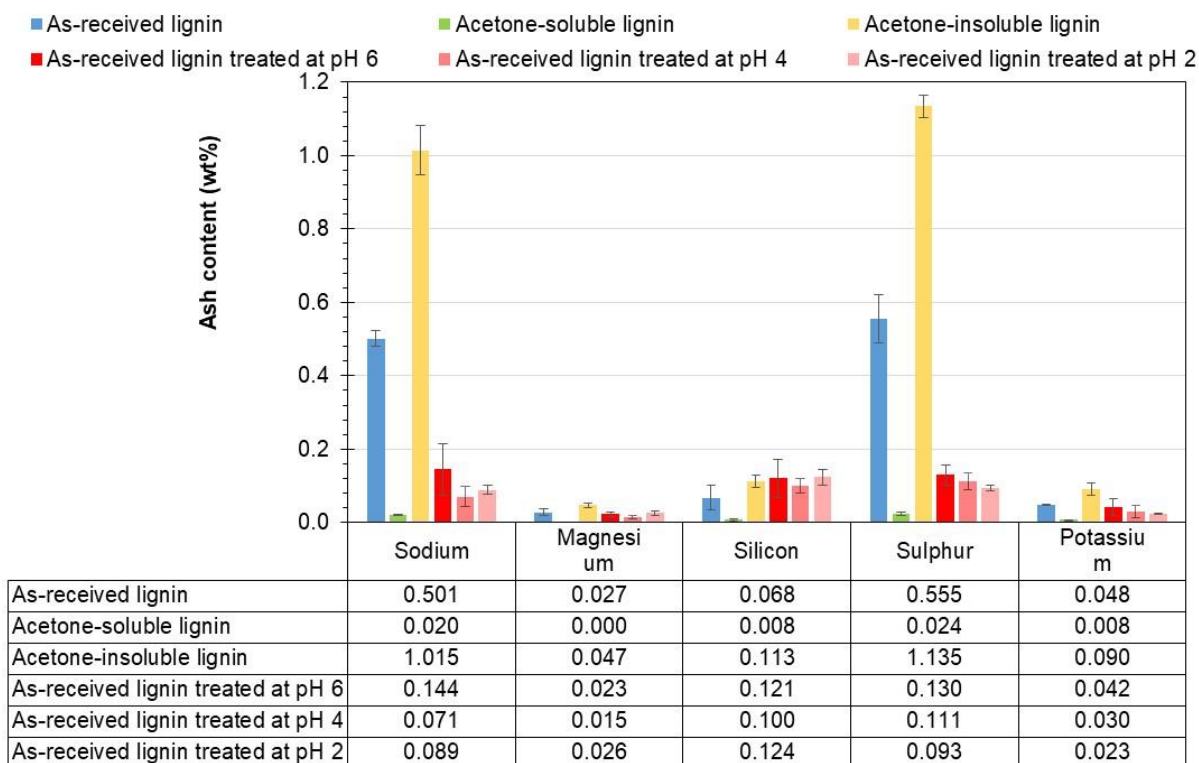
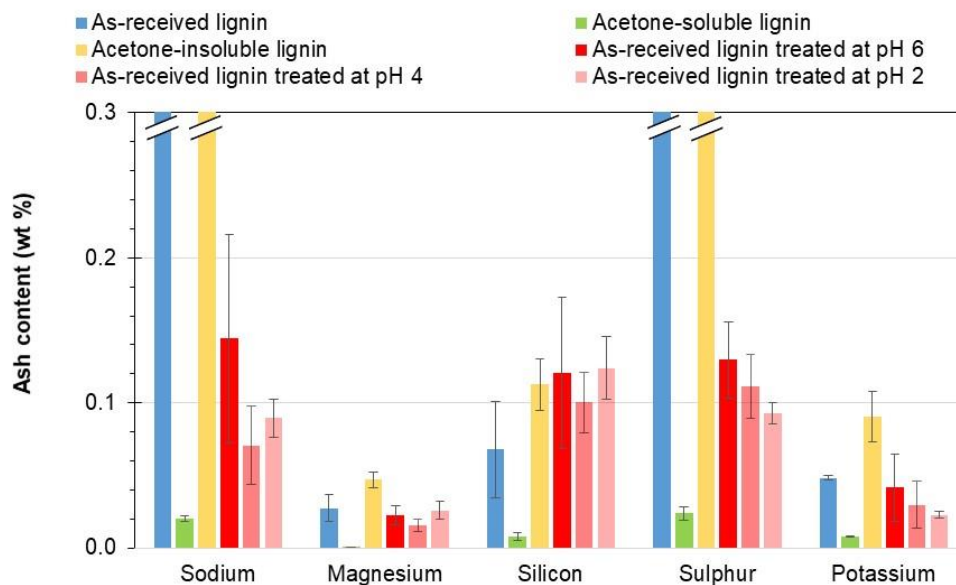


Figure 4.23 Inorganic elements found in the ash from: as-received lignin; acetone-soluble lignin; and acetone-insoluble lignin.

For comparison, as-received lignin was characterised and used as the reference point or benchmark for subsequent treatments carried out in this work. This includes (a) treating with acidified water; and (b) molecular weight fractionation using acetone. Figure 4.24 (a) shows the ash content found in lignin sample analysed in this work; the elements (sodium, magnesium, silica, sulphur and potassium) and their compositions are presented. The acetone-insoluble lignin has the highest content of each element and their contents are higher than those in the as-received lignin. On the other hand, the lowest ash content can be seen for the acetone-soluble lignin sample. The treatment using acidified water, i.e. lignin treated with acidified water (pH 2, pH 4 and pH 6), is significantly lower in sodium, sulphur and potassium when compared to the as-received lignin. The reduction of sodium and potassium has been ascribed as being due to the removal of alkaline ions by hydrolysis [270–272].



(a)



(b)

Figure 4.24 Elements and their contents detected in lignin samples used in this current study: (a) full view of the ash content from 0 to 1.2% and (b) enlarged view of a maximum ash content of 0.3%.

An enlarged view of the ash contents is displayed in Figure 4.24 (b) where a small amounts of the elements were detected in the acetone-soluble lignin, which can be explained by the fact that inorganic elements not being soluble in an organic solvent. Furthermore, the inorganic elements remain in the insoluble-fraction, which causes increases in the ash content in the insoluble-fraction [31,282]. In the case of treatment using acidified water, the concentration of sodium and sulphur is significantly reduced by 72% and 77%, respectively compared to those found in the as-received lignin.

Figure 4.25 shows the ash content of the lignin samples produced in this work. All the treated samples, except for the acetone-insoluble lignin are lower in ash content compared to the as-received lignin ($1.195 \pm 0.021\%$). The lowest ash content is seen in the acetone-soluble lignin ($0.055 \pm 0.021\%$), whilst the lignins from the acidified water treatment show the lowest ash content for the lignin that was treated with pH4 ($0.328 \pm 0.065\%$).

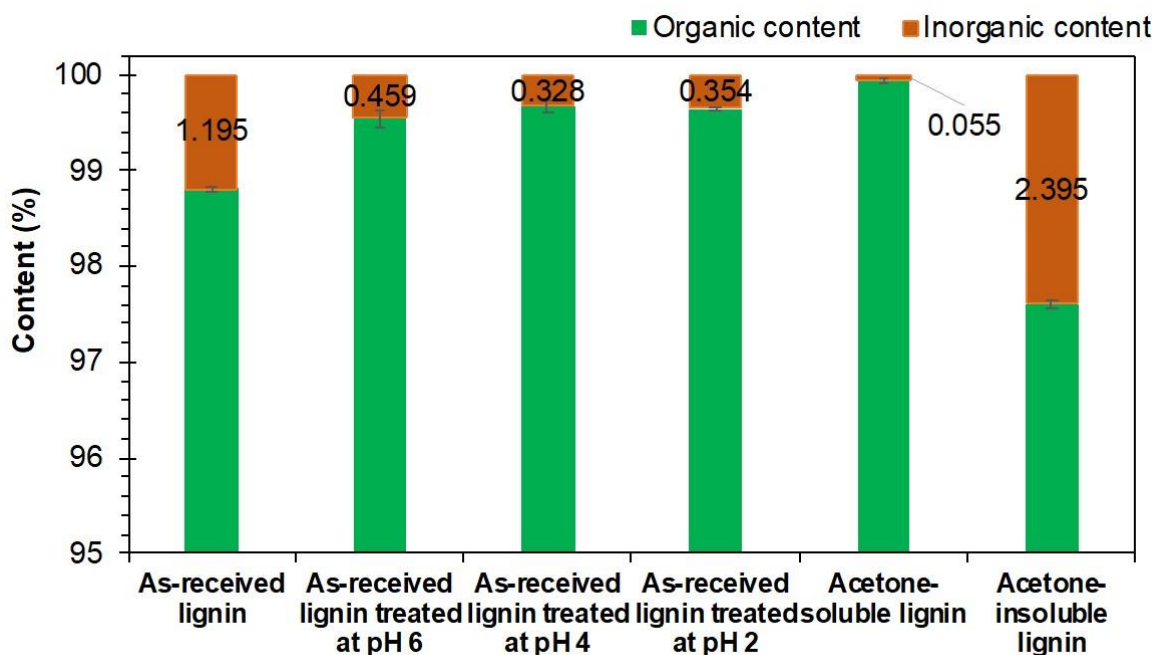


Figure 4.25 Ash content in the lignin samples determined in this current study in accordance with the TAPPI T211 om-02 standard.

The amount of inorganic content detected in lignin has been mentioned as a concern as it may lead the formation of defect in the fibres and reduce the mechanical properties [18,64]. Moreover, elementals such as sodium and potassium are known to act as catalysts for the chemical cracking of lignin. Liquid product yield was observed to decrease when the inorganic content in the lignin decreased [107,283]. It has been reported that the addition of an alkaline additive such as NaOH, KOH can enhance the yield of liquid products [284]. The presence of inorganic salt accelerated the reaction and led to the formation of a low molecular weight product [285,286].

The evidence from literature indicates that inorganic present in lignin can lead to a deterioration in the mechanical properties, therefore in the current study the lignin with the lowest inorganic content was selected for the production of fibres. When comparing the two treatment techniques: (a) treating with acidified water; and (b) molecular weight fractionation using acetone, the latter is a more effective technique in terms of reducing the ash content. The low ash content of acetone-soluble lignin reported in this section and its homogeneity reported in Section 4.4.2.2, lead to the selection of acetone-soluble lignin for fibre production; this is discussed in Chapter 5.

4.4.2.4 Lignin Content of Acetone-soluble and Acetone-insoluble Lignins

The lignin content was calculated from the total acid-insoluble lignin (Klason lignin) and acid-soluble lignin, as shown in Table 4.14; the as-received lignin is taken as the reference point. The purity of lignin is based on the Klason and acid-soluble lignin. Acetone-soluble lignin shows a total lignin content of $98.4 \pm 2.3\%$ and other components can be assigned to inorganic and carbohydrates [34,97,245]. A significant increase in acid-soluble lignin content was seen for the acetone-soluble lignin, compared to that for the as-received lignin, which increased from $4.45 \pm 0.01\%$ to $7.20 \pm 0.05\%$. This could be attributed to the low molecular weight component contained in acetone-soluble lignin. Similar results have been reported in the literature [34,85] which are compiled in Table 4.14. On the other hand, the content of acid-soluble lignin in the acetone-insoluble lignin decreased from $4.45 \pm 0.01\%$ to $3.68 \pm 0.01\%$.

Table 4.14 A summary of the lignin content in as-received, acetone-soluble and acetone-insoluble lignins.

Lignin samples	Klason lignin (%)	Acid-soluble lignin (%)	Lignin content (%)
Current work			
As-received lignin	92.7 ± 0.9	4.45 ± 0.01	97.2 ± 0.8
Acetone-soluble lignin	91.2 ± 2.3	7.20 ± 0.05	98.4 ± 2.3
Acetone-insoluble lignin	91.1 ± 1.2	3.68 ± 0.01	94.8 ± 1.2
Data from the literature			
IndulinAT lignin [34]	91.0 ± 0.4	2.51 ± 0.1	93.5 ± 0.5
Methanol-soluble Indulin AT lignin [34]	90.8 ± 0.8	3.13 ± 0.1	93.9 ± 0.8
Methanol-insoluble Indulin AT lignin [34]	90.8 ± 0.0	1.13 ± 0.1	92.1 ± 0.1
Softwood Kraft lignin [85]	92.3	2.5	94.8
Acetone-soluble softwood Kraft lignin [85]	64.4	16.9	80.9
Ethanol-soluble softwood Kraft lignin [85]	57.0	20.5	87.5

From the characterisations of the lignins obtained from fractionation using acetone, the acetone-soluble lignin has the lowest ash content ($0.055 \pm 0.021\%$) and the highest molecular weight homogeneity (PDI of 1.73 ± 0.07) and a lignin content of $98.4 \pm 2.3\%$. These again support the selection of acetone-soluble lignin as the material for the fibre formation. Other relevant properties of acetone-soluble lignin were characterised and are discussed in the following section.

4.4.2.5 Thermo-gravimetric Analysis of Acetone-soluble and Acetone-insoluble Lignins

Figure 4.26 and Figure 4.27 show the TGA and DTG data for acetone-soluble and acetone-insoluble lignins. Various distinct mass-loss stages were observed in both lignins. For comparison, the as-received lignin was used as a reference; the same four stages of mass-loss were applied for these two lignins. In the first stage, a small mass-loss of approximately 1-2% is seen below 150 °C. This was found in both the lignins. Figure 4.26 (b) displays an enlarged view of the first stage region for acetone-soluble lignin; the DTG curve displays a peak at 64.6 °C with the mass-loss rate of 0.3 %/°C and an endset DTG around 120 °C. Acetone-insoluble lignin shows a DTG peak at 72.1 °C and the endset DTG is around 135 °C. These two values are higher than those of acetone-soluble lignin, as shown in Figure 4.27 (b). This implies that the acetone-insoluble lignin rather than the acetone-soluble lignin may have a higher affinity for water. This statement is supported by the mass-loss rate of acetone-insoluble lignin which dropped from 0.3 %/°C for acetone-soluble lignin to 0.2 %/°C for acetone-insoluble lignin.

In the second stage, between 150 °C and 310 °C, the residual mass of acetone-soluble and acetone-insoluble lignins at 310 °C are $88.1 \pm 2.4\%$ and $89.9 \pm 0.9\%$, respectively.

The major mass-loss was found in the third stage, between 310 °C and 600 °C. In this stage, the mass-loss rates for acetone-soluble and acetone-insoluble lignin are $3.1 \pm 0.2\%$ and $2.9 \pm 0.2\%$. The mass-loss in this stage is 42.3% for acetone-soluble and 37.6% of acetone-insoluble lignin. The residual mass at 600 °C for acetone-soluble lignin ($45.5 \pm 2.8\%$) lower than that of acetone-insoluble lignin ($55.2 \pm 5.1\%$) and as-received lignin ($56.0 \pm 4.1\%$). The mass-loss and DTG curves of as-received lignin are overlaid with lignins obtained from fractionation using acetone, as displayed in Figure 4.28. The results from the TGA results are compiled in Table 4.15. The highest mass-loss rate was found for the acetone-soluble lignin. This trend correlates well with the results reported in the literature, which are summarised in Table 4.15 [34,98,124].

In the fourth stage above 600 °C the decrease in mass-loss rate was clearly observed in both acetone-soluble and acetone-insoluble lignins and are similar to the as-received lignin. The mass-loss for all three lignins (as-received, acetone-soluble and acetone-insoluble) is in the range of 8% to 10%, and the acetone-soluble lignin shows the highest mass-loss rate of 0.35 %/°C, as shown in Figure 4.28 (b). The lowest residual mass at 900 °C was exhibited in acetone-soluble lignin ($36.5 \pm 1.4\%$), whilst the residual masses of acetone-insoluble and as-received lignin are $41.0 \pm 3.7\%$ and $45.0 \pm 1.2\%$, respectively. The decrease in residue mass of the soluble-fraction lignin as compared to the parent lignin has been reported previously in the literature [34,98,124].

The residual char was calculated using the residual mass from TGA subtracted with the ash content analysed in accordance with the TAPPI T211 om-02 standard. The highest residual char was found for the as-received lignin which is $43.8 \pm 1.2\%$. After fractionation using acetone, the acetone-soluble and acetone-insoluble lignins have residual char content of $36.4 \pm 1.4\%$ and $38.6 \pm 3.7\%$, respectively.

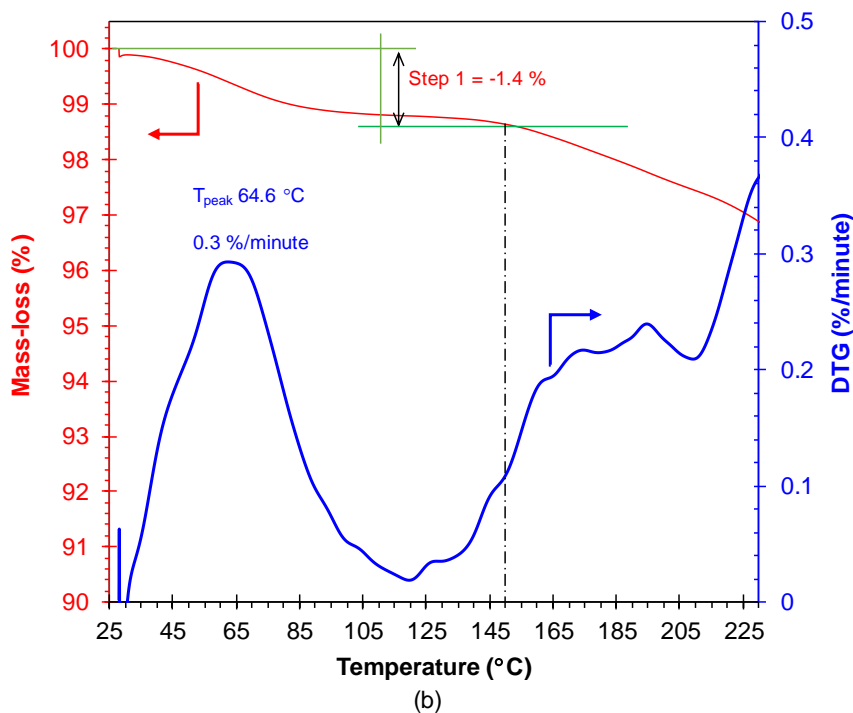
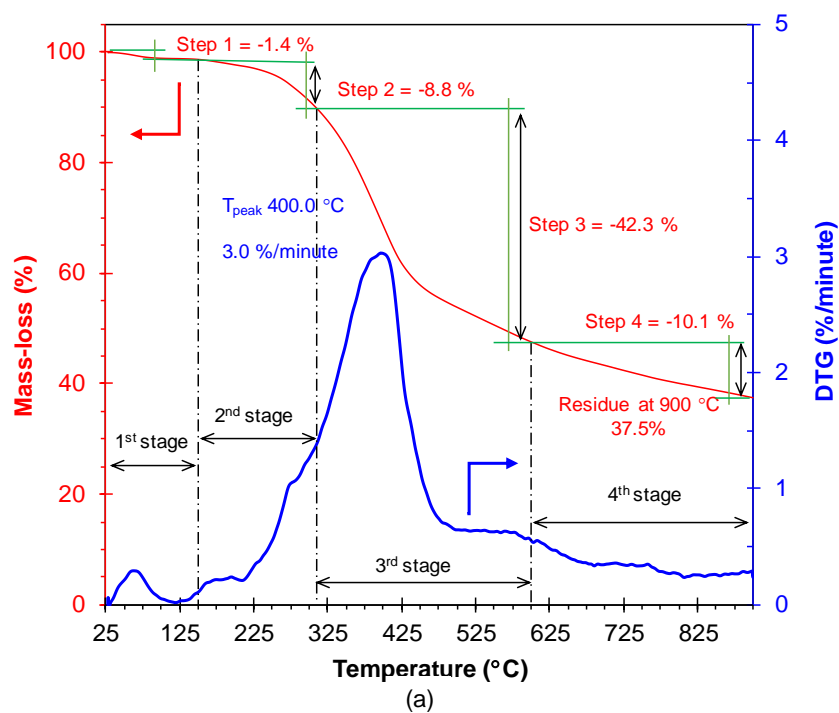
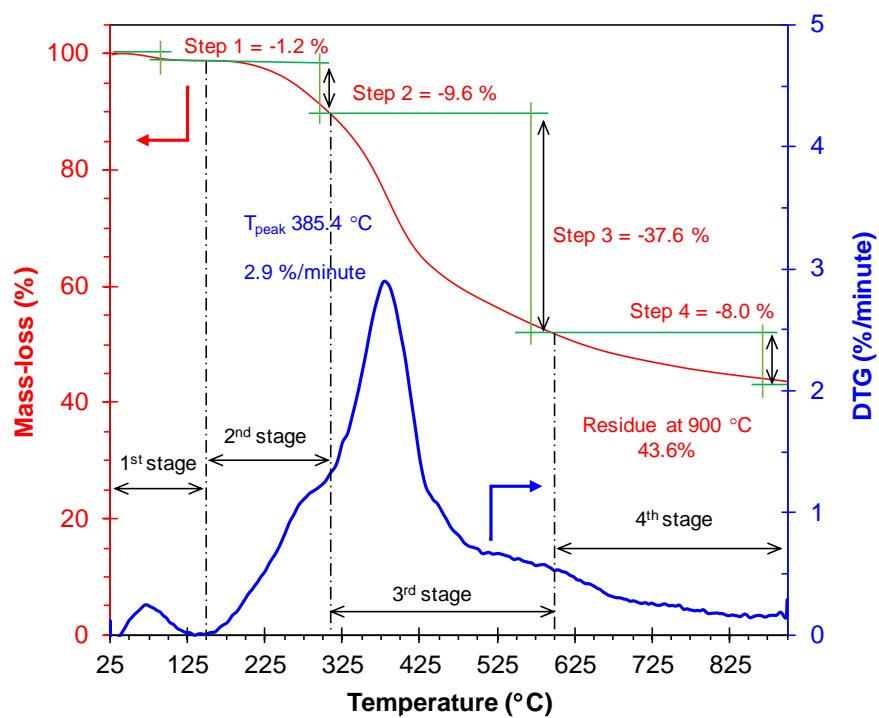
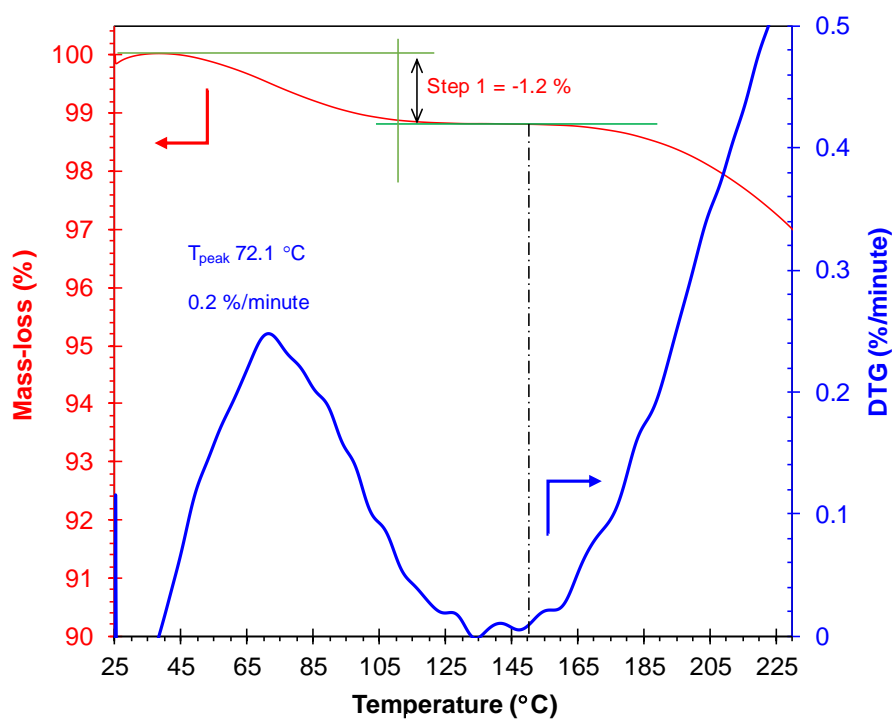


Figure 4.26 TGA and DTG curves for acetone-soluble lignin: (a) the thermal decomposition range from 25 °C to 900 °C divided into four main stages; and (b) enlarged view of the first stage.



(a)



(b)

Figure 4.27 TGA and DTG curves for acetone-insoluble lignin: (a) the thermal decomposition range from 25 °C to 900 °C divided into four main stages; and (b) enlarged view of the first stage region.

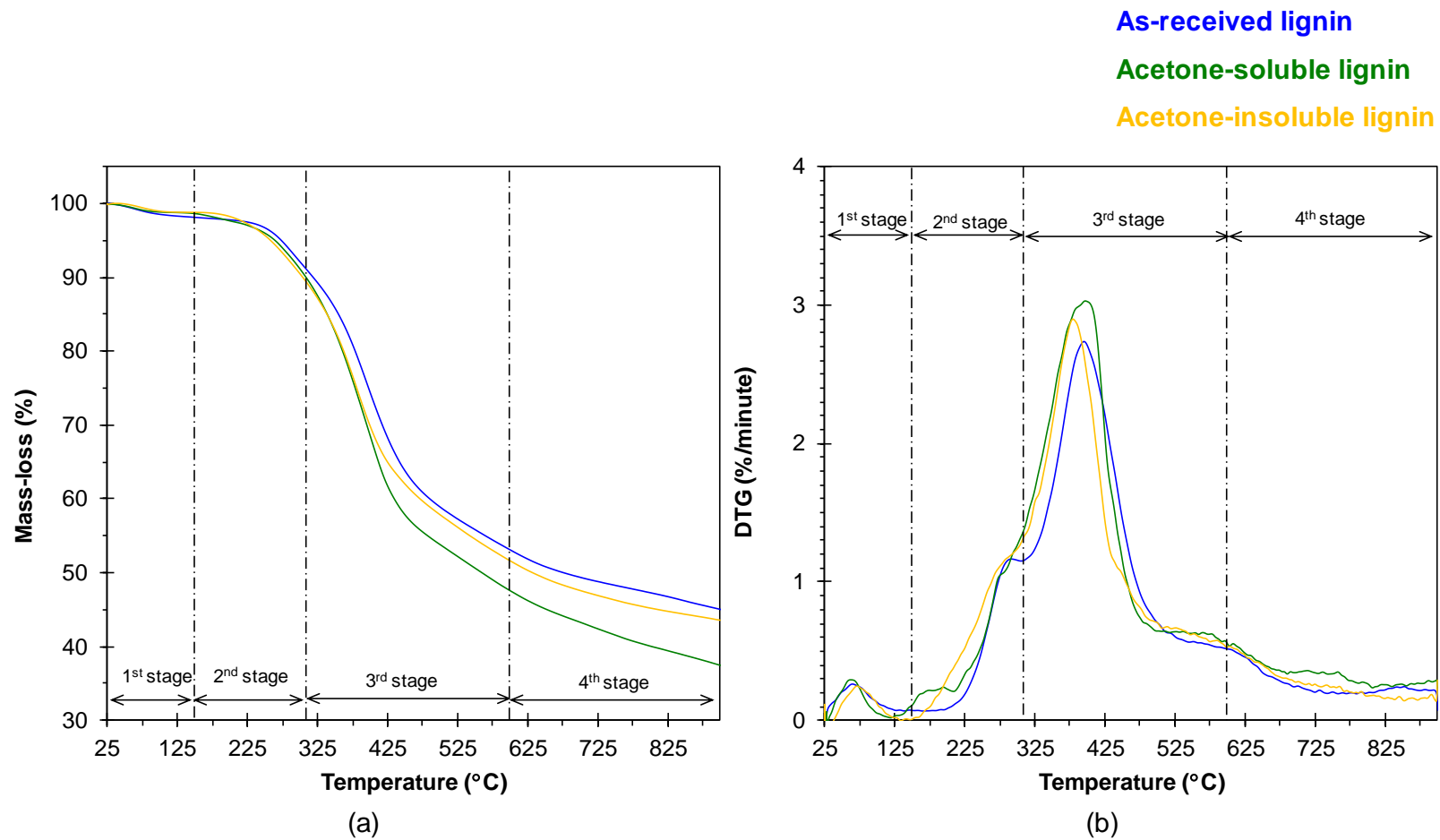


Figure 4.28 Overlaid TGA and DTG curves for pre-dried as-received lignin, acetone-soluble lignin and acetone-insoluble lignin: (a) and (b) the thermal decomposition range from 25 °C to 900 °C divided into four main stages.

Table 4.15 Compiled TGA results for as-received lignin and lignin from acetone fractionation. The TGA experiment conducted from 25 to 900 °C and heating rate 10 K·minute⁻¹ under an argon with a flow rate of 50 ml·minute⁻¹.

Lignin samples	Residual mass (%)				T _{50%} (°C)	T _{DTG, max} (°C)	Maximum mass- loss rate (%/°C)
	1 st stage (25-150 °C)	2 nd stage (150-310 °C)	3 rd stage (310-600 °C)	4 th stage (600-900 °C)			
Current work							
Pre-dried as-received lignin	98.0 ± 0.2	90.8 ± 0.3	56.0 ± 4.1	45.0 ± 1.2	675	391.5 ± 10.9	2.6 ± 0.1
Acetone-soluble lignin	97.5 ± 1.7	88.1 ± 2.4	45.5 ± 2.8	36.5 ± 1.4	559	393.6 ± 10.8	3.1 ± 0.2
Acetone-insoluble lignin	98.3 ± 0.7	89.9 ± 0.9	55.2 ± 5.1	41.0 ± 3.7	630	387.8 ± 5.8	2.9 ± 0.1
Data from the literature							
IndulinAT lignin [124]	98	86	52	48*	711	334	0.2
Methanol-soluble Indulin AT lignin	96	66	42	40*	434	313	0.2
Methanol-insoluble Indulin AT lignin	95	82	55	43*	652	329	0.18

Lignin samples	Residual mass (%)				T _{50%} (°C)	T _{DTG, max} (°C)	Maximum mass- loss rate (%/°C)
	1 st stage (25-150 °C)	2 nd stage (150-310 °C)	3 rd stage (310-600 °C)	4 th stage (600-900 °C)			
Softwood Kraft lignin [34]	98	89	50	35	600	384	4.5
Methanol-soluble softwood Kraft lignin	98	84	42	30	540	369	7.0
Methanol-insoluble softwood Kraft lignin	98	89	52	40	640	404	4.0
BioChoice [®] lignin [98]	97	87	45.2	45.2**	540	390	0.31
Methanol/acetone-soluble BioChoice [®] lignin	97	82	37.5	37.5**	420	375	0.4
Methanol/acetone-insoluble BioChoice [®] lignin	97	84	46.6	46.6**	540	360	0.23

Note: * The residual mass at 780 °C and ** The residual mass at 600 °C.

4.4.2.6 Differential Scanning Calorimetry of Acetone-soluble and Acetone-insoluble Lignins

The lignin samples were heated from 25 °C to 250 °C in the DSC in order to determine their T_g . A heating rate of 10 K·minute⁻¹ was used and three successive temperature scans were carried out as described in Section 3.4.5. Figure 4.29 shows DSC traces for the lignins obtained from fractionation using acetone. DSC traces for as-received lignin have been included to enable comparison. The same pattern was found in the DSC traces for these three lignins. The first heating scan shows a broad endothermic and a T_{g1} , but the endothermic peak disappeared in the second and third heating scans and a clear T_g was noticed.

The enthalpy of vaporisation for acetone-soluble lignin is 46.0 J·g⁻¹ which is significantly lower than that of acetone-insoluble lignin (96.9 J·g⁻¹) and as-received lignin (65.7 J·g⁻¹). This indicates the presence of moisture in the sample. This correlates with the analysis from the TGA results where a mass-loss of about 2- 2.5% was observed from 25 °C to 150 °C.

T_g s from three successive scans are plotted in Figure 4.30. The acetone-soluble lignin shows the lowest T_g , in all three heating scans, whereas acetone-insoluble lignin exhibits the highest T_g . T_g s data from the second heating scan of acetone-soluble and acetone-insoluble lignins are 145.8 ± 0.3 °C and 189.1 ± 0.4 °C, respectively whilst that for as-received lignin is 163.0 ± 1.5 °C. The reduction in T_g for lignin obtained from the soluble-fraction and the increase in T_g of the insoluble-fraction have been reported in the literature and they are compiled in Table 4.13 [29,83,124,276].

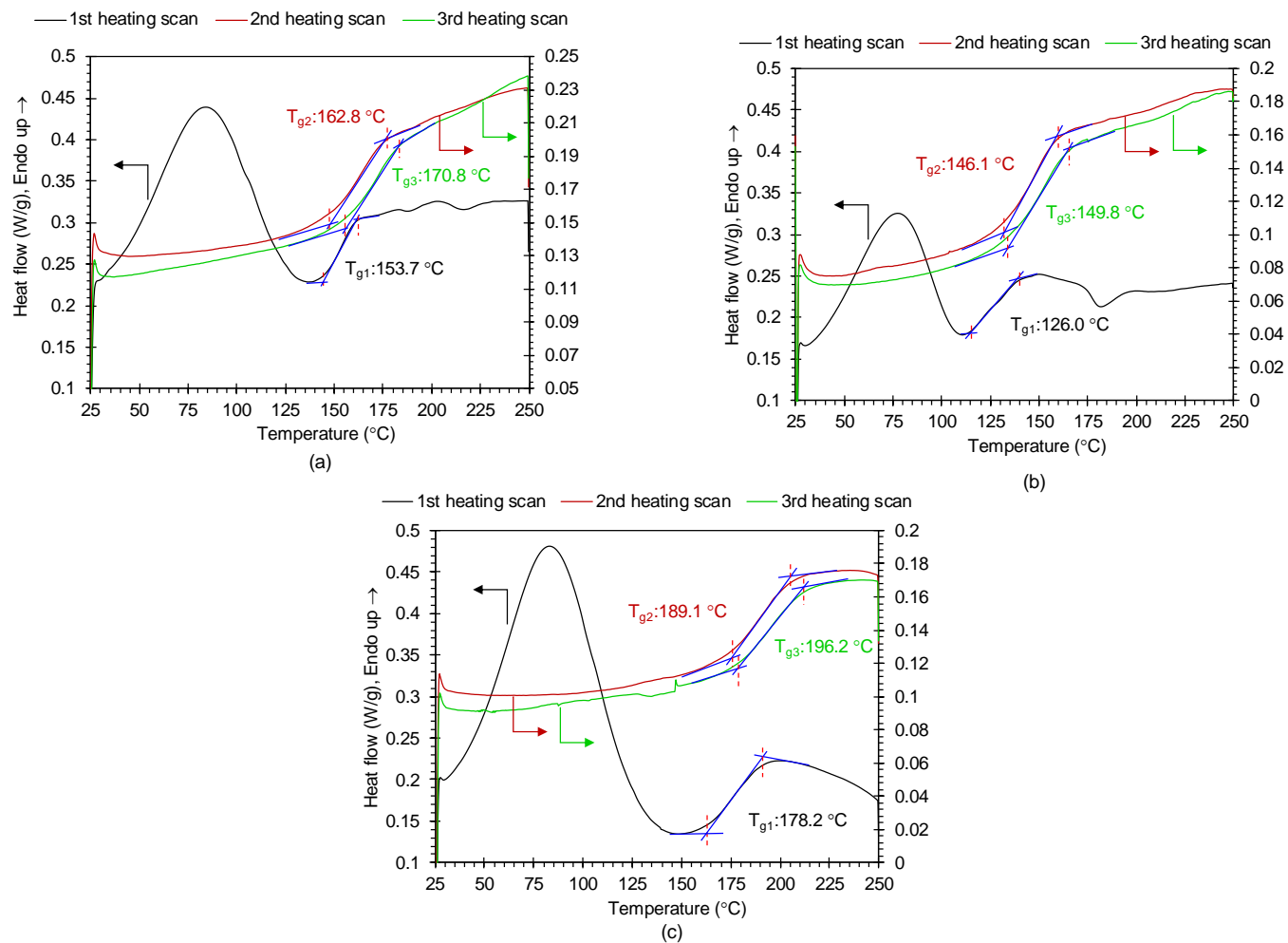


Figure 4.29 DSC thermograms for; (a) as-received lignin and lignins from fractionation using acetone; (b) acetone-soluble and (c) acetone-insoluble lignins.

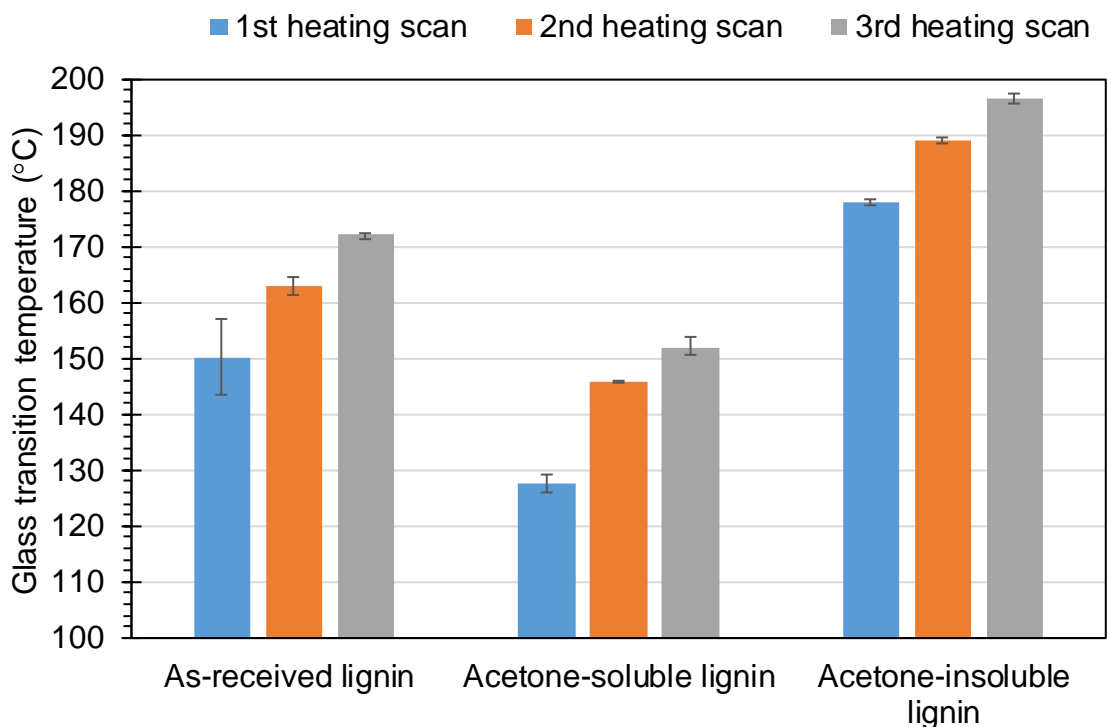


Figure 4.30 Glass transition temperatures analysed from as-received lignin and lignins obtained from fractionation using acetone.

Correlation between the T_g and M_w of lignins has been reported in the literature. In general the T_g increases with increasing M_w and a linear regression trend has been observed [29,83,124]. Figure 4.31 shows compiled T_g s and M_w for parent lignins and the lignins obtained from molecular weight fractionation. A linear correlation is seen. The red circles represent the T_g s of the as-received and the lignins from fractionation using acetone and these are plotted against the correspond M_w (determined by GPC) which are described in Sections 4.2.2 and 4.4.2.2. A linear relationship is observed where the correlation coefficient of determination (R^2) is 0.9944.

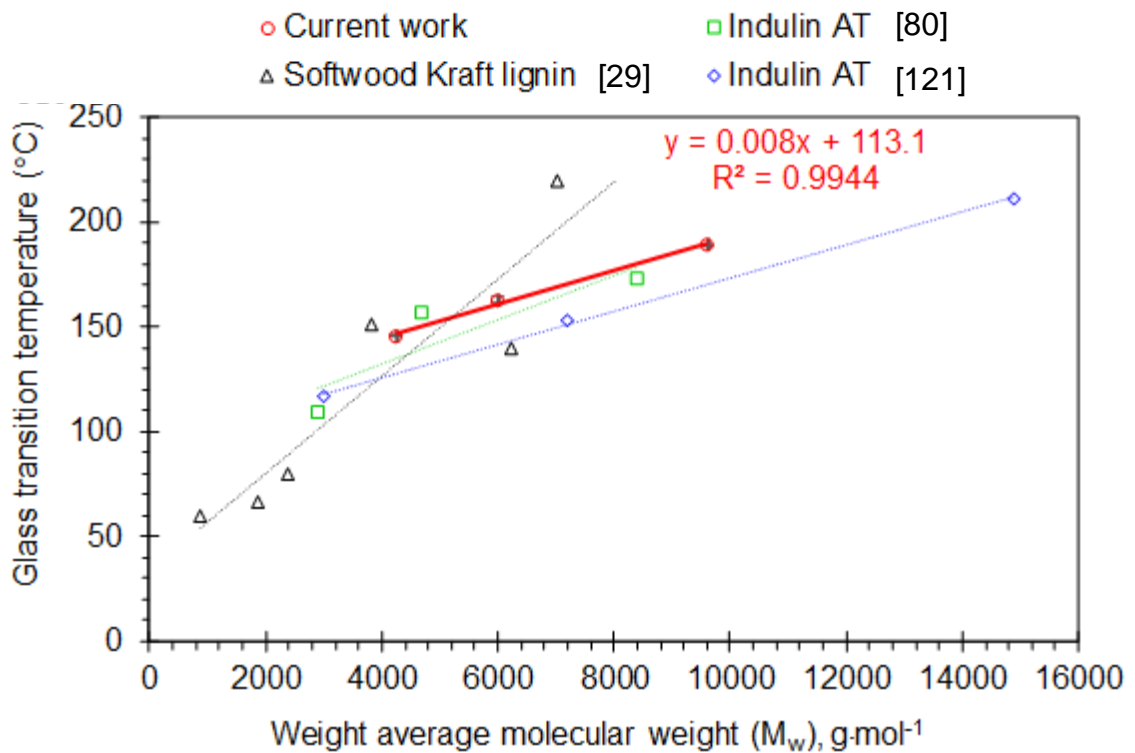


Figure 4.31 A plot of T_g s versus weight average molecular weight (M_w). The results from the current work are plotted as red circle and fitted with a linear regression line. The data and the data from the literature have also been plotted [29,83,124].

The correlation between the T_g and fractionation composition can be expressed using the Flory-Fox equation (Equation 4.7 [287]). The as-received lignin is composed of fraction representing acetone-soluble and acetone-insoluble lignin, therefore, the T_g can be estimated using Equation 4.7:

$$\frac{1}{T_g} = \frac{W_1}{T_{g1}} + \frac{W_2}{T_{g2}} \quad \text{Equation 4.7}$$

where W_1 and T_{g1} are the fractional yield and T_g (in K) of acetone-soluble lignin. W_2 and T_{g2} are the fractional yield and T_g of acetone-insoluble lignin.

The calculated and experimentally derived T_{gs} for the as-received lignin are 163.19 °C and 163.0 ± 1.5 °C, respectively.

4.4.2.7 Functional Group Analysis of Acetone-soluble and Acetone-insoluble Lignins by Fourier Transform Infrared Spectroscopy

FTIR spectra of as-received lignin, acetone-soluble lignin and acetone-insoluble lignin are shown in Figure 4.32. All three lignins show similar absorption spectra and the peak position deviated by only of 2-3 cm^{-1} .

The relative intensity of the absorption bands of O-H stretching (at 3,390 cm^{-1}), phenolic O-H (at 1,365 cm^{-1}), aliphatic secondary O-H (at 1,081 cm^{-1}) and aliphatic primary O-H (at 1,030 cm^{-1}), with reference to the aromatic vibration (at 1,514 cm^{-1}) were calculated in order to observe the concentration of the hydroxyl groups. The data are given in Table 4.16 where it seen that the lowest relative hydroxyl content is for acetone-soluble lignin. It has been reported that a decrease in the aliphatic O-H leads to an improvement in thermal mobility [155,168,266]. On the other hand, the acetone-insoluble lignin shows an increase in the aliphatic O-H concentration. These results suggest that the acetone-soluble lignin chain may have better thermal mobility when compared to as-received and acetone-insoluble lignin.

The FTIR spectra can be analysed for the condensation index (CI) to gain an insight into the structure of lignin. The condensation index [97,288] was calculated for the three lignin samples using Equation 4.8:

$$\text{Condensation Index (CI)} = \frac{\text{Sum of all minima between } 1500 \text{ and } 1050 \text{ cm}^{-1}}{\text{Sum of all maxima between } 1600 \text{ and } 1030 \text{ cm}^{-1}} \quad \text{Equation 4.8}$$

From Table 4.16, a lower CI value is seen for the acetone-soluble fraction whereas the acetone-insoluble lignin has an increased value when compared with the as-received lignin. The structural condensation index obtained via FTIR can be

related to molecular weight distribution. Lignins with a higher PDI value tends to possess more condensed structures. This suggests that fractionation using acetone can be employed to improve the homogeneity of lignin and enable the selection of fractions for fibres formation.

Table 4.16 Relative intensities of FTIR absorbance band for hydroxyl groups and condensation index for as-received, acetone-soluble and acetone-insoluble lignins.

Lignin samples	O-H at 3390 cm⁻¹	Phenolic O-H at 1365 cm⁻¹	Aliphatic secondary O-H at 1081 cm⁻¹	Aliphatic primary O-H at 1030 cm⁻¹	CI
As-received lignin	0.733	0.600	0.649	0.702	0.72
Acetone-soluble lignin	0.606	0.492	0.518	0.638	0.66
Acetone-insoluble lignin	0.782	0.651	0.793	0.919	0.75

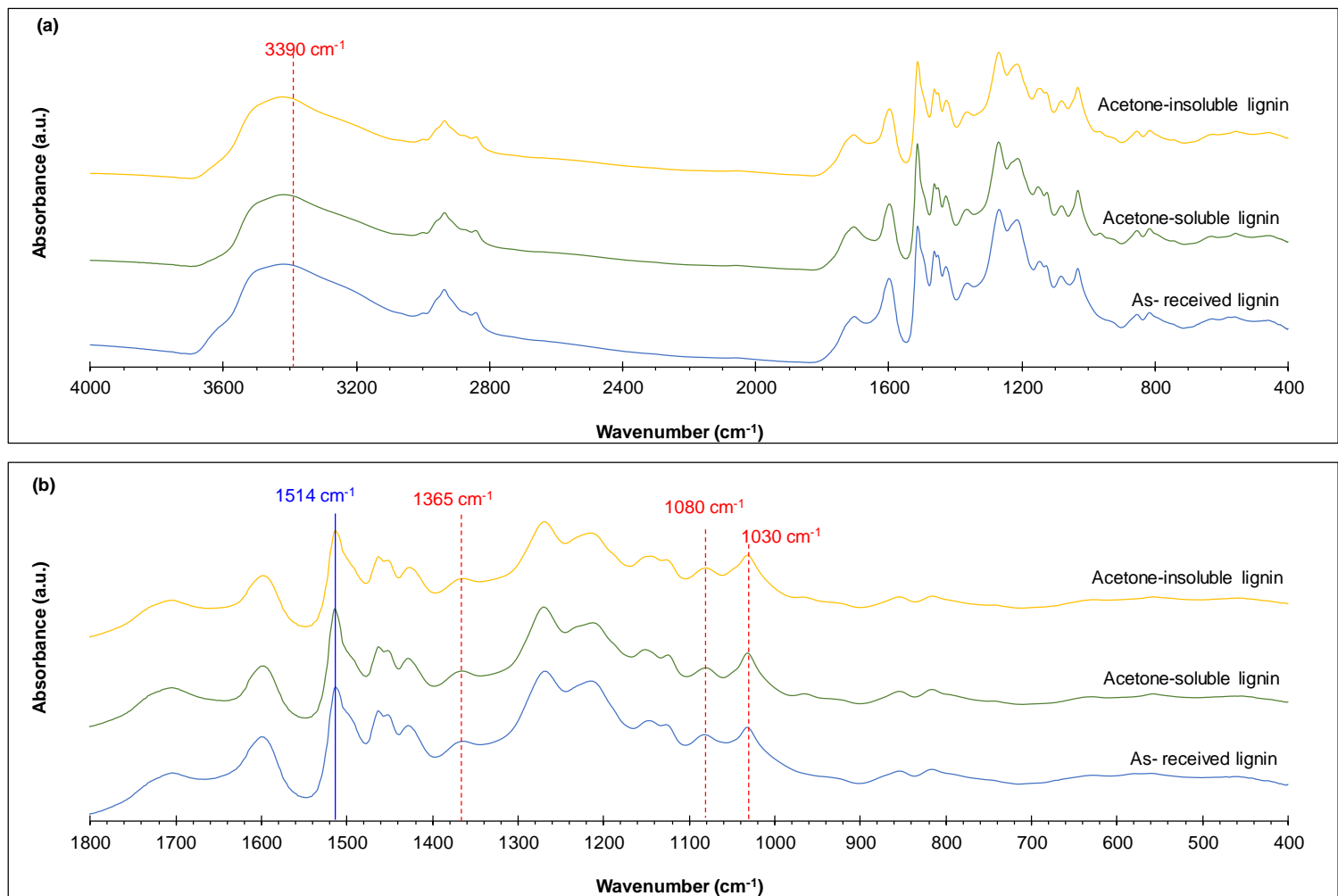


Figure 4.32 FTIR spectra of as-received, acetone-soluble and acetone-insoluble lignins: (a) whole spectral range; and (b) enlarged view from 1800- 600 cm⁻¹.

4.5 Treating Acetone-insoluble Lignin with Acidified Water

The ash content of the acetone-soluble and insoluble fractions are $0.055 \pm 0.021\%$ and $2.395 \pm 0.034\%$. As discussed in Section 4.4.2.3, acetone-soluble lignin can be one of the material choices for the production of fibres and this is reported in Chapter 5. On the other hand, acetone-insoluble lignin has a high ash content, so it requires an appropriate treatment before it can be used for manufacturing fibres.

With reference to the outcome of the Taguchi DoE discussed in Section 4.3, the optimum processing condition is the treatment of as-received lignin using pH 2 acidified water. In this instance, the acetone-insoluble lignin was treated with HCl at pH 2. The ash content in the acid-treated acetone-insoluble lignin decreased to $0.358 \pm 0.016\%$. This is 85% lower than that found in acetone-insoluble lignin. The elemental compositions (sulphur, sodium, magnesium, silica, potassium) for the ash are reduced; sodium, sulphur and potassium decrease by 91.6%, 90.2% and 84.2%, respectively when compared to the untreated acetone-insoluble lignin.

Figure 4.33 shows the ash contents at pH2 acetone-insoluble lignin compared with the other lignins produced in the current work. Ash content retained acetone-insoluble lignin after treatment at pH 2 is close to that the as-received lignin treated at pH 2 ($0.354 \pm 0.020\%$). This could imply that the lowest ash content retained in the acid treated lignins is between 0.3 - 0.4%.

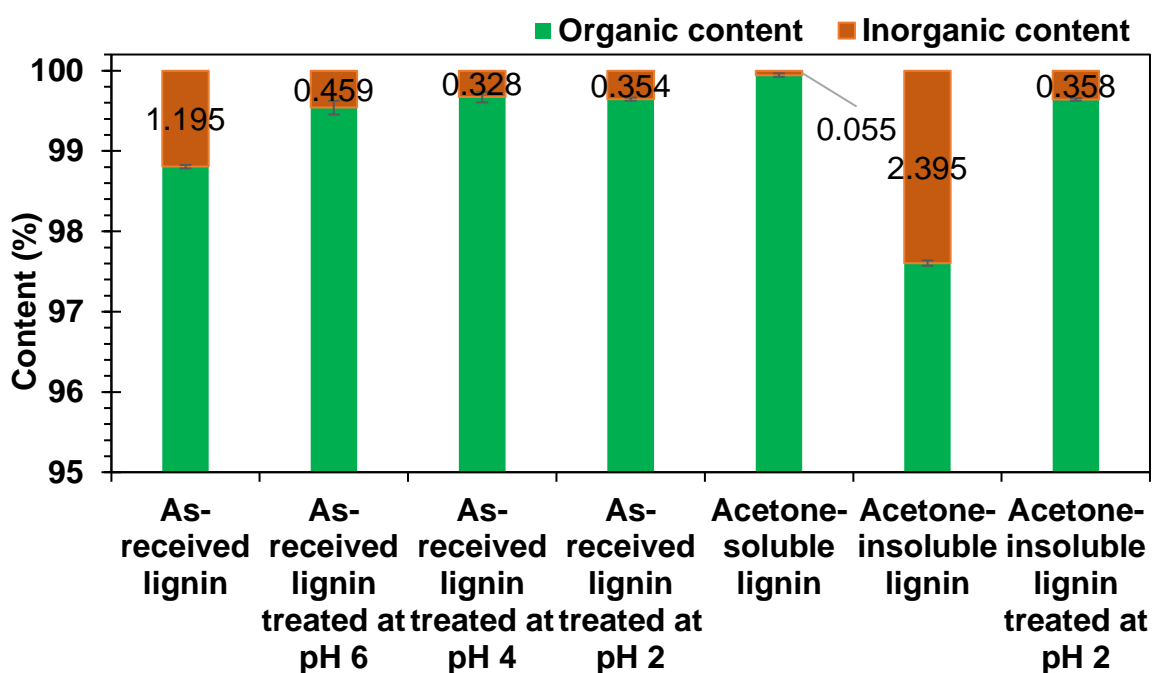


Figure 4.33 Inorganic elements found in the ash content from acid-treated acetone-insoluble lignin compared with other lignin samples produced in this work.

The characterisation of the moisture content, molecular weight, thermal properties and functional group determination were carried out on the acid-treated acetone-insoluble lignin. These results are compiled in Table 4.17. After treatment with pH 2 acidified water, slightly increase in M_w to $10,200 \pm 566 \text{ g}\cdot\text{mol}^{-1}$ and PDI to 3.04 ± 0.23 were found, compared to acetone-insoluble lignin (M_w of $9,600 \pm 566 \text{ g}\cdot\text{mol}^{-1}$ and PDI of 2.82 ± 0.28). The T_{g2} analysed from the second heating scan of pH 2 acetone-insoluble lignin is $188.3 \pm 3.4 \text{ }^\circ\text{C}$, and the predicted T_g using the linear model showed in Figure 4.31 and described in Section 4.4.2.6 is $194.7 \text{ }^\circ\text{C}$. According to Table 4.17, considering the results from TGA, the residue mass of pH 2 acetone-insoluble lignin are $38.4 \pm 4.2\%$. The calculated char residue of pH 2 acetone-insoluble lignin is $38.0 \pm 4.2\%$ which are comparable to that of acetone-insoluble lignin ($38.6 \pm 3.7\%$).

Table 4.17 Compiled properties of lignins produced and used for fibre fabrication.

Characteristics		Acetone-insoluble lignin	Acetone-insoluble lignin treated at pH 2
Moisture content (%)		3.94 ± 1.15	2.61 ± 0.08
Ash content (%)		2.395 ± 0.034	0.358 ± 0.016
Molecular weight	M _w (g·mol ⁻¹)	9,600 ± 566	10,200 ± 566
	M _n (g·mol ⁻¹)	3,400 ± 141	3,350 ± 71
	PDI	2.82 ± 0.28	3.04 ± 0.23
Results from TGA	T _{DTG,onset} (°C)	248.6 ± 22.8	266.3 ± 14.37
	T _{DTG,max} (°C)	387.8 ± 5.8	389.3 ± 4.98
	Maximum mass-loss rate (%/°C)	2.88 ± 0.02	3.16 ± 5.28
	Residue mass (%)	41.0 ± 3.7	38.4 ± 4.2
	Residue char (%)	38.6 ± 3.7	38.0 ± 4.2
Results from DSC			
First heating scan	Endothermic peak (°C)	83.5 ± 0.5	86.3 ± 0.7
	Enthalpy of vaporisation (J·g ⁻¹)	96.9 ± 6.9	69.2 ± 5.1
	T _{g1} (°C)	178.0 ± 0.5	179.4 ± 0.4
Second heating scan	T _{g2} (°C)	189.1 ± 0.4	188.3 ± 3.4
Third heating scan	T _{g3} (°C)	196.6 ± 0.9	191.2 ± 0.2

4.6 Summary

- As-received lignin has an ash content of $1.195 \pm 0.021\%$; two major elements found in the ash are sulphur and sodium at 46% and 42%, respectively. The ash content has been reported to have an effect on the char content and the mechanical properties of the fibres. Therefore, the as-received softwood Kraft lignin (BioChoice[®]lignin) needed subsequent treatment in order to reduce the inorganic content.

- Treating lignin with acidified water is a simple technique to remove inorganic impurities. The conditions for treating the lignin was optimised using Taguchi DoE. The optimum conditions are as follows: pH 4; acidified water-to-lignin ratio of 100 (cm³:g); washing time of 30 minutes; and the number of cycles equal to five. From ANOVA, the acidic level (pH) is the most influential factor in reducing the ash content found in lignin. It contributes a 65% influence for reducing the ash content. Fisher pairwise comparison showed that the use of pH 2 and pH 4 solutions has no statistically significant influence on the ash content. After treating with acidified water (pH 2), a 70% drop in the ash content in as-received lignin was found. A decrease in the sulphur and sodium content was also obvious. The T_g of acid-treated lignin was found in the range of 156-158 °C. The relative intensities of phenolic O-H and aliphatic O-H absorbances in the acid-treated lignin were reduced.

- Molecular weight fractionation using acetone can be used as an efficient and convenient technique to obtain acetone-soluble lignin with a $57.4 \pm 0.6\%$ yield. Acetone-soluble lignin has a lower ash content of $0.055 \pm 0.021\%$, lower M_w of $4,250 \pm 71 \text{ g}\cdot\text{mol}^{-1}$ and PDI of 1.73 and a lower T_{g2} of $145.8 \pm 0.3 \text{ °C}$, compared to those of as-received lignin. This indicates that the acetone fractionation can be employed to remove inorganics and separate out the high molecular weight fraction in softwood Kraft lignin.

- The procedure for the treatment of softwood Kraft lignin (BioChoice[®]lignin) is shown in Figure 4.34. After fractionation, the acetone can be recovered, and acetone-soluble lignin can be obtained. The acetone-insoluble lignin requires further

purification to remove the inorganic content. In this study, treatment with acidified water was carried out on the acetone-insoluble lignin. Acetone-insoluble lignin has an ash content of $2.395 \pm 0.034\%$. After treatment with acidified water (pH 2), the ash content reduced to $0.358 \pm 0.016\%$. The M_w , PDI and T_g of pH 2 acetone-insoluble lignin are $10,200 \pm 566 \text{ g}\cdot\text{mol}^{-1}$, 3.04 ± 0.23 and $188.3 \pm 3.4 \text{ }^\circ\text{C}$, respectively.

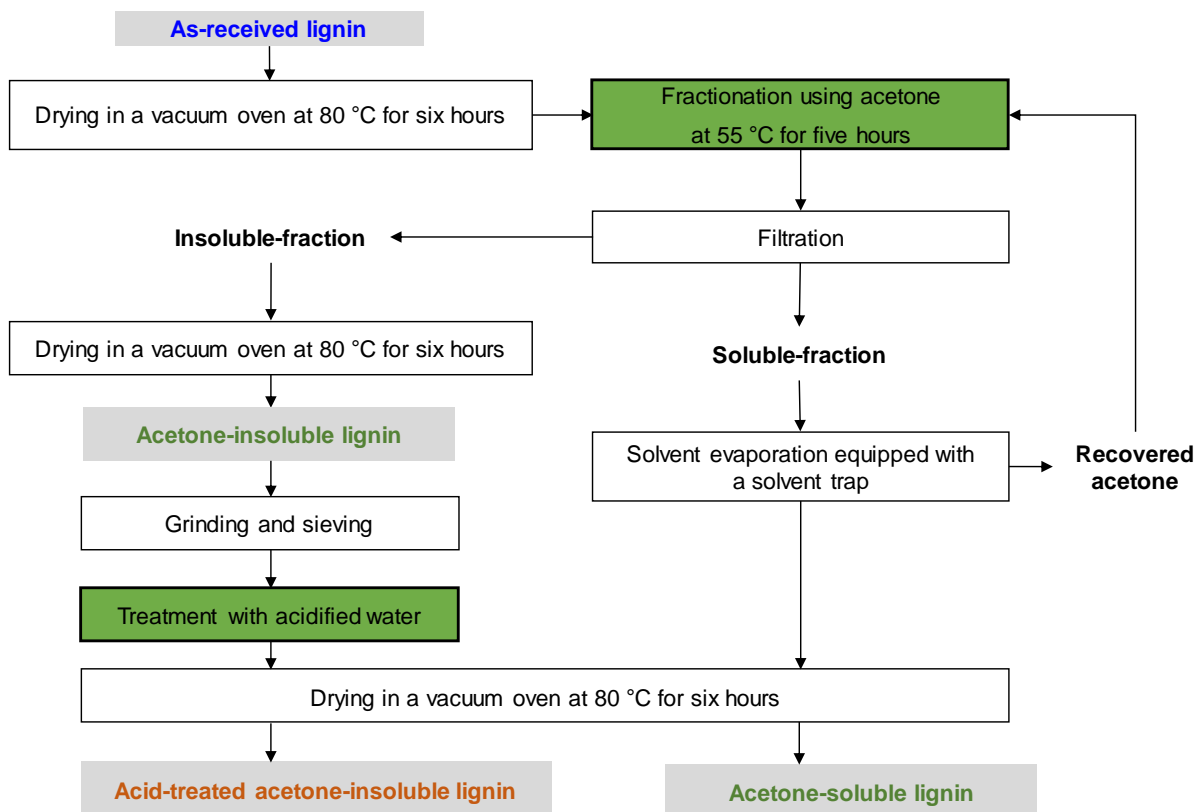


Figure 4.34 Flowchart showing the steps used for obtaining acetone-soluble lignin and acid-treated acetone-insoluble lignin.

- In summary, this chapter reported on an effective method (fractionation using acetone) to remove the inorganic content in BioChoice[®] lignin. Acetone-soluble lignin showed a reduced inorganic content and heterogeneity in the molecular weight distribution. Thus, acetone-soluble lignin was used for fibre spinning which is described in Chapter 5.

5. ELECTRO-SPINNING OF ACETONE-SOLUBLE LIGNIN

5.1 Introduction

This chapter reports on a novel approach that was developed for electro-spinning of acetone-soluble softwood Kraft lignin without the need of polymer blending or chemical modification. Furthermore, the primary solvent used for electro-spinning lignin (DMSO) is non-toxic and the secondary solvent (acetone) is significantly less toxic than the solvents reported in the literature. The parameters for the electro-spinning of acetone-soluble lignin were optimised to produce bead-free lignin fibres. Moreover, axially-aligned electro-spun lignin fibres were produced using a custom-made grounded graphite electrode collector. Subsequent steps for the production of carbonised lignin fibres which included the removal of residual solvents, thermo-stabilisation and carbonisation are discussed in detail.

The production of fibres from neat lignin has not been reported extensively. The majority of previous reports are based on hardwood Organosolv lignin dissolved in ethanol [103,183], whilst softwood lignin has required a blend involving PEO [35,36,143], PAN [192,229] and PVA [289] to produce fibres. It is claimed that softwood lignin alone does not possess sufficient viscoelasticity for spinning [35,139,143]. Moreover, electro-spinning using lignin requires it to be dissolved in an appropriate solvent. Several researchers have used N, N-dimethylformamide (DMF) [35,36,143,192,229] as the solvent. A compilation of solvent used for electro-spinning of lignin is summarised in Section 2.3.2, Chapter 2. However, DMF is a toxic with environmental and health concerns [143,144,149].

This thesis reports on a new approach for electro-spinning acetone-soluble softwood Kraft lignin without using a second polymer or blend. Acetone-soluble lignin with low ash content of $0.055 \pm 0.021\%$ was dissolved in a common and nontoxic binary solvent of acetone and dimethyl sulfoxide (DMSO). Subsequent to electro-spinning, a detailed study was undertaken to define the heating conditions to remove the retained solvents. The optimum conditions for thermo-stabilisation and

carbonisation were studied. The properties of the resultant fibres in each of the steps mentioned above were determined.

5.2 Criteria for Selecting the Solvent for Electro-spinning of Acetone-soluble lignin

Although the acetone-soluble lignin fraction is soluble in acetone, the resulting lignin solution cannot be used for extended periods due to the low boiling point of acetone (56 °C). This was observed to lead to the solidification of lignin at the tip of the needle. Therefore, a method was required to retard the evaporation rate of the lignin solution during electro-spinning. The options considered were to cool the solution or introduce a second solvent with a higher boiling point; the latter option was used.

In this work, DMSO was used as the second solvent due to the fact that it is mutually soluble and compatible with lignin and acetone. Selected properties of acetone and DMSO that are of relevance to electro-spinning, are presented in Table 5.1. Other alternative solvents for dissolving lignin for electro-spinning and their properties are presented in Appendix A. The solvents used by previous researchers for electro-spinning lignin are also included in Table 5.1. With reference to Table 5.1, as the boiling point of DMSO (189 °C) is higher than that of acetone. Hence, the overall evaporation rate of the solvents can be retarded.

As seen in Table 5.1, the majority of the solvents used in the literature are toxic. For example, DMF and DMA_c have been used extensively, which are reviewed and compiled in Table 2.8, Chapter 2. In the current project, the decision was taken not to use any toxic solvents, so DMSO was chosen because it has lower electrical conductivity and higher dielectric constant than DMF. Moreover, it is known that solvents with high dielectric constant can reduce the formation of beads during electro-spinning [169,174]. However, as seen in Section 2.3.2, a number of other factors can lead to the formation of beads. For example, the solution viscosity [171–173], surface tension [169], temperature [177], electrical conductivity [169] and dielectric constant [174].

Table 5.1 A compilation of solvents used for electro-spinning of lignin and their properties [290].

Solvents	Toxicity*	Hansen Solubility parameter (MPa ^{1/2})			Boiling point (°C)	Enthalpy of vaporisation (kJ·mol ⁻¹)	Freezing point (°C)	Surface tension (mN·m ⁻¹)	Electrical conductivity ohm ⁻¹ ·m ⁻¹	Dielectric constant
		δ _D	δ _P	δ _H						
Acetone		15.5	10.4	7	56	31.2	-95	23.3	5x10 ⁻⁹	20.6
DMSO	Not a hazardous substance	18.4	16.4	10.2	189	52.9	18.5	43.7	2x10 ⁻⁹	46.6
DMF		17.4	13.7	11.3	153	46.9	-61	35	6x10 ⁻⁹	20.6
DMAc		16.8	11.5	10.2	166	49	-20	34	2 x10 ⁻⁹	37.8
Ethanol		15.8	8.8	19.4	78	42.3	-114	22.3	1x10 ⁻⁹	22.4

* Toxicity is represented with hazard symbol;  : Serious health hazard,  : Flammable,  : Health hazards.

5.3 Influence of the Concentration of Acetone-soluble Lignin on the Solution Properties and Morphology of Electro-spun Fibres

The concentration of lignin in the binary solvent has an influence on the solution viscosity and electrical conductivity. This was investigated using lignin concentrations corresponding to 45, 48, 53 and 58 wt%. The volume ratio of acetone to DMSO was maintained at 2:1. The properties of the lignin solutions are discussed in the following section.

5.3.1 Viscosity and Electrical Conductivity of Acetone-soluble Lignin Solutions

Figure 5.1 shows a plot of the viscosity versus the shear rate for lignin solutions of specified concentrations. The data shows shear thinning behaviour and the extrapolated viscosities at zero shear viscosity are summarised in Table 5.2. The solution viscosity acquired from various lignin concentrations from 45- 58 wt% is in a range 0.2-0.6 Pa·s. As expected, the viscosity of the solution increased with increasing lignin concentration. The electrical conductivity of the solutions is summarised in Table 5.2. An increase of lignin concentration results in an increase in the electrical conductivity.

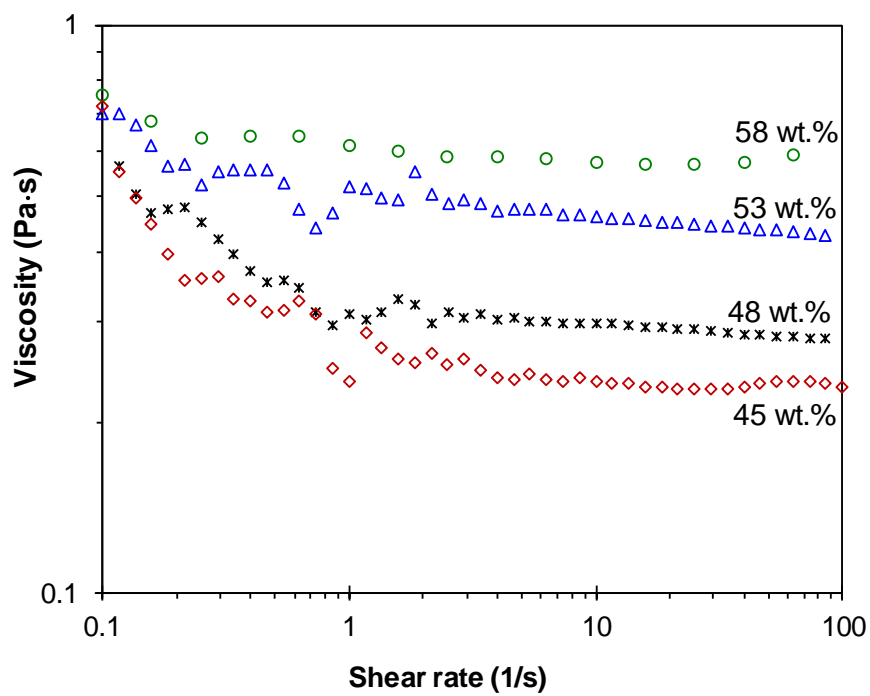


Figure 5.1 Observed relationship between the viscosity and shear rate for acetone-soluble lignin solutions at specified concentrations.

Table 5.2 Viscosity and electrical conductivity of lignin solutions at specified concentrations. The measurements were obtained at 25 °C.

Lignin concentration (wt%)	Viscosity (Pa·s)		Electrical conductivity ($\mu\text{S}\cdot\text{cm}^{-1}$)	
	Ave.	SD.	Ave.	SD.
45	0.23	0.00	2.29	0.05
48	0.31	0.03	2.33	0.07
53	0.43	0.01	2.37	0.02
58	0.62	0.04	2.41	0.04
Acetone	0.00036	0.00	1.83	0.01
DMSO	0.0019	0.00	2.17	0.02

Table 2.8, Section 2.3.2, provides a compilation of selected papers on the electro-spinning of lignin fibres was presented where bead-free electro-spun fibres were reported [103,118,183]. Total polymer concentration compiled in Table 2.8 varies from 9 - 50 wt%.

5.3.2 Morphology of Electro-spun Acetone-soluble Lignin Fibres

The electro-spinning of acetone-soluble lignin solution with different lignin concentrations was carried out using a custom-made electro-spinning unit as described in Section 3.3.2.1, Chapter 3. Figure 5.2 (a-d) shows micrographs of electro-spun fibres obtained from lignin solutions at specified concentrations. The micrographs have been coded and paired with low and higher magnification images at the top and bottom rows, respectively; “a” represents the low-magnification

micrographs and “a*” represents the corresponding higher magnification micrograph. Electro-spinning using a solution concentration of 45 wt% resulted in beaded fibres (see Figure 5.2 (a and a*)). By increasing the concentration of lignin to 48 wt%, the presence of the beads on the electro-spun fibres was eliminated; however, the spun fibres consisted of mixture circular fibres and flat ribbons. When the concentration of lignin to 53 wt% bead-free electro-spun fibres were produced, and the occurrence of flat fibres was reduced. However, increasing the lignin concentration to 58 wt% caused an increase in the presence of ribbon-like fibres and their relative widths increased. A number of fractured fibres were also observed. The fibre diameter distributions for the lignin concentrations corresponding to 48, 53 and 58 wt% acetone-soluble lignin in acetone/DMSO are presented in Figure 5.3 (a-c). A normal distribution trace has been superimposed on each dataset. The average fibre diameters for the 48, 53 and 58 wt% lignin are 0.69 ± 0.35 , 1.16 ± 0.21 and 1.67 ± 0.48 μm , respectively.

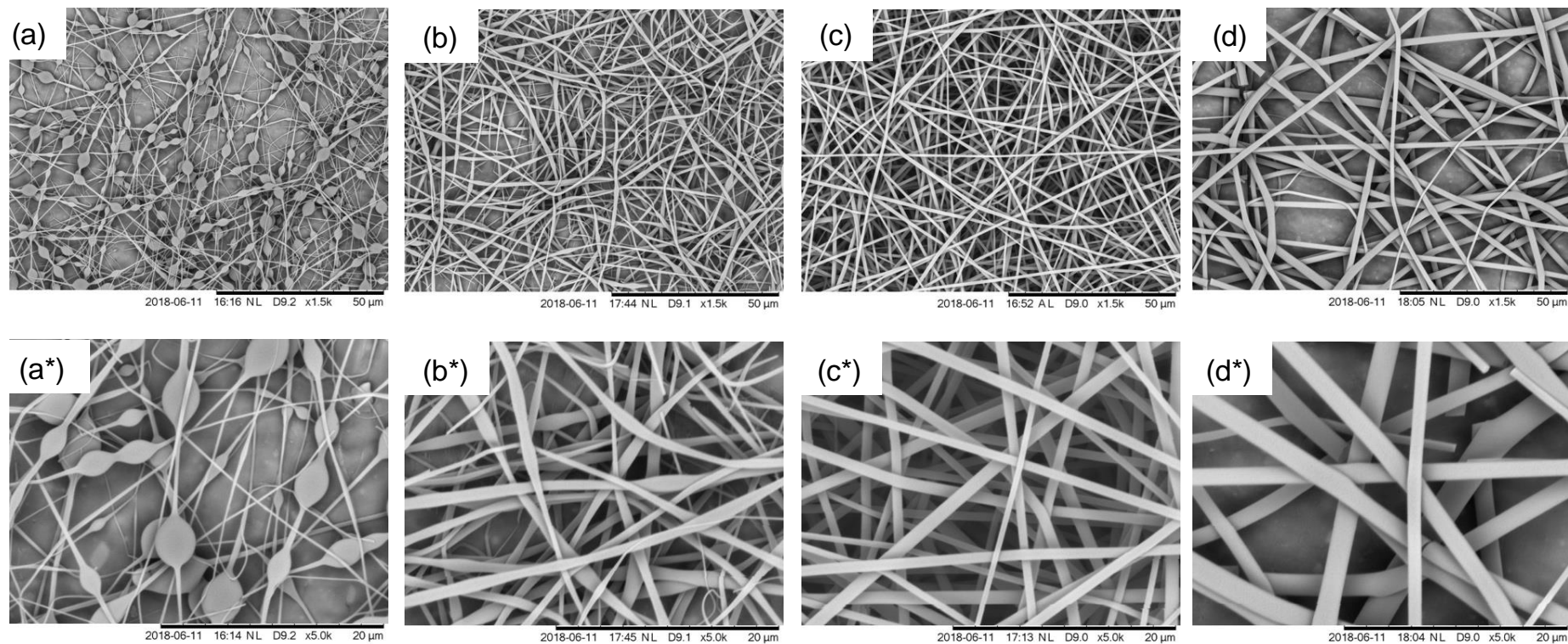


Figure 5.2 SEM micrographs showing the effect of the lignin concentrations on the fibre morphology: 45 wt% (a and a*) , 48 wt% (b and b*), 53 wt% (c and c*) and 58 wt% (d and d*).

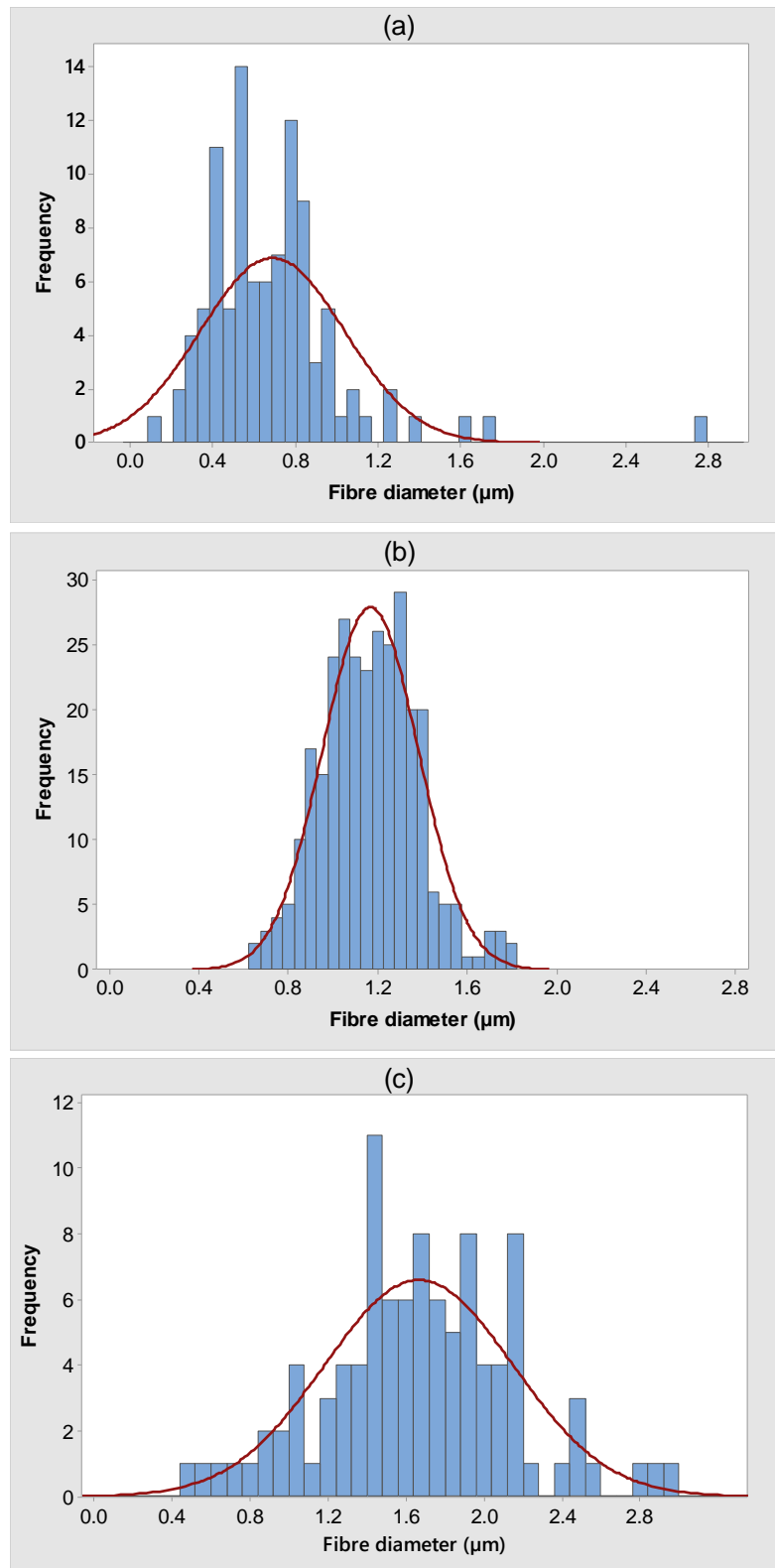
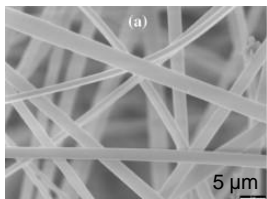
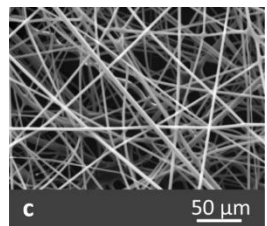


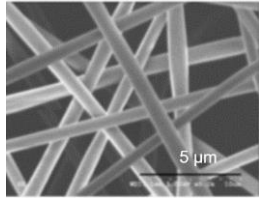
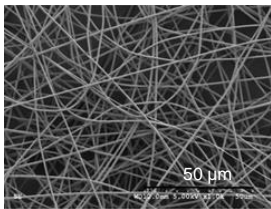
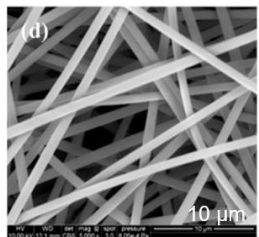
Figure 5.3 Histograms and normal distributions for the fibre diameters for electro-spun acetone-soluble lignin fibres at different lignin concentrations of: (a) 48 wt%, (b) 53 wt% and 58 wt%.

Some of the papers mentioned in Table 2.8, Section 2.3.2 were selected and are reproduced in Table 5.3. Information on the composition of the lignin solution and the morphology of the electro-spun fibres are included. In the majority of the cases, there is a view that hardwood lignin does not require to blend with a second polymer or blended to enable electro-spinning [103,183]. However, the equipment had to be modified to accommodate a co-axial needle. The consensus of opinion in the literature is that softwood Kraft lignin needs to be blended to enable electro-spinning [35,36,118,143,144,188,192,193].

With reference to Figure 5.2 and Table 5.3, it can be said that the current work demonstrates a new approach to produce bead-free electro-spun fibres from softwood Kraft lignin without using polymer blends. Moreover, the solvents used for electro-spinning is less toxicity when compared to the solvents have been reported in the literature. Characterisation of the electro-spun acetone-soluble lignin fibres produced in this study are described.

Table 5.3 Selected papers on electro-spinning of lignin with the relevant information on the solution, fibre morphology and fibre diameter.

Lignin	Blend ratio of lignin/ polymer blend	Total polymer concentration / solvent	Fibre diameter (nm)	Fibre morphology	Reference
Hardwood Organosolv (Alcell®)	N/A	50 wt% /Ethanol	800-3,000		[103,183]
Softwood Kraft (Indulin AT)	90/10 of PEO (w/w)	11 wt% /NaOH aqueous	500-10,000		[143,144]

Lignin	Blend ratio of lignin/polymer blend	Total polymer concentration / solvent	Fibre diameter (nm)	Fibre morphology	Reference
Softwood Kraft (Indulin AT)	99.6/0.4 of PEO (w/w)	45 wt% /DMF	1,401		[35]
Softwood Kraft (Indulin AT)	99.8 /0.2 of PEO (w/w)	32 (w/v) /DMF	900-1,200		[36]
Corn stover Organosolv	50/50 of PAN (w/w)	20 wt% /DMF	1,690		[185]

5.4 Randomly Aligned Electro-spun Acetone-soluble Lignin Fibres and Their Properties

Electro-spun acetone-soluble lignin fibres was produced using a solution concentration of 53 wt% in a binary solvent of 2/1 volume ratio of acetone and DMSO.

5.4.1 Scanning Electron Microscopy of Electro-spun Acetone-soluble Lignin Fibres

Figure 5.4 (a and b) shows typical SEM micrographs of electro-spun lignin fibres where a smooth surface is observed. Variability in fibre diameter can be seen clearly

in the high magnification micrographs as shown in Figure 5.4 (b). The determination of the fibre diameter was carried out on 300 measurements from six SEM micrographs taken from six random areas to obtain representative data on the fibre diameter distribution. The average fibre diameter is $1.16 \pm 0.21 \mu\text{m}$. The distribution of fibre diameters is presented in Figure 5.5 where the range is 0.6 -1.8 μm . The surface roughness of the electro-spun acetone-soluble lignin is presented in Appendix B.

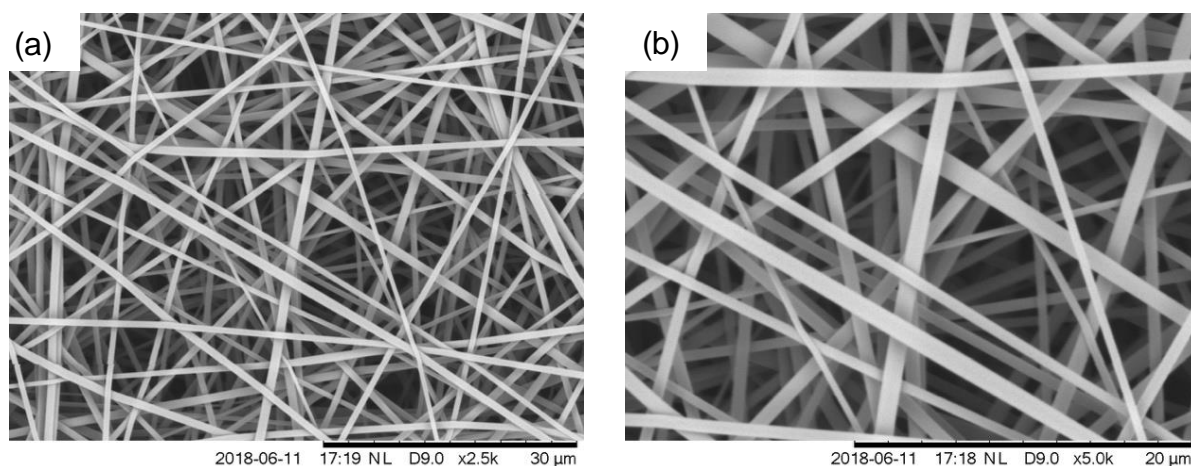


Figure 5.4 SEM micrographs of the surface of electro-spun acetone-soluble lignin.

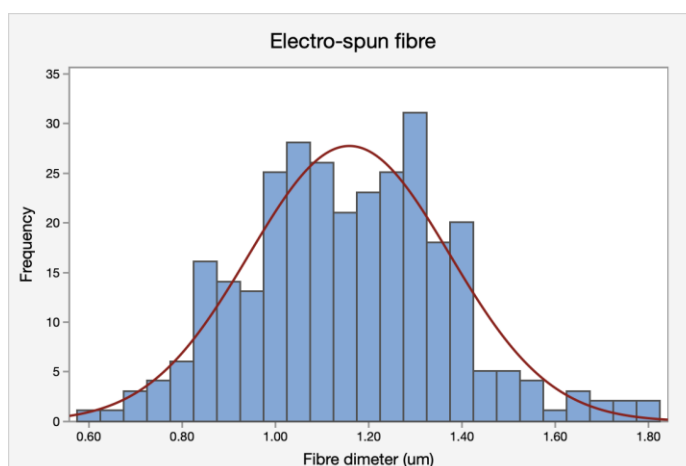


Figure 5.5 Histogram and normal distribution of the fibre diameter for the as-spun acetone-soluble lignin fibres.

Figure 5.6 (a-d) illustrates a cross-sectional view of electro-spun acetone-soluble lignin fibres. As inspection of the cross-sectional view of the fibres showed the presence of circular and elliptical fibres. The presence of the elliptical fibres may be due to the fibres being solvent-rich. This may also account for some deformation of the fibres at the fibre-to-fibre contact points (see Figure 5.6 (c and d)). It is proposed that the elliptical fibres cross-sections can be eliminated by optimising and controlling the evaporation rate of DMSO from the fibres as they travel from the Taylor cone to the ground-plate. This is not straightforward as it is necessary to prevent the premature evaporation of the acetone at the tip of the needle, whilst accelerating the evaporation of the solvent from the fibres in-flight, before they are deposited. Nevertheless, this study has shown that softwood Kraft lignin can be electro-spun without the need for blending.

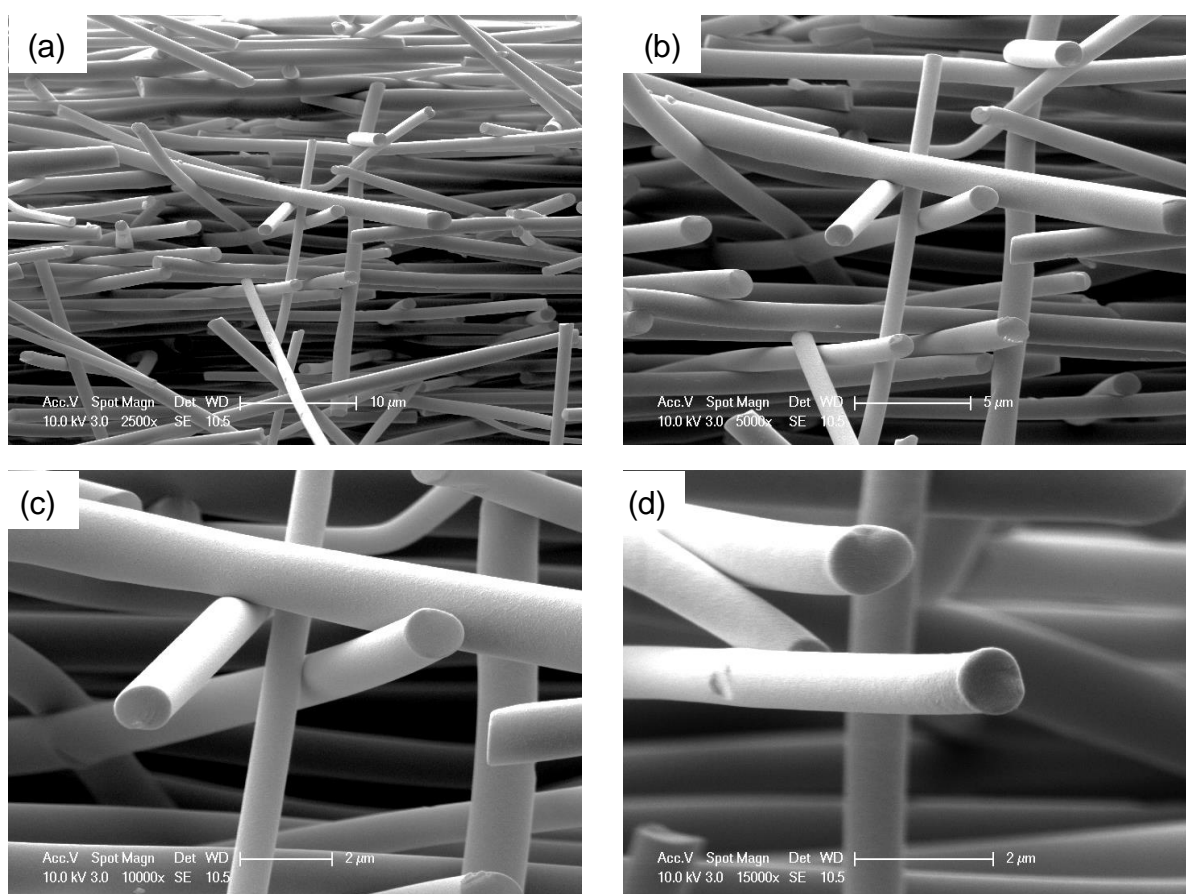


Figure 5.6 SEM micrographs of a cross-sectional views of electro-spun acetone-soluble lignin fibres.

5.4.2 Differential Scanning Calorimetry of Electro-spun Acetone-soluble Lignin Fibres

The electro-spun acetone-soluble lignin fibres were characterised using the DSC-1 from -60 °C to 250 °C. The thermograms are showed in Figure 5.7 (a). In the majority of cases, DSC data reported in the literature tend to ignore the first heating scan and only the data from the second scan are reported [134,185,191]. The reasons that have been given for this practice include erasing the “memory of the polymer”. This can be erroneous because the volume of solvent(s) retained in the material will influence the magnitude of the T_g in subsequent scans [135,291]. This approach of ignoring the data from the first heating scan can lead to incorrect conditions being adopted for subsequent heating regimes to remove solvents from the electro-spun fibres.

With reference to Figure 5.7 (a), this exponentially increasing baseline (i) is generally associated with mass-loss within the sample as a function of temperature. However, normally with events such as evaporation of low-molecular weight components (water and acetone in the current case) from the sample, the baseline will return to its original position – as indicated by (ii). The small but noticeable blip in the thermogram (iii) is most likely due to volatiles experiencing a sudden volatilisation from the sample. Coded item (iv) at 124.5 °C shows a sudden increase in the heat capacity trace and the baseline decreases; this can be attributed to an endothermic evaporation event. This may be water or water associated with DMSO [292,293] and DMSO with a boiling point of 189 °C [290]. The fact that the baseline shows a negative gradient after the peak suggests that this is likely to be evaporation.

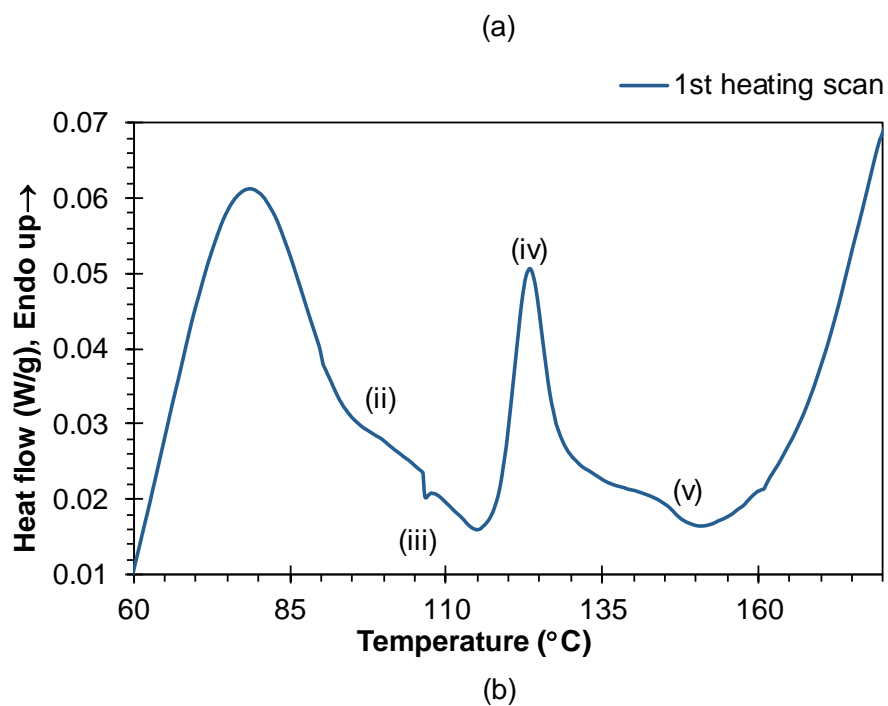
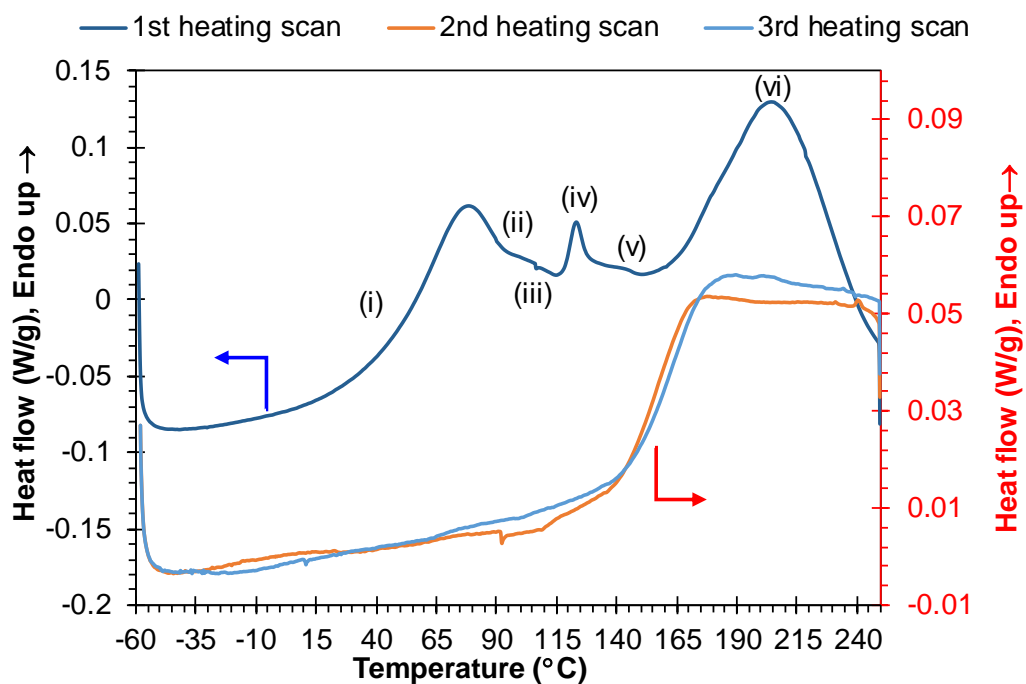


Figure 5.7 DSC thermograms; (a) showing three successive heating scans for electro-spun acetone-soluble lignin fibres where the thermal analysis was carried out in nitrogen and (b) expanded view of the first heating scan from 60-180 °C.

Figure 5.7 (b) shows an expanded plot for coded region (iv) where this feature is more akin to evaporation. A small endothermic peak is observed around 145 °C (v) but the origin of this peak is not known, and further research is required to elucidate its origin. However, it is possible that this endothermic feature is associated with a glass transition. In instance, where the polymer is in a strained state, for example, electro-spun fibres, an endothermic relaxation peak will be observed as it is heated past the glass transition temperature [294,295]. This endothermic relaxation peak is also observed in polymers that are aged or annealed at temperatures close to the glass transition temperature of the polymer. The large endothermic peak coded as (vi) is attributed to the evaporation of DMSO from the electro-spun fibres.

Another analysis of the electro-spun acetone-soluble lignin fibres was conducted from 25-250°C in nitrogen to observe the replication of the first heating scan. Figure 5.8 (a) illustrates the three thermograms and the codes (i–vi) are presented for the first heating scan with the same sequence as the previous results shown in Figure 5.7 (a). A similar pattern was observed for three endothermic peaks at 71.8, 117.0, 205.5 °C, respectively. A small blip located at (iii) is still detected, as shown in the expanded view in Figure 5.8 (b), and a small endotherm peak is observed around 145 °C (v) which is shown as an insert in Figure 5.8 (b). This is similar to the result described previously in Figure 5.7.

The successive second and third ramped heating scans are shown in Figure 5.7 (a) and Figure 5.8 (a) where the T_g is clearly visible. The T_{g2} from the second and third heating scans are 154.4 °C and 165 °C, respectively. Reconsidering of the coded feature (iv) in Figure 5.7 (b) and Figure 5.8 (b), it may be the manifestation of a T_g for plasticised lignin due to the presence of DMSO. However, its disappearance in the second and third scans may also represent volatility in the sample as a function of temperature.

The negative slope in the second scan after 240 °C may be indicative of cross-linking reactions in the lignin as this is an exothermic process. Previous researches have suggested that lignin can cross-link at temperatures above 230 °C [134,135,217,218,221]. This may explain the observed increase in the T_{g2} in the second scan.

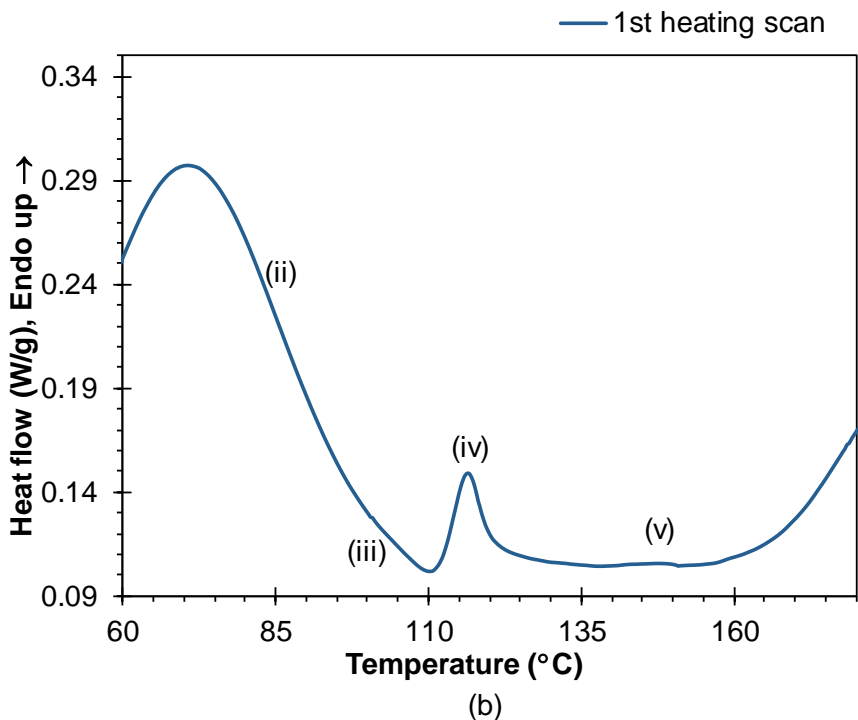
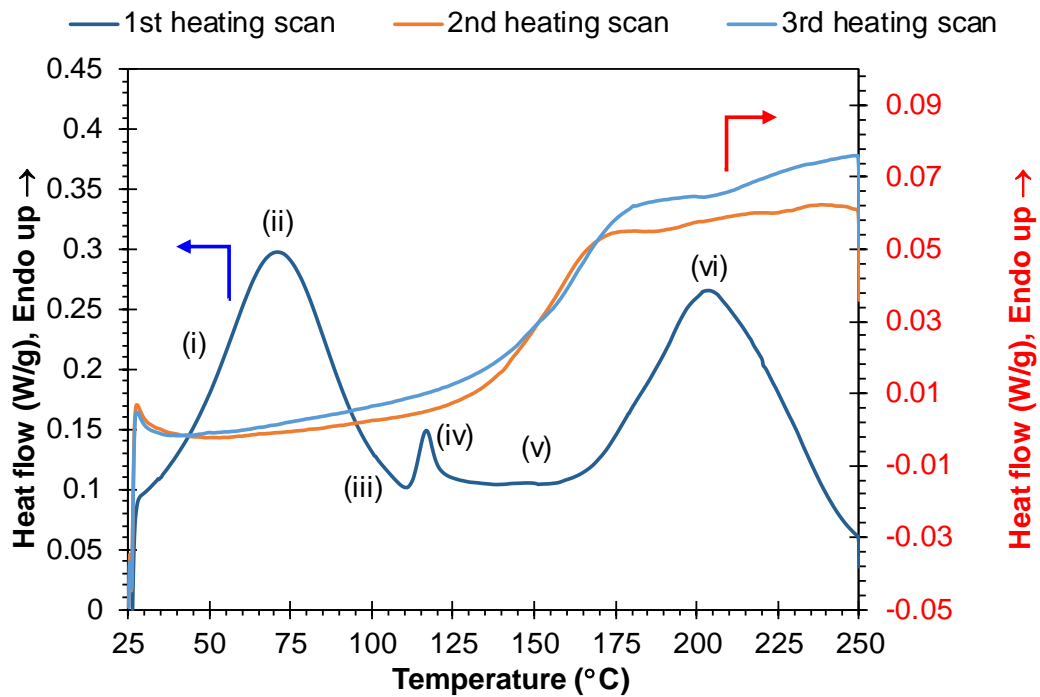


Figure 5.8 DSC thermograms where the thermal analysis was carried out in nitrogen from 25-250 °C: (a) showing three successive heating scans for electro-spun acetone-soluble lignin; and (b) expanded view of the first heating scan from 60-180 °C.

The weights of the electro-spun acetone-soluble lignin fibres were measured to determine the mass-loss after three successive scans. The mass-loss was measured to be between of 13.4 - 15.7%. TGA analysis of the electro-spun acetone-soluble lignin fibres is discussed in the next section where mass-loss data from the DSC are compared.

5.4.3 Thermo-gravimetric Analysis of Electro-spun Acetone-soluble Lignin Fibres

Figure 5.9 shows the TGA and DTG curves for the electro-spun acetone-soluble lignin fibres. The DTG trace for electro-spun fibres shows four major peaks and a minor peak. Peak-a at 62 °C is assigned to the evaporation of moisture or low molecular weight component (water and acetone). Peak-b at 132.1 °C is assumed to be due to the evaporation of water and water associated with DMSO. Peak-c at 221.3 °C is due to the evaporation of DMSO. The three DTG peaks (a, b and c) at 62 °C, 132.1 °C and 221.3 °C, respectively, correlate well with the results obtained from the first heating scan of DSC trace where the three endothermic peaks are seen and discussed in Section 5.4.2. Mass-loss at 250 °C for the electro-spun acetone-soluble lignin from the TGA data is 13.6% and this also correlates well with that measured after the DSC experiments. The origin of the shoulder peak-d at 269.3 °C is not known but it presents also in the lignin powder. Peak-e at 393.3 °C is thermal degradation of lignin.

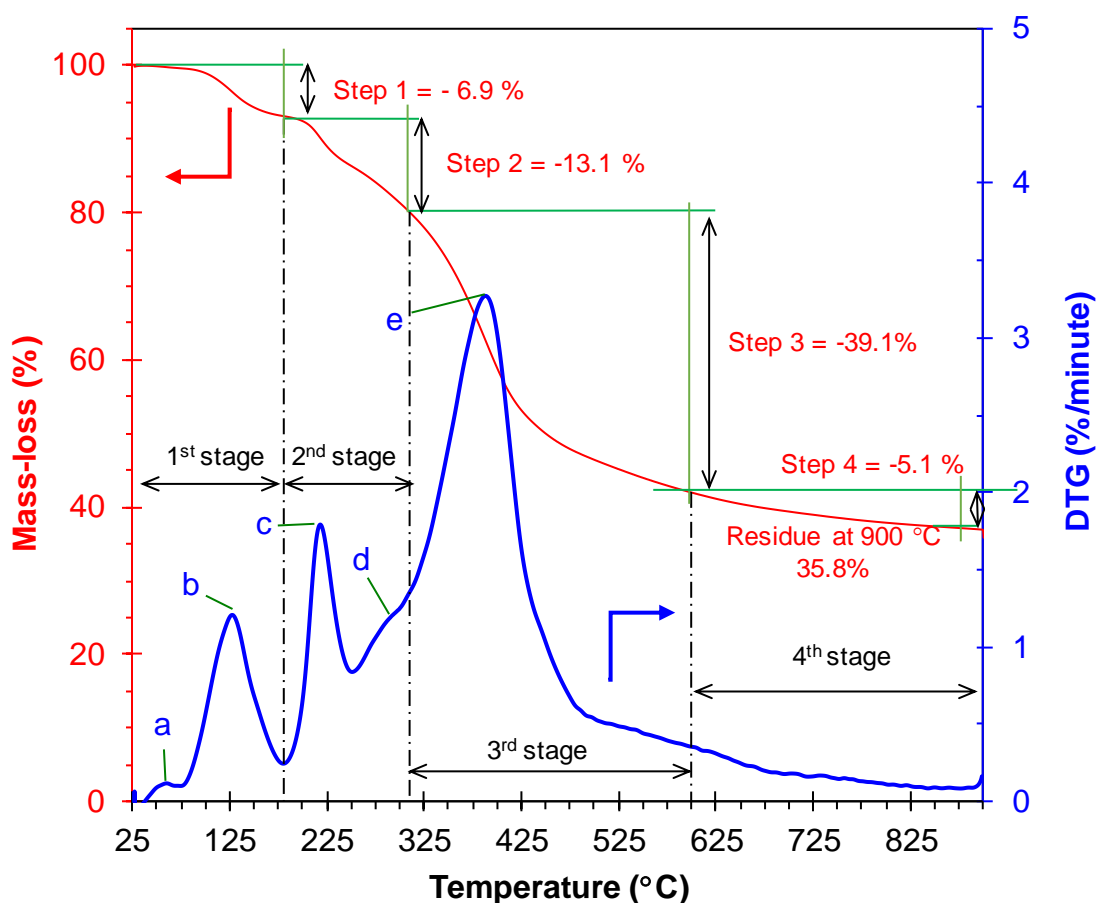


Figure 5.9 TGA and DTG curves for electro-spun acetone-soluble lignin fibres.

Figure 5.10 shows an overlaid plot of the TGA and DTG curves of the electro-spun acetone-soluble lignin fibres and acetone-soluble powder. On inspection the mass-loss data in Figure 5.10, the faster rate of mass-loss for electro-spin fibres is reasonable because the (i) surface area of the electro-spun fibres (fibre diameter of $1.16 \pm 0.21 \mu\text{m}$) when compared to powder (particle size of $13.2 \pm 0.16 \mu\text{m}$). (ii) the electro-spun fibres contain absorbed moisture, acetone and DMSO whereas, the powder has absorbed moisture.

Interestingly, the residual mass the two samples at $900 \text{ }^\circ\text{C}$ is approximately 36-38 %. This suggest that the presence of moisture and solvent does not influence the char content after pyrolysis at $900 \text{ }^\circ\text{C}$ in argon.

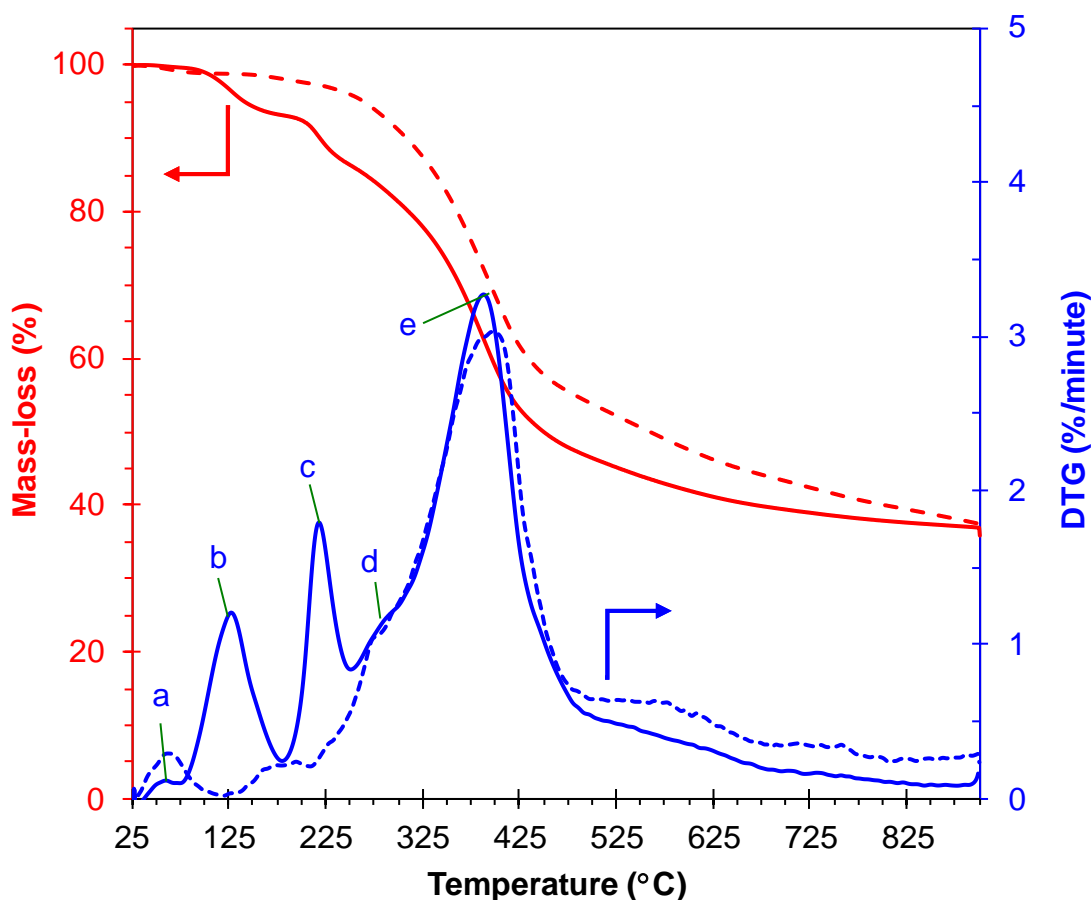


Figure 5.10 Overlaid TGA and DTG curves of electro-spun acetone-soluble lignin fibres plotted in solid line and acetone-soluble lignin powder plotted in dotted line.

5.5 Heating of Electro-spun Acetone-soluble Lignin Fibres to Remove Acetone and DMSO

Prior to thermo-stabilisation and carbonisation of the electro-spun acetone-soluble lignin fibres, it is essential to investigate and develop a procedure to remove the retained acetone and DMSO. Moreover, it is also necessary to establish the optimum processing conditions for thermo-stabilisation of the solvent-free fibres and the subsequent heat treatment procedures for carbonisation. The characteristic features of the resultant fibres after each step of processing are analysed and discussed in the following sections.

Prior to discussing the effect of the heating temperature before carbonisation, the author wishes to declare that it is recognised that the average diameters of the as-spun lignin fibres, and those were heated in nitrogen and air were 1.42 ± 0.15 , 1.17 ± 0.19 and 1.21 ± 0.25 μm , respectively. There are not similar possibly because of variation in the properties of solution and the time lapse between the production of the polymer solution and the production fibres. However, analyses of the electro-spun fibres from the same batch were used to study the effect of the heating temperature on the fibre morphology.

The heating experiments were carried out for six hours each, at 100 °C, 140 °C, 180 °C and 200 °C. The electro-spun acetone-soluble lignin fibres were heated in (i) air, (ii) nitrogen or (iii) a vacuum oven. In the case of (i) and (ii), the gas flow was consistent at 50 ml·minute⁻¹. The experimental set up is illustrated in Figure 3.10, Chapter 3. The heating temperatures were selected on the basis of the DSC results obtained for the electro-spun acetone-soluble lignin fibres, as explained in Section 5.4.2. The T_{g2} from the second heating scan of the electro-spun acetone-soluble fibres is 154.4 °C. Hence, the temperature regime for heating experiment was dictated by this temperature.

5.5.1 Scanning Electron Microscopy of Heated Electro-spun Acetone-soluble Lignin Fibres

The morphology of the electro-spun fibres that were heated at 100, 140, 180 and 200 °C for six hours, in air, nitrogen and in a vacuum oven is shown in Figure 5.11. Evidence of fibre fusion was not observed when the electro-spun fibres were heated at 100 or 140 °C, in air, nitrogen or a vacuum oven. However, it is clearly shown that all fibres fuse at the fibre cross-over regions when the temperature is 180 °C. At 200 °C, extensive fibre fusion was observed.

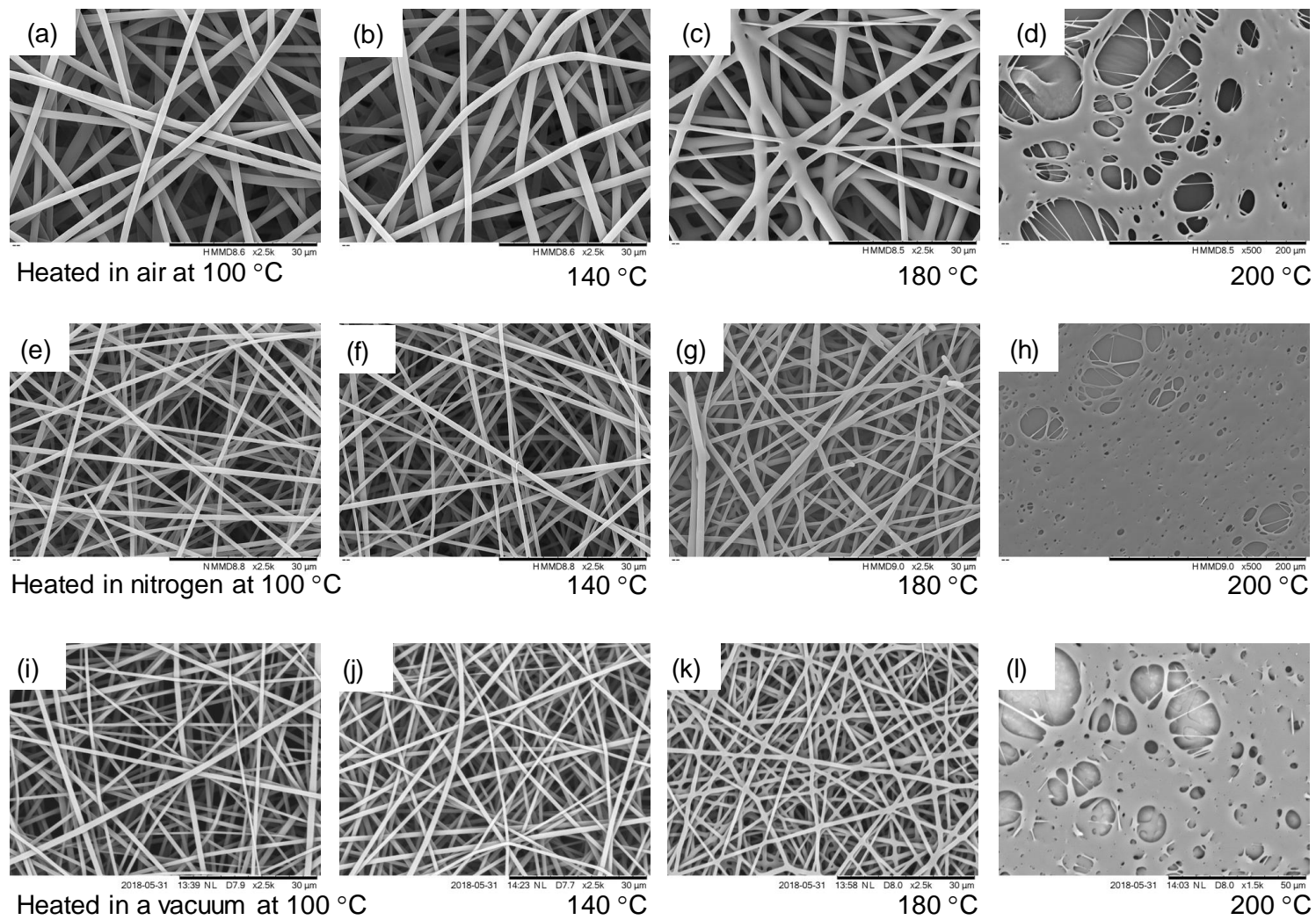


Figure 5.11 Fibre morphology as a function of temperatures and environments.

Since, the boiling point of DMSO is 189 °C, evaporating it at 140 °C will take significant amount of time. Moreover, the T_{g1} and T_{g2} of the electro-spun acetone-soluble fibres are approximately 140 °C (note the uncertainty in the T_{g1} because the fibres are solvent-rich) and 154.4 °C, respectively. Subjecting these fibres to temperature in excess of their T_g can cause sagging and fibres fusion at the contact point. The extent of fibres fusion can be influence of many factors. (i) The volume of solvent that is retained in the electro-spun fibres as they are deposited on the ground plate. (ii) The relative diameter of the electro-spun fibres as a function of electro-spinning time. This is stated in the context of variability in fibre diameter. (iii) The evaporation rate of the solvent as it resides on ground plate. This will be a function of the surface-properties of the fibres and the environmental temperature. (iv) Surface evaporation from the fibres will enable a skin to be formed, depending on its thickness and mechanical properties. The skin can enable retention of a circular geometry. (v) The storage conditions of the fibres can also influence its cross-section. For example, a solvent-loaded fibre will creep and sag under its own weight when subjecting them to heat treatment in a vacuum oven.

Heating the fibres in a vacuum oven is one way to accelerate the evaporation of solvents as it can increase the partial pressure difference and reduce the boiling point of the solvent. From the integration of the Clausius-Clapeyron equation (Equation (5.1)) [296], it can be figured out that the boiling point of DMSO is reduced to 140 °C when the vacuum is lowered to 200 mbar (see Figure 5.12). Therefore, heating the electro-spun acetone-soluble fibres at 140 °C in a vacuum oven can be an effective method to reduce the concentration of DMSO in the fibres.

$$\ln\left(\frac{P_2}{P_1}\right) = -\frac{\Delta H_{\text{vap}}}{R}\left(\frac{1}{T_2} - \frac{1}{T_1}\right) \quad \text{Equation 5.1}$$

where P_i in torr represents vapour pressure at temperature T_i (K), ΔH_{vap} is the enthalpy of vaporization ($\text{J}\cdot\text{mol}^{-1}$) and R is the ideal gas constant ($8.314 \text{ J}\cdot\text{mol}^{-1}$).

The boiling points and enthalpies of vaporization (ΔH_{vap}) for acetone are 56 °C and 40.65 k J·mol⁻¹ and 189 °C and 52.9 kJ·mol⁻¹ for DMSO, respectively.

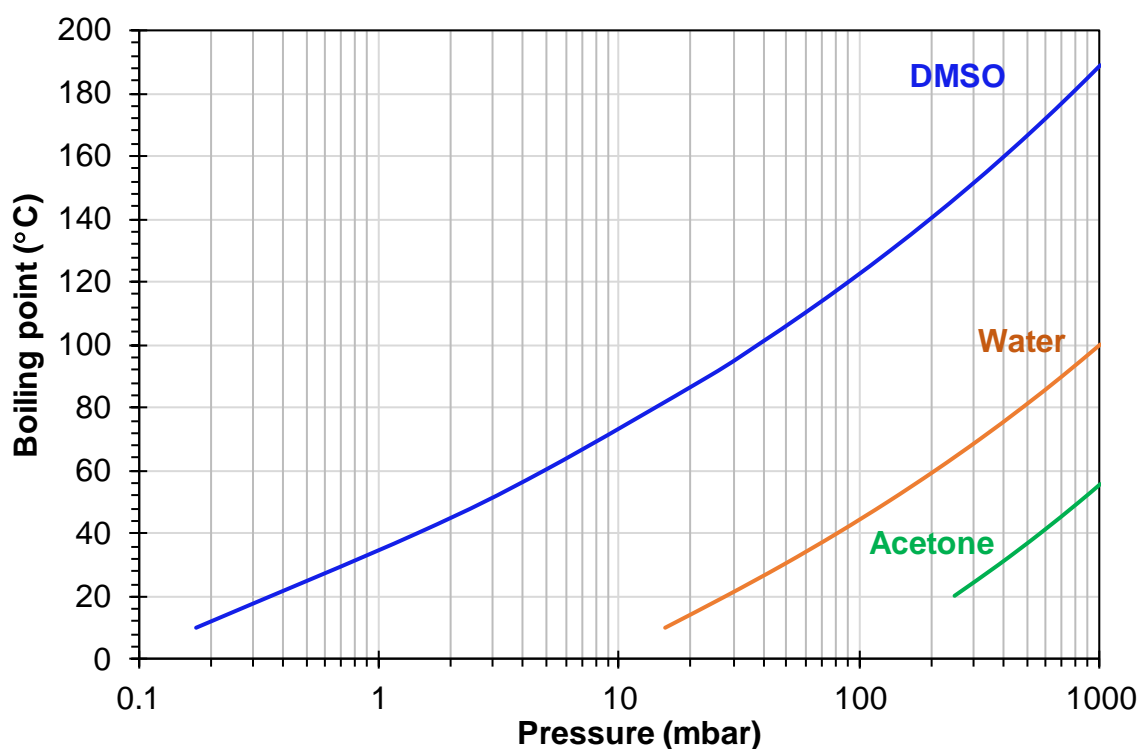


Figure 5.12 Relationship between boiling point and external pressure for DMSO, water and acetone [296].

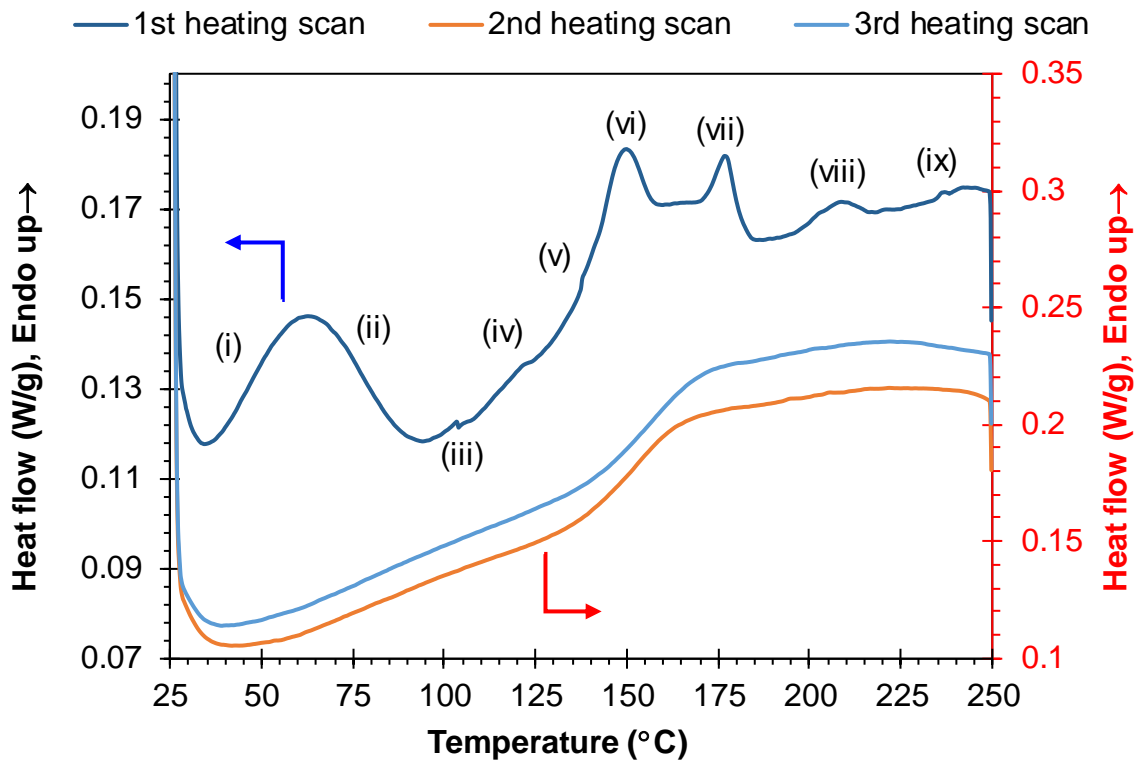
5.5.2 Differential Scanning Calorimetry of Heated Electro-spun Acetone-soluble Lignin Fibres

As discussed in Section 5.5.1, the electro-spun acetone-soluble lignin fibres were heated in a vacuum oven at 140 °C for six hours. Prior to venting the vacuum oven to atmosphere, the gas inlet was connected to a silica gel canister to prevent moisture from being introduced into the vacuum oven and the lignin sample. Moreover, the electro-spun lignin sample was stored in a desiccator until required. Therefore, the presence of the endotherm in the DSC scan (regions (i) and (ii)) as shown in Figure 5.13 (a) is puzzling. However, the moisture absorption can be expected due to

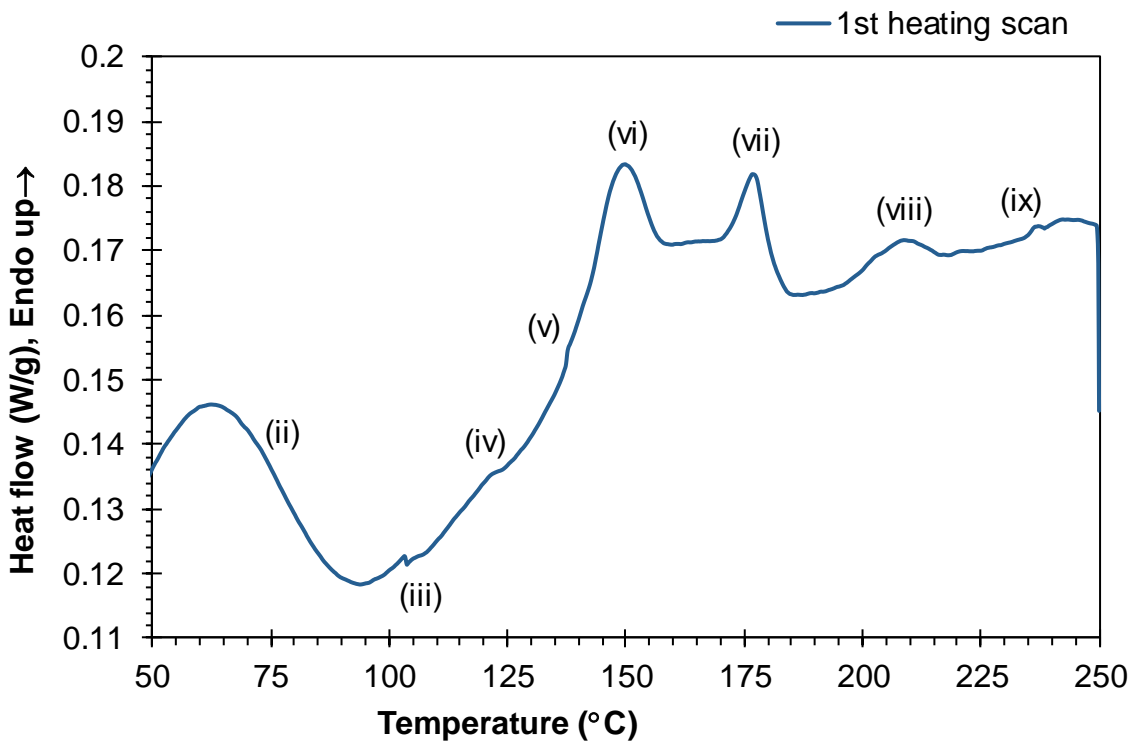
the sample being exposed to the atmosphere during preparation and weighing the sample for the DSC measurement. A noticeable blip located at (iii) is the same as that discovered in the electro-spun fibres. This is possibly due to volatiles escaping suddenly from the sample via the two holes on the crimped top-lid of the sample pan.

In Figure 5.13 (b) the baseline is seen to increase gradually as a function of temperature with a rapid increase between 105 and 151 °C; this is attributed to the T_g . During this increase, two small endothermic peaks at 122 °C (iv) and 134 °C (v) are noticeable, however, its origin is still unclear. Coded point (iv) and (v) may be attributed to enthalpy relaxation during solvent evaporation. Coded items (vi) and (vii) this can be attributed to the evaporation of DMSO associated with water and DMSO, respectively. The presence of two thermal events can be seen at 210°C (viii) and 245 °C (ix). However, the origin of these thermal events are still unclear in their explanation. T_g s reading from the second and third heating scans for the electro-spun soluble lignin fibres heated in a vacuum oven at 140 °C for six hours are 149.4 ± 0.8 °C and 154.5 ± 1.6 °C, respectively.

Figure 5.14 illustrates an overlaid plot for the first heating scan acquired from electro-spun fibres (dotted line) and the electro-spun fibres heated in a vacuum oven at 140 °C for six hours (solid line). Heating the electro-spun fibres for six hours at 140 °C in a vacuum oven result in a significant decrease in the peak areas (a, b and c). The observed trend indicates clearly that the electro-spun fibres contained moisture, acetone and DMSO. Peak-a is attributed to evaporation of acetone and water. Peak-b is possibly due to water associated with DMSO. Since the peak-b at 117 °C is not present in the electro-spun fibres heated in a vacuum oven, it can be attributed to the evaporation of DMSO. Peak-c at 205 °C decrease significantly when compared to the fibres heated in the vacuum oven. The reduction of the three peaks correlates with their mass-loss recorded prior to and after the DSC scans. The mass-loss of the electro-spun acetone-soluble lignin fibres heated in the vacuum oven is 4.2 - 4.4% which is significantly lower than that of the mass-loss of the electro-spun fibres (13.4 - 15.7%).



(a)



(b)

Figure 5.13 DSC thermograms illustrating three successive heating scans for electro-spun acetone-soluble lignin fibres heated in a vacuum oven at 140 °C for six hours.

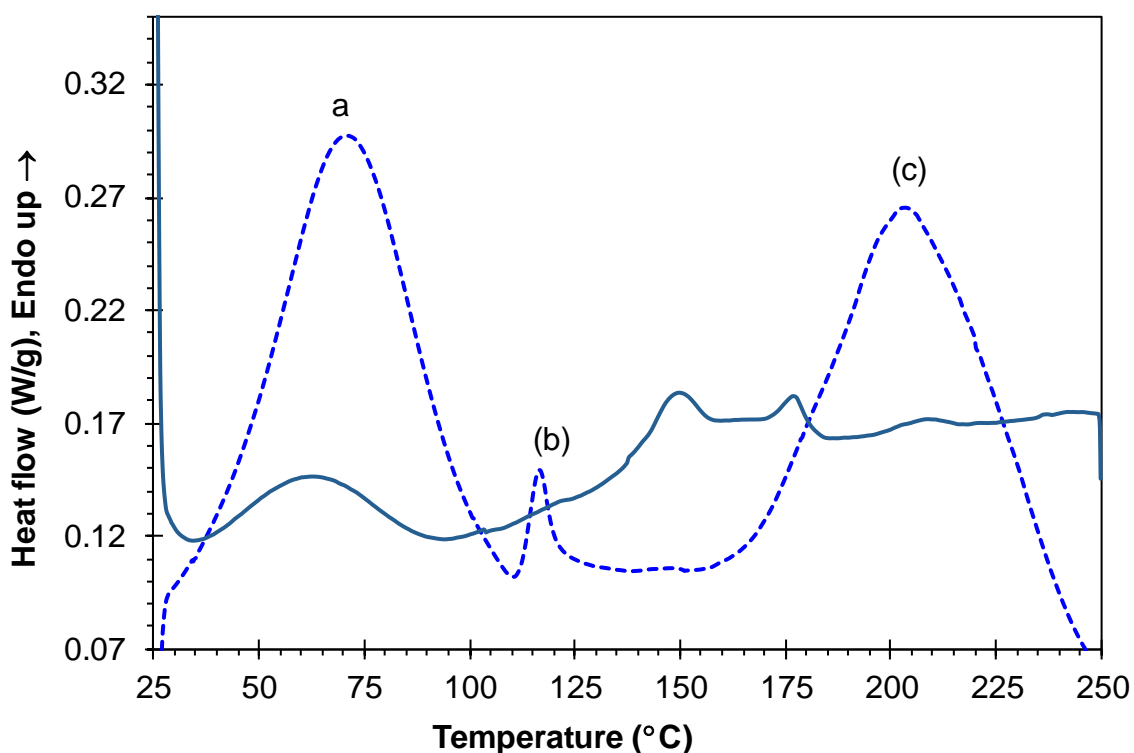


Figure 5.14 An overlaid the first heating scan thermogram of electro-spun acetone-soluble lignin (dotted line) and the electro-spun fibres heated in a vacuum oven at 140 °C for six hours (solid line).

5.5.3 Thermo-gravimetric Analysis of Heated Electro-spun Acetone-soluble Lignin Fibres

Figure 5.15 shows the mass-loss and DTG curves for electro-spun acetone-soluble lignin fibres heated in a vacuum oven at 140 °C for six hours. The mass-loss reading at 250 °C is 4.27%, which is in the same range of mass-loss recorded from the DSC measurement reported in Section 5.5.2 (4.2 - 4.4%).

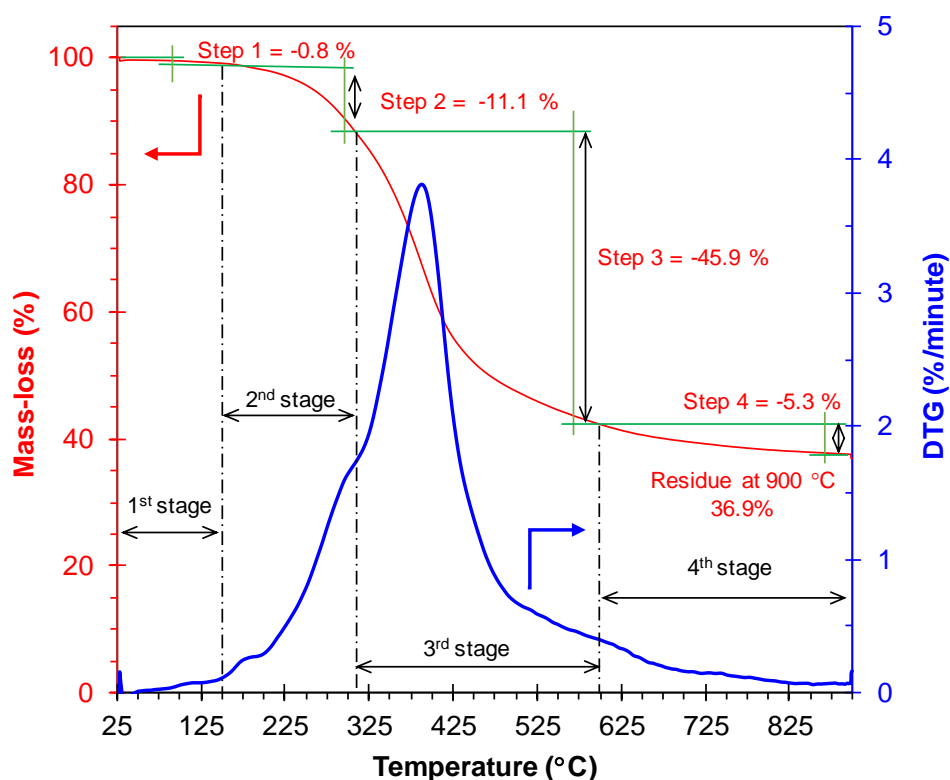


Figure 5.15 TGA and DTG curves for electro-spun lignin acetone-soluble lignin fibres heated on a vacuum oven at 140 °C for six hours.

Figure 5.16 illustrates overlaid DTG and mass-loss curves for: a- acetone-soluble lignin powder, b- electro-spun acetone-soluble lignin fibres and c- electro-spun acetone-soluble lignin fibres heated in a vacuum oven at 140 °C for six hours. The solid lines represent the DTG curves and the dotted lines correspond to mass-loss data. Considering trace-c, in Figure 5.16, the two sharp peaks at 132.1 °C and 221.3 °C are not present. This can be attributed to removal of volatile during heating in the vacuum oven. The DTG for trace-c, the electro-spun fibres heated in vacuum oven at 140 °C for six hours, is similar to that of trace-a, the acetone-soluble lignin powder. The electro-spun fibres heated in a vacuum oven exhibits a sharp peak at 393.3 °C. This corresponds to thermal degradation with a rate of 3.78 %/°C. This rate is noticeably higher than that of acetone-soluble lignin powder (trace-a). This may be due to the higher surface area of the electro-spun acetone-soluble lignin fibres. However, the residual mass at 900 °C for the three samples are in the range 35-36%.

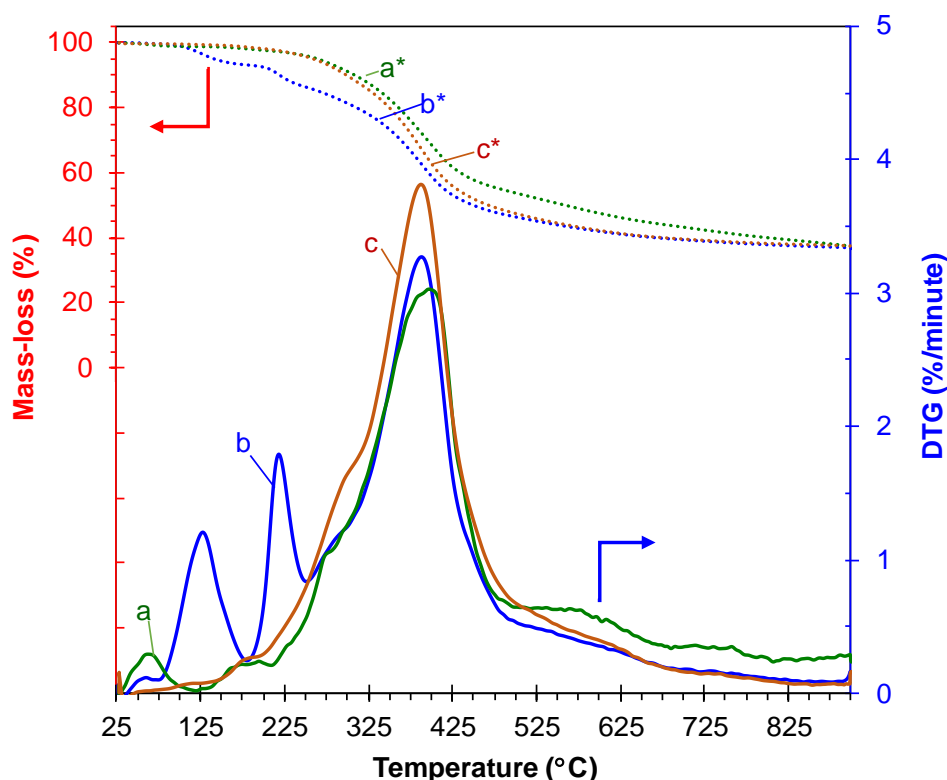


Figure 5.16 DTG and TGA and curves: a- acetone-soluble lignin powder, b- electro-spun acetone-soluble lignin fibres, c- electro-spun acetone-soluble lignin fibres heated in a vacuum oven at 140 °C for six hours. Sample code with an asterisk represents the mass-loss data.

5.5.4 Fourier Transform Infrared Spectroscopy of Heated Electro-spun Acetone-soluble Lignin Fibres

The FTIR spectra does not present any significant change for the electro-spun acetone-soluble lignin as a function of the heating temperature and environment. The FTIR spectra for the samples are compiled and shown in Appendix C. An example of overlaid FTIR spectra obtained from the sample heated in air, nitrogen and a vacuum at the same temperature of 140 °C are illustrated in Figure 5.17. The FTIR spectra of acetone-soluble lignin is plotted and used as a benchmark.

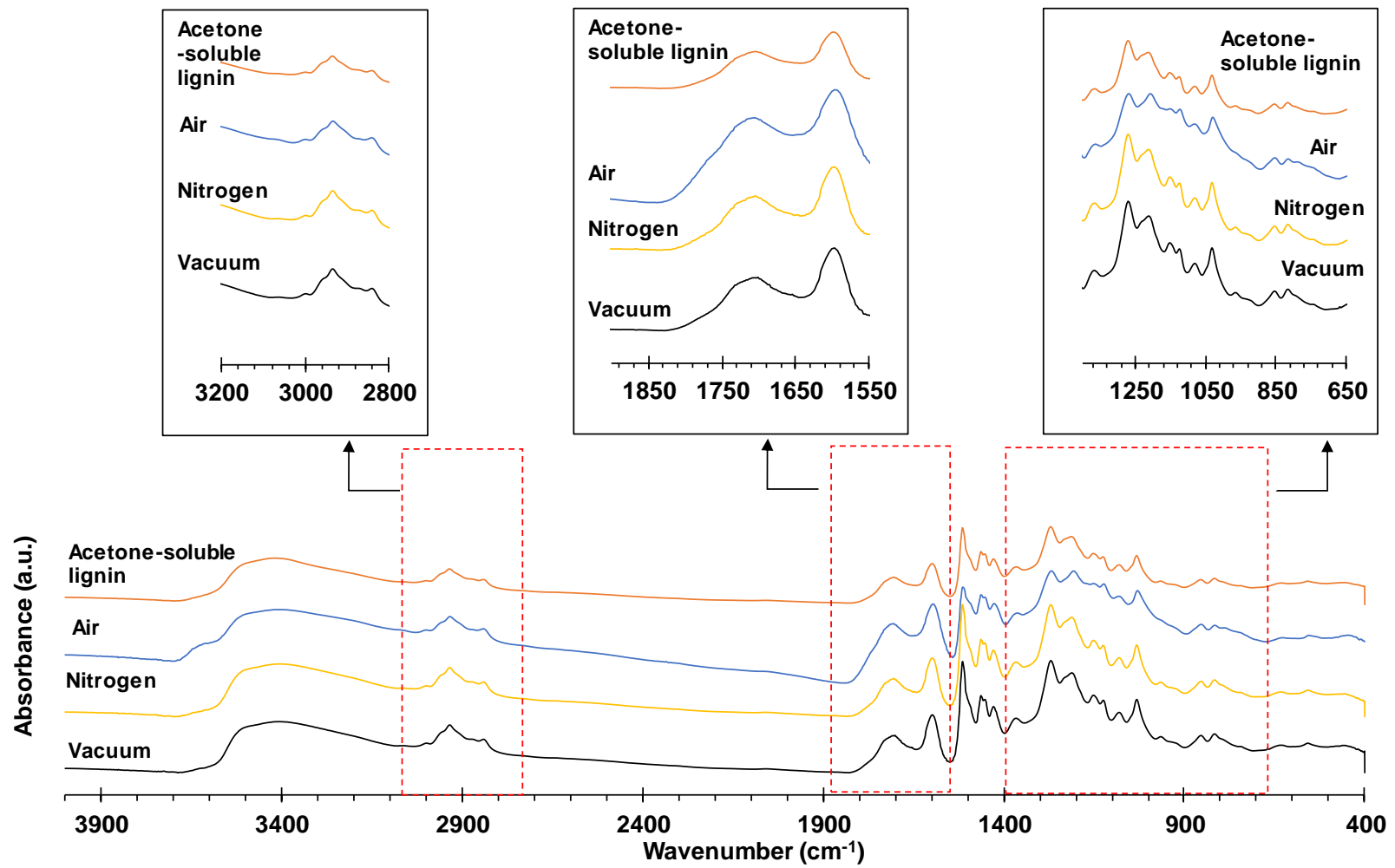


Figure 5.17 Overlaid FTIR spectra for lignin fibres dried in an air-circulating and nitrogen-circulating and a vacuum oven at 140 °C.

5.6 Thermo-stabilisation of Electro-spun Acetone-soluble Lignin Fibres

After heating the electro-spun acetone-soluble lignin fibres as discussed previously in Section 5.5, thermo-stabilisation experiments were conducted separately using air- and nitrogen-flow in a tube furnace. The selection of the temperature for thermo-stabilisation was based on the TGA data for the electro-spun acetone-soluble fibres heated in a vacuum oven, which is shown in Figure 5.15. The onset for maximum T_{DTG} was 263.35 °C, therefore the thermo-stabilisation temperature was selected to be 250 °C at 0.5 K·minute⁻¹. In order to remove moisture and the solvent retained in the sample, the electro-spun fibres were subjected to isothermal dwells at 100 °C, 150 °C and 250 °C for one hour in a sequential fashion. Fibre samples were removed after they were thermo-stabilised at 150°C, 180°C, 200°C, 220°C and 250°C in order to observe the changes in the fibre morphology.

Figure 5.18 shows a photograph of a set of the electro-spun fibres thermo-stabilised at different temperatures. The fibres did not show any evidence of fibre-to-fibre fusion after thermo-stabilisation in air. However, the electro-spun acetone-soluble lignin fibres that were thermo-stabilised in nitrogen were fused and could not retain their shape.

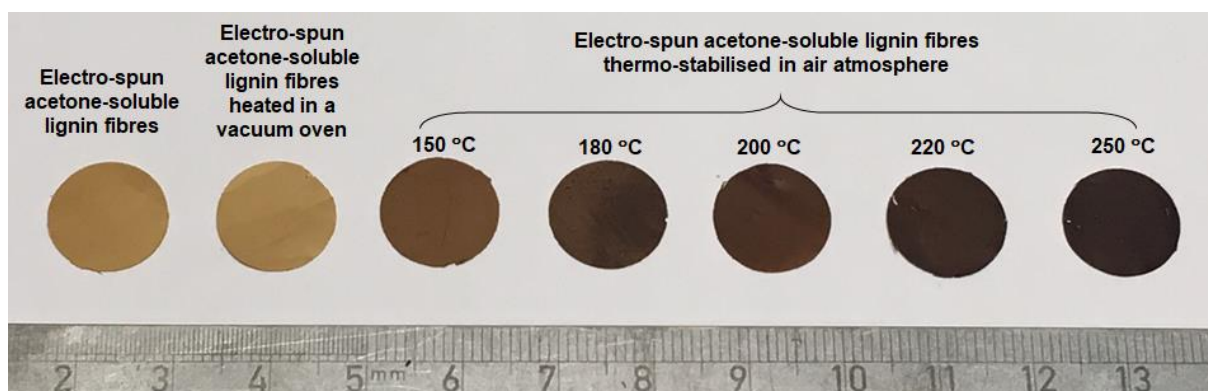


Figure 5.18 Photographs of the electro-spun acetone-soluble lignin fibres showing the colour after thermo-stabilisation in air.

5.6.1 Scanning Electron Microscopy of Thermo-stabilised Electro-spun Acetone-soluble Lignin Fibres

In Figure 5.19 (a-e), at first sight it seems that the electro-spun fibres that were thermo-stabilised in nitrogen were fused and that the degree of fibre fusion increased with increasing temperature. However, this was not the case with the electro-spun fibres that were thermo-stabilised in air. Figure 5.19 (f-j) show that these fibres retained their overall form and shape up to 250 °C.

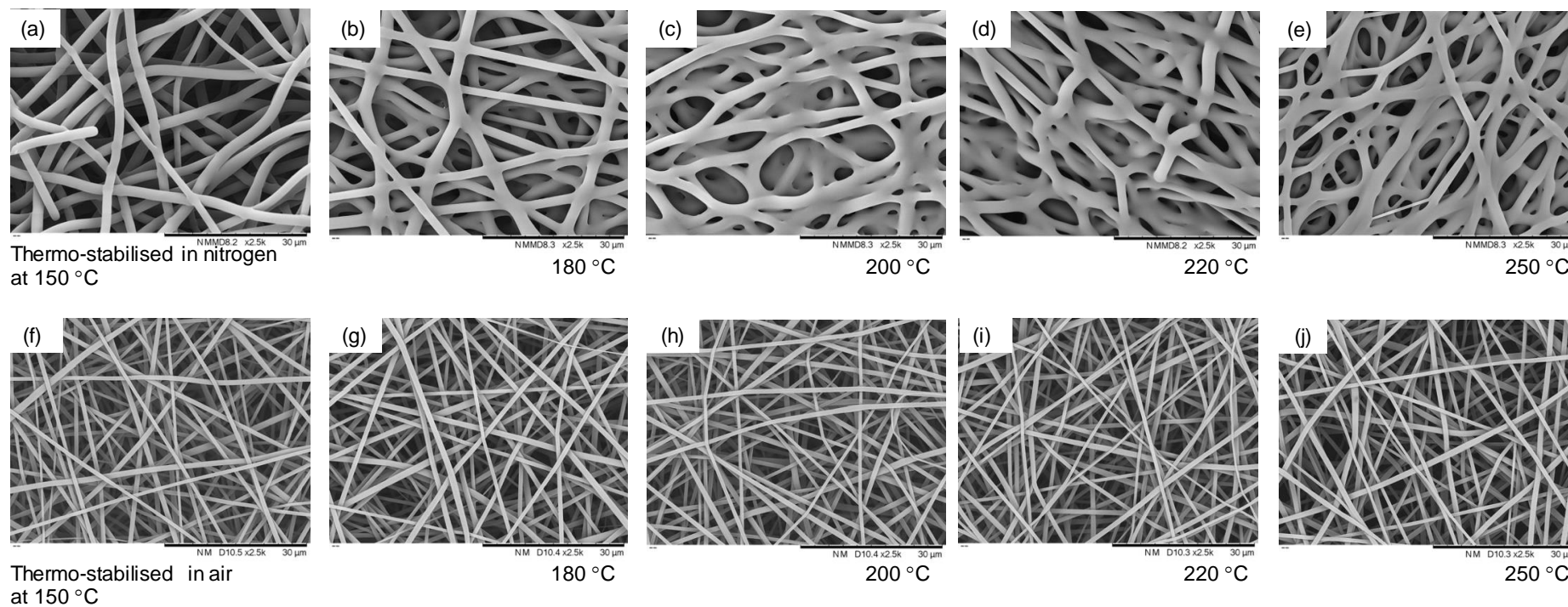


Figure 5.19 Fibres morphologies of the electro-spun acetone-soluble lignin fibres thermo-stabilised in: nitrogen (a-e) and air (f-j) at 150 to 250 °C with a dwell time of one hour.

5.6.2 Differential Scanning Calorimetry of Thermo-stabilised Electro-spun Acetone-soluble Lignin Fibres

The electro-spun acetone-soluble lignin fibres were characterised using DSC to study the effect of the environment (air or nitrogen) and the thermo-stabilisation temperature. The main focus was on determining the T_g of the electro-spun acetone-soluble lignin fibres. Correlation between the T_{g2} read from the second heating scan and fibre morphology was investigated as a function of the thermo-stabilisation conditions. DSC thermograms of the samples thermo-stabilised in air and nitrogen are presented in Figure 5.20 and Figure 5.21, respectively. The analysed values are compiled in Table 5.4. The DSC trace for the electro-spun acetone-soluble lignin fibres that were heated in a vacuum oven at 140 °C for six hours is plotted and used for comparison, which is labelled as an asterisk (*).

With reference to Figure 5.20 (a), traces from the first heating scan, the fibres showed a broad endothermic peak and a glass transition. The enthalpy of vaporisation obtained from the endothermic peak of the fibres stabilised at below 220 °C was approximately 5-10 J·g⁻¹. A significant increase in the enthalpy to about 42 J·g⁻¹ was noticed for the fibres stabilised at 250 °C. The T_{g1} from the first heating scan was found to be in the range 153-158 °C.

Figure 5.20 (b) shows a clear T_{g2} in the second heating scan, T_{g2} of the fibres thermo-stabilised in nitrogen increased slightly as compared to the fibres heated in the vacuum oven. T_{g2} increased to 163°C from 151 °C. Considering the T_{g2} of the fibres in thermo-stabilised in nitrogen, the thermo-stabilisation temperature and corresponding T_{g2} were expressed as a set of values: (150 °C, T_{g2} = 159.3 °C); (180 °C, T_{g2} = 157.4 °C); (200 °C, T_{g2} = 158.9 °C); and (220 °C, T_{g2} = 163.8 °C). As can be seen, the T_g values become lower than the thermo-stabilised temperature when the thermo-stabilised temperature is 180 °C. This can explain the fibres fusion reported previously in Figure 5.19 (a-e) where the fibres fusion is seen at 180 °C, and the degree of fibres fusion increased when thermo-stabilisation temperature was increased.

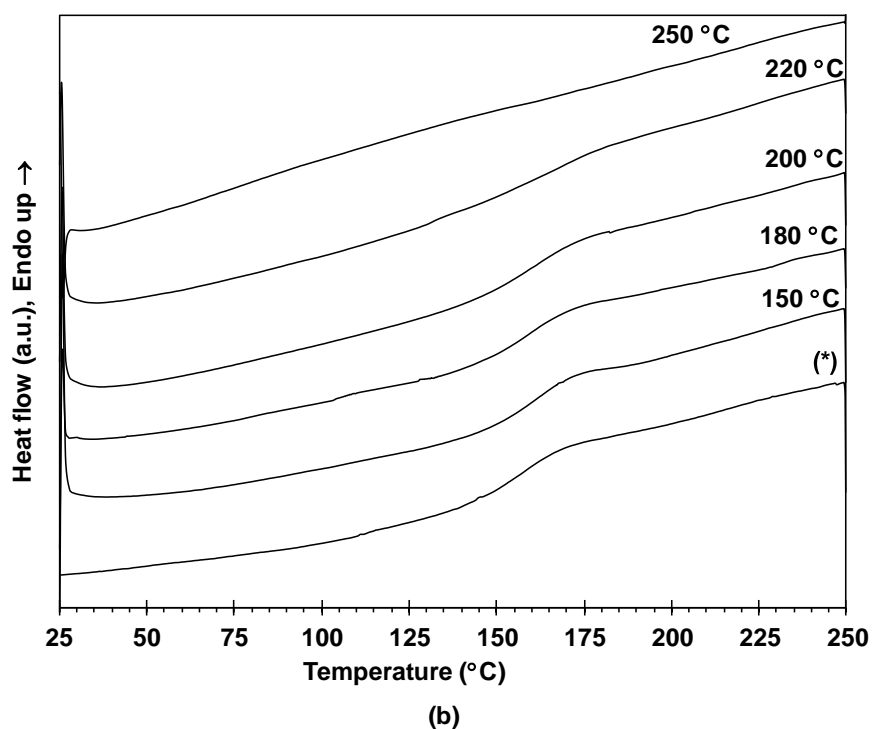
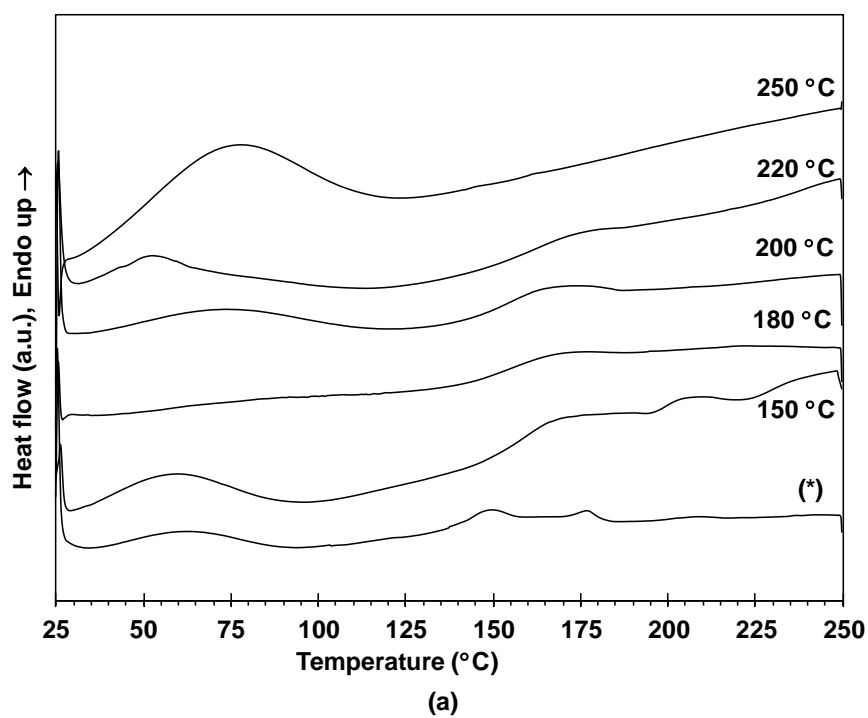
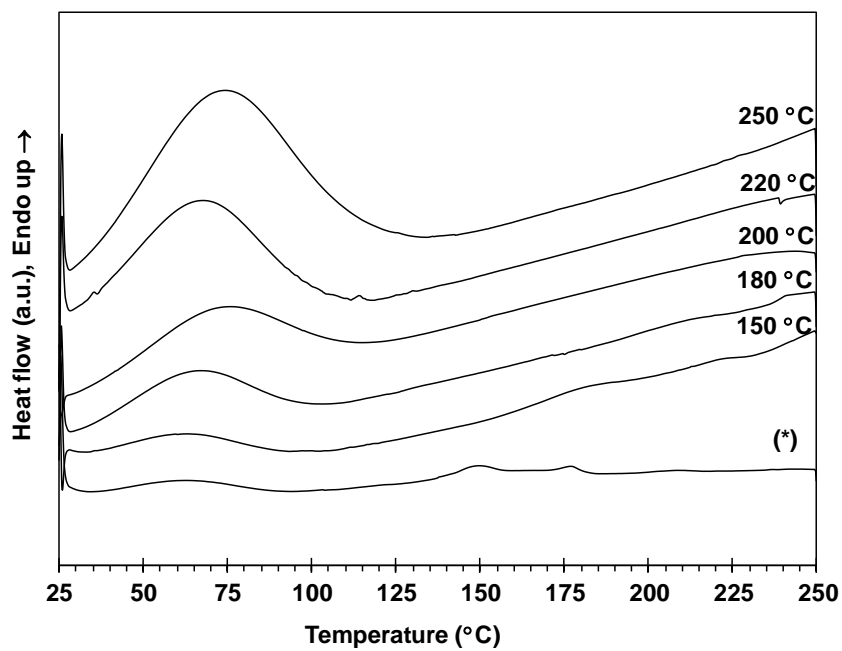
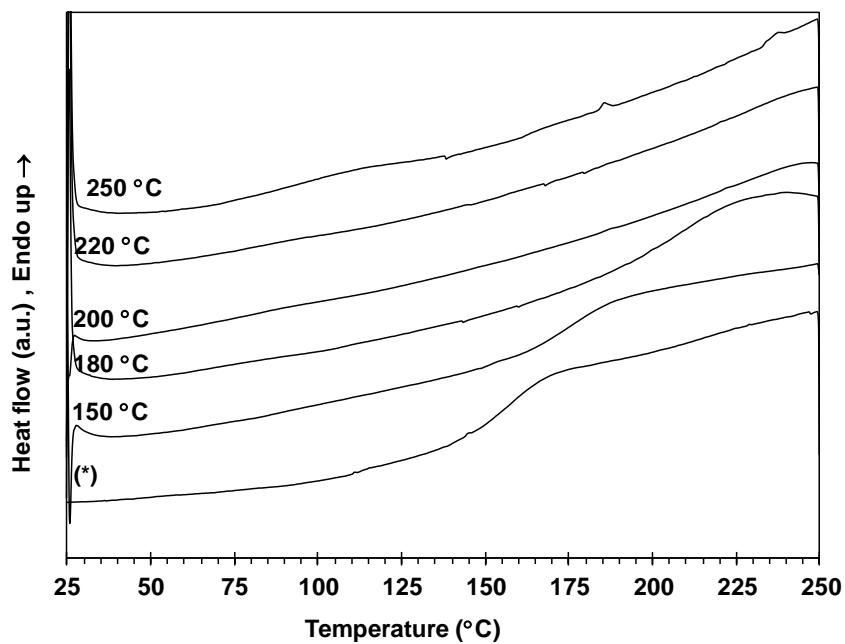


Figure 5.20 DSC thermograms of lignin fibres thermo-stabilised in nitrogen (a) first heating scan and (b) second heating scan. (*) DSC traces of the electro-spun acetone-soluble lignin fibres heated in a vacuum oven at 140 °C for six hours.



(a)



(b)

Figure 5.21 DSC thermograms for electro-spun acetone-soluble lignin fibres thermo-stabilised in nitrogen: (a) first heating scan and (b) second heating scan. (*) DSC traces for the electro-spun acetone-soluble lignin fibres heated in a vacuum oven at 140 °C for six hours.

Table 5.4 Compiled DSC results for thermo-stabilised samples.

Samples	Temperature	First heating scan					Second heating scan
		Endothermic peak					T _{g2} (°C)
		Onset (°C)	Peak (°C)	Endset (°C)	Enthalpy (J·g ⁻¹)	T _{g1} (°C)	
Electro-spun acetone-soluble lignin fibres heated in a vacuum oven	140 °C	39.5	62.5	86.9	4.8	N/A	150.7
Thermo-stabilisation of electro-spun acetone-soluble lignin fibres in nitrogen	150°C	33.5	59.7	85.3	11.4	158.1	159.3
	180°C	N/A	N/A	N/A	N/A	155.5	157.4
	200°C	26.5	74.3	124.1	10.2	153.0	158.9
	220°C	39.2	72.5	104.9	6.4	157.3	163.6
	250°C	27.5	74.3	113.6	42.5	N/A	N/A
Thermo-stabilisation of electro-spun acetone-soluble lignin fibres in air	150°C	25.4	63.2	96.8	8.4	168.3	173.8
	180°C	33.3	65.5	95.6	33.3	202.5	205.1
	200°C	34.9	72.5	109.2	42.6	N/A	N/A
	220°C	34.2	67.5	100.8	61.4	N/A	N/A
	250°C	33.6	73.7	114.6	124.4	N/A	N/A

With reference to Figure 5.21 (a) and the compiled data in Table 5.4, the first heating scans of the electro-spun fibres thermo-stabilised in air show a broad endothermic peak and the enthalpy increases as a function of the thermo-stabilisation temperature. The enthalpy of the fibres thermo-stabilised at 250 °C in air and in nitrogen are 124.4 J·g⁻¹ and 42.5 J·g⁻¹, respectively. These endothermic peaks indicate the presence of moisture in the samples. The higher in enthalpy of the fibres thermo-stabilised in air can be explained by the changes in chemical structure during thermo-stabilised in air. The changes in chemical structure and elemental composition will be reported in Sections 5.6.3 and 5.6.4.

Figure 5.21 (b) shows a clear T_{g2} in the second heating scan. The T_{g2} for the fibres thermo-stabilised in air increase significantly compared to the fibres heated in the vacuum oven. The T_{g2} increased from 150.7 °C to 205.1 °C when the sample was thermo-stabilised at 180 °C. T_{g2} could not be observed within the measurement range of 250 °C when the fibres were thermo-stabilised in air at above 200 °C. Increased T_g for lignin after oxidative thermo-stabilisation has been reported in the literature [134,217,218]. With reference to the morphology of electro-spun fibres thermo-stabilised in air presented in Figure 5.19 (f-j), it is seen that the fibres can retain their structure. The retaining fibre structure correlate well with their T_g. If the T_g is higher than the thermo-stabilisation temperature fibres fusion is prevented. The factors that can give rise to fibres fusion for electro-spinning fibres were discussed previously in section 5.5.1.

5.6.3 Fourier Transform Infrared Spectroscopy of Thermo-stabilised Electro-spun Acetone-soluble Lignin Fibres

The changes in the functional groups in the electro-spun acetone-soluble lignin fibres thermo-stabilised in different environments were investigated using FTIR spectroscopy. The spectra of the samples thermo-stabilised in nitrogen and air are shown in Figure 5.22 and Figure 5.23, respectively. The gas flow rate in each case was constant at 50 ml·minute⁻¹. Expanded views of the regions between 3,100-2,800 cm⁻¹, 1,900-1,550 cm⁻¹ and 1,400-650 cm⁻¹ are inserted in their parent

figures. FTIR spectra of the electro-spun fibres heated in a vacuum oven at 140 °C for six hours are included for cross-comparison and it is coded with an asterisk.

The fibres thermo-stabilised in nitrogen at 150, 180, 200, 220 and 250 °C did not show any significant changes in their FTIR spectra compared to the fibres heated in the vacuum oven, as shown in Figure 5.22. However, the electro-spun acetone-soluble lignin fibres thermo-stabilised in air showed significant changes.

With reference to Figure 5.23, the three absorbance bands between 2,930-3,000 cm^{-1} corresponding to C-H stretching [97,265,266] disappear completely when the thermo-stabilisation temperature was raised to 250 °C. This suggests the occurrence of demethylation had occurred [13,217,218,222,297]. In addition to the disappearance of the C-H stretching, an absorbance band between 1720-1690 cm^{-1} (C=O stretching) was observed to shift to the left and peak intensity increased with a function of temperature. The increasing C=O absorbance in the fibres thermo-stabilised in air at 220 and 250 °C may be attributable to the formation of unconjugated carbonyl, esters, ketone and aldehyde [198,218,220,291]. A decrease intensity of C-O absorbance at 1,218, 1,081 and 1,033 cm^{-1} was found on the fibres thermo-stabilised in air at 220 °C, and these bands became broader and disappeared when the sample was thermo-stabilised in air to 250 °C. The decrease in the C-O band can be explained by the cleavage of α -O-4' and β -O-4' bonds [134,217,221,222]. Moreover, when the temperature was raised to 250 °C, a new shoulder at 1,850 cm^{-1} corresponding to anhydride linkage was observed which reported in the literature [218]. The formation of aldehyde has also been reported in the literature [198,218,291,298]. In the wavelength range 800-1,400 cm^{-1} , no absorbance bands were presented. The peaks at 822 cm^{-1} and 855 cm^{-1} are assigned to C-H stretching of the G-unit diminished and disappeared when the thermo-stabilisation temperature was raised to 220 °C. This indicates a change in molecular structure via cross-linking at the C5-position [134,218,221]. Further evidence for the molecular structural changes via the increasing aromaticity was observed with the formation of the band at 750 cm^{-1} . This is assigned to aromatic out-of-plane bending of C-H bonds [107,291]. FTIR spectral results reported in this current work are similar to those for FTIR and NMR spectroscopy [134,221,223] reported in the literature.

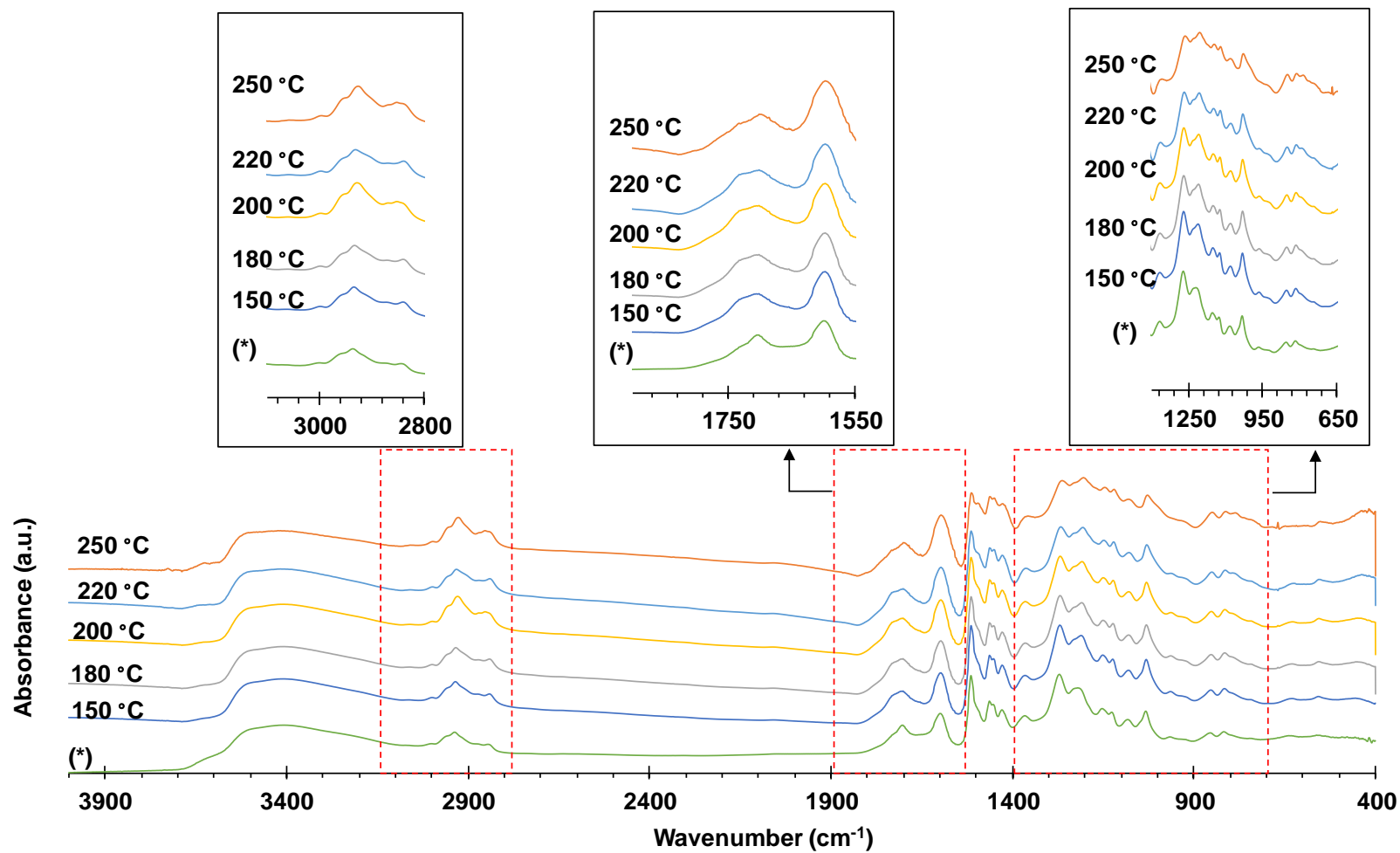


Figure 5.22 FTIR spectra of lignin thermo-stabilised in nitrogen ($50 \text{ ml}\cdot\text{minute}^{-1}$) at 150, 180, 200, 220 and 250 °C. (*) FTIR spectra of the electro-spun fibres heated in a vacuum oven at 140 °C for six hours.

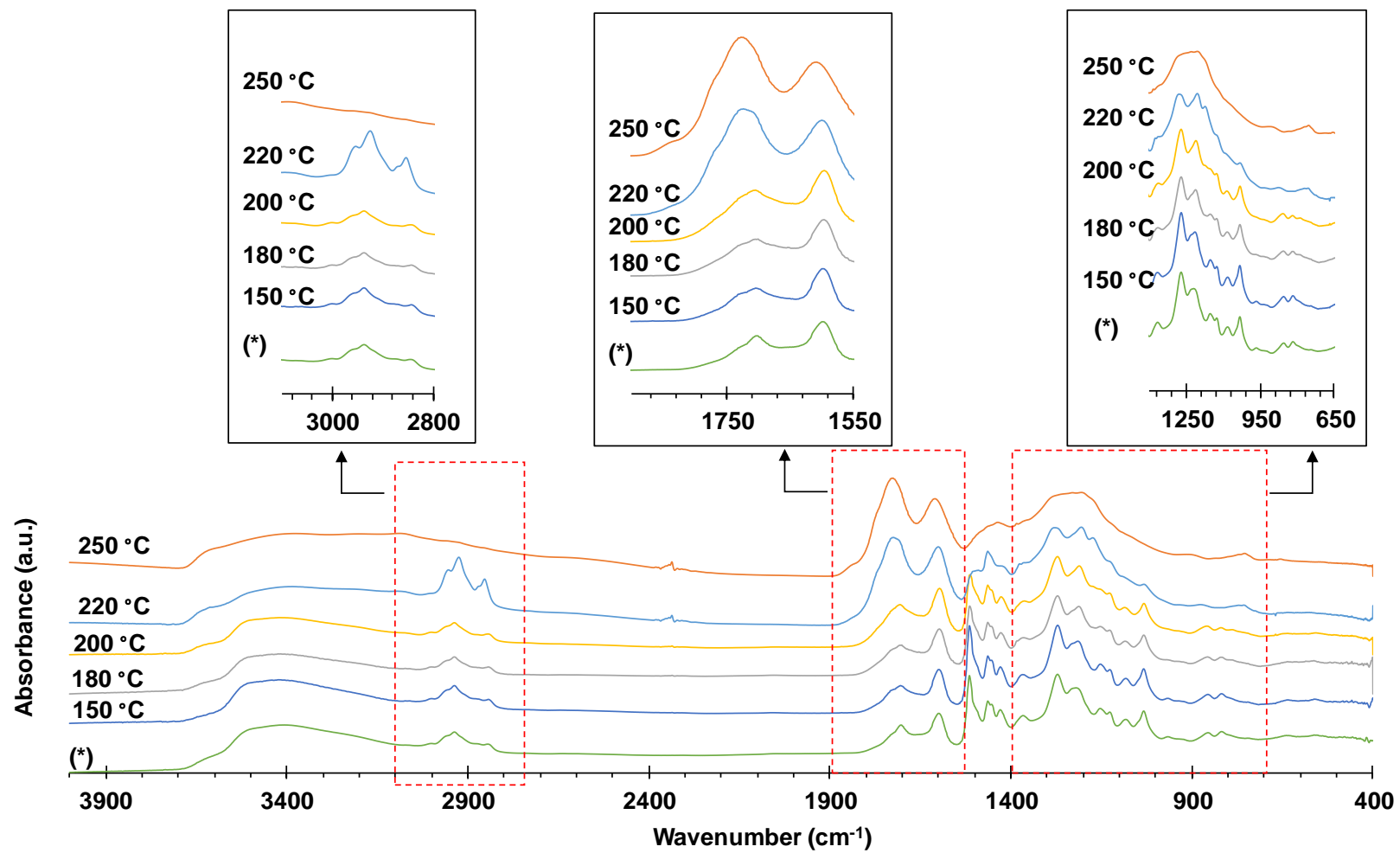


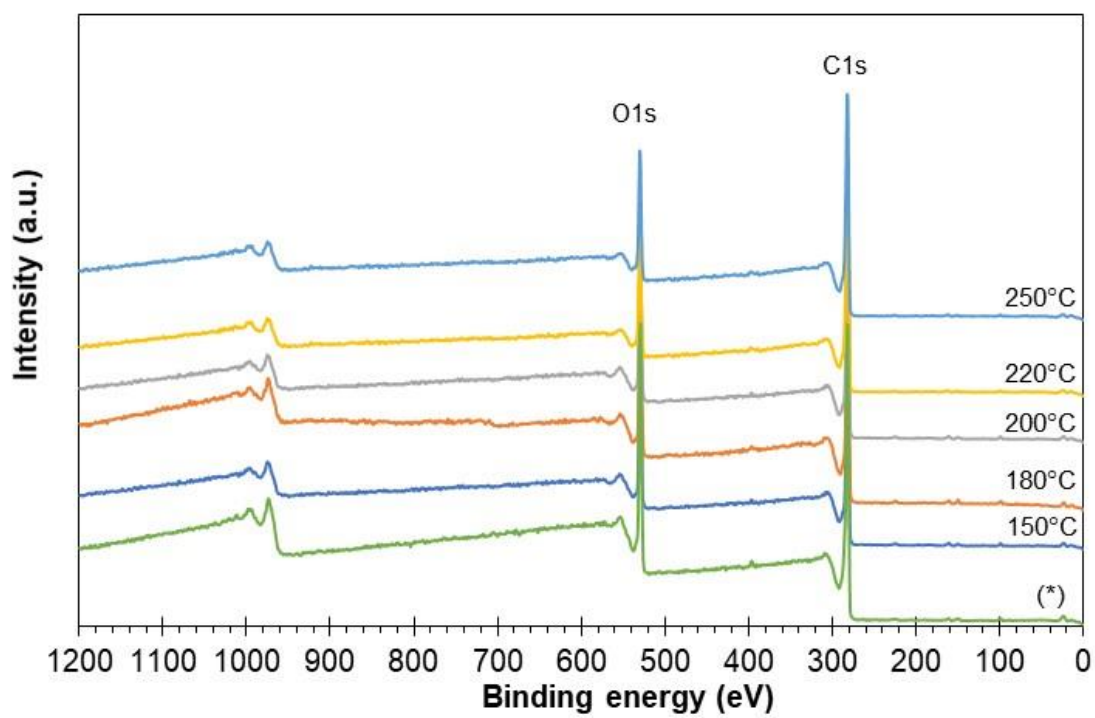
Figure 5.23 FTIR spectra of lignin thermo-stabilised in air (50 ml·minute⁻¹) at 150, 180, 200, 220 and 250 °C. (*) FTIR spectra of the electro-spun fibres heated in a vacuum oven at 140 °C for six hours.

5.6.4 X-ray Photoelectron Spectroscopy of Thermo-stabilised Electro-spun Acetone-soluble Lignin Fibres

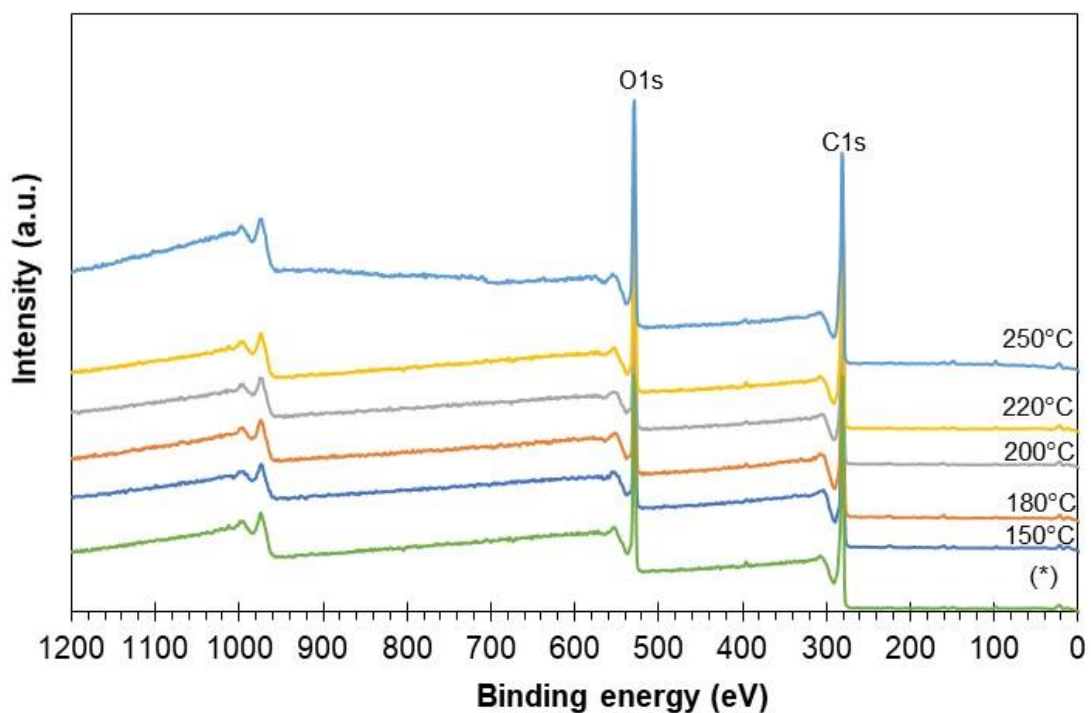
X-ray Photoelectron Spectroscopy (XPS) was used to study the chemical composition of oxidised lignin fibre surface. The formation of carboxyl (C(=O)-OH) and ester (O-C=O) groups have been detected on the surface of oxidative thermo-stabilised lignin [134,217]. In the current study, XPS was performed on the surface of electro-spun acetone-soluble lignin fibres that were thermo-stabilised in nitrogen and air.

Figure 5.24 (a and b) shows low-resolution XPS spectra. Spectra of electro-spun acetone-soluble lignin fibres heated in a vacuum oven at 140 °C for six hours are indicated by an asterisk. This spectral was used as the benchmark or refernce spectra for comparison. Carbon (C1s) and oxygen (O1s) peak at 284.93 eV and 533.33 eV, respectively [217,299,300] are the two major elements found on the fibre surface. Sulphur (S2p) at 164.7 eV was also detected. The compositions of carbon, oxygen and sulphur are 79-82, 17-20 and below 1 atomic %, respectively, and the relative concentrations of C1s, O1s and S2p as a function of thermo-stabilisation temperature is summarised in Table 5.5. The presence of sulphur is consistent with the results from the analysis of the ash discussed in Section 4.4.2.3 and the use of DMSO.

After thermo-stabilisation in nitrogen, no significant changes could be noticed, except for the sample that was processed at 250 °C. An increase in the carbon content and a lower of oxygen content was noticed when compared the electro-spun fibres that were heated in the vacuum oven. On the other hand, a significant change could be seen in the carbon and oxygen content for the lignin fibres that were thermo-stabilised in air. An obvious reduction in the carbon content and an increase oxygen content is seen as a function of temperature. This indicates that air thermo-stabilisation leads to the formation of oxygen contain structural unit lignin. This trend correlates well with that reported the literature [134,217,218,220]. The increase in the oxygen content can influence the moisture absorption characteristics.



(a)



(b)

Figure 5.24 XPS spectra of electro-spun acetone-soluble lignin heated in: (a) nitrogen and (b) air. (*) XPS spectra of the electro-spun acetone-soluble lignin fibres heated in a vacuum oven at 140 °C for six hours.

Table 5.5 Carbon, oxygen and sulphur contents for as-spun lignin fibres heated in a vacuum oven and in nitrogen or oxygen at specified temperatures.

Samples	Temperature	Carbon (atomic%)		Oxygen (atomic%)		Sulphur (atomic%)	
		Ave	SD	Ave	SD	Ave	SD
Electro-spun fibres heated in vacuum oven for six hours	140 °C	82.12	0.21	17.33	0.21	0.55	0.04
Electro-spun fibres thermo-stabilised in nitrogen	150 °C	82.34	0.27	17.12	0.26	0.54	0.09
	180 °C	82.02	0.26	17.66	0.25	0.32	0.07
	200 °C	79.30	0.28	20.04	0.28	0.66	0.18
	220 °C	80.57	0.29	19.04	0.28	0.39	0.10
	250 °C	85.23	0.29	14.56	0.29	0.21	0.07
Electro-spun fibres thermo-stabilised in air	150 °C	82.73	0.24	16.78	0.23	0.49	0.07
	180 °C	81.62	0.24	17.82	0.23	0.56	0.08
	200 °C	79.92	0.27	19.83	0.26	0.25	0.06
	220 °C	78.46	0.26	21.27	0.25	0.27	0.07
	250 °C	74.94	0.27	24.90	0.26	0.16	0.05

High-resolution XPS spectra of the C1s peak were curve-fitted in order to determine the chemical state of carbon on the fibre surface. Four carbon peaks of C1, C2, C3 and C4 were fitted and the deconvoluted peaks were correlated to different functional groups between carbon and oxygen. The C-C component of the C1s spectrum of carbon (at 285.0 eV) was used to set the binding energy scale. Shifting of the deconvoluted bands relative to the C1 at 285.0 eV and functional groups are listed in Table 5.6.

Table 5.6 Chemical state of carbons and their binding energy and function groups between carbon and oxygen [299,301–303].

Chemical state	Band shifting relative to C1 (eV)	Functional groups
C1	285	C-C, C=C, C-H
C2	286.4 - 286.6	C-O, C-O-C
C3	287.7 - 287.9	C=O, O-C-O
C4	289.0 - 289.4	O-C=O, (C=O)-OH

Figure 5.25 (a and b) shows examples of the deconvoluted peaks of high-resolution spectra within the C1s region; other deconvoluted spectra are compiled in Appendix D. Overlaid spectra of electro-spun acetone-soluble lignin fibres thermo-stabilised in nitrogen and air within the C1s region are given in Figure 5.26 (a and b). Spectra of electro-spun acetone-soluble lignin fibres heated in a vacuum oven at 140 °C for six hours are plotted for comparison.

Regarding Figure 5.26 (a), i.e. the electro-spun acetone-soluble lignin fibres thermo-stabilised in nitrogen, obvious change in the spectra was observed when the temperature was raised to 250 °C. A band at 285 eV (C1) declined, while bands at 287.7 eV (C3) and 289 eV (C4) increased.

Upon thermo-stabilisation in air, as shown in Figure 5.26 (b), a significant increase in C4 with a function of temperature was found and C3 disappeared completely at 250 °C. The presence of the band at C4 corresponds to the formation of carboxyl (C(=O)-OH) and ester (O-C=O) groups [134,217,218]. It can be said that thermo-stabilisation in air promotes the formation of oxygen containing bonds with carbon including the formation of carboxyl (C(=O)-OH) and ester (O-C=O) groups. This result is consistent with the increase in the oxygen content reported in Table 5.5. This correlates with the observed increase in the FTIR absorbance between 1,720-1,690 cm⁻¹ corresponding to C=O stretching, as discussed in Section 5.6.3.

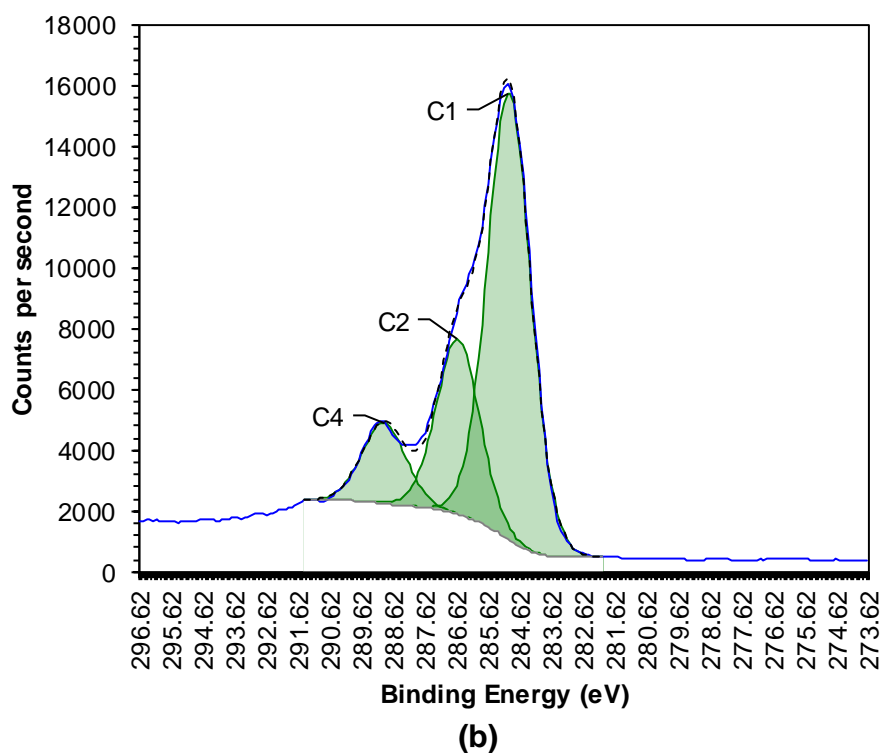
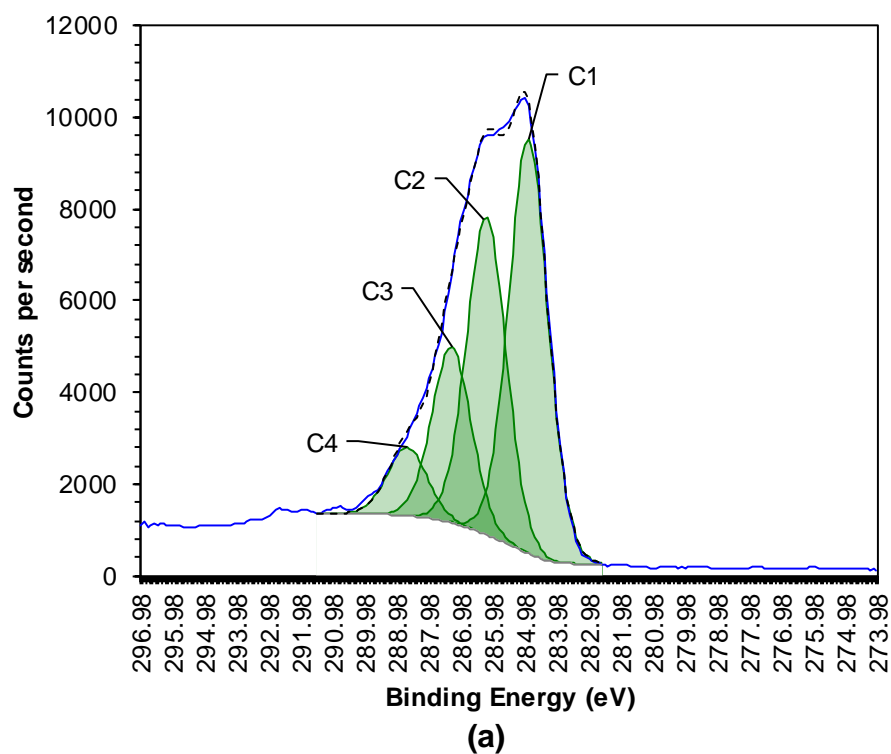


Figure 5.25 XPS spectra of electro-spun acetone-soluble lignin fibres thermo-stabilised at 250 °C in (a) nitrogen and (b) air. XPS spectra of the electro-spun fibres heated in a vacuum oven at 140 °C for six hours coded in (*).

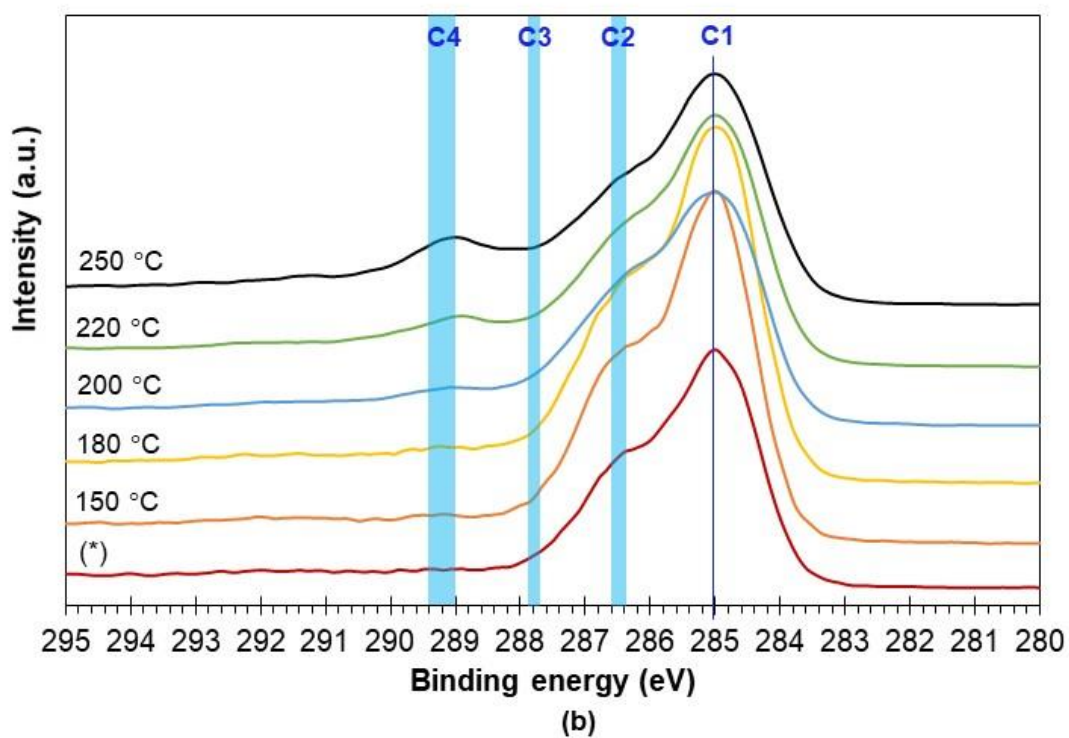
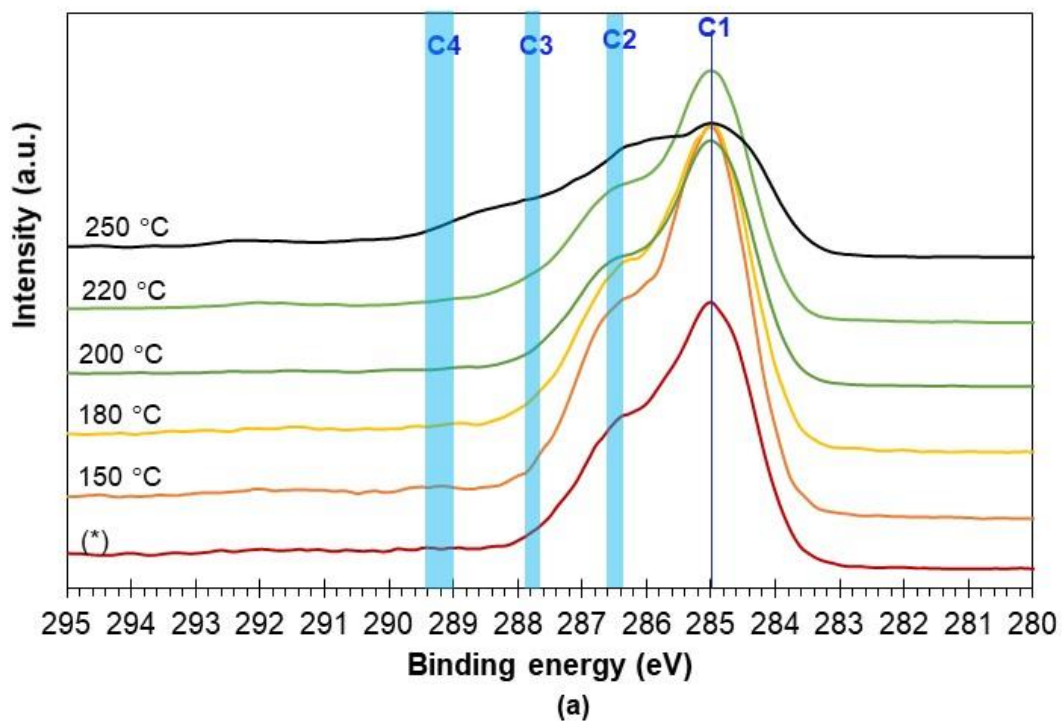


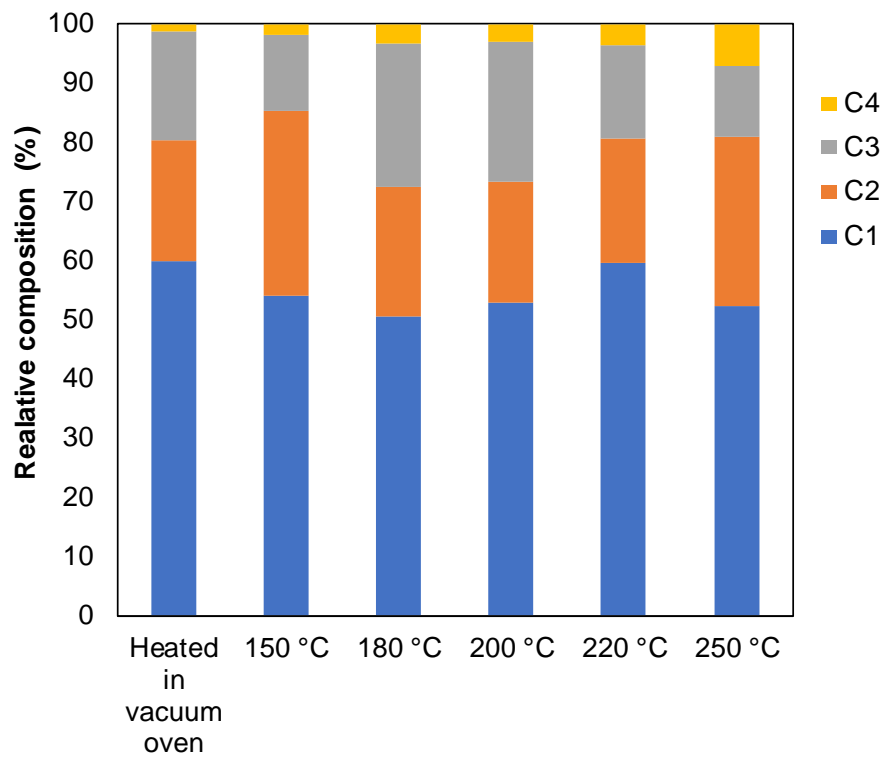
Figure 5.26 Overlaid high-resolution XPS spectra of the electro-spun acetone-soluble lignin fibres thermo-stabilised in: (a) nitrogen; and (b) air. (*) XPS spectra of the electro-spun fibres heated in a vacuum oven at 140 °C for six hours.

Figure 5.27 (a and b) shows the relative composition (%) of C1-C4 obtained from deconvoluted XPS spectra. The electro-spun fibres thermo-stabilised in nitrogen have no significant changes in C1, C2, C3 and C4 until the temperature is increased to 250 °C. C4 shows an increase from 1 at% to 7 atomic% and C3 decreases from 18 to 12 atomic % when stabilised at 250 °C as shown in Figure 5.27 (a).

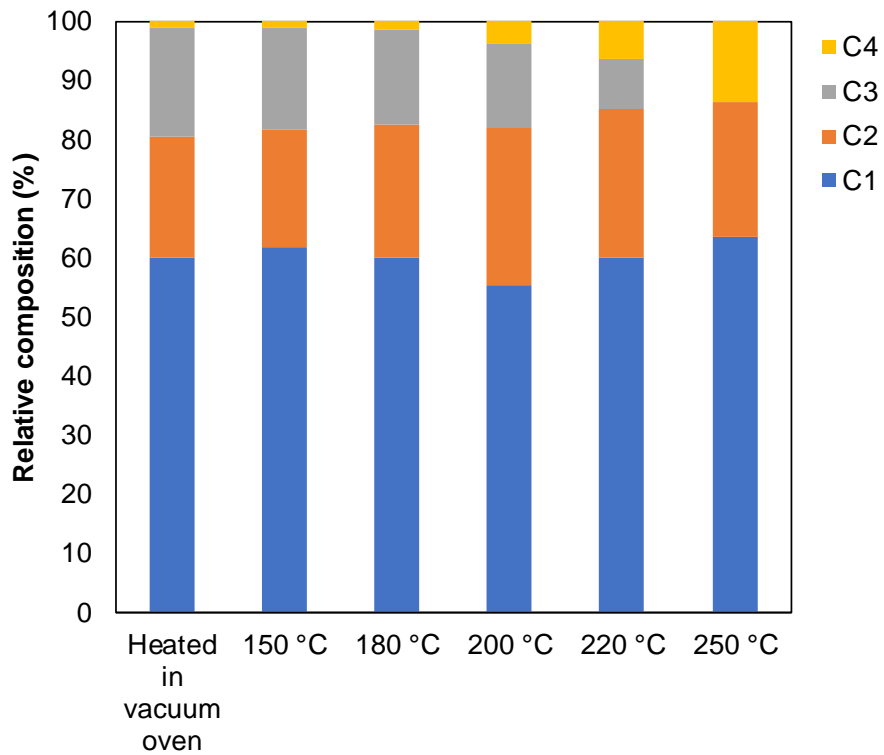
Regarding the electro-spun fibres thermo-stabilised in air shown in Figure 5.27 (b), there is a decrease in C3 and increase in C4 with an increase in the thermo-stabilisation temperature. This could be explained by the oxidation of aldehyde (C3) to form ester (C4) as proposed in the literature [13,218]. Furthermore, the results from the experiment at 250 °C show that the thermo-oxidised fibres possessed a lower C2 concentration when compared to those heated in nitrogen. The lower C2 concentration under oxidative conditions involves the cleavage of interunit linkages such as α -O-4' and β -O-4' [134,217,221,222] and these have low bond dissociation energies [222,304].

In summary, thermo-stabilisation under air or oxidative thermo-stabilisation can retain the structure of the electro-spun fibres, as shown in Figure 5.19. Retaining the fibre structure can be accounted for an increase in the T_g when the fibres are thermo-stabilised in air and/or the formation of an oxidised skin on the fibres. This may also be due to cross-linking as evidence in the FTIR spectra at 822 cm^{-1} and 855 cm^{-1} assigned to C-H stretching of the G-unit diminished and disappeared when the thermo-stabilisation temperature was raised to 220 °C. This indicates a change in molecular structure via cross-linking at the C5-position [134,218,221]. Under oxidative thermo-stabilisation of lignin fibres, a decrease in the intensity of C-O at 1,218 cm^{-1} , 1,081 cm^{-1} and 1,033 cm^{-1} and increase in the intensity of C=O at 1,720-1,690 cm^{-1} were found. The formation of carboxyl (C(=O)-OH) and ester (O-C=O) groups was confirmed by XPS.

In the current work, the electro-spun acetone-soluble lignin were thermo-stabilised by heating them from 25-250 °C at 0.5 K·minutes⁻¹. The air flow was maintained at 50 ml·minutes⁻¹. The next section reports on the carbonisation of these fibres.



(a)



(b)

Figure 5.27 Relative concentration of C1- C4 under specified thermo-stabilisation conditions: (a) thermo-stabilised in nitrogen and (b) thermo-stabilised in air.

5.7 Carbonisation of Electro-spun Acetone-soluble Lignin Fibres

After thermo-stabilisation in air, the acetone-soluble electro-spun lignin fibres, were carbonised under different conditions. In this section, a Taguchi design of experiments was used to study the effect of carbonisation conditions on the carbonised electro-spun acetone-soluble lignin fibres and to optimise carbonisation process-parameters. The parameters investigated are (i) heating rate, (ii) carbonisation temperature and (iii) dwell time. Each parameter was chosen to have three levels as indicated in Table 5.7.

Table 5.7 The parameters investigated and their levels for the carbonisation of electro-spun lignin fibres.

Parameters	Heating rate (K·minute ⁻¹)	Carbonisation temperature (°C)	Dwell time (hour)
Level 1	2.5	1,000	0
Level 2	5	1,200	1
Level 3	10	1,500	3

A L₉ orthogonal array representing 3³ experiments was selected. Table 5.8 shows the combinations of nine experiments. The fibre diameters of the carbonised electro-spun fibres were measured by Image J software (version 1.52p) and averaged over 300 individual measurements. The effect of each parameter used on the properties of the electro-spun acetone-soluble lignin fibres are discussed in Sections 5.7.1 and 5.7.2.

Table 5.8 Combination factors of nine experiments and measured fibre diameter of the carbonised fibres.

Experiment number	Heating rate (K·minute ⁻¹)	Temperature (°C)	Dwell time (hour)	Fibre diameter (µm)	
				Ave.	SD
Exp. 1	2.5	1,000	0	0.569	0.141
Exp. 2	2.5	1,200	1	0.522	0.153
Exp. 3	2.5	1,500	3	0.473	0.113
Exp. 4	5	1,000	1	0.655	0.185
Exp. 5	5	1,200	3	0.581	0.163
Exp. 6	5	1,500	0	0.473	0.113
Exp. 7	10	1,000	3	0.556	0.137
Exp. 8	10	1,200	0	0.555	0.135
Exp. 9	10	1,500	1	0.521	0.130

5.7.1 Taguchi Analysis on the Effect of Carbonisation Condition on Fibre Diameter

Regarding Table 5.8, the average fibre diameter of the carbonised electro-spun acetone-soluble lignin fibres obtained from nine experiments ranges between 0.47 - 0.65 µm. Figure 5.28 shows SEM micrographs of the morphology of the electro-spun acetone-soluble lignin fibres carbonised under different conditions. The fibres that were heated at 2.5 and 5 K·minute⁻¹ preserved their structure, whereas the sample carbonised at 10 K·minute⁻¹ exhibited sagging in the fibres.

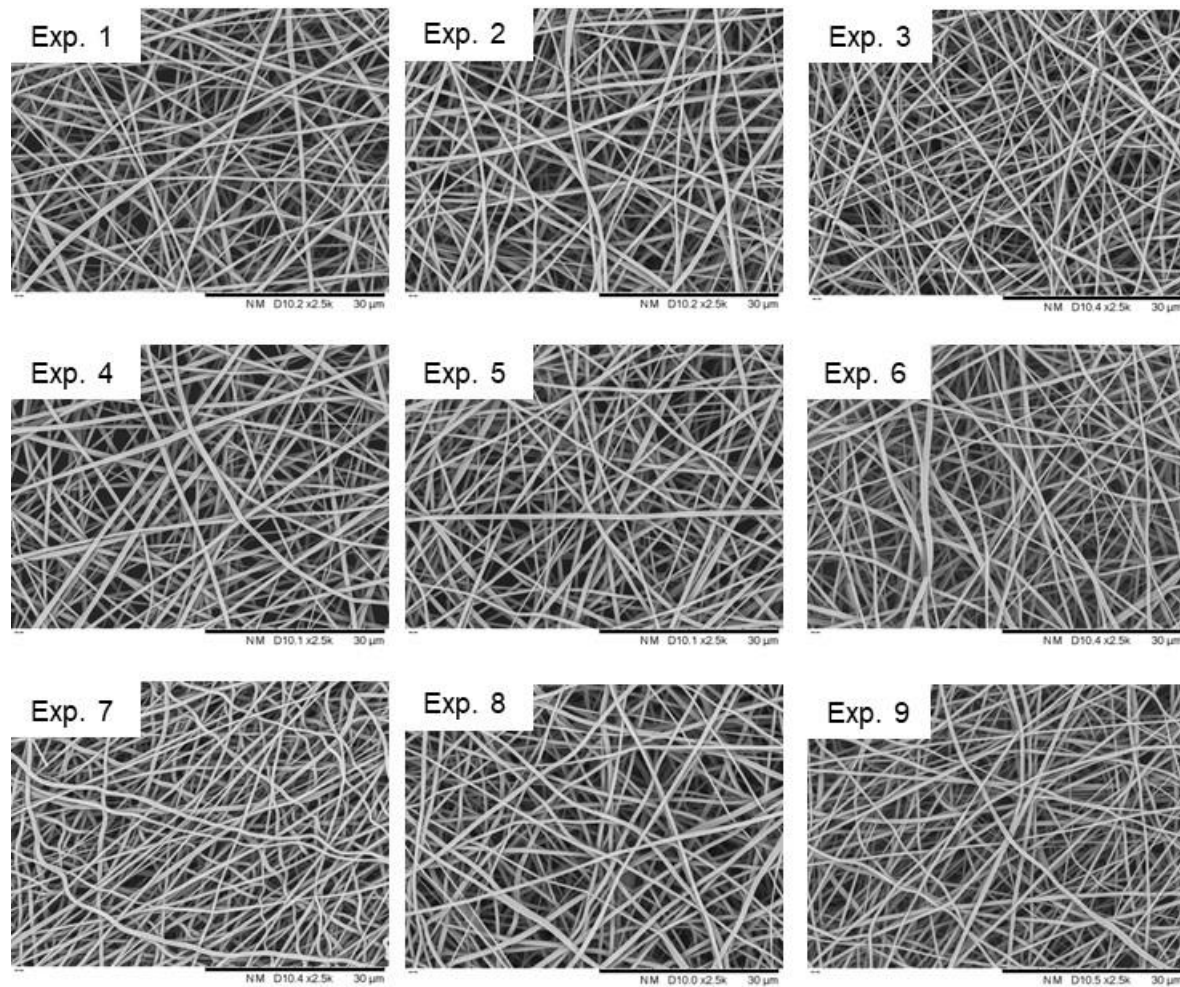


Figure 5.28 SEM micrographs of carbonised electro-spun acetone-soluble lignin fibres. The labels from (a) to (i) represent the fibre morphology obtained from experiment 1-9 detailed in Table 5.8.

The distribution of the measured fibre diameter is shown in Figure 5.29. From the distribution curve, the fibre diameters are plotted in range from 0.1-1.3 μm for cross-comparison. A noticeable narrow fibre distribution is seen for the fibres carbonised at 1,500 $^{\circ}\text{C}$, corresponding to Exp.3, Exp.6 and Exp. 9 in Table 5.8. However, in this analysis, the measured fibre diameter and the distribution of fibre diameter were considered to be from the combined effects of the three factors. Therefore, Taguchi analysis and ANOVA were conducted in order to clarify the contribution each factor. The ANOVA tables for the fibre diameter and their distribution are compiled in Appendix E.

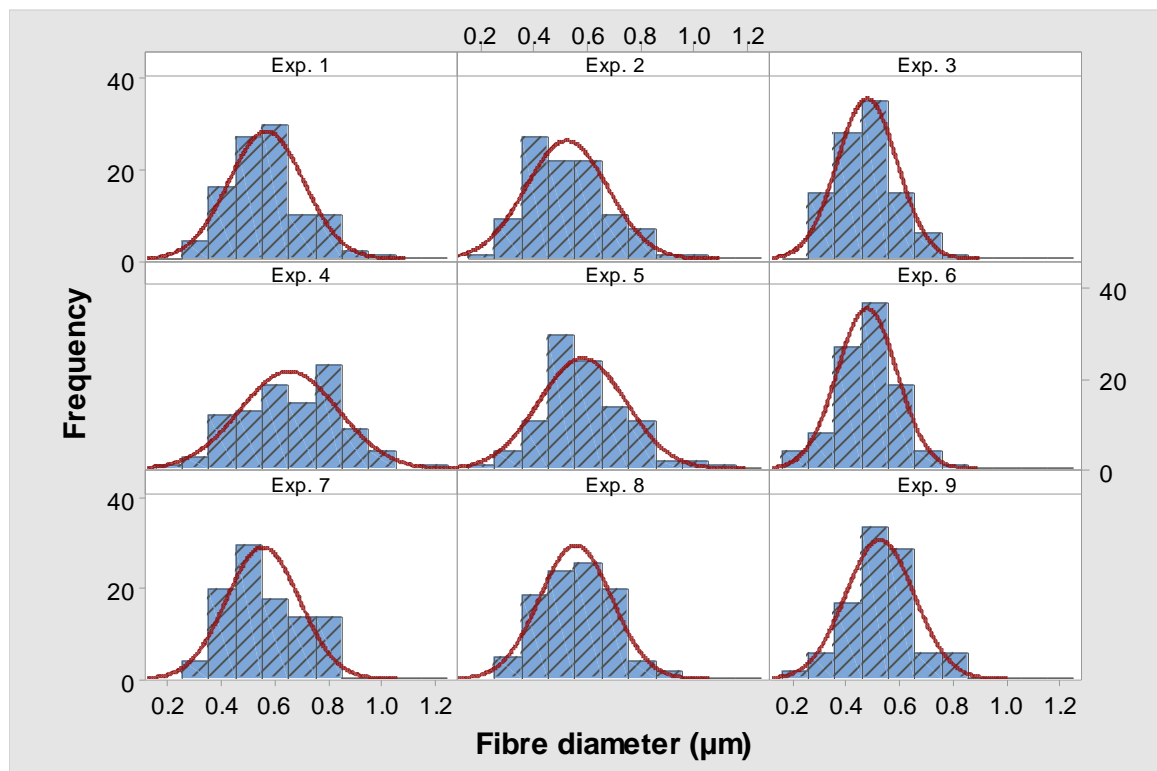


Figure 5.29 The distribution of measured fibres diameters from the carbonised lignin fibres obtained from nine experiments (see Table 5.8).

Figure 5.30 (a) and (b) show the analysis of the mean values of fibre diameter and signal-to-noise ratio (S/N), respectively. In Figure 5.30 (a), the fibre diameter increased to 0.57 μm when the heating rate was increased from 2.5 to 5 $\text{K}\cdot\text{minute}^{-1}$, but the fibre diameter decreased when using a heating rate of 10 $\text{K}\cdot\text{minute}^{-1}$. However,

the ANOVA result showed that there is no statistically significant difference (with $p < 0.05$) between the diameters for fibres carbonised at 2.5 and 5 $\text{K}\cdot\text{minute}^{-1}$.

The effect of carbonisation temperature was found to be the dominant factor affecting the fibre diameter (with supporting evidence from ANOVA) with a 64.4 % contribution. Regarding the Taguchi analysis, the fibre diameter is reduced when the carbonisation temperature is increased. At 1,500 $^{\circ}\text{C}$, the average diameter of the carbonised fibres is 0.49 μm . Similar reductions in fibre diameter have been reported for carbonised lignin fibres [36,184,225]. For instance, the average fibre diameter for the electro-spun lignin fibres reduced from 700 nm to 561 nm when the carbonisation temperature increased from 1,000 to 1,400 $^{\circ}\text{C}$ [184]. Variations in dwell time, from one to three hours did not influence the fibre diameter. Previous studies reported that dwell times increased from three to 10 hours showed a significant decrease in fibre diameter [144].

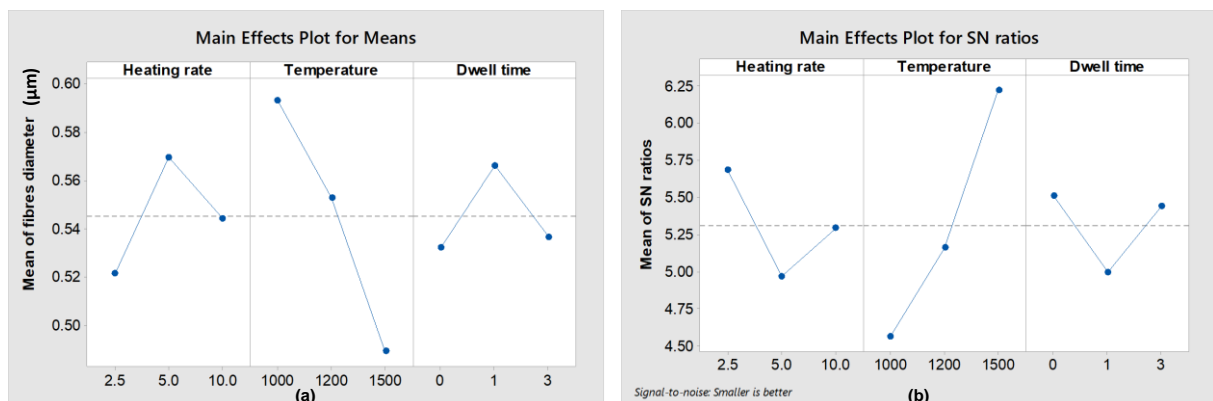


Figure 5.30 Main effect and signal-to-noise ratio plots for the diameters of carbonised lignin fibres.

An interaction plot of the controllable factors is shown in Figure 5.31. The interaction plots show that the sample carbonised at 10 $\text{K}\cdot\text{minute}^{-1}$ showed that the carbonisation temperature and dwell time did not affect the fibre diameter. Moreover, heating rate and dwell time showed a low effect on fibre diameter when the carbonisation temperature was 1,500 $^{\circ}\text{C}$.

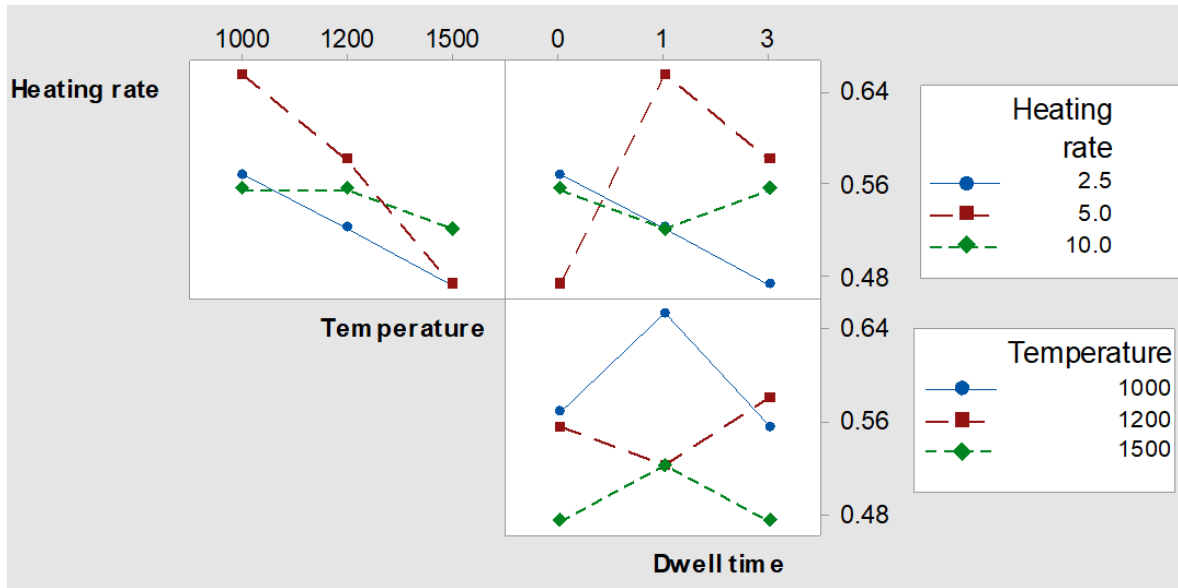


Figure 5.31 Interaction plots for the fibre diameter of carbonised electro-spun lignin fibres.

With regard to Figure 5.29, a narrow distribution for the fibre diameter is noticeable on the sample carbonised at 1,500 °C. The same result was reported from the Taguchi analysis; increasing the carbonisation temperature narrowed the fibre diameter distribution, whilst heating rate and dwell time did not show any clear influence, as seen in Figure 5.32.

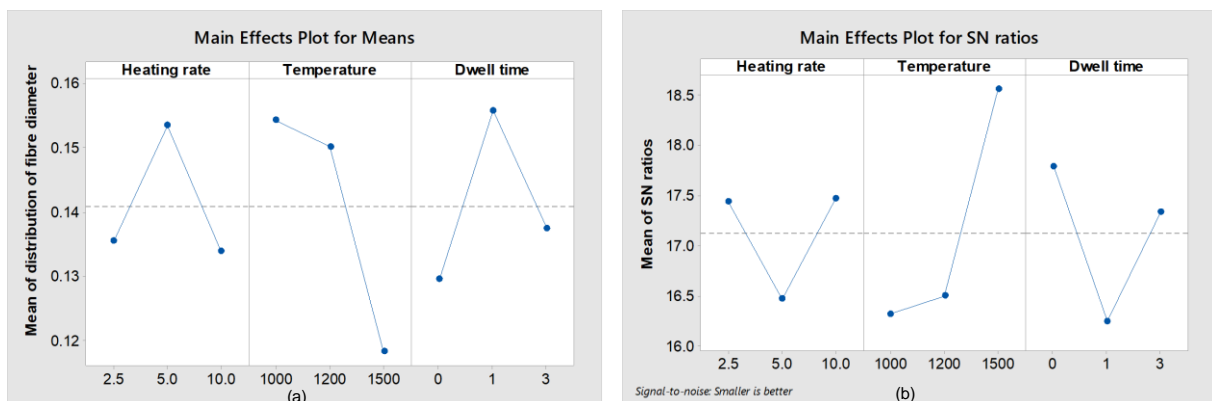


Figure 5.32 Main effect and signal-to-noise ratio plots for the distribution of fibre diameter of carbonised electro-spun lignin fibres.

The interaction plots for the distribution of the fibre diameter of carbonised electro-spun acetone-soluble lignin are presented in Appendix F. When the fibres were heated at $10 \text{ K}\cdot\text{minute}^{-1}$, carbonisation temperature and dwell time had no significant effect on the distribution of fibre diameter. When fibres were carbonised at $1,500 \text{ }^\circ\text{C}$, the heating rates and dwell times showed an insignificant effect on the distribution of fibre diameter, as compared to those that were carbonised at $1,000 \text{ }^\circ\text{C}$ and $1,200 \text{ }^\circ\text{C}$.

Apart from the analysis on fibre diameter and the distribution of fibre diameter, the structure of the carbonised electro-spun acetone-soluble lignin fibres were analysed using Raman spectroscopy and this is discussed in the following section.

5.7.2 Taguchi Analysis on the Effect of Carbonisation Condition on Graphitic Structure of Lignin Analysed using Raman Spectroscopy

Raman spectroscopy was performed to compare the graphite-like structure formed under different carbonisation conditions. Figure 5.33 shows an example of the deconvolution Raman spectra taken from Experiment 1. There are two broad characteristic bands, D-band and G-band are centred about $1,340 \text{ cm}^{-1}$ and $1,590 \text{ cm}^{-1}$, respectively [226–228,305,306]. The D-band represents the breathing mode of the 6-carbon atom in an aromatic ring and this refers to disordered carbon. The G-band is attributed to the in-plane stretching mode of sp^2 carbon, indicating an ordered carbon structure [145,215,229,307–309].

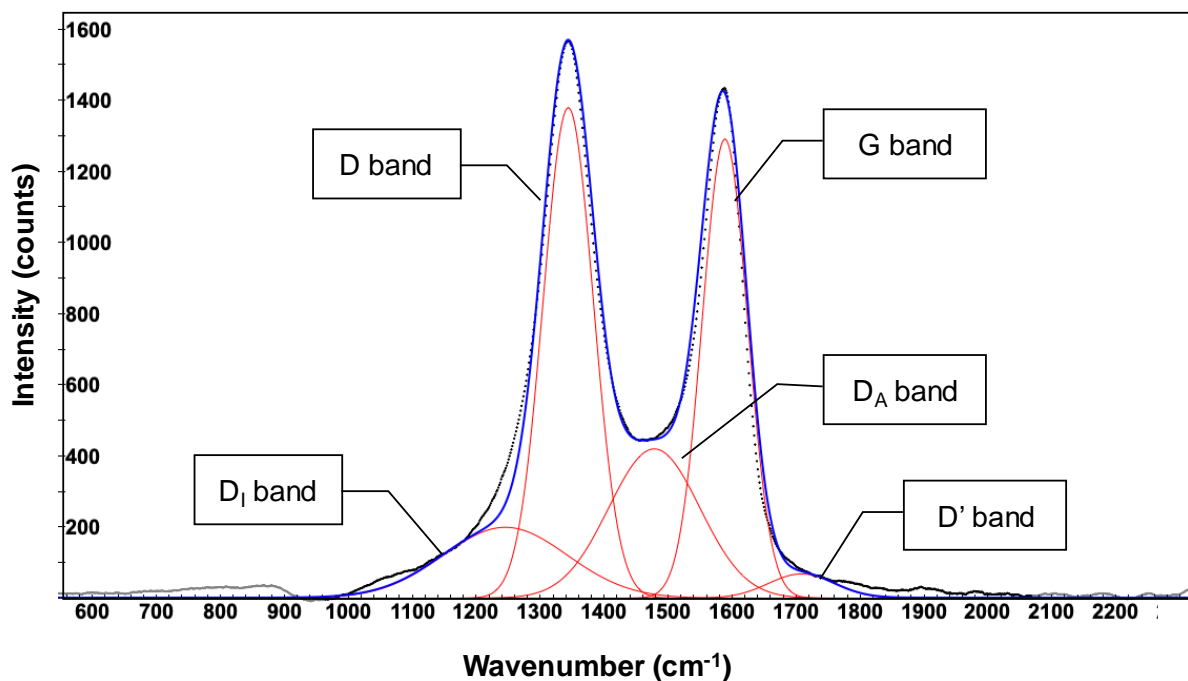


Figure 5.33 Deconvolution of typical Raman spectra for electro-spun acetone-soluble lignin fibres carbonised at 1,500 °C.

The spectra were deconvoluted using Gaussian and Lorentzian line shapes to extract information on the band characteristics such as intensity, width and the area under them. The R^2 value of the curve fittings was more than 95%. With regard to amorphous carbon, three sub-bands (D_1 , D_A and D') are commonly presented [103,185,299,300,310–312]. The deconvolution spectra show the three bands at 1,100-1,200 cm^{-1} (D_1), 1,450-1,500 cm^{-1} (D_A) and 1,600-1,700 cm^{-1} (D'). D_1 corresponds to defects present in a heterogeneous structure caused by the incomplete volatilisation of nitrogen or oxygen. The D_A represents amorphous carbon and D' is attributed to vibration of the disordered graphitic lattice [185,311–313].

Analysis of the characteristics in the D and G bands such as their peak position, intensity ratio of (I_D/I_G), full width half max (FWHM) and ratio of the integrated intensity (A_D/A_G) are summarised in Table 5.9. Taguchi analysis and ANOVA are discussed in subsequent sections.

Table 5.9 The combinations of L9 Taguchi orthogonal array, the results of the analysed data from Raman spectra.

Expt. No.	D-band position		G-band position		I_D/I_G		FWHM of D-band (cm ⁻¹)		FWHM of G-band (cm ⁻¹)		A_D/A_G	
	Ave.	SD	Ave.	SD	Ave.	SD	Ave.	SD	Ave.	SD	Ave.	SD
Exp.1	1,345.1	1.0	1,589.5	1.0	0.82	0.02	211.7	2.0	103.1	9.9	1.7	0.2
Exp.2	1,345.8	4.1	1,590.2	2.0	0.86	0.02	171.8	22.1	101.0	1.0	1.5	0.1
Exp.3	1,345.7	1.8	1,588.8	0.0	1.00	0.09	104.1	0.8	83.5	0.0	1.3	0.1
Exp.4	1,352.3	2.0	1,590.9	1.0	0.82	0.05	200.7	11.5	107.3	17.9	1.6	0.3
Exp.5	1,348.0	3.0	1,590.2	0.0	0.86	0.01	169.7	7.0	99.6	3.0	1.5	0.0
Exp.6	1,340.4	3.5	1,587.3	2.0	1.00	0.01	129.0	16.2	95.4	5.0	1.4	0.1
Exp.7	1,345.5	6.4	1,589.7	2.6	0.82	0.02	192.3	9.5	123.5	26.7	1.3	0.2
Exp.8	1,345.1	3.0	1,592.9	0.1	0.86	0.04	209.5	25.2	102.3	5.0	1.8	0.4
Exp.9	1,346.4	0.8	1,587.4	2.0	0.92	0.13	157.5	56.4	99.6	18.8	1.4	0.1

The ratio of the peak height of the deconvoluted D-band and G-band (I_D/I_G) was taken to indicate the degree of order in the structure [36,103,145,184,215,220,229]. A lower value of I_D/I_G represents a higher graphitic structure. Therefore, a “small is better” quality characteristic was set for the Taguchi analysis. Response values for the main effects and S/N ratio are shown in Figure 5.34. The carbonisation temperature was found to be the highest dominant factor. Increasing the carbonised temperature increased the I_D/I_G ratio. However, the heating rate and dwell time did not show a clear effect on the I_D/I_G ratio. This was confirmed by ANOVA: the contributions from the of carbonisation temperature, heat rate and dwell time were 89.6%, 3.5% and 3.1%, respectively.

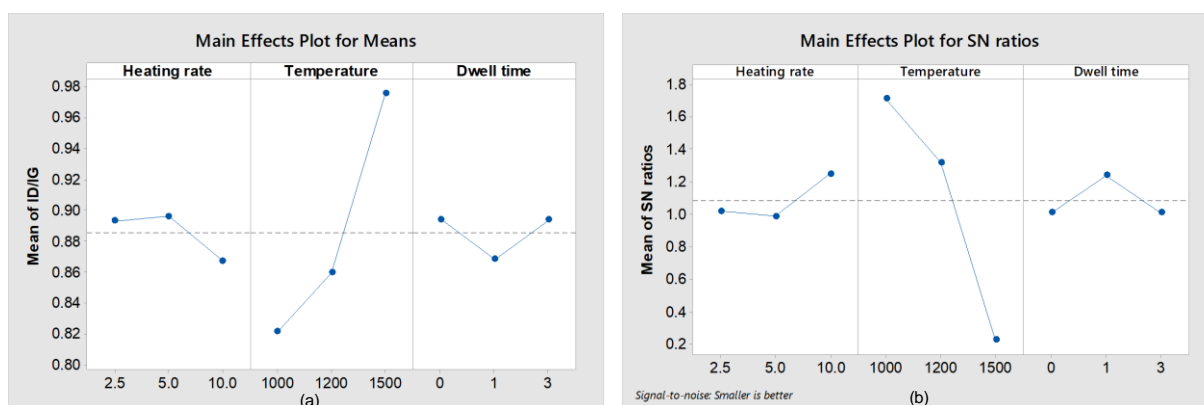


Figure 5.34 Main effect and S/N ratio plots for the I_D/I_G ratio for the carbonised electro-spun lignin fibres.

The same statistical analysis with the “small is better” quality characteristic was performed on full width at half maximum (FWHM) for the D- and G-bands. A narrow FWHM indicates a homogeneous structure. Figure 5.35 and Figure 5.36 show the Taguchi analysis for the D and G-bands, where in the analysis includes the mean values of and S/N, respectively.

With reference to the Taguchi analysis shown in Figure 5.35 (a), the lowest response mean value of the FWHM D-band was found for the sample carbonised at 1,500 °C at 2.5 K·minute⁻¹ and a dwell time of three hours. This analysis was supported

by the analysis of S/N shown in Figure 5.35 (b). The carbonisation temperature was ranked main factor contributing to the FWHM of the D-band with a 75.9% contribution.

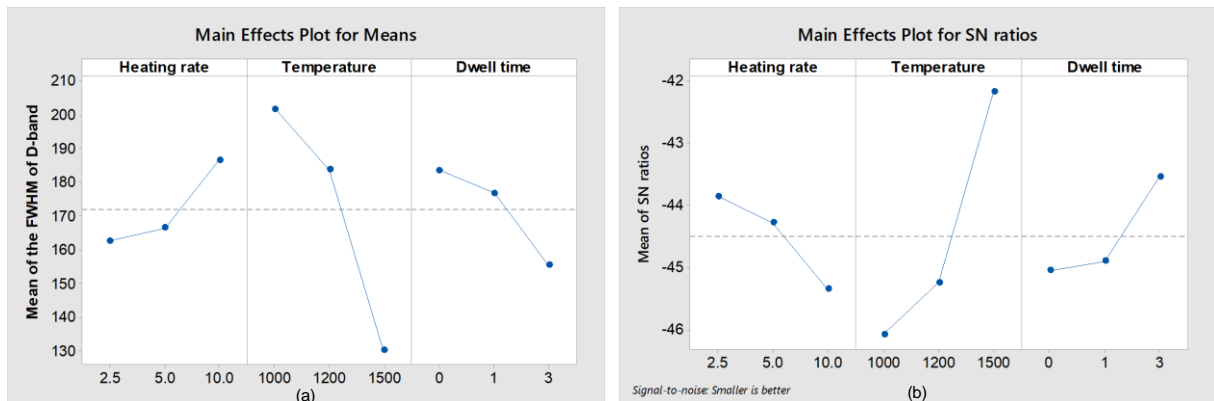


Figure 5.35 Main effect and S/N ratio plots for the FWHM for the D-band for the carbonised electro-spun lignin fibres.

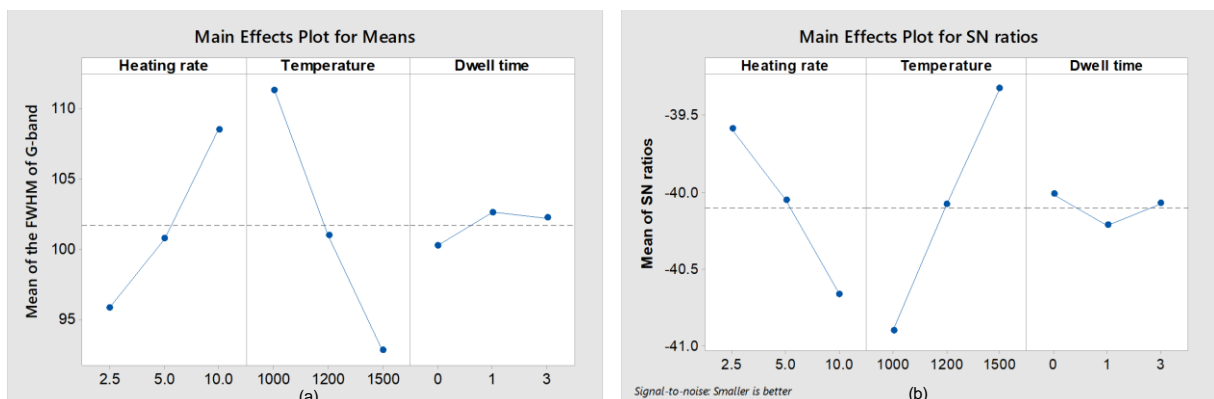


Figure 5.36 Main effects and S/N ratio plots for the FWHM for the G-band for the carbonised electro-spun lignin fibres.

With reference to Figure 5.36 (a), the carbonisation temperature is the most dominant factor contributing a 57.6 % impact effect on the FWHM for the G-band. An increase of carbonisation temperature leads to a decrease in the FWHM of the G-band. Figure 5.36 (b) shows the outcome of the Taguchi analysis where the best condition to obtain the lowest FWHM of the G-band is by using a carbonisation temperature of 1,500 °C and at 2.5 K·minute⁻¹.

From the Taguchi analysis of the FWHM of D and G-bands shown in Figure 5.35 and Figure 5.36, the carbonised acetone-soluble lignin fibres exhibited an improvement in the structure with the increase in carbonisation temperature.

The integrated areas under D and G-bands were denoted as A_D and A_G , respectively. The ratio of A_D/A_G can be used to measure the degree of graphitisation. The “small is better” quality characteristic was conducted on the A_D/A_G ratio. It was confirmed that the degree of graphitisation increased as the A_D/A_G decreased. The response mean value for the A_D/A_G ratio and S/N are illustrated in Figure 5.37.

From the Taguchi analysis and ANOVA, the dwell time is the most influential factor that affected the A_D/A_G ratio contributing 44%, and carbonising for a longer period showed a lower A_D/A_G . The second most influential factor on A_D/A_G is carbonisation temperature. However, this result is different from I_D/I_G which shows that carbonisation temperature is the most influential factor.

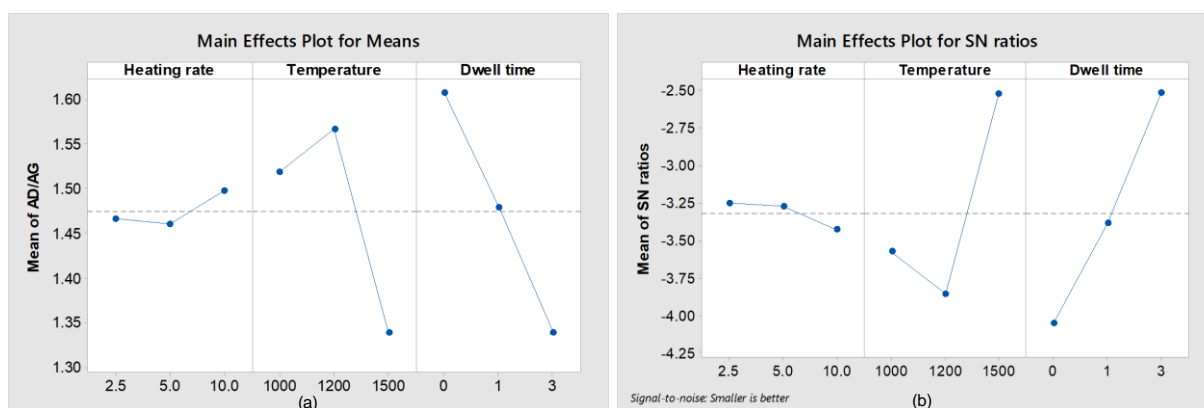


Figure 5.37 Main effects and S/N ratio plots for the A_D/A_G ratio for the carbonised electro-spun lignin fibres.

Analysis of the interaction plots of all parameters are compiled in Appendix F. They correlate well with the analysis of the mean value. Carbonisation conditions for electro-spun acetone-soluble lignin fibres derived from the Taguchi analysis are compiled in Table 5.10. The suggested condition is considered based on the results of the carbonised fibre diameter, the diameter distribution and the graphitic structure. The suggested condition consists at $2.5 \text{ K}\cdot\text{minute}^{-1}$ at $1,500 \text{ }^\circ\text{C}$ and longer dwell time.

Table 5.10 A summary of the Taguchi analysis for the carbonisation parameters for acetone-soluble electro-spun lignin fibres.

Responses	Controlled parameters								
	Heating rate (K·minute ⁻¹)			Temperature (°C)			Dwell time (hour)		
	2.5	5.0	10.0	1,000	1,200	1,500	0	1	3
Fibre diameter	✓					✓	✓		
Distribution of fibre diameter	✓					✓	✓		
I _D /I _G			✓	✓				✓	
FWHM of D-band	✓					✓			✓
FWHM of G-band	✓					✓			✓
A _D /A _G	✓					✓			✓

The same conclusion on the dominant effect (carbonisation temperature) was reached from the ANOVA analysis. A bar chart showing the percentage contribution of the main factors for each property of interest is shown in Figure 5.38.

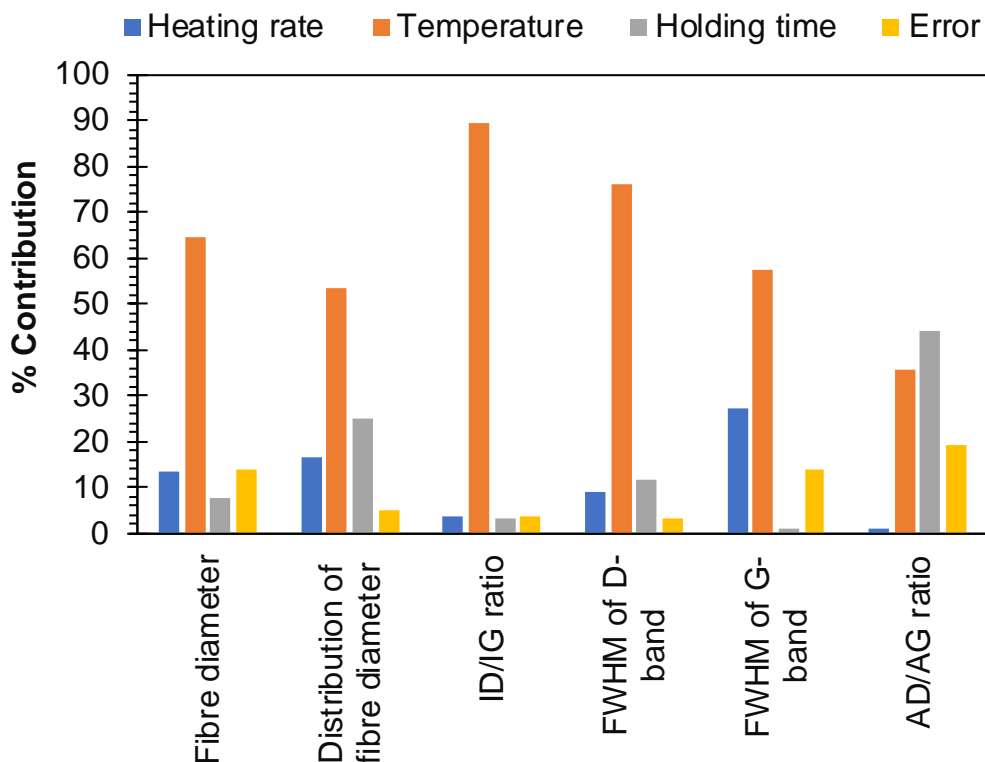


Figure 5.38 Percentage contribution of main effect on interested properties.

Regarding the ANOVA for the effects of carbonisation on the carbonised electro-spun acetone-soluble lignin fibres discussed in Sections 5.7.1 and 5.7.2. The temperature is found to be a dominant key parameter for the properties of carbonised fibres. Validation of the effect of carbonisation temperature on other characteristics of the carbonised fibre was also undertaken.

5.7.3 Scanning Electron Microscopy Carbonised Electro-spun Acetone-soluble Lignin Fibres

The effect of carbonisation temperature on the microstructure of the fibres was studied using SEM. The fibres were carbonised at 1,000 °C, 1,200 °C and 1,500 °C at 2.5 K·minute⁻¹ with a dwell time of one hour. The surface and cross-sectional morphologies of the carbonised fibres are shown in Figure 5.39. The fibre diameter and its normal distribution are shown in Figure 5.40.

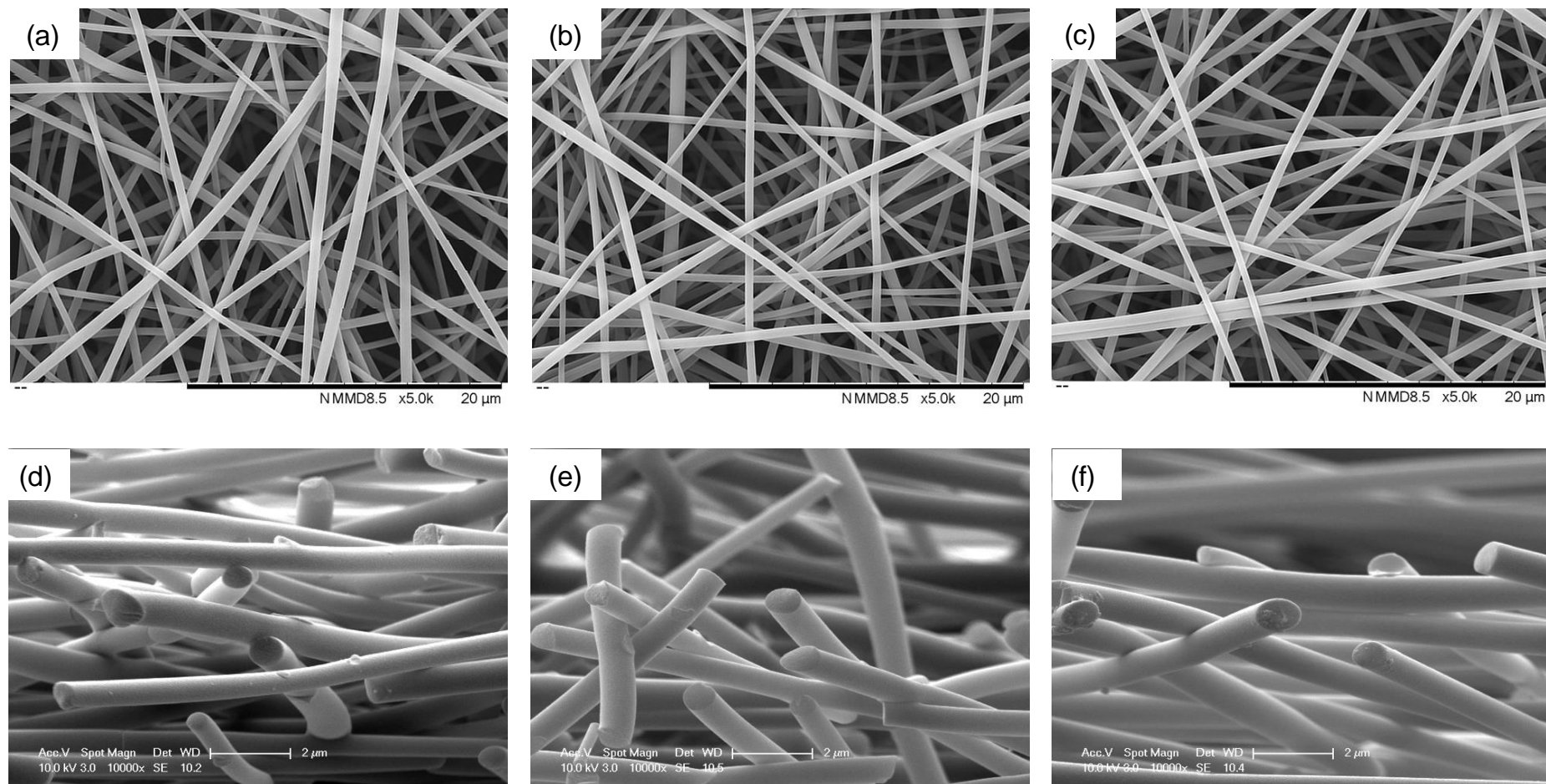


Figure 5.39 SEM micrographs of the surface morphology and cross-sectional view of electro-spun acetone-soluble lignin fibres.

Fibres carbonised at 1,000 °C ((a) and (d)), 1,200 °C ((b) and (e)) and 1,500 °C ((c) and (f)).

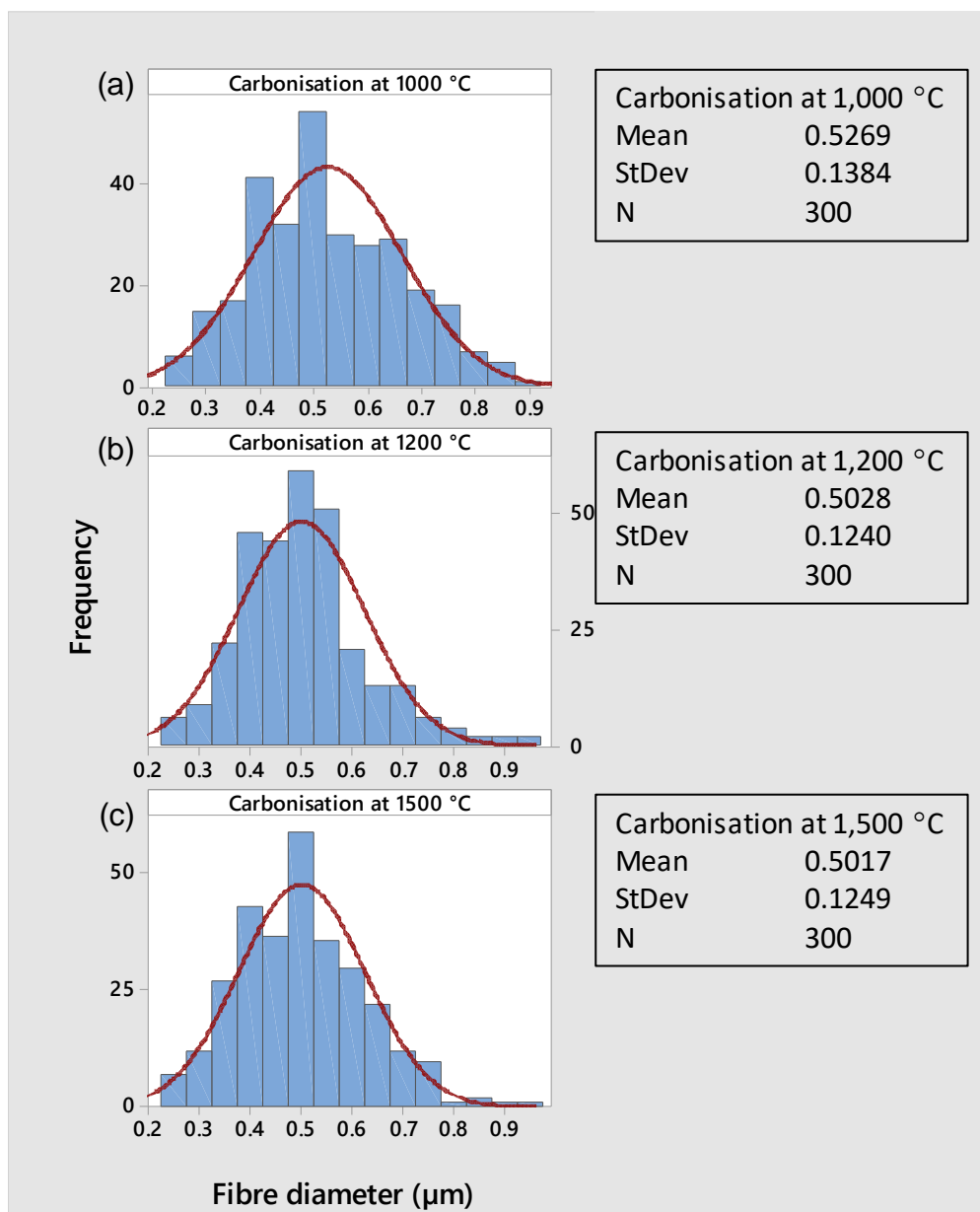


Figure 5.40 Average fibre diameter and distribution of electro-spun acetone-soluble lignin fibres carbonised at (a) 1,000 °C, (b) 1,200 °C and (c) 1,500 °C.

The average diameter of the carbonised lignin fibres was estimated using a sample size of 300 random measurements. The average diameters of fibres carbonised at 1,000 °C, 1,200 °C and 1,500 °C are 526 ± 138 nm, 502 ± 124 nm and 501 ± 125 nm, respectively. The fibre diameter decreased as the carbonisation temperature was increased from 1,000 °C to 1,200 °C; increasing the temperature to 1,500 °C did not lead to any further decreasing in the fibre diameter. These are in contrast to the results

obtained from the Taguchi analysis reporting the fibre diameter continuously decreasing with the increase in carbonisation temperature. However, the predicted diameter of the fibres carbonised at 1,500 °C (590 nm) is close to the diameter from the experimental measurement (501 ± 125 nm).

5.7.4 Raman Spectroscopy Carbonised Electro-spun Acetone-soluble Lignin Fibres

Raman spectroscopy was conducted on the electro-spun acetone-soluble lignin fibres that were carbonised at 1,000 °C, 1,200 °C and 1,500 °C. Their spectra are illustrated in Figure 5.41. The Raman spectra, all the carbonised electro-spun fibres exhibit D-and G-bands centred at about $1,340\text{ cm}^{-1}$ and $1,590\text{ cm}^{-1}$. The details of these two bands are described in Section 5.7.2. The intensity of D and G-bands increase when the carbonisation temperature was increase from 1,200 °C to 1,500 °C. This attributes to the formation of graphite-like structure. However, I_D/I_G ratio increased from 0.82 ± 0.03 to 0.86 ± 0.02 and 1.00 ± 0.08 when the carbonisation temperature was increased from 1,000 °C to 1,200 °C and 1,500 °C, respectively. These represent more disordered graphitic structure are formed when increase temperature. The increase of disorder structure of carbonised lignin is ascribed due to irregular and complex of lignin structure which inhibit a rearrange into ordered graphitic structure [223,312,314]. The I_D/I_G ratios measured in this study are lower than those reported in the literature, which range from 1.2 to 2.5 [144,185,220,312,315]. This means carbonised lignin fibres produced from this work have more order graphitic structure compared to the values reported in the literature.

Considering the effect of carbonisation temperature, an increasing carbonisation temperature results in an increase of the I_D/I_G ratio. A similar rising trend of the I_D/I_G ratio when increasing the carbonisation temperatures has been reported [103,146,299,306,312]. On the other hand, copolymer of lignin/PAN [184] and PAN [146,316,317] precursors exhibited a decline in the I_D/I_G ratio when the carbonisation temperature was increased.

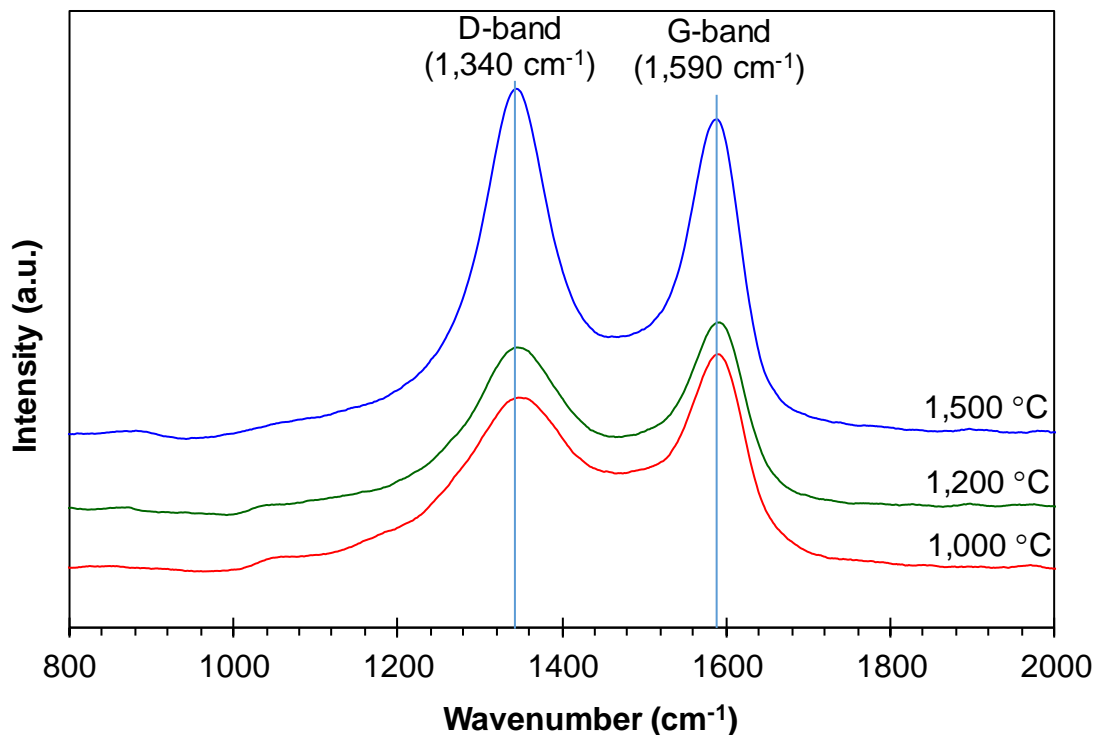


Figure 5.41 An overlaid plot of Raman spectra for electro-spun acetone-soluble lignin fibres carbonised at 1,000 °C, 1,200 °C and 1,500 °C.

5.7.5 X-ray Photoelectron Spectroscopy of Carbonised Electro-spun Acetone-soluble Lignin Fibres

The elemental and chemical composition of the carbonised electro-spun acetone-soluble lignin fibres were determined using XPS. XPS has previously been used to analyse lignin [301–303,318,319], the chemical composition of lignin-derived carbon materials [303] and the carbonised lignin fibres [103,217,224,299]. The XPS survey spectra of the electro-spun fibres carbonised at 1,000 °C, 1,200 °C and 1,500 °C are presented in Figure 5.42.

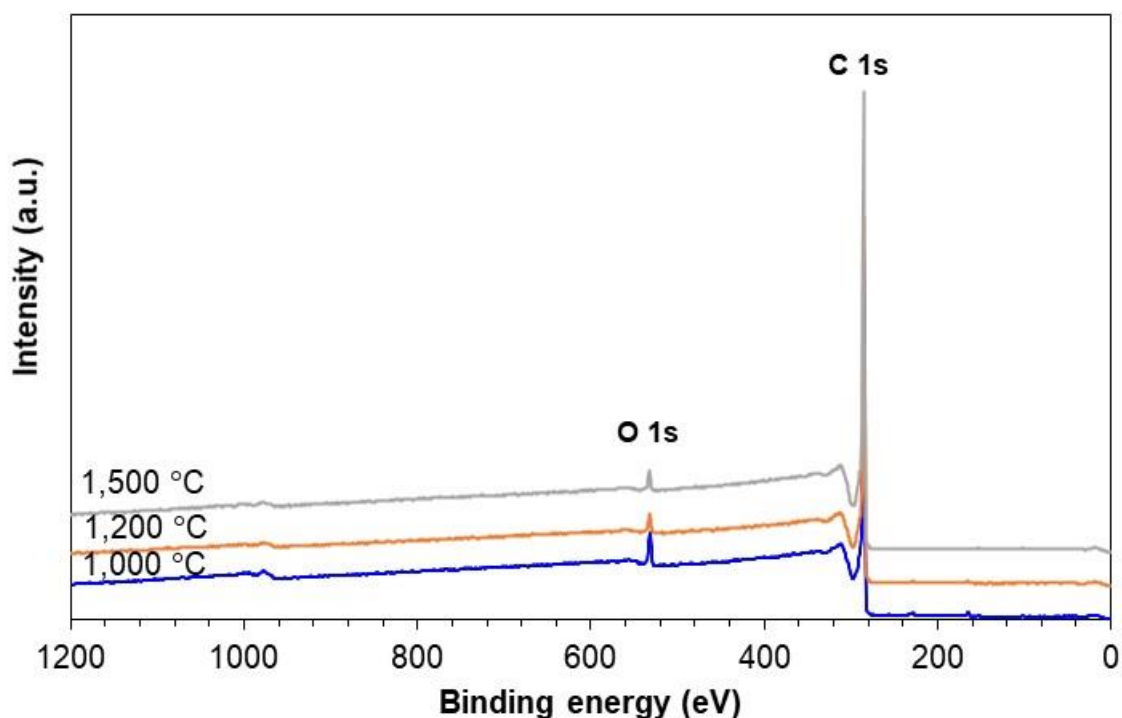


Figure 5.42 XPS spectra of carbonised electro-spun acetone-soluble lignin fibres which are carbonised at 1,000 °C, 1,200 °C and 1,500 °C.

The carbonised fibres exhibit two peaks, which are seen at 532.46 eV and 284.96 eV representing carbon and oxygen, respectively [217,224,303,319,320]. The intensity of the peak at 284.96 eV was higher than that of the peak at 532.46 eV, it is because the content of carbon is much higher than that of oxygen. The composition of the two elements in the carbonised electro-spun acetone-soluble lignin fibres is summarised in Table 5.11. The carbonised fibres show carbon content greater 90 atomic % and it increases with temperature increase. The carbon content of carbonised electro-spun acetone-soluble lignin fibres reported in this work is comparable to that reported in the literature [103,224,321]. It has been reported that carbon content is higher than 90 atomic % when the lignin precursor is carbonised at temperatures over 800 °C [103,321–324] and that the carbon content increased with increase in carbonisation temperature [103,322].

Table 5.11 Carbon and oxygen contents in the electro-spun acetone-soluble lignin fibres carbonised at 1,000 °C, 1,200 °C and 1,500 °C.

Carbonisation temperature (°C)	Carbon (atomic%)	Oxygen (atomic%)
1,000 °C	90.52	9.48
1,200 °C	94.29	5.71
1,500 °C	94.07	5.93

5.8 Production of Aligned Electro-spun Acetone-soluble Lignin Fibres and their Properties

In this work, the electro-spinning of acetone-soluble lignin without a polymer blend was demonstrated. A pair of parallel-edge, ground electrodes was used to align lignin fibres. Graphite was used as the ground electrode material and a schematic illustration is presented in Figure 3.8 (d), Chapter 3.

Using the unmodified parallel-plated graphite ground electrode, the fibres were deposited preferentially on the top of the ground electrode and only a few fibres were aligned perpendicular to the parallel electrodes shown in Figure 5.43 (a). On the other hand, using the modified parallel-plate graphite ground electrode, the fibres were aligned perpendicular to the two parallel electrodes shown in Figure 5.43 (b).

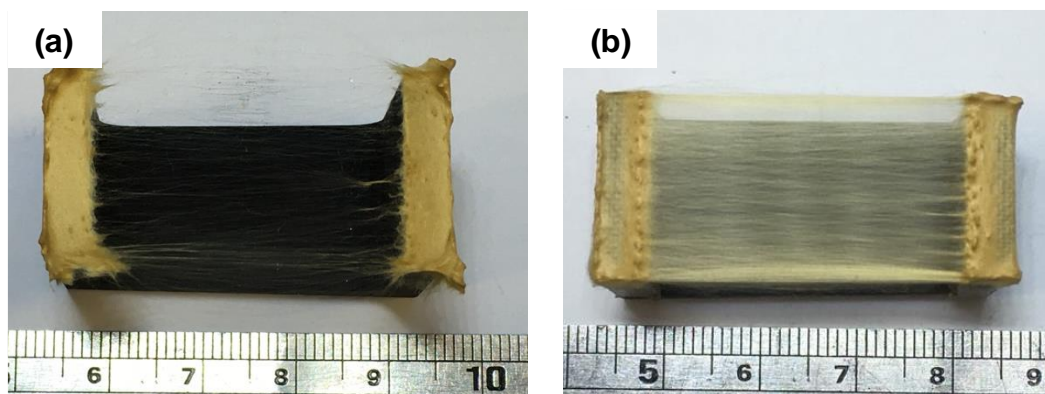


Figure 5.43 Photographs of electro-spun acetone-soluble lignin fibres collected on: (a) an unmodified parallel-plated graphite ground electrode and (b) modified parallel-plate graphite ground electrode. The ruler is in centimetre scale.

The morphology of the aligned electro-spun fibres obtained from the modified-graphite collector are shown in Figure 5.44. In Figure 5.44 (a), at a low magnification, it is seen that the fibres are aligned on the top layer whilst misaligned fibres can be observed clearly at the bottom layer, as indicated by the higher magnification and shown in Figure 5.44 (b). The misalignment is probably due to the whipping action as the electro-spinning jet oscillates between the ground electrodes. The average fibre diameter of the as-spun fibre was $1.48 \pm 0.23 \mu\text{m}$. The cross-sectional views of the aligned lignin fibres are shown in Figure 5.44 (c and d) where a circular form is presented.

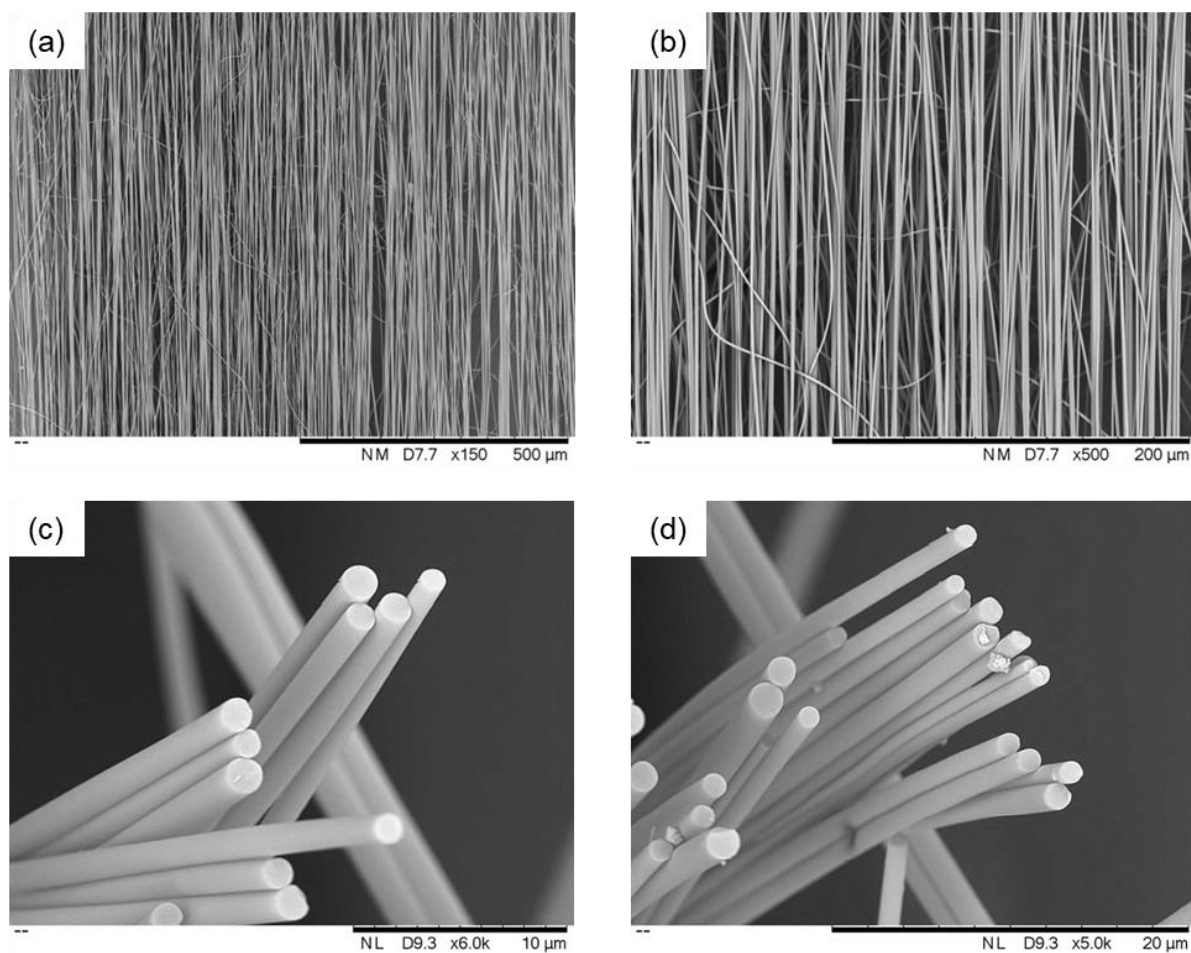


Figure 5.44 SEM micrographs of aligned electro-spun acetone-soluble lignin fibres: fibre surface morphology ((a) and (b)) and cross-sectional view ((c) and (d)).

The electro-spun acetone-soluble lignin fibres were produced using the optimised heating, thermo-stabilisation and carbonisation processes that were discussed in Sections 5.5, 5.6 and 5.7, respectively. The aligned fibres were heated in a vacuum oven at 140 °C for six hours. This was followed by oxidative thermo-stabilisation in a tube furnace where the fibres were heated at 0.5 K·minutes⁻¹ in air from room temperature to 250 °C with one-hour dwells at 100 °C, 150 °C and 250 °C. The thermo-stabilised fibres were carbonised at 1,000 °C, 1,200 °C and 1,500 °C for one hour at each temperature.

Figure 5.45 shows SEM micrographs of the aligned lignin fibres carbonised at 1,000, 1,200 and 1,500 °C. The presence of misaligned fibres is probably due to the alignment being disturbed during transportation and sample preparation. The fibre diameters and their distributions of the carbonised fibres are shown in Figure 5.46. The average fibre diameter was calculated from 50 measurements. The diameters of fibres carbonised at 1,000 °C, 1,200 °C and 1,500 °C were 639 ± 93 nm, 550 ± 74 nm and 547 ± 94 nm, respectively. This represents a reduction of 57%, 63% and 63%, respectively from the electro-spun acetone-soluble fibres.

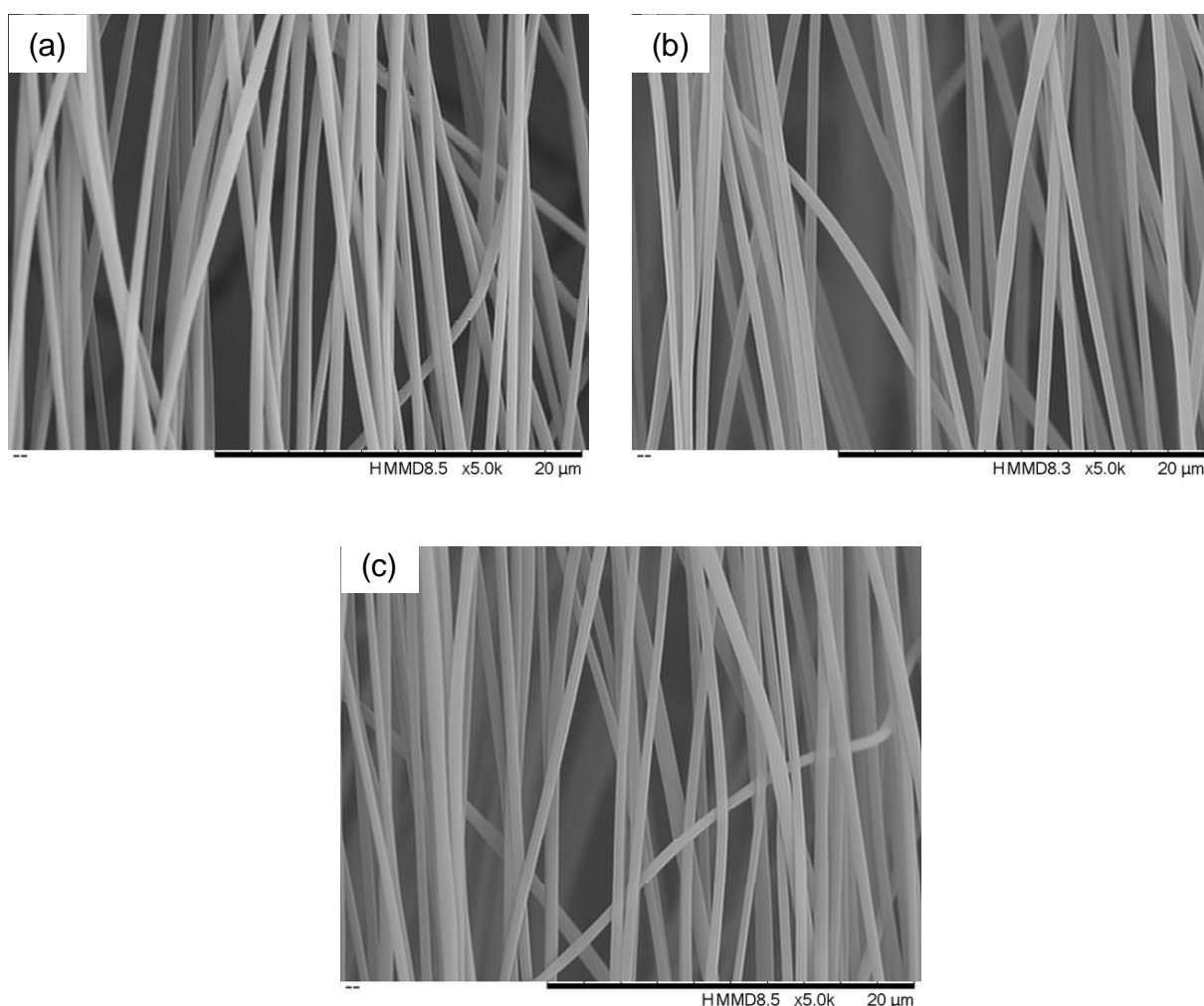


Figure 5.45 SEM micrographs of aligned electro-spun fibres carbonised at: (a) 1,000 °C, (b) 1,200 °C and (c) 1,500 °C.

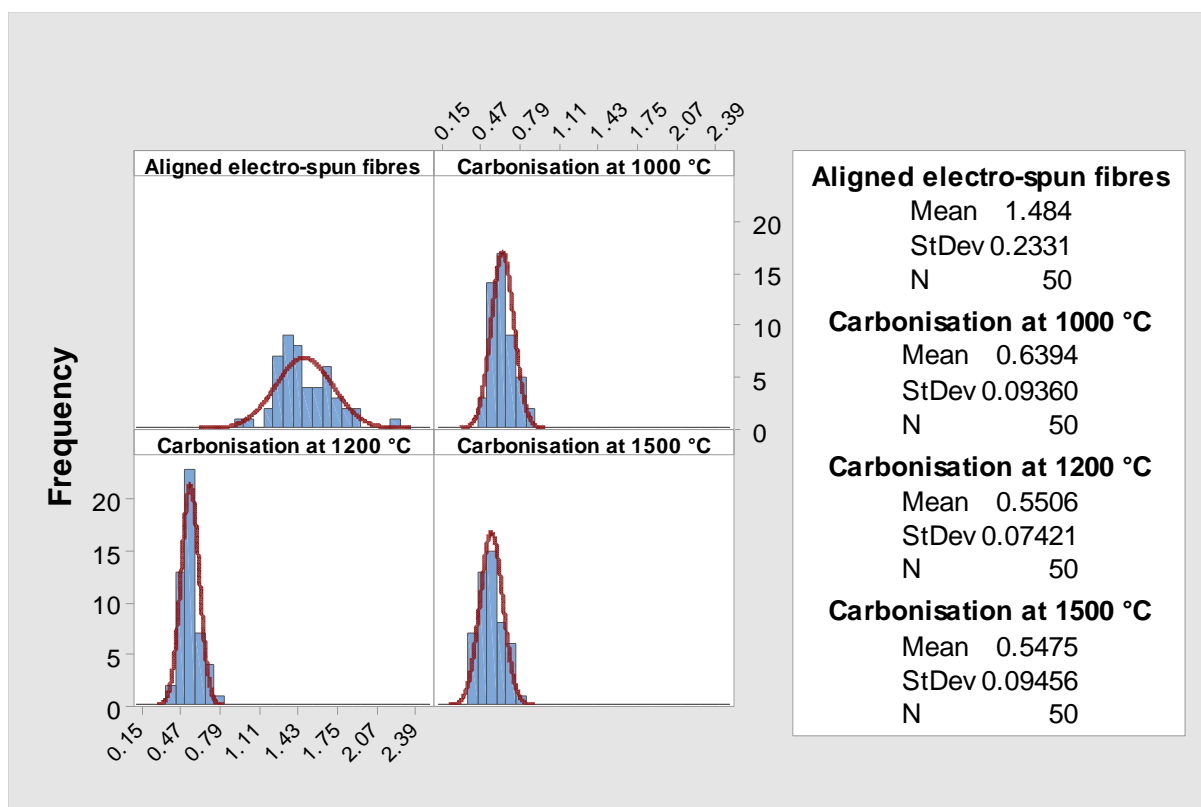


Figure 5.46 Fibre diameter and distribution of fibre diameter of as-spun aligned fibres and carbonised fibres at various carbonisation temperatures.

5.9 Summary

- The electrospinning of 100% softwood Kraft lignin was demonstrated successfully. 53 wt% of acetone-soluble lignin was dissolved in a binary solvent of acetone and DMSO. The viscosity and conductivity of the lignin solution are 0.43 ± 0.01 Pa·s and 2.37 ± 0.02 $\mu\text{S}\cdot\text{cm}^{-1}$, respectively. Electro-spun lignin fibres with a diameter of 1.16 ± 0.21 μm were produced. Lignin fibres were void-free and had a circular cross-section and smooth surface.
- After electro-spinning, the solvent retained in the fibres was reduced by heating in a vacuum oven at 140 °C for six hours. Increasing temperature to 180 °C and 200 °C resulted in fibres fusion.

- Thermo-stabilisation was carried out in air. The air flow rate was kept constant at 50 ml·minute⁻¹ with a heating rate of 0.5 °C·minute⁻¹. The temperature was ramped from ambient to 100 °C, 150 °C and 250 °C with a dwell time of one hour in each temperature. It was established that thermo-stabilisation in air can retain the circular cross-sectional of fibre. However, thermo-stabilisation in nitrogen lead fibre fusion. Retaining of fibre structure can be linked to changes in the chemical structure of lignin and it was verified by FTIR spectroscopy and XPS. From the FTIR results, carbonyl (C=O) bonds and the formation of aromatic out-of-plane bending of C-H were detected in the fibres stabilised in air. From XPS, in the sample thermo-stabilised in air, the C2 carbon (C-O-C, O-C) decreased, which involved demethylation and cleavage of interunit linkages of α -O-4' and β -O-4'. Increased C4 carbon (C(=O)-OH, O-C=O) was observed, revealing the auto-oxidation of aldehyde or ketone and formation of carboxylic acid (C(=O)-OH) and ester (O-C=O) from FTIR spectroscopy.

- Taguchi design of experiments and ANOVA were carried out to determine the main effect of the carbonisation condition on electro-spun acetone-soluble lignin fibres. From the Taguchi analysis, the carbonisation temperature is the dominant factor influencing the formation of graphite-like structures, which contributes over 50% of all factors.

- Carbonised fibres from the electro-spun acetone-soluble lignin precursor were produced where the average diameter was between 500-530 nm. The carbonised fibres showed a carbon content of over 90 at%.

- Aligned lignin fibres were produced successfully by using a modified-graphite collector. The diameter of aligned fibres was $1.48 \pm 0.23 \mu\text{m}$ where circular cross-section with a smooth surface. Based on semi-inspection, the fibres were void-free.

- Acetone-soluble lignin with a processing aid (vanillin; PEG) shows a drop in T_g . Electro-spun fibres from lignin with vanillin and PEG possessed a smaller fibre diameter and narrower distribution of diameter as compared to lignin without processing aid. After carbonisation at 1,500 °C, carbon fibre production with 450-550 nm fibre diameter was established. These results are presented in Appendix G.

- A flowchart for the production of carbonised lignin fibres from electro-spun acetone-soluble lignin is illustrated in Figure 5.47.

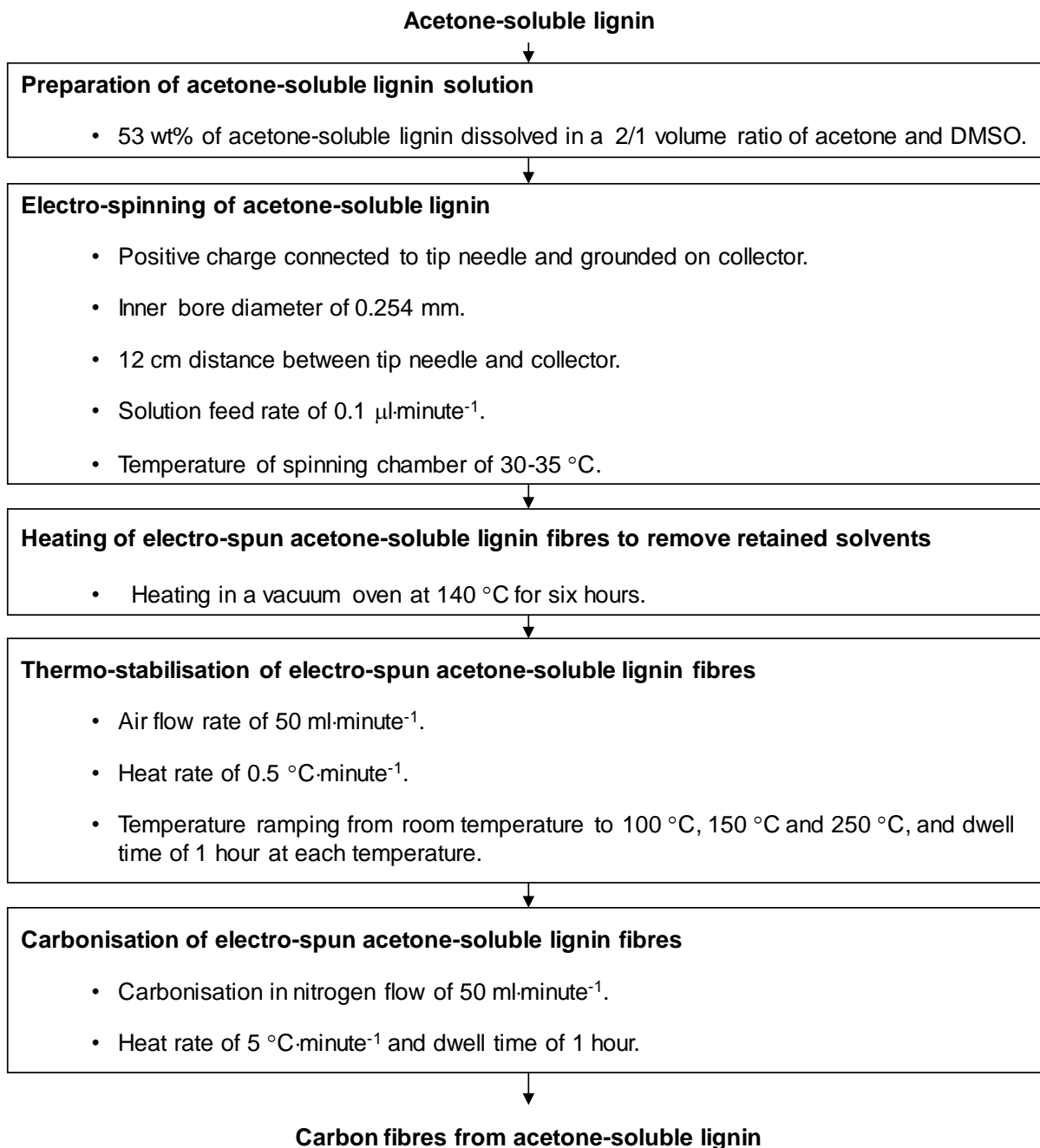


Figure 5.47 Illustration of the procedure for the production of carbon fibres from electro-spun acetone-soluble lignin fibres.

6. CONCLUSION AND RECCOMENDATION FOR FUTURE RESEARCH

6.1 Conclusion and Contribution to Knowledge

The aim of this research was to utilise softwood Kraft lignin as a bio-based precursor for the production of carbonised lignin fibres. A novel approach for electro-spinning of acetone-soluble softwood Kraft lignin, without polymer blending and/or chemical modification, was established for the first time in this current work.

An effective method of removing inorganic content from as-received lignin (BioChoice[®]lignin) was demonstrated. This method involved the fractionation of lignin with acetone. Fractionated lignin (acetone-soluble lignin) showed an inorganic content of $0.055 \pm 0.021\%$ with a fractionation yield of $57.4 \pm 0.6\%$.

Acetone-soluble lignin was electro-spun successfully without polymer blending. A combination of acetone and dimethyl sulfoxide was used for electro-spinning. Bead-free electro-spun acetone-soluble lignin fibres with a near circular cross-section were demonstrated for the first time in this work. With reference to the experimental conditions and laboratory environment, a 53 wt% of acetone-soluble lignin in a binary solvent of 2/1 volume ratio of acetone and DMSO was found to be the optimal concentration for electro-spinning. An operating voltage of 12 kV was applied between the capillary needle and the grounded electrode. The distance between the tip of the needle and the ground plate was kept at 20 cm. During electro-spinning, the temperature within the chamber was maintained between 30 and 35 °C. The collected electro-spun fibres had an average diameter of $1.16 \pm 0.21 \mu\text{m}$. Sequential procedures for producing carbonised lignin fibres including removing residuals solvent from the as-electro-spun fibres, thermo-stabilisation and carbonisation were investigated in detail. The electro-spun fibres made from acetone-soluble lignin were heated in a vacuum oven at 140 °C for six hours prior to thermo-stabilisation in air using a flow rate of 50 ml·minute⁻¹ with a heating rate of 0.5 °C·minute⁻¹ to 250 °C. After carbonisation,

carbonised lignin fibres with a near circular cross-section were obtained with diameters between 500-530 nm.

This research also demonstrated production of aligned softwood Kraft lignin fibres via electro-spinning using a novel custom-made grounded electrode collector. The grounded electrode improved degree of fibre alignment of the electro-spun lignin fibres and they could heat-treated without removing them from the collector.

6.2 Other Research Outcomes

Acetone-soluble lignin was also electro-spun successfully with processing aids such as vanillin and PEG. Electro-spun fibres of acetone-soluble lignin with the processing aids displayed a smaller fibre diameter with narrow distribution when compared to lignin fibres produced without the processing aids.

6.3 Recommendation for Future Research

Further characterisations of carbonised electro-spun acetone-soluble lignin fibres such as mechanical properties, electrical conductivity and surface area will be useful data for the application of the lignin-derived carbon fibres.

Acetone-insoluble lignin was produced from the molecular weight fraction using acetone. It was not used in this current work due to lack of time. After treatment with pH 2 acidified water, its ash content was reduced from to 2.395 ± 0.034 % to 0.358 ± 0.016 %. It could be blended with polymer blend such as cellulose acetate or cellulose to enable fibre formation.

APPENDICES

Appendix A: Alternative Solvent for Electro-spinning of Lignin.

Table A.1 A compilation of solvents that are enable for electro-spinning of lignin.

Solvents	Toxicity	Hansen Solubility parameter (MPa ^{1/2})			Boiling point (°C)	Enthalpy of vaporization, $\Delta_{\text{vap}}H^\circ$, (kJ/mol)
		δ_D	δ_P	δ_H		
Dimethyl sulfoxide	Not a hazardous substance or mixture	18.4	16.4	10.2	189	52.9
Dimethyl formamide		17.4	13.7	11.3	153	46.9
Dipropylene glycol	Not a hazardous substance or mixture	16.5	10.6	17.7	230	61.2
Diethylene glycol		16.6	12.0	20.7	245	66.5
Triethylene glycol	Not a hazardous substance or mixture	16.0	12.5	18.6	285	60.5
Ethylene glycol monomethyl ether		16.2	9.2	16.4	124	45.2
Propylene glycol	Not a hazardous substance or mixture	16.8	9.4	23.3	188	67
Ethanol		15.8	8.8	19.4	78	42.3
Propylene glycol monophenyl ether		16.2	7.8	12.6	243	
Ethylene glycol		17.0	11.0	26.0	250	65

Appendix B: Surface Roughness of Electro-spun Acetone-soluble Lignin Fibres

Figure A.1 (a) shows the surface topography obtained from atomic force microscopy (AFM). The average surface roughness (R_a) of the fibres was measured using three-line scans over 8 μm length as shown in Figure A.1 (b and c). The average surface roughness is 0.93 ± 0.19 nm.

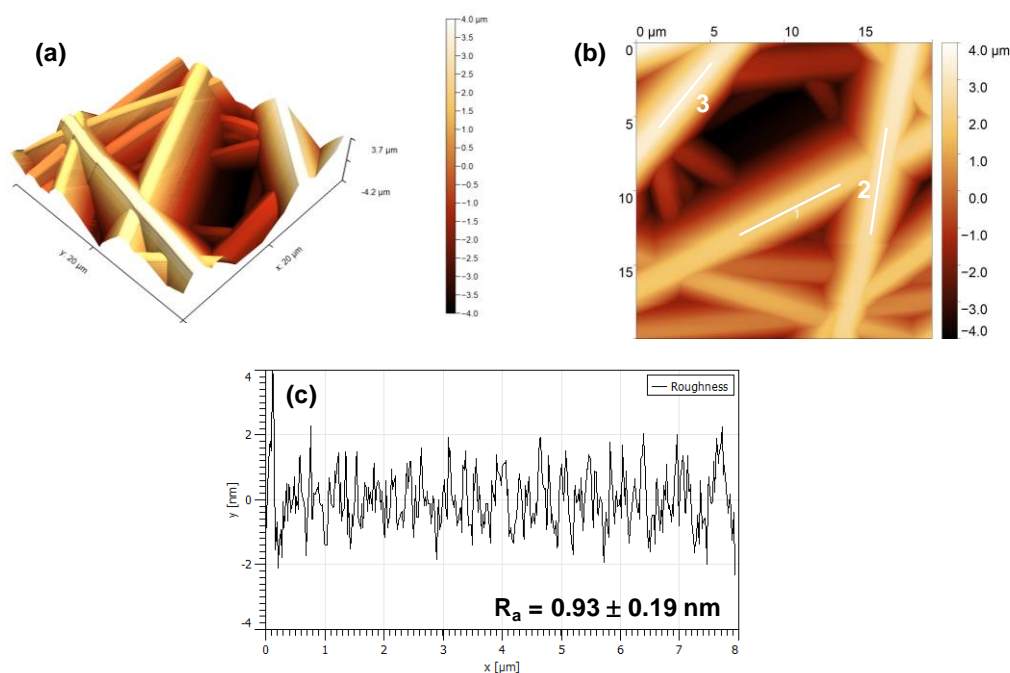


Figure A.1 AFM-based surface analysis of electro-spun acetone-soluble lignin fibres: (a) surface topography; (b) surface roughness measurement area; and (c) line profile of the surface roughness measurement.

Surface roughness of the carbonised fibres was measured using an AFM. Figure A.2 illustrates the AFM analysis including the 3-D image, surface morphology and the measurement of surface roughness of the electro-spun acetone-soluble lignin carbonised at 1,000 $^{\circ}\text{C}$, 1,200 $^{\circ}\text{C}$ and 1,500 $^{\circ}\text{C}$. After carbonisation, all the carbonised fibres showed a higher surface roughness compared to the surface roughness of as-spun fibres (0.93 ± 0.19 nm), as shown in Figure A.1. The average roughness of carbonised fibres is found to be in the range of 1.1-2.5 nm. [325].

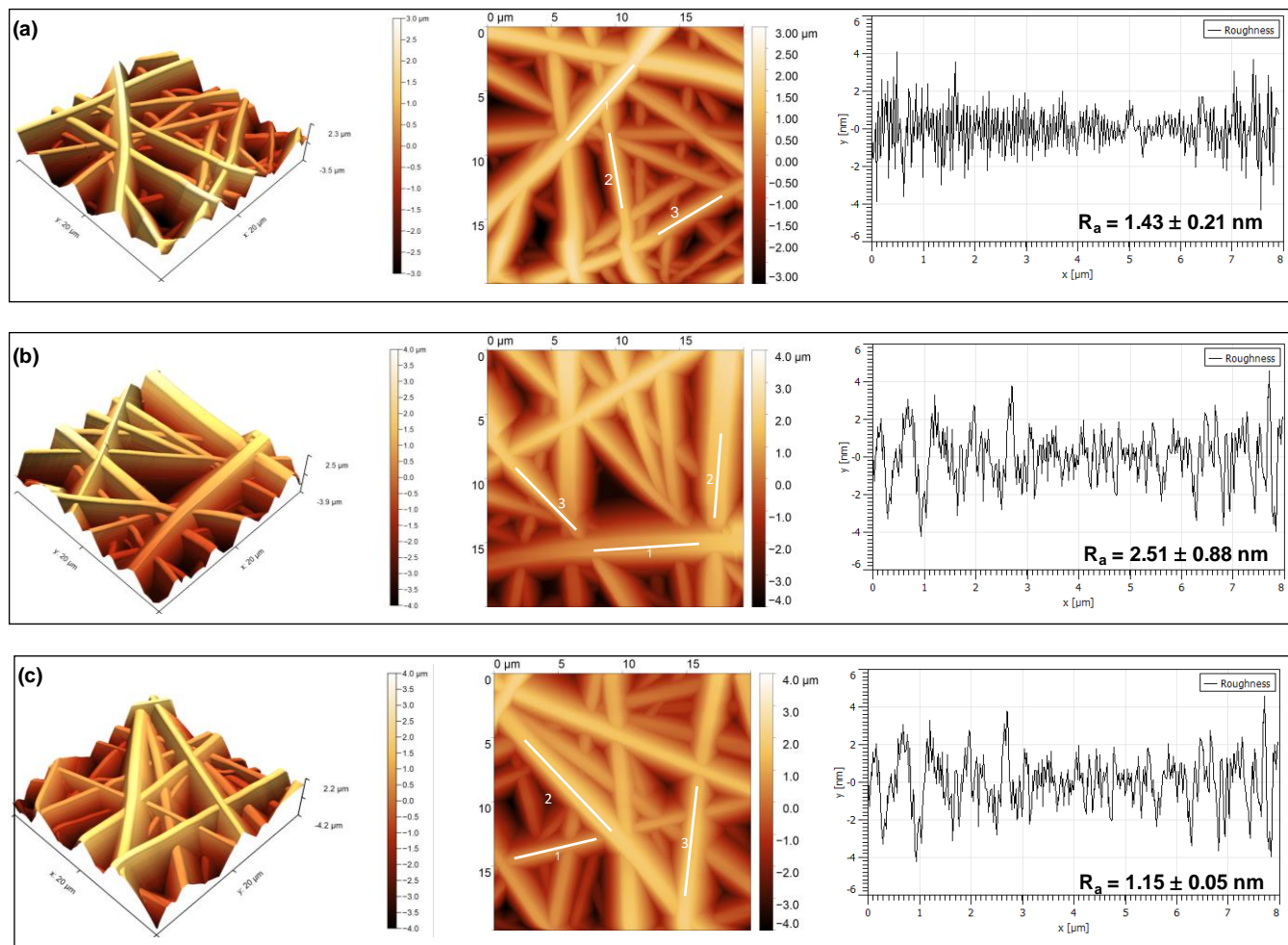


Figure A.2 AFM results of carbonised electro-spun acetone-soluble lignin fibres which are carbonised at: (a) 1,000 °C, (b) 1,200 °C and (c) 1,500 °C.

The surface roughness of the aligned electro-spun acetone-soluble lignin fibres and the carbonised fibres were characterised within a scanned square area of $0.25\ \mu\text{m} \times 0.25\ \mu\text{m}$. All the carbonised fibres possess a rougher surface than the electro-spun fibres. Figure A.3 presents the surface roughness of aligned carbonised electro-spun fibres, in the range of 2.8-5.0 nm.

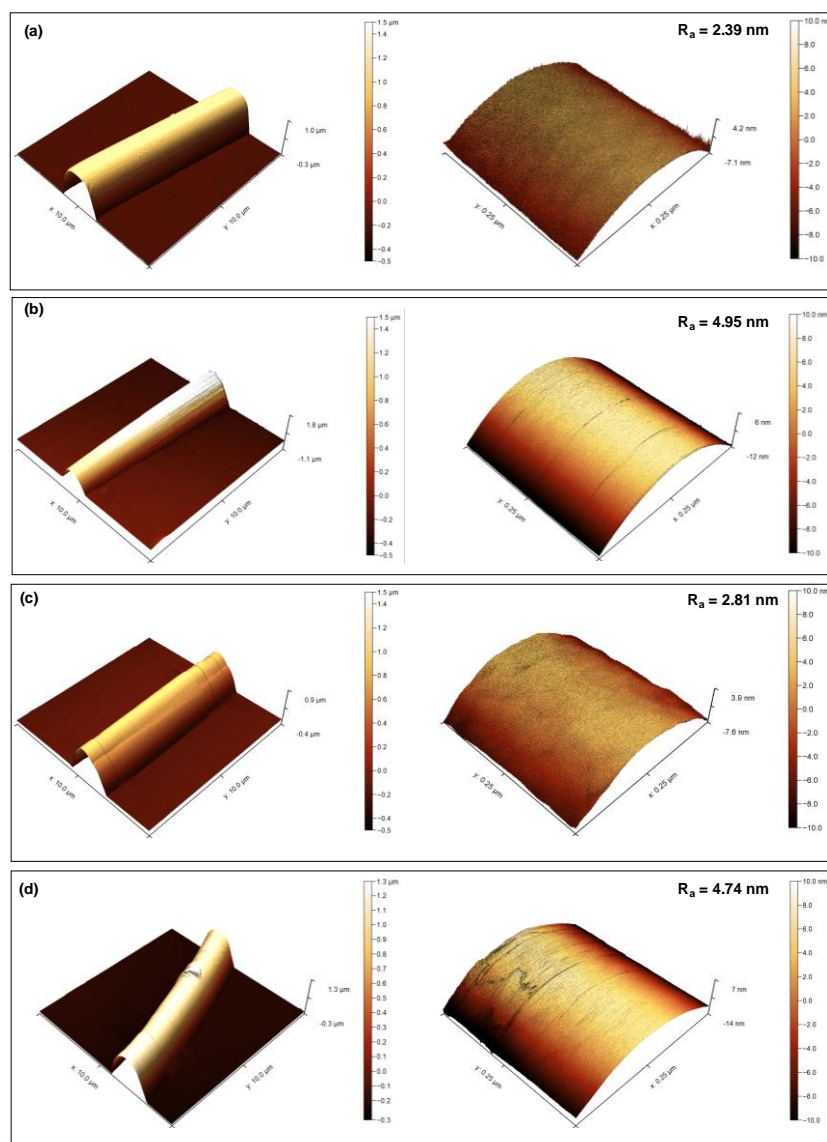


Figure A.3 Surface topography and roughness measurements of aligned electro-spun acetone-soluble lignin for: (a) electro-spun fibres, and the fibres carbonised at (b) 1,000 °C, (c) 1,200 °C and (d) 1,500 °C.

Appendix C: FTIR Spectra of Lignin Fibres Heated in a Vacuum Oven, Nitrogen and Air.

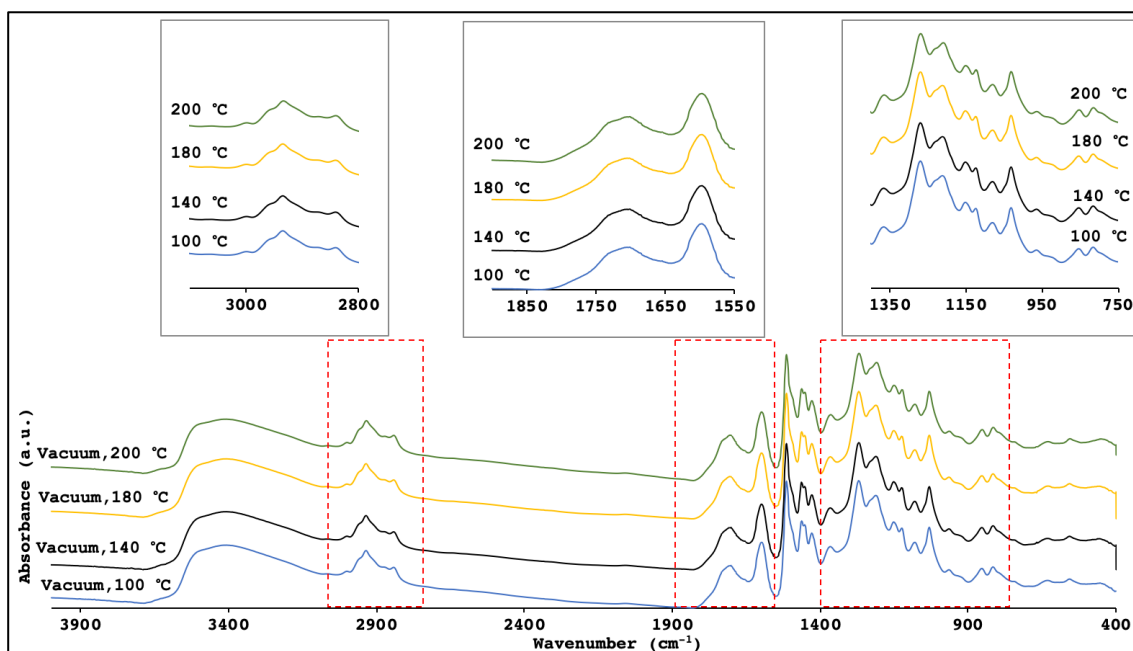


Figure A.4 Overlaid FTIR spectra of the electro-spun acetone-soluble lignin fibres heated in a vacuum oven.

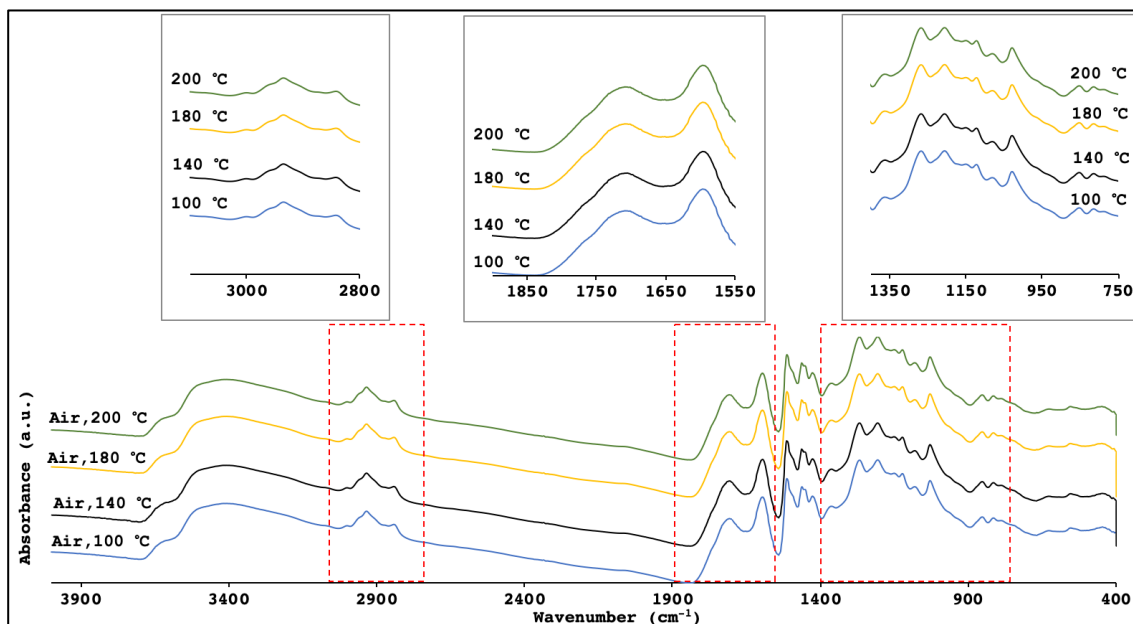


Figure A.5 Overlaid FTIR spectra of the electro-spun acetone-soluble lignin fibres heated in air

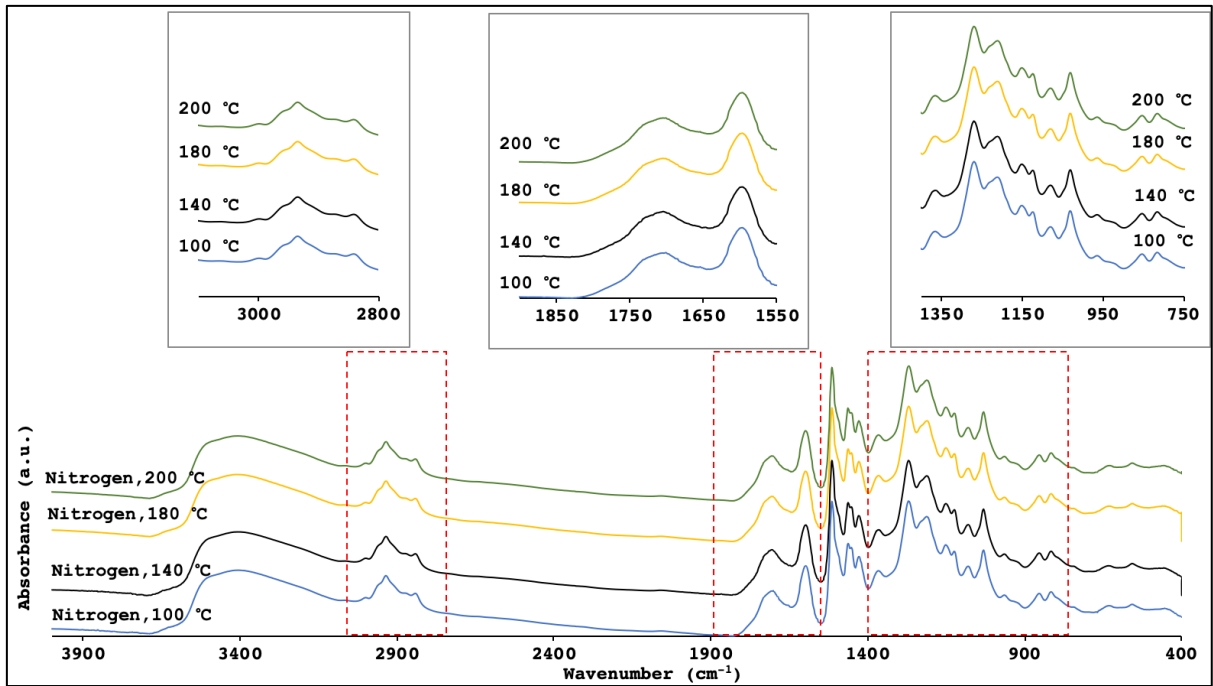


Figure A.6 Overlaid FTIR spectra of the electro-spun acetone-soluble lignin fibres heated in nitrogen

Appendix D: Deconvolution Curve Fitting for XPS spectra.

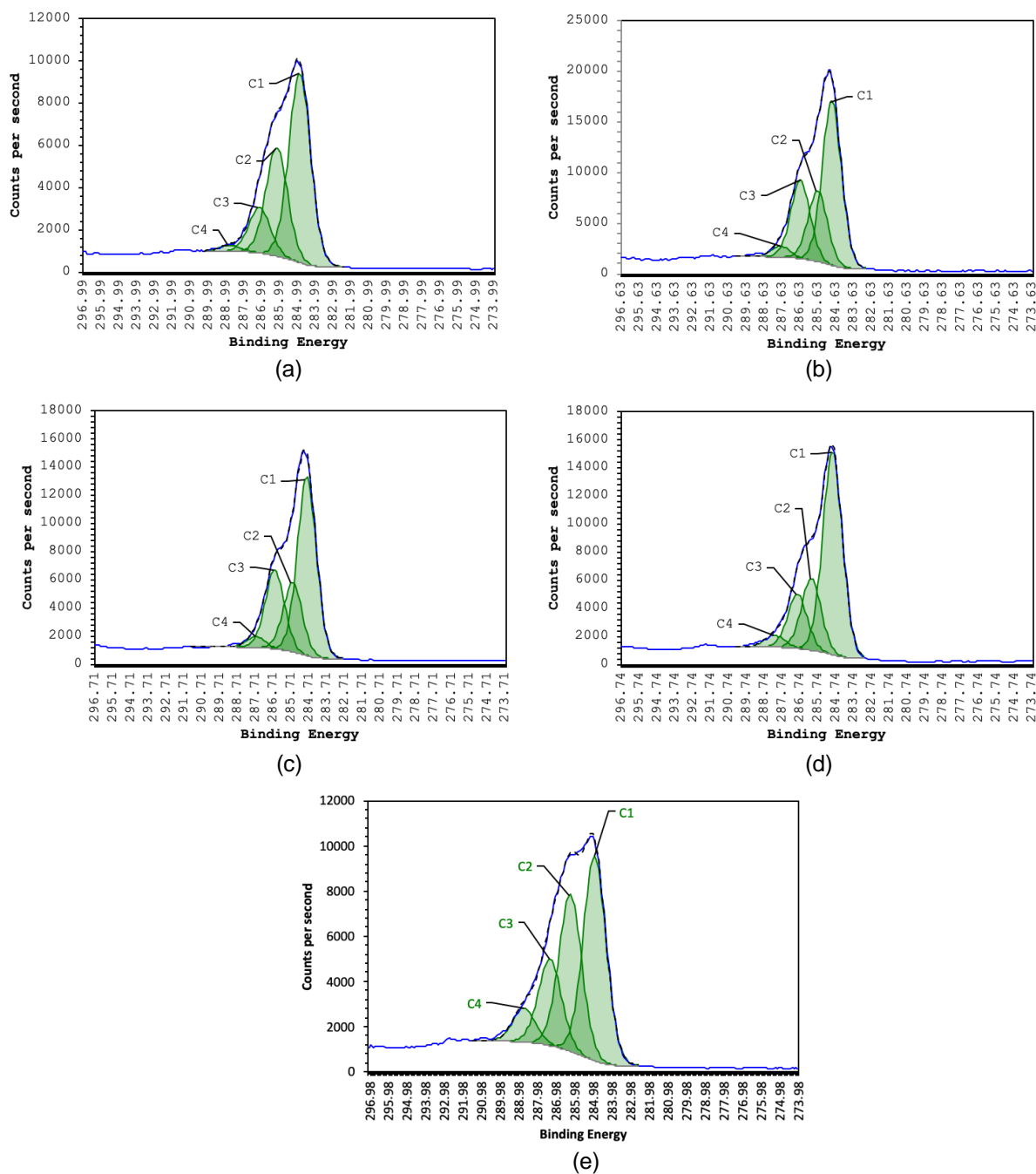


Figure A.7 High-resolution C1s of XPS spectra; spectra of the electro-spun acetone-soluble lignin fibres thermo-stabilised in air at: (a) 150 °C; (b) 180 °C; (c) 200; (d) 220 and (d) 250°C.

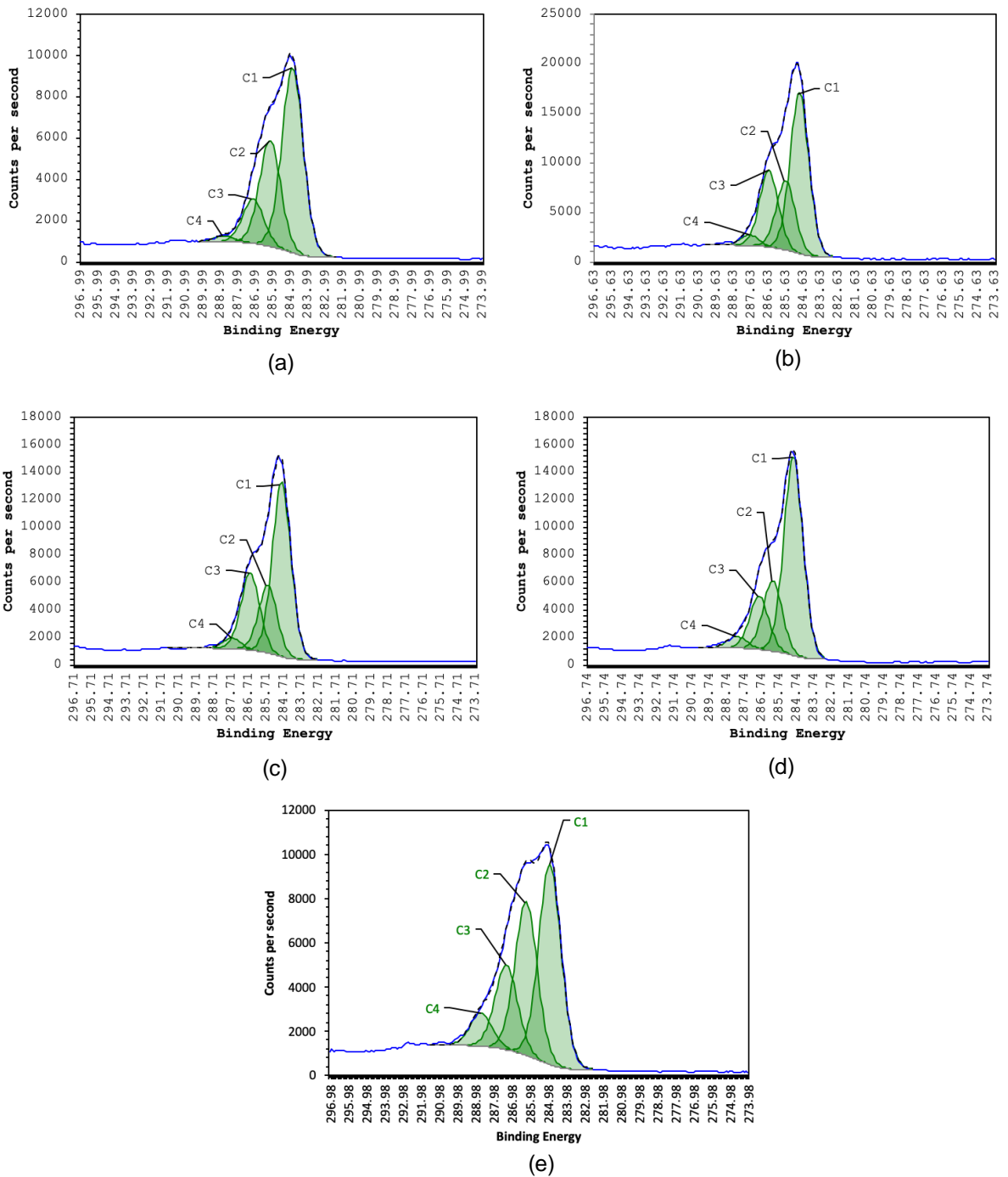


Figure A.8 High-resolution C1s of XPS spectra; spectra of the electro-spun acetone-soluble lignin fibres thermo-stabilised in nitrogen at: (a) 150 °C; (b) 180 °C; (c) 200 °C; (d) 220 °C and (d) 250°C.

Appendix E: Response table of Analysis of Variance (ANOVA)

Table A.2 Analysis of Variance for fibre diameter

Source	DF	Adj SS	Adj MS	F-Value	P-Value	% contribution
Heating rate	2	0.003485	0.001742	0.98	0.506	13.65
Temperature	2	0.016461	0.008231	4.62	0.178	64.46
Dwell time	2	0.002024	0.001012	0.57	0.638	7.93
Error	2	0.003566	0.001783			13.96
Total	8	0.025536				100

Table A.3 Analysis of Variance for distribution of fibre diameter

Source	DF	Adj SS	Adj MS	F-Value	P-Value	% contribution
Heating rate	2	0.000709	0.000354	3.26	0.235	16.39
Temperature	2	0.002317	0.001159	10.65	0.086	53.57
Dwell time	2	0.001082	0.000541	4.98	0.167	25.02
Error	2	0.000217	0.000109			5.02
Total	8	0.004325				100.00

Table A.4 Analysis of Variance for I_D/I_G

Source	DF	Adj SS	Adj MS	F-Value	P-Value	% contribution
Heating rate	2	0.001504	0.000752	0.92	0.52	3.51
Temperature	2	0.038458	0.019229	23.56	0.041	89.64
Holding time	2	0.001309	0.000655	0.8	0.555	3.05
Error	2	0.001633	0.000816			3.81
Total	8	0.042903				100.00

Table A.5 Analysis of Variance for FWHM of D-band

Source	DF	Adj SS	Adj MS	F-Value	P-Value	% contribution
Heating rate	2	987.3	493.7	2.83	0.261	9.07
Temperature	2	8266.7	4133.3	23.69	0.04	75.94
Holding time	2	1282.4	641.2	3.68	0.214	11.78
Error	2	348.9	174.5			3.21
Total	8	10885.3				100.00

Table A.6 Analysis of Variance for FWHM of G band

Source	DF	Adj SS	Adj MS	F-Value	P-Value	% contribution
Heating rate	2	243.346	121.673	1.97	0.337	27.39
Temperature	2	512.116	256.058	4.15	0.194	57.64
Holding time	2	9.438	4.719	0.08	0.929	1.06
Error	2	123.528	61.764			13.90
Total	8	888.428				100.00

Table A.7 Analysis of Variance for A_D/A_G

Source	DF	Adj SS	Adj MS	F-Value	P-Value	% contribution
Heating rate	2	0.002413	0.001207	0.05	0.951	1.00
Temperature	2	0.086115	0.043057	1.86	0.35	35.57
Holding time	2	0.10723	0.053615	2.31	0.302	44.29
Error	2	0.046351	0.023175			19.14
Total	8	0.242109				100.00

Appendix F: Interaction Plot of Carbonisation Parameters

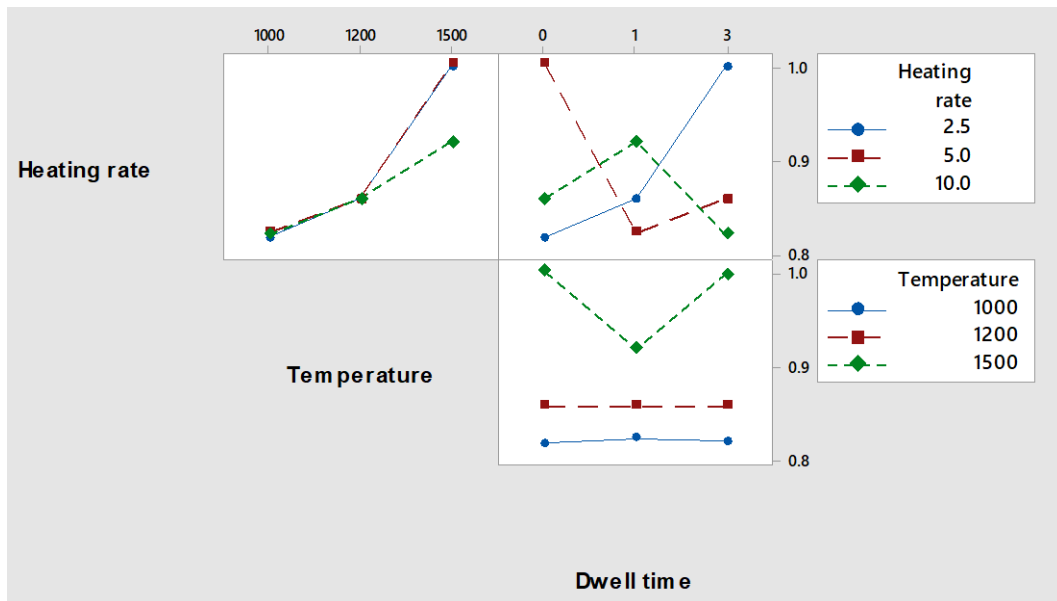


Figure A.9 Interaction effect plot for I_D/I_G ratio of carbonised electro-spun acetone-soluble lignin fibres.

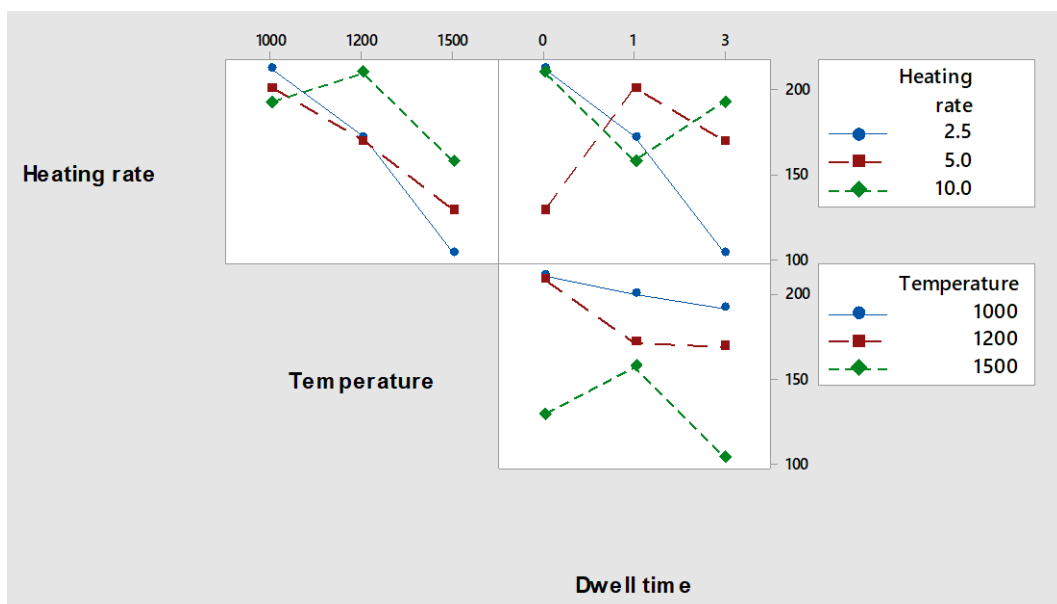


Figure A.10 Interaction effect plot for FWHM of D band of carbonised electro-spun acetone-soluble lignin fibres.

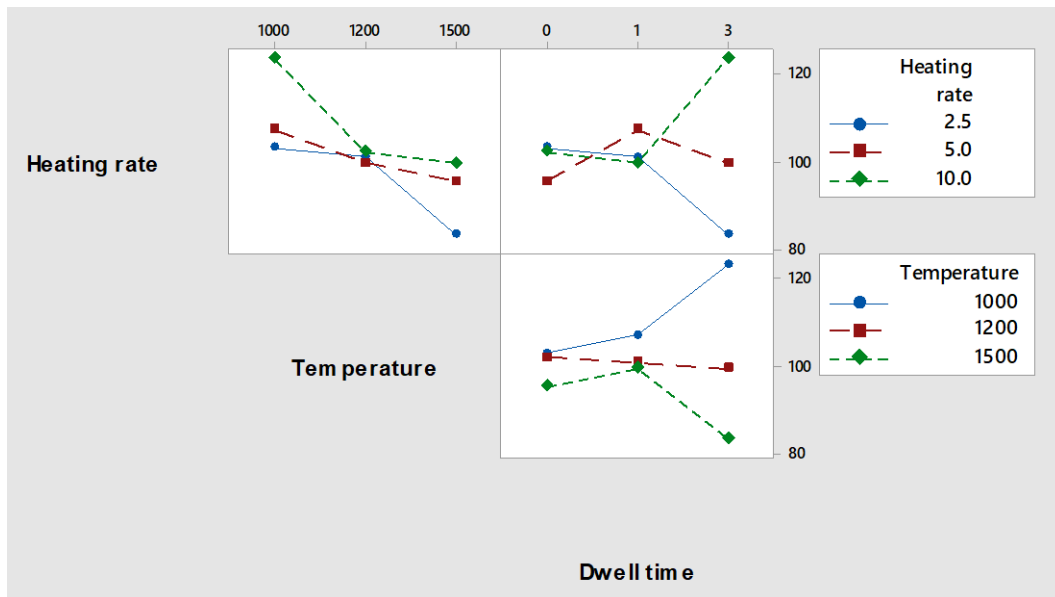


Figure A.11 Interaction effect plot for FWHM of G band of carbonised electro-spun acetone-soluble lignin fibres.

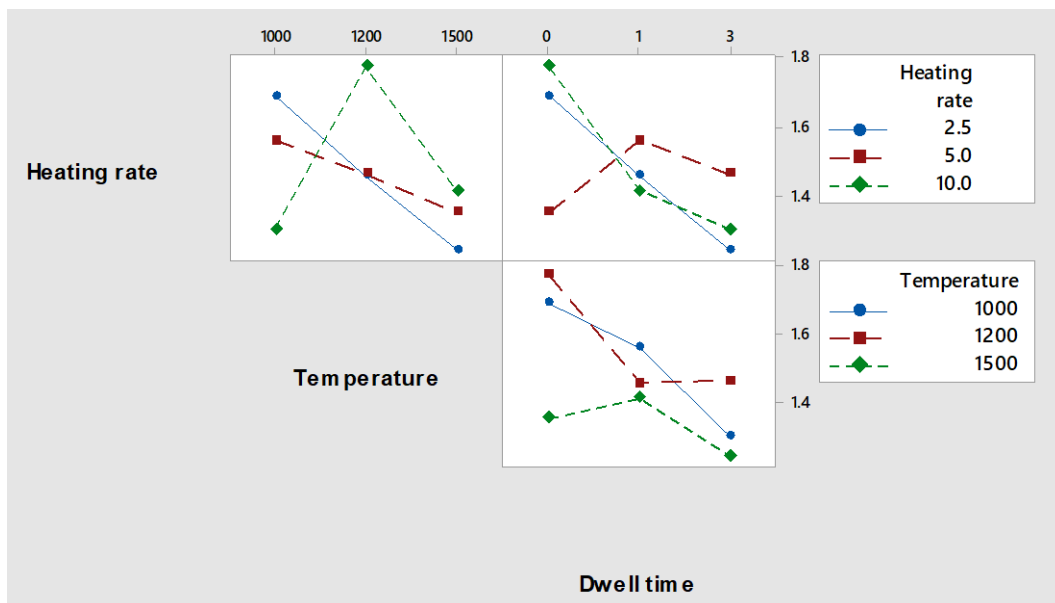


Figure A.12 Interaction effect plot for A_D/A_G ratio of carbonised electro-spun acetone-soluble lignin fibres.

Appendix G: Processing Aid for Electro-spinning of Acetone-soluble Lignin

This section describes the use of vanillin and polyethylene glycol (PEG) as processing aids for electro-spinning lignin. The basis for using additives to lignin was discussed by Bouajila *et al.* [326]. The requirements for the processing aid were stated as having to be an aromatic molecule with a structure that is similar to the repeat unit of lignin. This was the basis for the selection of vanillin as the processing aid in the current study. The T_g of lignin was said to be lowered by 60 °C by adding 20 wt% of vanillin [326]. PEG was selected as it is the low molecular weight form of polyethylene oxide (PEO) and it is miscible with lignin [102,138,153].

The chemical structure of vanillin and PEG are illustrated in Figure A.13. Vanillin possesses aldehyde, hydroxy and ether functional groups. PEG is a linear polyether compound.

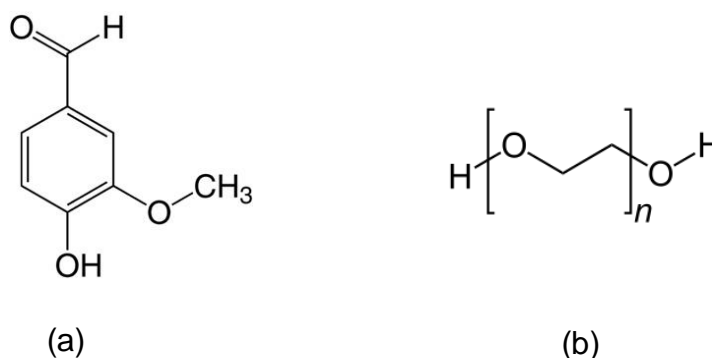


Figure A.13 Molecular structure of (a) vanillin and (b) polyethylene glycol.

In this work, vanillin was added to acetone-soluble lignin in the range of 0 to 2 grams per 100 grams of lignin. The effect of the processing aid content on the T_g of acetone-soluble lignin and the uniformity of the diameter of the electro-spun fibres was investigated.

DSC was conducted to study the effect of the processing aids on the T_g of acetone-soluble lignin. A single T_g is observed clearly in the second and third heating traces. The T_g s are shown in Figure A.14. The presence of a single T_g indicates that lignin

and vanillin are miscible. The T_g of lignin decrease with an increasing concentration of vanillin in the blend. For instance, the T_g is lowered to 133.8 °C when two grams of vanillin were mixed to 100 grams of acetone-soluble lignin.

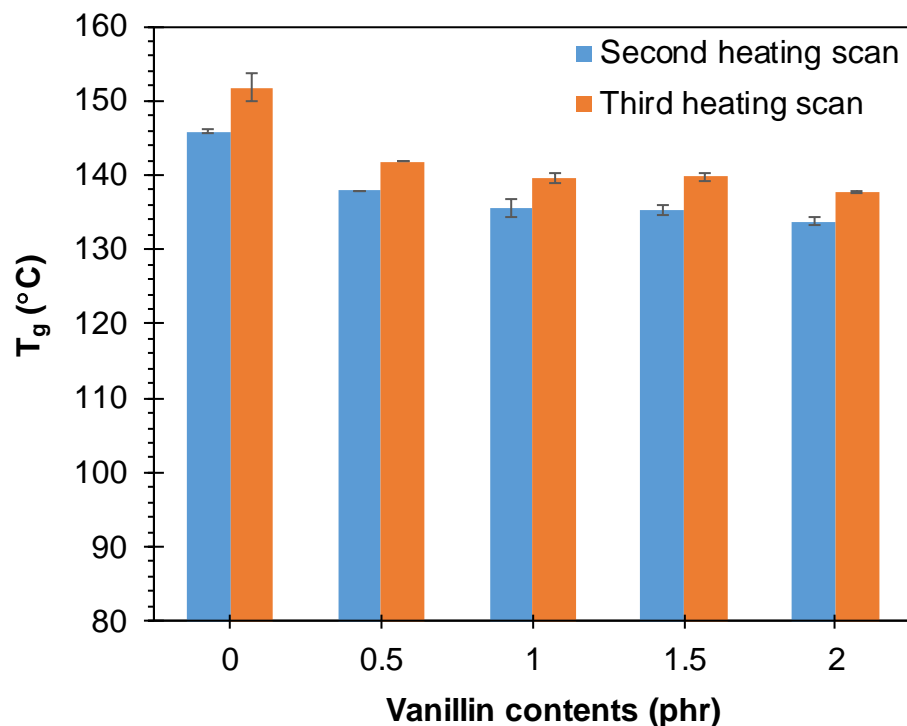


Figure A.14 T_g from the second and third heating scans of lignin blended with vanillin.

In the case of the PEG-lignin blend, a single T_g was detected due to the good miscibility between the two polymer. Figure A.15 shows a bar chart of T_g for the lignin blended with PEG. At 2.5 phr of PEG, the T_g of lignin drops from 145.8 °C to 119.5 °C.

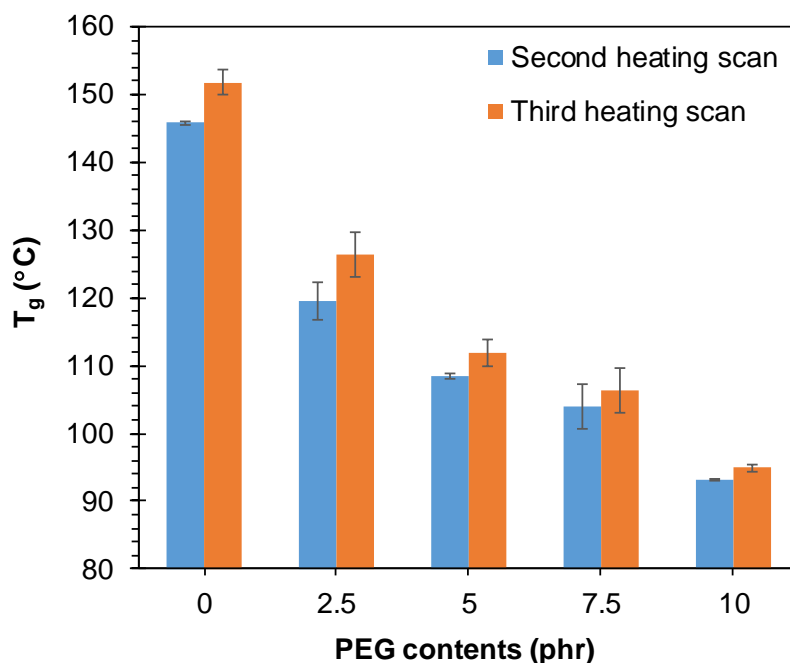


Figure A.15 T_g from second and third heating scans of lignin/PEG.

Lignin with 2 phr of vanillin and lignin with 2.5 phr PEG were used for electro-spinning. The viscosity and conductivity of lignin/vanillin are 0.39 ± 0.02 Pa·s and 2.40 ± 0.02 $\mu\text{S}\cdot\text{cm}^{-1}$, respectively. The lignin/PEG solutions are 0.38 ± 0.03 Pa·s and 2.38 ± 0.03 $\mu\text{S}\cdot\text{cm}^{-1}$, respectively. The viscosity and conductivity of the lignin solutions with the processing aid were found to be in a similar range when compared to the acetone-soluble lignin solution without the processing aid as reported in Section 5.3.

Both lignin/vanillin and lignin/PEG solutions were found to be suitable for electro-spinning. The fibre morphology of electro-spun and carbonised fibres from lignin with the processing aid are presented in Figure A.16 and Figure A.17. A noticeable difference in fibre diameter distribution between neat lignin and the lignin with the processing aids.

The electro-spun fibre obtained from lignin with vanillin and PEG (see Figure A.18 and Figure A.19) showed a narrower distribution when compared to the lignin without processing aid (Figure 5.5). The fibre diameter of the lignin/vanillin blend is in the

range 0.6-1.4 μm and that for lignin/PEG fibres is 0.6-1.6 μm , both of which are narrower than that of neat lignin (0.6-1.8 μm).

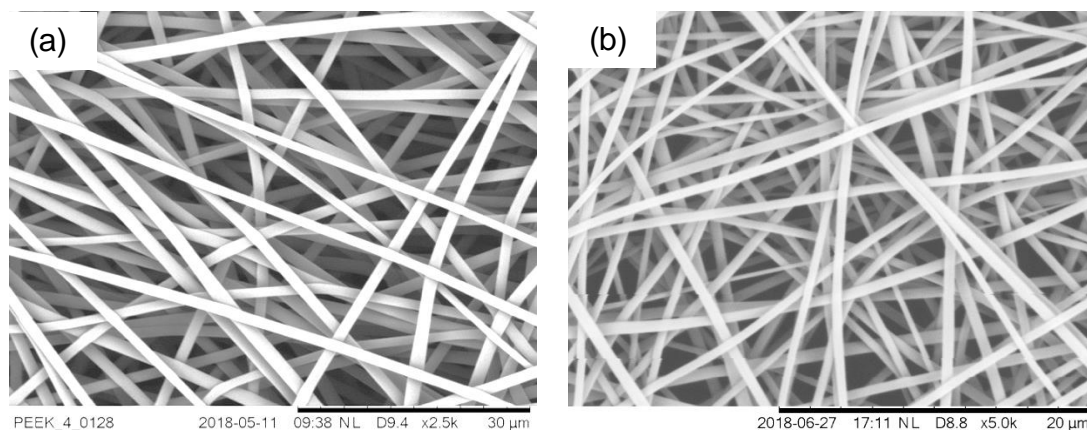


Figure A.16 SEM micrographs of lignin/vanillin fibres; (a) electro-spun fibres and (b) the fibres carbonised at 1,500 $^{\circ}\text{C}$.

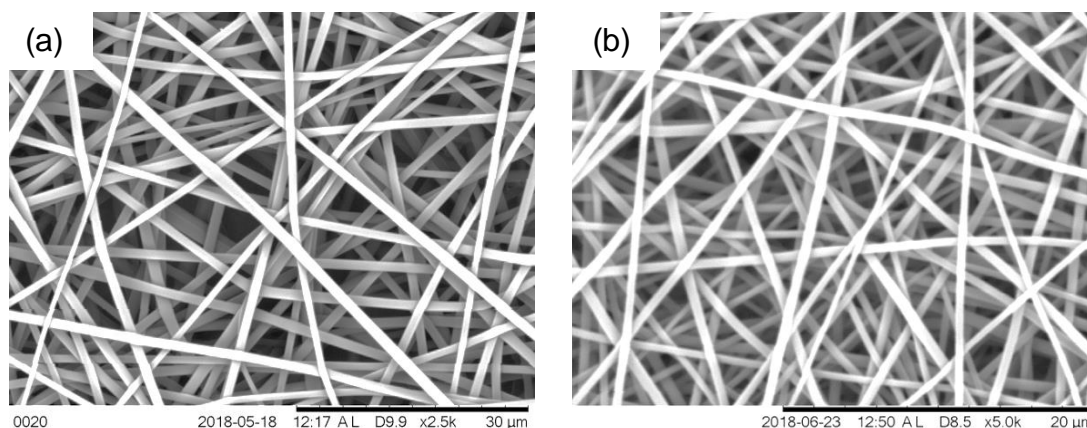


Figure A.17 SEM micrographs of lignin/PEG fibres; (a) electro-spun fibres and (b) the fibres carbonised at 1,500 $^{\circ}\text{C}$.

With regard to the lignin/vanillin blended, the average fibres diameter decreased from 1,040 nm (the electro-spun fibres) to 530 nm carbonised at 1,500 $^{\circ}\text{C}$. The changing the average diameter for the lignin/PEG blend was 1052 nm and after

carbonisation at 1,500°C was 496 nm. Moreover, the use of a processing aid can assist in improving the smoothness of the fibre surface to 1 nm R_a as shown in Figure A.20.

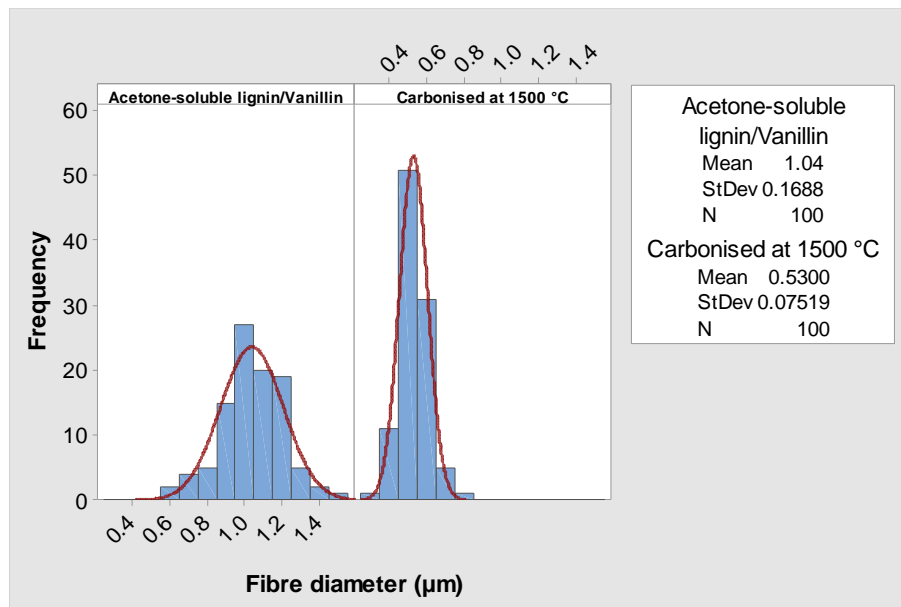


Figure A.18 Fibres diameter and distribution of electro-spun acetone-soluble lignin with vanillin.

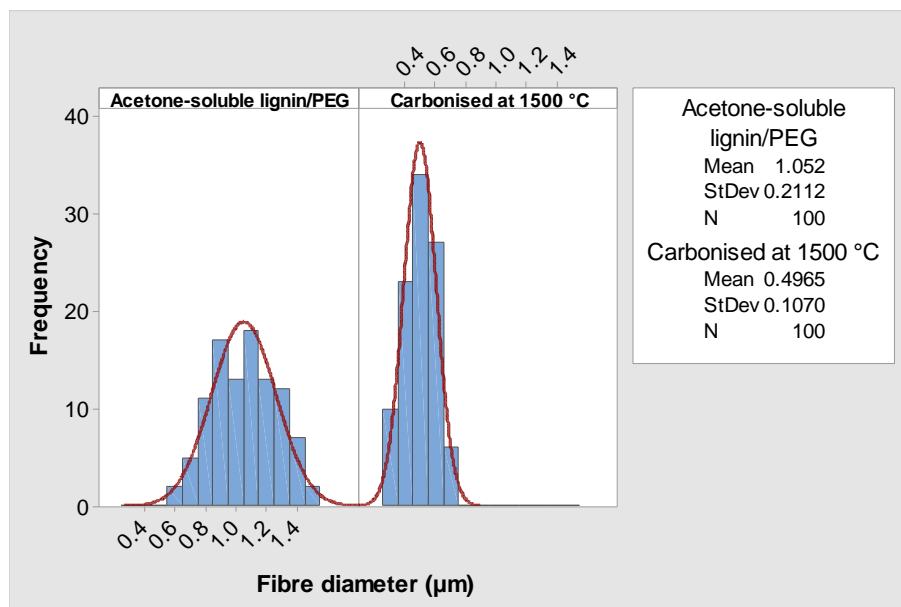


Figure A.19 Fibres diameter and distribution of electro-spun acetone-soluble lignin with PEG.

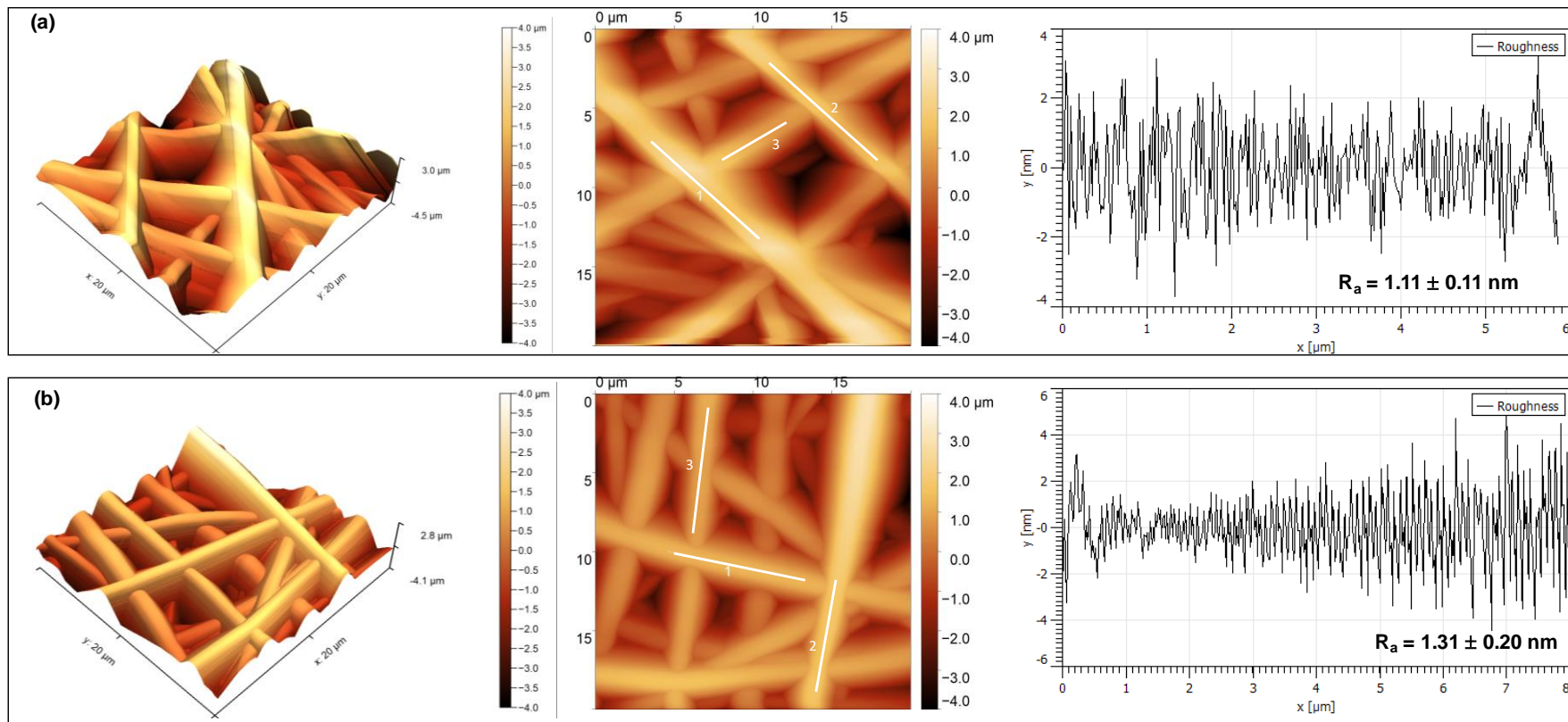


Figure A.20 Surface topography and surface roughness measurement: (a) electro-spun fibres and (b) carbon fibres derived from acetone-soluble lignin with vanillin.

LIST OF REFERENCES

- [1] A. Al-Lami, P. Hilmer, M. Sinapius, Eco-efficiency assessment of manufacturing carbon fiber reinforced polymers (CFRP) in aerospace industry, *Aerosp. Sci. Technol.* 79 (2018) 669–678.
<https://doi.org/10.1016/j.ast.2018.06.020>.
- [2] P. Morgan, *Carbon Fibers and Their Composites*, CRC Press, 2005.
<https://doi.org/10.1201/9781420028744>.
- [3] H. Ogawa, Architectural application of carbon fibers Development of new carbon fiber reinforced glulam, *Carbon N. Y.* 38 (2000) 211–226.
[https://doi.org/10.1016/s0008-6223\(99\)00146-3](https://doi.org/10.1016/s0008-6223(99)00146-3).
- [4] H. Fang, Y. Bai, W. Liu, Y. Qi, J. Wang, Connections and structural applications of fibre reinforced polymer composites for civil infrastructure in aggressive environments, *Compos. Part B Eng.* 164 (2019) 129–143.
<https://doi.org/10.1016/j.compositesb.2018.11.047>.
- [5] A.M. Figliolini, L.A. Carlsson, Mechanical properties of carbon fiber/vinylester composites exposed to marine environments, *Polym. Compos.* 35 (2014) 1559–1569. <https://doi.org/10.1002/pc.22809>.
- [6] D.Z. Tang, The Application of Carbon Fiber Materials in Sports Equipment, *Appl. Mech. Mater.* 443 (2013) 613–616.
<https://doi.org/10.4028/www.scientific.net/amm.443.613>.
- [7] B.A. Newcomb, Processing, structure, and properties of carbon fibers, *Compos. Part A Appl. Sci. Manuf.* 91 (2016) 262–282.
<https://doi.org/10.1016/j.compositesa.2016.10.018>.
- [8] K. Brown, C. Gallé, D. Kosson, F. Sanchez, J.M. Torrenti, Materials and properties, in: *Perform. Assess. Concr. Struct. Eng. Barriers Nucl. Appl.*, Springer Netherlands, Dordrecht, 2016: pp. 9–29. https://doi.org/10.1007/978-94-024-0904-8_2.
- [9] B. Pratima, *Updates on Carbon Fibre*, Smithers Rapra Technology, Shawbury, Shrewsbury, Shropshire, U.K., 2013.
- [10] M. Garside, Leading countries based on carbon fiber production capacity in 2018 (in 1,000 metric tons), Dec 18, 2018. (2018).
<https://www.statista.com/statistics/380549/leading-countries-by-carbon-fiber-production-capacity/> (accessed June 25, 2019).
- [11] M. Kühnel, T. Kraus, *The global CFRP market 2016*. Experience Composites, 2016.
- [12] T. Kraus, M. Kühnel, *Composites Market Report 2015*, 2015.
- [13] H. Mainka, O. Täger, E. Körner, L. Hilfert, S. Busse, F.T. Edelmann, A.S. Herrmann, Lignin - An alternative precursor for sustainable and cost-effective automotive carbon fiber, *J. Mater. Res. Technol.* 4 (2015) 283–296.

- <https://doi.org/10.1016/j.jmrt.2015.03.004>.
- [14] W. Fang, S. Yang, X.-L. Wang, T.-Q. Yuan, R.-C. Sun, Manufacture and application of lignin-based carbon fibers (LCFs) and lignin-based carbon nanofibers (LCNFs), *Green Chem.* 19 (2017) 1794–1827. <https://doi.org/10.1039/c6gc03206k>.
- [15] 5000M TORAY Torayca 12K T700SC Carbon Fiber tow continuous carbon fiber filament Yarn thread tape. 5000 meters, (n.d.). <https://directvoltage.com/shop/carbon-fiber-material/5000m-toray-torayca-12k-t700sc-carbon-fiber-tow-continuous-carbon-fiber-filament-yarn-thread-tape-5000-meters/> (accessed June 28, 2019).
- [16] C.D. Warren, F.L. Paulauskas, F.S. Baker, C.C. Eberle, A. Naskar, Development of Commodity Grade, Lower Cost Carbon Fiber-Commercial Applications, in: SAMPE Fall Tech. Conf. 2008, Memphis, TN, USA, 2009: pp. 24–36.
- [17] S.J. Park, G.Y. Heo, Precursors and manufacturing of carbon fibers, *Springer Ser. Mater. Sci.* 210 (2015) 31–66. https://doi.org/10.1007/978-94-017-9478-7_2.
- [18] A.A. Ogale, M. Zhang, J. Jin, Recent advances in carbon fibers derived from biobased precursors, *J. Appl. Polym. Sci.* 133 (2016). <https://doi.org/10.1002/app.43794>.
- [19] E. Frank, L.M. Steudle, D. Ingildeev, J.M. Spörl, M.R. Buchmeiser, Carbon fibers: Precursor systems, processing, structure, and properties, *Angew. Chemie - Int. Ed.* 53 (2014) 5262–5298. <https://doi.org/10.1002/anie.201306129>.
- [20] F.G. Calvo-Flores, J.A. Dobado, J. Isac-García, F.J. Martín-Martínez, Lignin and Lignans as Renewable Raw Materials: Chemistry, Technology and Applications, John Wiley & Sons Ltd, 2015. <https://doi.org/10.1002/9781118682784>.
- [21] L. Hodásová, M. Jablonsky, S. Andrea, A. Haz, Lignin, potential products and their market value, *Wood Res.* 60 (2015) 973–986.
- [22] J. Miller, A.-C. Bodart, Nanocellulose: Technology , Applications and Markets Special Market Analysis Study, 2014.
- [23] S. Takahashi, M. Hattori, M. Morimoto, Y. Uraki, T. Yamada, Performance of softwood soda-anthraquinone lignin as water-reducing chemical admixture in concrete, *J. Wood Chem. Technol.* 34 (2014) 31–38. <https://doi.org/10.1080/02773813.2013.820322>.
- [24] S. Kalami, M. Arefmanesh, E. Master, M. Nejad, Replacing 100% of phenol in phenolic adhesive formulations with lignin, *J. Appl. Polym. Sci.* 134 (2017) 45124. <https://doi.org/10.1002/app.45124>.
- [25] H. Zhang, B. Yu, W. Zhou, X. Liu, F. Chen, High-value utilization of eucalyptus kraft lignin: Preparation and characterization as efficient dye dispersant, *Int. J. Biol. Macromol.* 109 (2018) 1232–1238. <https://doi.org/10.1016/j.ijbiomac.2017.11.118>.

- [26] S. Laurichesse, L. Avérous, Chemical modification of lignins: Towards biobased polymers, *Prog. Polym. Sci.* 39 (2014) 1266–1290. <https://doi.org/10.1016/j.progpolymsci.2013.11.004>.
- [27] J. Miller, M. Faleiros, L. Bodart, A.-C. Bodart, *Lignin: Technology, Applications and Markets*, 2016.
- [28] D. Watkins, M. Nuruddin, M. Hosur, A. Tcherbi-Narteh, S. Jeelani, Extraction and characterization of lignin from different biomass resources, *J. Mater. Res. Technol.* 4 (2015) 26–32. <https://doi.org/10.1016/j.jmrt.2014.10.009>.
- [29] A.P. Dodd, J.F. Kadla, S.K. Straus, Characterization of fractions obtained from two industrial softwood kraft lignins, *ACS Sustain. Chem. Eng.* 3 (2015) 103–110. <https://doi.org/10.1021/sc500601b>.
- [30] L. Lagerquist, A. Pranovich, I. Sumerskii, S. von Schoultz, L. Vähäsalo, S. Willför, P. Eklund, Structural and Thermal Analysis of Softwood Lignins from a Pressurized Hot Water Extraction Biorefinery Process and Modified Derivatives, *Molecules.* 24 (2019) 335. <https://doi.org/10.3390/molecules24020335>.
- [31] J. Domínguez-Robles, T. Tamminen, T. Liitiä, M.S. Peresin, A. Rodríguez, A.S. Jääskeläinen, Aqueous acetone fractionation of kraft, organosolv and soda lignins, *Int. J. Biol. Macromol.* 106 (2018) 979–987. <https://doi.org/10.1016/j.ijbiomac.2017.08.102>.
- [32] Z. Hu, X. Du, J. Liu, H.M. Chang, H. Jameel, Structural Characterization of Pine Kraft Lignin: BioChoice Lignin vs Indulin AT, *J. Wood Chem. Technol.* 36 (2016) 432–446. <https://doi.org/10.1080/02773813.2016.1214732>.
- [33] L. Kouisni, P. Holt-Hindle, M.M.K. Paleologou, The Lignoforce System™: A New Process for the Production of High-Quality Lignin from Black Liquor. *Journal of Science & Technology for Forest Products and processes: VOL.2, NO.4, Pulp Pap. Canada.* 2012 (2012) 6–10.
- [34] H. Li, A.G. McDonald, Fractionation and characterization of industrial lignins, *Ind. Crops Prod.* 62 (2014) 67–76. <https://doi.org/10.1016/j.indcrop.2014.08.013>.
- [35] I. Dallmeyer, F. Ko, J.F. Kadla, Correlation of elongational fluid properties to fiber diameter in electrospinning of softwood kraft lignin solutions, *Ind. Eng. Chem. Res.* 53 (2014) 2697–2705. <https://doi.org/10.1021/ie403724y>.
- [36] I. Dallmeyer, S. Chowdhury, J.F. Kadla, Preparation and characterization of kraft lignin-based moisture-responsive films with reversible shape-change capability, *Biomacromolecules.* 14 (2013) 2354–2363. <https://doi.org/10.1021/bm400465p>.
- [37] R. Ding, H. Wu, M. Thunga, N. Bowler, M.R. Kessler, Processing and characterization of low-cost electrospun carbon fibers from organosolv lignin/polyacrylonitrile blends, *Carbon N. Y.* 100 (2016) 126–136. <https://doi.org/10.1016/j.carbon.2015.12.078>.
- [38] S.J. Park, S.Y. Lee, History and structure of carbon fibers, in: *Springer Ser. Mater. Sci.*, Springer Netherlands, Dordrecht, 2014: pp. 1–30.

https://doi.org/10.1007/978-94-017-9478-7_1.

- [39] D.D.L. Chung, ed., *Front Matter*, in: *Carbon Fiber Compos.*, Butterworth-Heinemann, Boston, 2015: p. iii. <https://doi.org/10.1016/b978-0-08-050073-7.50001-4>.
- [40] X. Zhang, Y. Lu, H. Xiao, H. Peterlik, Effect of hot stretching graphitization on the structure and mechanical properties of rayon-based carbon fibers, *J. Mater. Sci.* 49 (2014) 673–684. <https://doi.org/10.1007/s10853-013-7748-0>.
- [41] T. Matsumoto, Mesophase pitch and its carbon fibers, *Pure Appl. Chem.* 57 (1985) 1553–1562. <https://doi.org/10.1351/pac198557111553>.
- [42] X. Huang, Fabrication and properties of carbon fibers, *Materials (Basel)*. 2 (2009) 2369–2403. <https://doi.org/10.3390/ma2042369>.
- [43] M. Dumont, G. Chollon, M.A. Dourges, R. Paillet, X. Bourrat, R. Naslain, J.L. Bruneel, M. Couzi, Chemical, Microstructural and thermal analyses of a naphthalene-derived mesophase pitch, *Carbon N. Y.* 40 (2002) 1475–1486. [https://doi.org/10.1016/S0008-6223\(01\)00320-7](https://doi.org/10.1016/S0008-6223(01)00320-7).
- [44] H.C. Liu, A.T. Chien, B.A. Newcomb, Y. Liu, S. Kumar, Processing, Structure, and Properties of Lignin- and CNT-Incorporated Polyacrylonitrile-Based Carbon Fibers, *ACS Sustain. Chem. Eng.* 3 (2015) 1943–1954. <https://doi.org/10.1021/acssuschemeng.5b00562>.
- [45] S.J. Park, M.K. Seo, Element and Processing, in: S.J. Park, M.K. Seo (Eds.), *Interface Sci. Technol.*, Elsevier, 2011: pp. 431–499. <https://doi.org/10.1016/B978-0-12-375049-5.00006-2>.
- [46] R.C. Houtz, “Orlon” Acrylic Fiber: Chemistry and Properties, *Text. Res. J.* 20 (1950) 786–801. <https://doi.org/10.1177/004051755002001107>.
- [47] E. Fitzer, D.J. Müller, The influence of oxygen on the chemical reactions during stabilization of pan as carbon fiber precursor, *Carbon N. Y.* 13 (1975) 63–69. [https://doi.org/10.1016/0008-6223\(75\)90259-6](https://doi.org/10.1016/0008-6223(75)90259-6).
- [48] L. Henderson, B. Fox, M. Huson, M. Maghe, C. Creighton, S. Nunna, N. Byrne, S. Atkiss, Using ionic liquids to reduce energy consumption for carbon fibre production, *J. Mater. Chem. A*. 4 (2016). <https://doi.org/10.1039/C6TA06842A>.
- [49] S.A. White, J.E. Spruiell, F.L. Paulauskas, Fundamental studies of stabilization of polyacrylonitrile precursor, part 1: Effects of thermal and environmental treatments, *Int. SAMPE Symp. Exhib.* 51 (2006) 51.
- [50] E. Fitzer, W. Frohs, M. Heine, Optimization of stabilization and carbonization treatment of PAN fibres and structural characterization of the resulting carbon fibres, *Carbon N. Y.* 24 (1986) 387–395. [https://doi.org/10.1016/0008-6223\(86\)90257-5](https://doi.org/10.1016/0008-6223(86)90257-5).
- [51] A. Bismarck, M.E. Kumru, J. Springer, J. Simitzis, Surface properties of PAN-based carbon fibers tuned by anodic oxidation in different alkaline electrolyte systems, *Appl. Surf. Sci.* 143 (1999) 45–55. [https://doi.org/10.1016/S0169-4332\(98\)00929-5](https://doi.org/10.1016/S0169-4332(98)00929-5).
- [52] N. V. Salim, S. Blight, C. Creighton, S. Nunna, S. Atkiss, J.M. Razal, The Role

- of Tension and Temperature for Efficient Carbonization of Polyacrylonitrile Fibers: Toward Low Cost Carbon Fibers, *Ind. Eng. Chem. Res.* 57 (2018) 4268–4276. <https://doi.org/10.1021/acs.iecr.7b05336>.
- [53] P.J. Goodhew, A.J. Clarke, J.E. Bailey, A review of the fabrication and properties of carbon fibres, *Mater. Sci. Eng.* 17 (1975) 3–30. [https://doi.org/10.1016/0025-5416\(75\)90026-9](https://doi.org/10.1016/0025-5416(75)90026-9).
- [54] E.D. Weil, Carbon fibers, 2nd edition by J. B. Donnet and R. C. Bansal, Marcel Dekker, *Polym. Adv. Technol.* 3 (1992) 47–47. <https://doi.org/10.1002/pat.1992.220030109>.
- [55] N. Yusof, A.F. Ismail, Post spinning and pyrolysis processes of polyacrylonitrile (PAN)-based carbon fiber and activated carbon fiber: A review, *J. Anal. Appl. Pyrolysis.* 93 (2012) 1–13. <https://doi.org/10.1016/j.jaap.2011.10.001>.
- [56] J. Dietrich, P. Hirt, H. Herlinger, Electron-beam-induced cyclisation to obtain C-fibre precursors from polyacrylonitrile homopolymers, *Eur. Polym. J.* 32 (1996) 617–623. [https://doi.org/10.1016/0014-3057\(95\)00185-9](https://doi.org/10.1016/0014-3057(95)00185-9).
- [57] C.D. Warren, F.L. Paulauskas, F.S. Baker, C.C. Eberle, A. Naskar, Multi-task research program to develop commodity grade, lower cost carbon fiber, 40th, SAMPE Fall Tech. Conf. Multifunct. Mater. 2008; Memphis, TN. (2008) 36.
- [58] J.L. Wertz, M. Deleu, S. Coppée, A. Richel, Hemicelluloses and lignin in biorefineries, Boca Raton: CRC Press, 2017. <https://doi.org/10.1201/b22136>.
- [59] F.H. Isikgor, C.R. Becer, Lignocellulosic biomass: a sustainable platform for the production of bio-based chemicals and polymers, *Polym. Chem.* 6 (2015) 4497–4559. <https://doi.org/10.1039/c5py00263j>.
- [60] N.D. Patil, N.R. Tanguy, N. Yan, Lignin Interunit Linkages and Model Compounds, in: *Lignin Polym. Compos.*, William Andrew Publishing, 2015: pp. 27–47. <https://doi.org/10.1016/B978-0-323-35565-0.00003-5>.
- [61] K. Sudo, K. Shimizu, A new carbon fiber from lignin, *J. Appl. Polym. Sci.* 44 (1992) 127–134. <https://doi.org/10.1002/app.1992.070440113>.
- [62] J.F. Kadla, S. Kubo, R.D. Gilbert, R.A. Venditti, Lignin-Based Carbon Fibers, in: *Chem. Modif. Prop. Usage Lignin*, 2011: pp. 121–137. https://doi.org/10.1007/978-1-4615-0643-0_7.
- [63] A. Compere, W. Griffith, Low cost carbon fiber from renewable resources, in: 33rd Int. SAMPE Tech. Conf., 2001: pp. 1–28.
- [64] J.F. Kadla, S. Kubo, R.A. Venditti, R.D. Gilbert, A.L. Compere, W. Griffith, Lignin-based carbon fibers for composite fiber applications, *Carbon N. Y.* 40 (2002) 2913–2920. [https://doi.org/10.1016/S0008-6223\(02\)00248-8](https://doi.org/10.1016/S0008-6223(02)00248-8).
- [65] S.Y. Lin, C.W. Dence, *Methods in Lignin Chemistry*, Springer Series in Wood Science, 2008. [https://doi.org/10.1016/0305-0491\(93\)90261-3](https://doi.org/10.1016/0305-0491(93)90261-3).
- [66] J.C. Del Río, P. Prinsen, J. Rencoret, L. Nieto, J. Jiménez-Barbero, J. Ralph, Á.T. Martínez, A. Gutiérrez, Structural characterization of the lignin in the cortex and pith of elephant grass (*Pennisetum purpureum*) stems, *J. Agric. Food Chem.* 60 (2012) 3619–3634. <https://doi.org/10.1021/jf300099g>.

- [67] E. Adler, Lignin chemistry-past, present and future, *Wood Sci. Technol.* 11 (1977) 169–218. <https://doi.org/10.1007/BF00365615>.
- [68] J.H. Banoub, M. Delmas, Structural elucidation of the wheat straw lignin polymer by atmospheric pressure chemical ionization tandem mass spectrometry and matrix-assisted laser desorption/ionization time-of-flight mass spectrometry, *J. Mass Spectrom.* 38 (2003) 900–903. <https://doi.org/10.1002/jms.503>.
- [69] C. Crestini, F. Melone, M. Sette, R. Saladino, Milled wood lignin: A linear oligomer, *Biomacromolecules.* 12 (2011) 3928–3935. <https://doi.org/10.1021/bm200948r>.
- [70] F. Souto, V. Calado, N. Pereira, Lignin-based carbon fiber: a current overview, *Mater. Res. Express.* 5 (2018).
- [71] N. Mandlekar, A. Cayla, F. Rault, S. Giraud, F. Salaün, G. Malucelli, J.-P. Guan, An Overview on the Use of Lignin and Its Derivatives in Fire Retardant Polymer Systems, in: M. Poletto (Ed.), *Lignin - Trends Appl.*, IntechOpen, Rijeka, 2018. <https://doi.org/10.5772/intechopen.72963>.
- [72] T. Aro, P. Fatehi, Production and Application of Lignosulfonates and Sulfonated Lignin, *ChemSusChem.* 10 (2017) 1861–1877. <https://doi.org/10.1002/cssc.201700082>.
- [73] T. Li, S. Takkellapati, The current and emerging sources of technical lignins and their applications, *Biofuels, Bioprod. Biorefining.* 12 (2018) 756–787. <https://doi.org/10.1002/bbb.1913>.
- [74] Z. Wang, T.Q. Lam, J.Y. Zhu, Lignosulfonate and elevated pH can enhance enzymatic saccharification of lignocelluloses, *Biotechnol. Biofuels.* 6 (2013). <https://doi.org/10.1186/1754-6834-6-9>.
- [75] A. Vishtal, A. Kraslawski, Challenges in industrial applications of technical lignins, *BioResources.* 6 (2011) 3547–3568.
- [76] D. Daniel, L. Khachatryan, C. Astete, R. Asatryan, C. Marculescu, D. Boldor, Sulfur contaminations inhibit depolymerization of Kraft lignin, *Bioresour. Technol. Reports.* 8 (2019) 100341. <https://doi.org/https://doi.org/10.1016/j.biteb.2019.100341>.
- [77] A.N. Evdokimov, A. V. Kurzin, O. V. Fedorova, P. V. Lukanin, V.G. Kazakov, A.D. Trifonova, Desulfurization of kraft lignin, *Wood Sci. Technol.* 52 (2018) 1165–1174. <https://doi.org/10.1007/s00226-018-1014-1>.
- [78] H. Erdtman, Lignins: Occurrence, formation, structure and reactions, *J. Polym. Sci. Part B Polym. Lett.* 10 (1972) 228–230. <https://doi.org/10.1002/pol.1972.110100315>.
- [79] S. Svensson, Minimizing the sulphur content in Kraft lignin, Degree Project, ECTS 30.0 At STFI-Packforsk, (2008).
- [80] J.W.A.-G. Gaskin J.W. A4 - Steiner, C. A4 - Harris, K. A4 - Das, K.C. A4 - Bibens, B., Effect of low-temperature pyrolysis conditions on biochar for agricultural use, *Trans. ASABE.* v. 51 (2008) 2061-2069–2008 v.51 no.6.

- [81] J. Qi, K. Han, Q. Wang, J. Gao, Carbonization of biomass: Effect of additives on alkali metals residue, SO₂ and NO emission of chars during combustion, *Energy*. 130 (2017) 560–569. <https://doi.org/https://doi.org/10.1016/j.energy.2017.04.109>.
- [82] R.J.A. Gosselink, A. Abächerli, H. Semke, R. Malherbe, P. Käuper, A. Nadif, J.E.G. Van Dam, Analytical protocols for characterisation of sulphur-free lignin, *Ind. Crops Prod.* 19 (2004) 271–281. <https://doi.org/10.1016/j.indcrop.2003.10.008>.
- [83] T. Saito, J.H. Perkins, F. Vautard, H.M. Meyer, J.M. Messman, B. Tolnai, A.K. Naskar, Methanol fractionation of softwood Kraft lignin: Impact on the lignin properties, *ChemSusChem*. 7 (2014) 221–228. <https://doi.org/10.1002/cssc.201300509>.
- [84] S.Y. Park, J.-Y. Kim, H.J. Youn, J.W. Choi, Fractionation of lignin macromolecules by sequential organic solvents systems and their characterization for further valuable applications., *Int. J. Biol. Macromol.* 106 (2018) 793–802. <https://doi.org/10.1016/j.ijbiomac.2017.08.069>.
- [85] A.S. Jääskeläinen, T. Liitiä, A. Mikkelsen, T. Tamminen, Aqueous organic solvent fractionation as means to improve lignin homogeneity and purity, *Ind. Crops Prod.* 103 (2017) 51–58. <https://doi.org/10.1016/j.indcrop.2017.03.039>.
- [86] F. Xu, J.X. Sun, R. Sun, P. Fowler, M.S. Baird, Comparative study of organosolv lignins from wheat straw, *Ind. Crops Prod.* 23 (2006) 180–193. <https://doi.org/10.1016/j.indcrop.2005.05.008>.
- [87] C. Arato, E.K. Pye, G. Gjennestad, The Lignol Approach to Biorefining of Woody Biomass to Produce Ethanol and Chemicals, in: B.H. Davison, B.R. Evans, M. Finkelstein, J.D. McMillan (Eds.), *Appl. Biochem. Biotechnol.*, Humana Press, Totowa, NJ, 2005: pp. 0871–0882. <https://doi.org/10.1385/abab:123:1-3:0871>.
- [88] M. Vallejos, F. Felissia, A. Curvelo, M.D. Zambon, L. Ramos, M. Area, Chemical and physico-chemical characterization of lignins obtained from ethanol-water fractionation of bagasse, *BioResources*. 6 (2011) 1158–1171.
- [89] N.M. Stark, D.J. Yelle, U.P. Agarwal, Techniques for Characterizing Lignin, in: O. Faruk, M. Sain (Eds.), *Lignin Polym. Compos.*, William Andrew Publishing, 2015: pp. 49–66. <https://doi.org/10.1016/B978-0-323-35565-0.00004-7>.
- [90] S. Constant, H.L.J. Wienk, A.E. Frissen, P. De Peinder, R. Boelens, D.S. Van Es, R.J.H. Grisel, B.M. Weckhuysen, W.J.J. Huijgen, R.J.A. Gosselink, P.C.A. Bruijninx, New insights into the structure and composition of technical lignins: A comparative characterisation study, *Green Chem.* 18 (2016) 2651–2665. <https://doi.org/10.1039/c5gc03043a>.
- [91] J.C. Parajó, J.L. Alonso, D. Vázquez, On the behaviour of lignin and hemicelluloses during the acetosolv processing of wood, *Bioresour. Technol.* 46 (1993) 233–240. [https://doi.org/https://doi.org/10.1016/0960-8524\(93\)90126-V](https://doi.org/https://doi.org/10.1016/0960-8524(93)90126-V).
- [92] F. Öhman, H. Theliander, P. Tomani, P. Axegard, Method for separating lignin

- from black liquor. US Patent 8,486,224 B2, US8486224B2, 2013.
- [93] F. Öhman, H. Theliander, M. Norgren, P. Tomani, P. Axegård, Method for separating lignin from a lignin containing liquid/slurry. US Patent 8,815,052, B2, 2009.
- [94] P. Tomani, The LignoBoost process, *Cellul. Chem. Technol.* 44 (2010) 53–58.
- [95] C. Ma, Z. Li, J. Li, Q. Fan, L. Wu, J. Shi, Y. Song, Lignin-based hierarchical porous carbon nanofiber films with superior performance in supercapacitors, *Appl. Surf. Sci.* 456 (2018) 568–576.
<https://doi.org/10.1016/j.apsusc.2018.06.189>.
- [96] L. Kouisni, A. Gagné, K. Maki, P. Holt-Hindle, M. Paleologou, LignoForce System for the Recovery of Lignin from Black Liquor: Feedstock Options, Odor Profile, and Product Characterization, *ACS Sustain. Chem. Eng.* 4 (2016) 5152–5159. <https://doi.org/10.1021/acssuschemeng.6b00907>.
- [97] D. Schorr, P.N. Diouf, T. Stevanovic, Evaluation of industrial lignins for biocomposites production, *Ind. Crops Prod.* 52 (2014) 65–73.
<https://doi.org/10.1016/j.indcrop.2013.10.014>.
- [98] X. Jiang, D. Savithri, X. Du, S. Pawar, H. Jameel, H.M. Chang, X. Zhou, Fractionation and Characterization of Kraft Lignin by Sequential Precipitation with Various Organic Solvents, *ACS Sustain. Chem. Eng.* 5 (2017) 835–842.
<https://doi.org/10.1021/acssuschemeng.6b02174>.
- [99] K. Maki, M. Paleologou, Y. Zhang, M. Feng, P. Fatehi, LignoForce™ Kraft Lignin Extraction: Process Scale-Up, and Product Development, in: *Kraft Lignin Innov. Forum*, 2017.
- [100] L. Kouisni, P. Holt-Hindle, K. Maki, M. Paleologou, The LignoForce System™: A new process for the production of high-quality lignin from black liquor, *J. Sci. Technol. For. Prod. Process.* 2 (2012) 6–10.
- [101] S. Kubo, J.F. Kadla, Thermal decomposition study of isolated lignin using temperature modulated TGA, *J. Wood Chem. Technol.* 28 (2008) 106–121.
<https://doi.org/10.1080/02773810802124928>.
- [102] S. Kubo, J.F. Kadla, Poly(ethylene oxide)/organosolv lignin blends: Relationship between thermal properties, chemical structure, and blend behavior, *Macromolecules.* 37 (2004) 6904–6911.
<https://doi.org/10.1021/ma0490552>.
- [103] R. Ruiz-Rosas, J. Bedia, M. Lallave, I.G. Loscertales, A. Barrero, J. Rodríguez-Mirasol, T. Cordero, The production of submicron diameter carbon fibers by the electrospinning of lignin, *Carbon N. Y.* 48 (2010) 696–705.
<https://doi.org/10.1016/j.carbon.2009.10.014>.
- [104] O.Y. Abdelaziz, K. Li, P. Tunå, C.P. Hulteberg, Continuous catalytic depolymerisation and conversion of industrial kraft lignin into low-molecular-weight aromatics, *Biomass Convers. Biorefinery.* 8 (2018) 455–470.
<https://doi.org/10.1007/s13399-017-0294-2>.
- [105] J. Sameni, S. Krigstin, D. dos S. Rosa, A. Leao, M. Sain, Thermal characteristics of lignin residue from industrial processes, *BioResources.* 9

(2014) 725–737.

- [106] V. Fierro, V. Torné-Fernández, A. Celzard, D. Montané, Influence of the demineralisation on the chemical activation of Kraft lignin with orthophosphoric acid, *J. Hazard. Mater.* 149 (2007) 126–133.
<https://doi.org/https://doi.org/10.1016/j.jhazmat.2007.03.056>.
- [107] R.K. Sharma, J.B. Wooten, V.L. Baliga, X. Lin, W. Geoffrey Chan, M.R. Hajaligol, Characterization of chars from pyrolysis of lignin, *Fuel*. 83 (2004) 1469–1482. <https://doi.org/https://doi.org/10.1016/j.fuel.2003.11.015>.
- [108] D.L. Dalluge, K.H. Kim, R.C. Brown, The influence of alkali and alkaline earth metals on char and volatile aromatics from fast pyrolysis of lignin, *J. Anal. Appl. Pyrolysis*. 127 (2017) 385–393.
<https://doi.org/https://doi.org/10.1016/j.jaap.2017.07.011>.
- [109] Suhas, P.J.M. Carrott, M.M.L.R. Carrott, Using alkali metals to control reactivity and porosity during physical activation of demineralised kraft lignin, *Carbon N. Y.* 47 (2009) 1012–1017.
<https://doi.org/https://doi.org/10.1016/j.carbon.2008.12.001>.
- [110] D. Mohan, C.U. Pittman, P.H. Steele, Single, binary and multi-component adsorption of copper and cadmium from aqueous solutions on Kraft lignin—a biosorbent, *J. Colloid Interface Sci.* 297 (2006) 489–504.
<https://doi.org/https://doi.org/10.1016/j.jcis.2005.11.023>.
- [111] J. Sameni, S. Krigstin, M. Sain, Characterization of Lignins Isolated from Industrial Residues and their Beneficial Uses, *BioResources*. 11 (2016) 8435–8456. <https://doi.org/10.15376/biores.11.4.8435-8456>.
- [112] W.F. DeGroot, F. Shafizadeh, The influence of exchangeable cations on the carbonization of biomass, *J. Anal. Appl. Pyrolysis*. 6 (1984) 217–232.
[https://doi.org/https://doi.org/10.1016/0165-2370\(84\)80019-4](https://doi.org/https://doi.org/10.1016/0165-2370(84)80019-4).
- [113] E. Jakab, O. Faix, F. Till, Thermal decomposition of milled wood lignins studied by thermogravimetry/mass spectrometry, *J. Anal. Appl. Pyrolysis*. 40–41 (1997) 171–186. [https://doi.org/https://doi.org/10.1016/S0165-2370\(97\)00046-6](https://doi.org/https://doi.org/10.1016/S0165-2370(97)00046-6).
- [114] M. Kleen, G. Gellerstedt, Influence of inorganic species on the formation of polysaccharide and lignin degradation products in the analytical pyrolysis of pulps, *J. Anal. Appl. Pyrolysis*. 35 (1995) 15–41.
[https://doi.org/https://doi.org/10.1016/0165-2370\(95\)00893-J](https://doi.org/https://doi.org/10.1016/0165-2370(95)00893-J).
- [115] S. Wang, Z. Li, X. Bai, W. Yi, P. Fu, Influence of inherent hierarchical porous char with alkali and alkaline earth metallic species on lignin pyrolysis, *Bioresour. Technol.* 268 (2018) 323–331.
<https://doi.org/https://doi.org/10.1016/j.biortech.2018.07.117>.
- [116] R. Mahadevan, S. Adhikari, R. Shakya, K. Wang, D. Dayton, M. Lehrich, S.E. Taylor, Effect of Alkali and Alkaline Earth Metals on in-Situ Catalytic Fast Pyrolysis of Lignocellulosic Biomass: A Microreactor Study, *Energy & Fuels*. 30 (2016) 3045–3056. <https://doi.org/10.1021/acs.energyfuels.5b02984>.
- [117] D.A. Baker, N.C. Gallego, F.S. Baker, On the characterization and spinning of an organic-purified lignin toward the manufacture of low-cost carbon fiber, *J.*

- Appl. Polym. Sci. 124 (2012) 227–234. <https://doi.org/10.1002/app.33596>.
- [118] I. Dallmeyer, F. Ko, J.F. Kadla, Electrospinning of technical lignins for the production of fibrous networks, *J. Wood Chem. Technol.* 30 (2010) 315–329. <https://doi.org/10.1080/02773813.2010.527782>.
- [119] M. Zhang, *Carbon Fibers Derived from Dry-Spinning of Modified Lignin Precursors*, Clemson University, 2016.
- [120] N. Giummarella, C. Lindgren, M.E. Lindström, G. Henriksson, Lignin Prepared by Ultrafiltration of Black Liquor, *Bioresour. Technol.* 11 (2016) 3494–3510.
- [121] C. Pouteau, B. Cathala, P. Dole, B. Kurek, B. Monties, Structural modification of Kraft lignin after acid treatment: Characterisation of the apolar extracts and influence on the antioxidant properties in polypropylene, *Ind. Crops Prod.* 21 (2005) 101–108. <https://doi.org/10.1016/j.indcrop.2004.01.003>.
- [122] S. Yasuda, N. Terashima, T. Ito, Chemical structures of sulfuric acid lignin. I. Chemical structures of condensation products from monolignols, *Mokuzai Gakkaishi.* 26 (1980) 552–557.
- [123] W. Fang, M. Ståhl Alekhina, O. Ershova, S. Heikkinen, H. Sixta, Purification and characterization of kraft lignin, *Holzforschung.* 69 (2015) 943–950. <https://doi.org/10.1515/hf-2014-0200>.
- [124] V. Passoni, C. Scarica, M. Levi, S. Turri, G. Griffini, Fractionation of Industrial Softwood Kraft Lignin: Solvent Selection as a Tool for Tailored Material Properties, *ACS Sustain. Chem. Eng.* 4 (2016) 2232–2242. <https://doi.org/10.1021/acssuschemeng.5b01722>.
- [125] W. Goldmann Valdes, J. Ahola, M. Mikola, J. Tanskanen, Solubility and fractionation of Indulin AT kraft lignin in ethanol-water media, *Sep. Purif. Technol.* 209 (2018). <https://doi.org/10.1016/j.seppur.2018.06.054>.
- [126] A. Tagami, C. Gioia, M. Lauberts, T. Budnyak, R. Moriana, M.E. Lindström, O. Sevastyanova, Solvent fractionation of softwood and hardwood kraft lignins for more efficient uses: Compositional, structural, thermal, antioxidant and adsorption properties, *Ind. Crops Prod.* 129 (2019) 123–134. <https://doi.org/10.1016/j.indcrop.2018.11.067>.
- [127] P. Ma, Y. Gao, H. Zhai, Fractionated Wheat Straw Lignin and Its Application as Antioxidant, *Bioresour. Vol 8, No 4.* (2013).
- [128] R. Sun, J. Tomkinson, Fractional separation and physico-chemical analysis of lignins from the black liquor of oil palm trunk fibre pulping, *Sep. Purif. Technol.* 24 (2001) 529–539. [https://doi.org/10.1016/S1383-5866\(01\)00153-8](https://doi.org/10.1016/S1383-5866(01)00153-8).
- [129] T. V. Lourençon, F.A. Hansel, T.A. Da Silva, L.P. Ramos, G.I.B. De Muniz, W.L.E. Magalhães, Hardwood and softwood kraft lignins fractionation by simple sequential acid precipitation, *Sep. Purif. Technol.* 154 (2015) 82–88. <https://doi.org/10.1016/j.seppur.2015.09.015>.
- [130] A. Toledano, L. Serrano, A. Garcia, I. Mondragon, J. Labidi, Comparative study of lignin fractionation by ultrafiltration and selective precipitation, *Chem. Eng. J.* 157 (2010) 93–99. <https://doi.org/10.1016/j.cej.2009.10.056>.

- [131] S.I. Mussatto, M. Fernandes, I.C. Roberto, Lignin recovery from brewer's spent grain black liquor, *Carbohydr. Polym.* 70 (2007) 218–223. <https://doi.org/10.1016/j.carbpol.2007.03.021>.
- [132] A. Toledano, A. García, I. Mondragon, J. Labidi, Lignin separation and fractionation by ultrafiltration, *Sep. Purif. Technol.* 71 (2010) 38–43. <https://doi.org/10.1016/j.seppur.2009.10.024>.
- [133] M.H. Hussin, A.A. Rahim, M.N. Mohamad Ibrahim, D. Perrin, N. Brosse, Enhanced properties of oil palm fronds (OPF) lignin fractions produced via tangential ultrafiltration technique, *Ind. Crop. Prod.* 66 (4896) 1–10. <https://doi.org/10.1016/j.indcrop.2014.12.027>.
- [134] I. Norberg, Y. Nordström, R. Drougge, G. Gellerstedt, E. Sjöholm, A new method for stabilizing softwood kraft lignin fibers for carbon fiber production, *J. Appl. Polym. Sci.* 128 (2013) 3824–3830. <https://doi.org/10.1002/app.38588>.
- [135] Y. Nordström, I. Norberg, E. Sjöholm, R. Drougge, A new softening agent for melt spinning of softwood kraft lignin, *J. Appl. Polym. Sci.* 129 (2013) 1274–1279. <https://doi.org/10.1002/app.38795>.
- [136] C. Compere, AL., Griffith, WL. and Leitten, Improving the Fundamental Properties of Lignin-Based Carbon Fibre for Transport Applications, *Int. SAMPE Symp. Exhib.* 49 (2001).
- [137] J.F. Kadla, S. Kubo, R.A. Venditti, R.D. Gilbert, Novel hollow core fibers prepared from lignin polypropylene blends, *J. Appl. Polym. Sci.* 85 (2002) 1353–1355. <https://doi.org/10.1002/app.10640>.
- [138] S. Kubo, J.F. Kadla, Kraft lignin/poly(ethylene oxide) blends: Effect of lignin structure on miscibility and hydrogen bonding, *J. Appl. Polym. Sci.* 98 (2005) 1437–1444. <https://doi.org/10.1002/app.22245>.
- [139] S. Kubo, J.F. Kadla, Lignin-based carbon fibers: Effect of synthetic polymer blending on fiber properties, *J. Polym. Environ.* 13 (2005) 97–105. <https://doi.org/10.1007/s10924-005-2941-0>.
- [140] G. Husman, Development and Commercialization of a Novel Low-Cost Carbon Fiber, in: *DOE Hydrog. Fuel Cells Progr. Veh. Technol. Progr. Annu. Merit Rev. Peer Eval. Meet.*, 2014: pp. 1–20.
- [141] P.J. Bissett, C.W. Herriott, Lignin/Polyacrylonitrile-Containing Dopes, Fibers, and Methods of Making Same. US Patent US20120003471A1, US20120003471A1, 2010.
- [142] X. Dong, C. Lu, P. Zhou, S. Zhang, L. Wang, D. Li, Polyacrylonitrile/lignin sulfonate blend fiber for low-cost carbon fiber, *RSC Adv.* 5 (2015) 42259–42265. <https://doi.org/10.1039/c5ra01241d>.
- [143] V. Poursorkhabi, A.K. Mohanty, M. Misra, Electrospinning of aqueous lignin/poly(ethylene oxide) complexes, *J. Appl. Polym. Sci.* 132 (2015). <https://doi.org/10.1002/app.41260>.
- [144] V. Poursorkhabi, A.K. Mohanty, M. Misra, Statistical analysis of the effects of carbonization parameters on the structure of carbonized electrospun organosolv lignin fibers, *J. Appl. Polym. Sci.* 133 (2016) n/a-n/a.

<https://doi.org/10.1002/app.44005>.

- [145] N.Y. Teng, I. Dallmeyer, J.F. Kadla, Incorporation of multiwalled carbon nanotubes into electrospun softwood kraft lignin-based fibers, *J. Wood Chem. Technol.* 33 (2013) 299–316. <https://doi.org/10.1080/02773813.2013.795807>.
- [146] I. Dallmeyer, L.T. Lin, Y. Li, F. Ko, J.F. Kadla, Preparation and characterization of interconnected, Kraft lignin-based carbon fibrous materials by electrospinning, *Macromol. Mater. Eng.* 299 (2014) 540–551. <https://doi.org/10.1002/mame.201300148>.
- [147] X. Xu, J. Zhou, L. Jiang, G. Lubineau, S.A. Payne, D. Gutschmidt, Lignin-based carbon fibers: Carbon nanotube decoration and superior thermal stability, *Carbon N. Y.* 80 (2014) 91–102. <https://doi.org/10.1016/j.carbon.2014.08.042>.
- [148] D.K. Seo, J.P. Jeun, H.B. Kim, P.H. Kang, Preparation and characterization of the carbon nanofiber mat produced from electrospun pan/lignin precursors by electron beam irradiation, *Rev. Adv. Mater. Sci.* 28 (2011) 31–34.
- [149] J. Roman, W. Neri, A. Derré, P. Poulin, Electrospun lignin-based twisted carbon nanofibers for potential microelectrodes applications, *Carbon N. Y.* 145 (2019) 556–564. <https://doi.org/10.1016/j.carbon.2019.01.036>.
- [150] M. Ago, J.E. Jakes, L.S. Johansson, S. Park, O.J. Rojas, Interfacial properties of lignin-based electrospun nanofibers and films reinforced with cellulose nanocrystals, *ACS Appl. Mater. Interfaces.* 4 (2012) 6849–6856. <https://doi.org/10.1021/am302008p>.
- [151] C. Lai, Z. Zhou, L. Zhang, X. Wang, Q. Zhou, Y. Zhao, Y. Wang, X.F. Wu, Z. Zhu, H. Fong, Free-standing and mechanically flexible mats consisting of electrospun carbon nanofibers made from a natural product of alkali lignin as binder-free electrodes for high-performance supercapacitors, *J. Power Sources.* 247 (2014) 134–141. <https://doi.org/10.1016/j.jpowsour.2013.08.082>.
- [152] D.R. Paul, C.B. Bucknall, *Polymer Blends: Formulation and Performance*, Wiley, 2000.
- [153] J.F. Kadla, S. Kubo, Miscibility and hydrogen bonding in blends of poly(ethylene oxide) and kraft lignin, *Macromolecules.* 36 (2003) 7803–7811. <https://doi.org/10.1021/ma0348371>.
- [154] S. Kubo, J.F. Kadla, The formation of strong intermolecular interactions in immiscible blends of poly(vinyl alcohol) (PVA) and lignin, *Biomacromolecules.* 4 (2003) 561–567. <https://doi.org/10.1021/bm025727p>.
- [155] M. Thunga, K. Chen, D. Grewell, M.R. Kessler, Bio-renewable precursor fibers from lignin/polylactide blends for conversion to carbon fibers, *Carbon N. Y.* 68 (2014) 159–166. <https://doi.org/10.1016/j.carbon.2013.10.075>.
- [156] M. Thunga, K. Chen, M.R. Kessler, Process of making carbon fibers from compositions including esterified lignin and poly(lactic acid), US9340425B2, 2016.
- [157] V.B. Gupta, Melt-spinning processes, in: V.B. Gupta, V.K. Kothari (Eds.), *Manuf. Fibre Technol.*, Springer Netherlands, Dordrecht, 2011: pp. 67–97.

- https://doi.org/10.1007/978-94-011-5854-1_4.
- [158] P. Bajpai, *Carbon Fibre from Lignin*, Springer Singapore, 2017.
<https://doi.org/10.1007/978-981-10-4229-4>.
- [159] K. Sudo, K. Shimizu, N. Nakashima, A. Yokoyama, A new modification method of exploded lignin for the preparation of a carbon fiber precursor, *J. Appl. Polym. Sci.* 48 (1993) 1485–1491.
<https://doi.org/10.1002/app.1993.070480817>.
- [160] K. Sudo, K. Shimizu, Method for Manufacturing Lignin for Carbon Fiber Spinning. US Patent US5344921A, US5344921A, 1994.
- [161] Y. Uraki, S. Kubo, N. Nigo, Y. Sano, T. Sasaya, Preparation of Carbon Fibers from Organosolv Lignin Obtained by Aqueous Acetic Acid Pulping, *Holzforschung.* 49 (1995) 343–350. <https://doi.org/10.1515/hfsg.1995.49.4.343>.
- [162] S. Kubo, Y. Uraki, Y. Sano, Preparation of carbon fibers from softwood lignin by atmospheric acetic acid pulping, *Carbon N. Y.* 36 (1998) 1119–1124.
[https://doi.org/10.1016/S0008-6223\(98\)00086-4](https://doi.org/10.1016/S0008-6223(98)00086-4).
- [163] L.M. Steudle, E. Frank, A. Ota, U. Hageroth, S. Henzler, W. Schuler, R. Neupert, M.R. Buchmeiser, Carbon Fibers Prepared from Melt Spun Peracylated Softwood Lignin: an Integrated Approach, *Macromol. Mater. Eng.* 302 (2017) 1600441. <https://doi.org/10.1002/mame.201600441>.
- [164] O. Hosseinaei, D.P. Harper, J.J. Bozell, T.G. Rials, Improving processing and performance of pure lignin carbon fibers through hardwood and herbaceous lignin blends, *Int. J. Mol. Sci.* 18 (2017). <https://doi.org/10.3390/ijms18071410>.
- [165] O. Hosseinaei, D.P. Harper, J.J. Bozell, T.G. Rials, Role of Physicochemical Structure of Organosolv Hardwood and Herbaceous Lignins on Carbon Fiber Performance, *ACS Sustain. Chem. Eng.* 4 (2016) 5785–5798.
<https://doi.org/10.1021/acssuschemeng.6b01828>.
- [166] V.B. Gupta, V.K. Kothari, *Manufactured fibre technology*, Chapman & Hall, London, 1997.
- [167] R.J. Young, P.A. Lovell, *Introduction to Polymers*, Third Edit, CRC Press, Boca Raton, FL, USA, 2011.
- [168] S. Wang, Y. Li, H. Xiang, Z. Zhou, T. Chang, M. Zhu, Low cost carbon fibers from bio-renewable Lignin/Poly(lactic acid) (PLA) blends, *Compos. Sci. Technol.* 119 (2015) 20–25. <https://doi.org/10.1016/j.compscitech.2015.09.021>.
- [169] S. Ramakrishna, K. Fujihara, W.-E. Teo, T.-C. Lim, Z. Ma, *An Introduction to Electrospinning and Nanofibers*, WORLD SCIENTIFIC, 2012.
<https://doi.org/10.1142/5894>.
- [170] D.H. Reneker, I. Chun, Nanometre diameter fibres of polymer, produced by electrospinning, *Nanotechnology.* 7 (1996) 216–223.
<https://doi.org/10.1088/0957-4484/7/3/009>.
- [171] S.L. Shenoy, W.D. Bates, H.L. Frisch, G.E. Wnek, Role of chain entanglements on fiber formation during electrospinning of polymer solutions: Good solvent, non-specific polymer-polymer interaction limit, *Polymer (Guildf).* 46 (2005)

3372–3384. <https://doi.org/10.1016/j.polymer.2005.03.011>.

- [172] S. Tungprapa, T. Puangparn, M. Weerasombut, I. Jangchud, P. Fakum, S. Semongkhol, C. Meechaisue, P. Supaphol, Electrospun cellulose acetate fibers: Effect of solvent system on morphology and fiber diameter, *Cellulose*. 14 (2007) 563–575. <https://doi.org/10.1007/s10570-007-9113-4>.
- [173] J.M. Deitzel, J. Kleinmeyer, D. Harris, N.C. Beck Tan, The effect of processing variables on the morphology of electrospun nanofibers and textiles, *Polymer (Guildf)*. 42 (2001) 261–272. [https://doi.org/10.1016/S0032-3861\(00\)00250-0](https://doi.org/10.1016/S0032-3861(00)00250-0).
- [174] W.K. Son, J.H. Youk, T.S. Lee, W.H. Park, The effects of solution properties and polyelectrolyte on electrospinning of ultrafine poly(ethylene oxide) fibers, *Polymer (Guildf)*. 45 (2004) 2959–2966. <https://doi.org/10.1016/j.polymer.2004.03.006>.
- [175] A. Celebioglu, T. Uyar, Electrospun porous cellulose acetate fibers from volatile solvent mixture, *Mater. Lett.* 65 (2011) 2291–2294. <https://doi.org/10.1016/j.matlet.2011.04.039>.
- [176] S.A. Theron, E. Zussman, A.L. Yarin, Experimental investigation of the governing parameters in the electrospinning of polymer solutions, *Polymer (Guildf)*. 45 (2004) 2017–2030. <https://doi.org/10.1016/j.polymer.2004.01.024>.
- [177] C. Mit-Uppatham, M. Nithitanakul, P. Supaphol, Ultrafine electrospun polyamide-6 fibers: Effect of solution conditions on morphology and average fiber diameter, *Macromol. Chem. Phys.* 205 (2004) 2327–2338. <https://doi.org/10.1002/macp.200400225>.
- [178] S. Chuangchote, T. Sagawa, S. Yoshikawa, Electrospinning of poly(vinyl pyrrolidone): Effects of solvents on electrospinnability for the fabrication of poly(p-phenylene vinylene) and TiO₂ nanofibers, *J. Appl. Polym. Sci.* 114 (2009) 2777–2791. <https://doi.org/10.1002/app.30637>.
- [179] P. Supaphol, S. Chuangchote, On the electrospinning of poly(vinyl alcohol) nanofiber mats: A revisit, *J. Appl. Polym. Sci.* 108 (2008) 969–978. <https://doi.org/10.1002/app.27664>.
- [180] X.Y. Yuan, Y.Y. Zhang, C. Dong, J. Sheng, Morphology of ultrafine polysulfone fibers prepared by electrospinning, *Polym. Int.* 53 (2004) 1704–1710. <https://doi.org/10.1002/pi.1538>.
- [181] C. Zhang, X. Yuan, L. Wu, Y. Han, J. Sheng, Study on morphology of electrospun poly(vinyl alcohol) mats, *Eur. Polym. J.* 41 (2005) 423–432. <https://doi.org/10.1016/j.eurpolymj.2004.10.027>.
- [182] C.L. Casper, J.S. Stephens, N.G. Tassi, D.B. Chase, J.F. Rabolt, Controlling surface morphology of electrospun polystyrene fibers: Effect of humidity and molecular weight in the electrospinning process, *Macromolecules*. 37 (2004) 573–578. <https://doi.org/10.1021/ma0351975>.
- [183] M. Lallave, J. Bedia, R. Ruiz-Rosas, J. Rodríguez-Mirasol, T. Cordero, J.C. Otero, M. Marquez, A. Barrero, I.G. Loscertales, Filled and hollow carbon nanofibers by coaxial electrospinning of Alcell lignin without binder polymers, *Adv. Mater.* 19 (2007) 4292–4296. <https://doi.org/10.1002/adma.200700963>.

- [184] W.J. Youe, S.M. Lee, S.S. Lee, S.H. Lee, Y.S. Kim, Characterization of carbon nanofiber mats produced from electrospun lignin-g-polyacrylonitrile copolymer, *Int. J. Biol. Macromol.* 82 (2016) 497–504. <https://doi.org/10.1016/j.ijbiomac.2015.10.022>.
- [185] R. Ding, H. Wu, M. Thunga, N. Bowler, M.R. Kessler, Processing and characterization of low-cost electrospun carbon fibers from organosolv lignin/polyacrylonitrile blends, *Carbon N. Y.* 100 (2016) 126–136. <https://doi.org/10.1016/j.carbon.2015.12.078>.
- [186] M. Schreiber, S. Vivekanandhan, A.K. Mohanty, M. Misra, Iodine treatment of lignin-cellulose acetate electrospun fibers: Enhancement of green fiber carbonization, *ACS Sustain. Chem. Eng.* 3 (2015) 33–41. <https://doi.org/10.1021/sc500481k>.
- [187] S.X. Wang, L. Yang, L.P. Stubbs, X. Li, C. He, Lignin-derived fused electrospun carbon fibrous mats as high performance anode materials for lithium ion batteries, *ACS Appl. Mater. Interfaces.* 5 (2013) 12275–12282. <https://doi.org/10.1021/am4043867>.
- [188] A. Oroumei, B. Fox, M. Naebe, Thermal and rheological characteristics of biobased carbon fiber precursor derived from low molecular weight organosolv lignin, *ACS Sustain. Chem. Eng.* 3 (2015) 758–769. <https://doi.org/10.1021/acssuschemeng.5b00097>.
- [189] S. Hu, Y. Lo Hsieh, Ultrafine microporous and mesoporous activated carbon fibers from alkali lignin, *J. Mater. Chem. A.* 1 (2013) 11279–11288. <https://doi.org/10.1039/c3ta12538f>.
- [190] C. Salas, M. Ago, L.A. Lucia, O.J. Rojas, Synthesis of soy protein-lignin nanofibers by solution electrospinning, *React. Funct. Polym.* 85 (2014) 221–227. <https://doi.org/10.1016/j.reactfunctpolym.2014.09.022>.
- [191] D. Kai, S. Jiang, Z.W. Low, X.J. Loh, Engineering highly stretchable lignin-based electrospun nanofibers for potential biomedical applications, *J. Mater. Chem. B.* 3 (2015) 6194–6204. <https://doi.org/10.1039/c5tb00765h>.
- [192] M. Cho, M.A. Karaaslan, S. Renneckar, F. Ko, Enhancement of the mechanical properties of electrospun lignin-based nanofibers by heat treatment, *J. Mater. Sci.* 52 (2017) 9602–9614. <https://doi.org/10.1007/s10853-017-1160-0>.
- [193] M. Cho, M. Karaaslan, S. Chowdhury, F. Ko, S. Renneckar, Skipping Oxidative Thermal Stabilization for Lignin-Based Carbon Nanofibers, *ACS Sustain. Chem. Eng.* 6 (2018) 6434–6444. <https://doi.org/10.1021/acssuschemeng.8b00209>.
- [194] V.B. Gupta, Solution-spinning processes, in: V.B. Gupta, V.K. Kothari (Eds.), *Manuf. Fibre Technol.*, Springer Netherlands, Dordrecht, 2011: pp. 124–138. https://doi.org/10.1007/978-94-011-5854-1_6.
- [195] S. Otani, Y. Fukuoka, B. Igarashi, K. Sasaki, Method for Producing Carbonized Lignin Fiber. US Patent 3,461,082, US3461082A, 1965.
- [196] M. Zhang, A.A. Ogale, Carbon fibers from dry-spinning of acetylated softwood kraft lignin, *Carbon N. Y.* 69 (2014) 626–629.

<https://doi.org/10.1016/j.carbon.2013.12.015>.

- [197] M. Zhang, A.A. Ogale, Effect of temperature and concentration of acetylated-lignin solutions on dry-spinning of carbon fiber precursors, *J. Appl. Polym. Sci.* 133 (2016) n/a--n/a. <https://doi.org/10.1002/app.43663>.
- [198] M. Zhang, J. Jin, A. Ogale, Carbon Fibers from UV-Assisted Stabilization of Lignin-Based Precursors, *Fibers*. 3 (2015) 184–196. <https://doi.org/10.3390/fib3020184>.
- [199] A.S. Klett, A.M. Payne, M.C. Thies, Continuous-Flow Process for the Purification and Fractionation of Alkali and Organosolv Lignins, *ACS Sustain. Chem. Eng.* 4 (2016) 6689–6694. <https://doi.org/10.1021/acssuschemeng.6b01560>.
- [200] A.S. Klett, P. V. Chappell, M.C. Thies, Recovering ultraclean lignins of controlled molecular weight from Kraft black-liquor lignins, *Chem. Commun.* 51 (2015) 12855–12858. <https://doi.org/10.1039/c5cc05341b>.
- [201] J. Jin, J. Ding, A. Klett, M.C. Thies, A.A. Ogale, Carbon Fibers Derived from Fractionated-Solvated Lignin Precursors for Enhanced Mechanical Performance, *ACS Sustain. Chem. Eng.* 6 (2018) 14135–14142. <https://doi.org/10.1021/acssuschemeng.8b02697>.
- [202] C. Hou, R. Qu, Y. Liang, C. Wang, Kinetics of diffusion in polyacrylonitrile fiber formation, *J. Appl. Polym. Sci.* 96 (2005) 1529–1533. <https://doi.org/10.1002/app.21526>.
- [203] D.R. Paul, Diffusion during the coagulation step of wet-spinning, *J. Appl. Polym. Sci.* 12 (1968) 383–402. <https://doi.org/10.1002/app.1968.070120301>.
- [204] J. Kaur, K. Millington, S. Smith, Producing high-quality precursor polymer and fibers to achieve theoretical strength in carbon fibers: A review, *J. Appl. Polym. Sci.* 133 (2016). <https://doi.org/doi:10.1002/app.43963>.
- [205] T.-Y. Wang, H.-C. Chang, Y.-T. Chiu, J.-L. Tsai, The index of dry-jet wet spinning for polyacrylonitrile precursor fibers, *J. Appl. Polym. Sci.* 132 (2015). <https://doi.org/10.1002/app.41265>.
- [206] B. Zhang, C. Lu, Y. Liu, P. Zhou, Wet spun polyacrylonitrile-based hollow fibers by blending with alkali lignin, *Polymer (Guildf)*. 149 (2018) 294–304. <https://doi.org/10.1016/j.polymer.2018.07.019>.
- [207] J. Jin, A.A. Ogale, Carbon fibers derived from wet-spinning of equi-component lignin/polyacrylonitrile blends, *J. Appl. Polym. Sci.* 135 (2018) 45903. <https://doi.org/10.1002/app.45903>.
- [208] A. Oroumei, M. Naebe, Mechanical property optimization of wet-spun lignin/polyacrylonitrile carbon fiber precursor by response surface methodology, *Fibers Polym.* 18 (2017) 2079–2093. <https://doi.org/10.1007/s12221-017-7363-9>.
- [209] H. Mirbaha, P. Nourpanah, P. Scardi, M. D'incal, G. Greco, L. Valentini, S. Bittolo Bon, S. Arbab, N. Pugno, The Impact of Shear and Elongational Forces on Structural Formation of Polyacrylonitrile/Carbon Nanotubes Composite Fibers during Wet Spinning Process, *Mater. (Basel, Switzerland)*. 12 (2019)

2797. <https://doi.org/10.3390/ma12172797>.
- [210] Q. Ouyang, Y.-S. Chen, N. Zhang, G.-M. Mo, D.-H. Li, Q. Yan, Effect of Jet Swell and Jet Stretch on the Structure of Wet-Spun Polyacrylonitrile Fiber, *J. Macromol. Sci. Part B.* 50 (2011) 2417–2427. <https://doi.org/10.1080/00222348.2011.564104>.
- [211] A. Mataram, A.F. Ismail, D.S.A. Mahmud, T. Matsuura, Characterization and mechanical properties of polyacrylonitrile/silica composite fibers prepared via dry-jet wet spinning process, *Mater. Lett.* 64 (2010) 1875–1878. <https://doi.org/https://doi.org/10.1016/j.matlet.2010.05.031>.
- [212] S.P. Maradur, C.H. Kim, S.Y. Kim, B.H. Kim, W.C. Kim, K.S. Yang, Preparation of carbon fibers from a lignin copolymer with polyacrylonitrile, *Synth. Met.* 162 (2012) 453–459. <https://doi.org/10.1016/j.synthmet.2012.01.017>.
- [213] C. Lu, C. Blackwell, Q. Ren, E. Ford, Effect of the Coagulation Bath on the Structure and Mechanical Properties of Gel-Spun Lignin/Poly(vinyl alcohol) Fibers, *ACS Sustain. Chem. Eng.* 5 (2017) 2949–2959. <https://doi.org/10.1021/acssuschemeng.6b02423>.
- [214] N. Byrne, R. De Silva, Y. Ma, H. Sixta, M. Hummel, Enhanced stabilization of cellulose-lignin hybrid filaments for carbon fiber production, *Cellulose.* 25 (2018) 723–733. <https://doi.org/10.1007/s10570-017-1579-0>.
- [215] X. Shi, X. Wang, B. Tang, Z. Dai, K. Chen, J. Zhou, Impact of lignin extraction methods on microstructure and mechanical properties of lignin-based carbon fibers, *J. Appl. Polym. Sci.* 135 (2018). <https://doi.org/10.1002/app.45580>.
- [216] L. Salmén, E. Bergnor, A.-M. Olsson, M. Åkerström, A. Uhlin, Extrusion of Softwood Kraft Lignins as Precursors for Carbon Fibres, *BioResources.* 10 (2015). <https://doi.org/10.15376/biores.10.4.7544-7554>.
- [217] I. Brodin, M. Ernstsson, G. Gellerstedt, E. Sjöholm, Oxidative stabilisation of kraft lignin for carbon fibre production, *Holzforschung.* 66 (2012) 141–147. <https://doi.org/10.1515/HF.2011.133>.
- [218] J.L. Braun, K.M. Holtman, J.F. Kadla, Lignin-based carbon fibers: Oxidative thermostabilization of kraft lignin, *Carbon N. Y.* 43 (2005) 385–394. <https://doi.org/10.1016/j.carbon.2004.09.027>.
- [219] Y. Li, D. Cui, Y. Tong, L. Xu, Study on structure and thermal stability properties of lignin during thermostabilization and carbonization, *Int. J. Biol. Macromol.* 62 (2013) 663–669. <https://doi.org/https://doi.org/10.1016/j.ijbiomac.2013.09.040>.
- [220] M. Cho, F.K. Ko, S. Renneckar, Impact of Thermal Oxidative Stabilization on the Performance of Lignin-Based Carbon Nanofiber Mats, *ACS Omega.* 4 (2019) 5345–5355. <https://doi.org/10.1021/acsomega.9b00278>.
- [221] H. Mainka, L. Hilfert, S. Busse, F. Edelmann, E. Haak, A.S. Herrmann, Characterization of the major reactions during conversion of lignin to carbon fiber, *J. Mater. Res. Technol.* 4 (2015) 377–391. <https://doi.org/10.1016/j.jmrt.2015.04.005>.
- [222] A. Beste, ReaxFF study of the oxidation of lignin model compounds for the most common linkages in softwood in view of carbon fiber production, *J. Phys.*

- Chem. A. 118 (2014) 803–814. <https://doi.org/10.1021/jp410454q>.
- [223] M. Foston, G.A. Nunnery, X. Meng, Q. Sun, F.S. Baker, A. Ragauskas, NMR a critical tool to study the production of carbon fiber from lignin, *Carbon N. Y.* 52 (2013) 65–73. <https://doi.org/10.1016/j.carbon.2012.09.006>.
- [224] M. Nar, H.R. Rizvi, R.A. Dixon, F. Chen, A. Kovalcik, N. D'Souza, Superior plant based carbon fibers from electrospun poly-(caffeyl alcohol) lignin, *Carbon N. Y.* 103 (2016) 372–383. <https://doi.org/10.1016/j.carbon.2016.02.053>.
- [225] H. Kleinhans, L. Salmén, Development of lignin carbon fibers: Evaluation of the carbonization process, *J. Appl. Polym. Sci.* 133 (2016). <https://doi.org/10.1002/app.43965>.
- [226] A. Ferrari, J. Robertson, Interpretation of Raman spectra of disordered and amorphous carbon, *Phys. Rev. B - Condens. Matter Mater. Phys.* 61 (2000) 14095–14107. <https://doi.org/10.1103/PhysRevB.61.14095>.
- [227] M.A. Pimenta, G. Dresselhaus, M.S. Dresselhaus, L.G. Cançado, A. Jorio, R. Saito, Studying disorder in graphite-based systems by Raman spectroscopy, *Phys. Chem. Chem. Phys.* 9 (2007) 1276–1291. <https://doi.org/10.1039/b613962k>.
- [228] A.C. Ferrari, J. Robertson, Resonant Raman spectroscopy of disordered, amorphous, and diamondlike carbon, *Phys. Rev. B - Condens. Matter Mater. Phys.* 64 (2001). <https://doi.org/10.1103/PhysRevB.64.075414>.
- [229] Q. Li, M.T. Naik, H.S. Lin, C. Hu, W.K. Serem, L. Liu, P. Karki, F. Zhou, J.S. Yuan, Tuning hydroxyl groups for quality carbon fiber of lignin, *Carbon N. Y.* 139 (2018) 500–511. <https://doi.org/10.1016/j.carbon.2018.07.015>.
- [230] J. Ayutsede, M. Gandhi, S. Sukigara, M. Micklus, H.-E. Chen, F. Ko, Regeneration of Bombyx mori silk by electrospinning. Part 3: characterization of electrospun nonwoven mat, *Polymer (Guildf)*. 46 (2005) 1625–1634. <https://doi.org/https://doi.org/10.1016/j.polymer.2004.11.029>.
- [231] Z. Dai, X. Shi, H. Liu, H. Li, Y. Han, J. Zhou, High-strength lignin-based carbon fibers via a low-energy method, *RSC Adv.* 8 (2018) 1218–1224. <https://doi.org/10.1039/c7ra10821d>.
- [232] A. Bahi, J. Shao, M. Mohseni, F. Ko, Membranes based on Electrospun Lignin-Zeolite Composite Nanofibers, *Sep. Purif. Technol.* 187 (2017). <https://doi.org/10.1016/j.seppur.2017.06.015>.
- [233] F. Croisier, A.S. Duwez, C. Jérôme, A.F. Léonard, K.O. Van Der Werf, P.J. Dijkstra, M.L. Bennink, Mechanical testing of electrospun PCL fibers, *Acta Biomater.* 8 (2012) 218–224. <https://doi.org/10.1016/j.actbio.2011.08.015>.
- [234] C.R. Carlisle, C. Coulais, M. Guthold, The mechanical stress-strain properties of single electrospun collagen type I nanofibers, *Acta Biomater.* 6 (2010) 2997–3003. <https://doi.org/10.1016/j.actbio.2010.02.050>.
- [235] S.R. Baker, S. Banerjee, K. Bonin, M. Guthold, Determining the mechanical properties of electrospun poly- ϵ -caprolactone (PCL) nanofibers using AFM and a novel fiber anchoring technique, *Mater. Sci. Eng. C.* 59 (2016) 203–212. <https://doi.org/10.1016/j.msec.2015.09.102>.

- [236] R. Ramachandramoorthy, A. Beese, H. Espinosa, In situ electron microscopy tensile testing of constrained carbon nanofibers, *Int. J. Mech. Sci.* 149 (2018) 452–458. <https://doi.org/10.1016/j.ijmecsci.2017.09.028>.
- [237] TAPPI Press, TAPPI T 257 cm-02 Sampling and Preparing Wood for Analysis, Atlanta, GA, USA, 2002.
- [238] TAPPI Press, TAPPI T 264 cm-07 Preparation of Wood for Chemical Analysis, Atlanta, GA, USA, 2007.
- [239] TAPPI Press, TAPPI T211 om-02 Ash in Wood, Pulp, Paper and Paperboard: Combustion at 525 Degrees Celsius, Atlanta, GA, USA, 1993.
- [240] TAPPI Press, T 222 om-02 Acid-insoluble lignin in wood and pulp, Atlanta, GA, USA, 2006.
- [241] TAPPI Press, TAPPI UM 250 Acid-Soluble Lignin in Wood and Pulp, Atlanta, GA, USA, 2000.
- [242] D. Nečas, P. Klapetek, Gwyddion: an open-source software for SPM data analysis, *Cent. Eur. J. Phys.* 10 (2012) 181–188. <https://doi.org/10.2478/s11534-011-0096-2>.
- [243] UPM BioPiva product family, (n.d.). <https://www.upmbiochemicals.com/products/lignin/UPM-BioPiva-product-family/> (accessed March 16, 2019).
- [244] B. Ahvazi, É. Cloutier, O. Wojciechowicz, T.-D. Ngo, Lignin Profiling: A Guide for Selecting Appropriate Lignins as Precursors in Biomaterials Development, *ACS Sustain. Chem. Eng.* 4 (2016) 5090–5105. <https://doi.org/10.1021/acssuschemeng.6b00873>.
- [245] G. Gellerstedt, I. Brodin, E. Sjöholm, Kraft lignin as feedstock for chemical products, in: 2007.
- [246] M. Alekhina, O. Ershova, A. Ebert, S. Heikkinen, H. Sixta, Softwood kraft lignin for value-added applications: Fractionation and structural characterization, *Ind. Crops Prod.* 66 (2015) 220–228. <https://doi.org/10.1016/j.indcrop.2014.12.021>.
- [247] G. Taguchi, S. Chowdhury, Y. Wu, Taguchi's Quality Engineering Handbook, 2007. <https://doi.org/10.1002/9780470258354>.
- [248] N.-E. El Mansouri, J. Salvadó, Structural characterization of technical lignins for the production of adhesives: Application to lignosulfonate, kraft, soda-anthraquinone, organosolv and ethanol process lignins, *Ind. Crops Prod.* 24 (2006) 8–16. <https://doi.org/https://doi.org/10.1016/j.indcrop.2005.10.002>.
- [249] B.A. Jawad, C.H. Riedel, A.A. Bazzari, Determination of Particle Size Distribution Using Laser Diffraction Technique, *Tech. - New Mater.* 21 (2008) 71–78. <https://doi.org/10.1115/imece2004-60510>.
- [250] G.M. Henk, Particle Size Measurements : Fundamentals, Practice, Quality, 2009. <https://doi.org/10.1007/978-1-4020-9016-5>.
- [251] E.M.L. Ehrnrooth, Change in Pulp Fibre Density With Acid-Chlorite Delignification, *J. Wood Chem. Technol.* 4 (1984) 91–109. <https://doi.org/10.1080/02773818408062285>.

- [252] R. Kumar Singla, S.N. Maiti, A.K. Ghosh, Crystallization, Morphological, and Mechanical Response of Poly(Lactic Acid)/Lignin-Based Biodegradable Composites, *Polym. Plast. Technol. Eng.* 55 (2016) 475–485. <https://doi.org/10.1080/03602559.2015.1098688>.
- [253] H. Chung, N.R. Washburn, Extraction and Types of Lignin, in: *Lignin Polym. Compos.*, 2015: pp. 13–25. <https://doi.org/10.1016/B978-0-323-35565-0.00002-3>.
- [254] W.M. Goldmann, J. Ahola, O. Mankinen, A.M. Kantola, S. Komulainen, V.-V. Telkki, J. Tanskanen, Determination of Phenolic Hydroxyl Groups in Technical Lignins by Ionization Difference Ultraviolet Spectrophotometry ($\Delta\varepsilon$ -IDUS method), *Period. Polytech. Chem. Eng.* 61 (2016). <https://doi.org/10.3311/ppch.9269>.
- [255] O.Y. Abdelaziz, C.P. Hulteberg, Physicochemical Characterisation of Technical Lignins for Their Potential Valorisation, *Waste and Biomass Valorization*. 8 (2017) 859–869. <https://doi.org/10.1007/s12649-016-9643-9>.
- [256] A. Gancone, J. Pubule, M. Rosa, D. Blumberga, Evaluation of agriculture eco-efficiency in Latvia, *Energy Procedia*. 128 (2017) 309–315. <https://doi.org/10.1016/j.egypro.2017.08.318>.
- [257] M. Brebu, T. Tamminen, I. Spiridon, Thermal degradation of various lignins by TG-MS/FTIR and Py-GC-MS, *J. Anal. Appl. Pyrolysis*. 104 (2013) 531–539. <https://doi.org/10.1016/j.jaap.2013.05.016>.
- [258] C. Liu, J. Hu, H. Zhang, R. Xiao, Thermal conversion of lignin to phenols: Relevance between chemical structure and pyrolysis behaviors, *Fuel*. 182 (2016) 864–870. <https://doi.org/https://doi.org/10.1016/j.fuel.2016.05.104>.
- [259] Z. Ma, Q. Sun, J. Ye, Q. Yao, C. Zhao, Study on the thermal degradation behaviors and kinetics of alkali lignin for production of phenolic-rich bio-oil using TGA-FTIR and Py-GC/MS, *J. Anal. Appl. Pyrolysis*. 117 (2016) 116–124. <https://doi.org/10.1016/j.jaap.2015.12.007>.
- [260] J. Zhao, W. Xiuwen, J. Hu, Q. Liu, D. Shen, R. Xiao, Thermal degradation of softwood lignin and hardwood lignin by TG-FTIR and Py-GC/MS, *Polym. Degrad. Stab.* 108 (2014) 133–138. <https://doi.org/https://doi.org/10.1016/j.polymdegradstab.2014.06.006>.
- [261] D. Shen, G. Liu, J. Zhao, J. Xue, S. Guan, R. Xiao, Thermo-chemical conversion of lignin to aromatic compounds: Effect of lignin source and reaction temperature, *J. Anal. Appl. Pyrolysis*. 112 (2015) 56–65. <https://doi.org/https://doi.org/10.1016/j.jaap.2015.02.022>.
- [262] H. Yang, R. Yan, H. Chen, D.H. Lee, C. Zheng, Characteristics of hemicellulose, cellulose and lignin pyrolysis, *Fuel*. 86 (2007) 1781–1788. <https://doi.org/https://doi.org/10.1016/j.fuel.2006.12.013>.
- [263] M. Zhang, F.L.P. Resende, A. Moutsoglou, D.E. Raynie, Pyrolysis of lignin extracted from prairie cordgrass, aspen, and Kraft lignin by Py-GC/MS and TGA/FTIR, *J. Anal. Appl. Pyrolysis*. 98 (2012) 65–71. <https://doi.org/10.1016/j.jaap.2012.05.009>.

- [264] X. Lin, S. Sui, S. Tan, U.C. Pittman, J. Sun, Z. Zhang, Fast Pyrolysis of Four Lignins from Different Isolation Processes Using Py-GC/MS, *Energies*. 8 (2015). <https://doi.org/10.3390/en8065107>.
- [265] K.K. Pandey, A study of chemical structure of soft and hardwood and wood polymers by FTIR spectroscopy, *J. Appl. Polym. Sci.* 71 (2004) 1969–1975. [https://doi.org/10.1002/\(sici\)1097-4628\(19990321\)71:12<1969::aid-app6>3.0.co;2-d](https://doi.org/10.1002/(sici)1097-4628(19990321)71:12<1969::aid-app6>3.0.co;2-d).
- [266] S. Kubo, J.F. Kadla, Hydrogen bonding in lignin: A fourier transform infrared model compound study, *Biomacromolecules*. 6 (2005) 2815–2821. <https://doi.org/10.1021/bm050288q>.
- [267] R. Berenguer, F.J. García-Mateos, R. Ruiz-Rosas, D. Cazorla-Amorós, E. Morallón, J. Rodríguez-Mirasol, T. Cordero, Biomass-derived binderless fibrous carbon electrodes for ultrafast energy storage, *Green Chem.* 18 (2016) 1506–1515. <https://doi.org/10.1039/C5GC02409A>.
- [268] Taguchi.G, S. Konishi, Taguchi methods, orthogonal arrays and linear graphs: Tools for quality engineering, Dearborn, Mich. : American Supplier Institute, Center for Taguchi Methods, 1987.
- [269] C. Douglas, *Montgomery: Design and Analysis of Experiments*, New York: John Wiley, 2000.
- [270] D. Mourant, Z. Wang, M. He, X.S. Wang, M. Garcia-Perez, K. Ling, C.-Z. Li, Mallee wood fast pyrolysis: Effects of alkali and alkaline earth metallic species on the yield and composition of bio-oil, *Fuel*. 90 (2011) 2915–2922. <https://doi.org/https://doi.org/10.1016/j.fuel.2011.04.033>.
- [271] M.T. Reza, R. Emerson, M.H. Uddin, G. Gresham, C.J. Coronella, Ash reduction of corn stover by mild hydrothermal preprocessing, *Biomass Convers. Biorefinery*. 5 (2015) 21–31. <https://doi.org/10.1007/s13399-014-0122-x>.
- [272] D.S. Scott, L. Paterson, J. Piskorz, D. Radlein, Pretreatment of poplar wood for fast pyrolysis: rate of cation removal, *J. Anal. Appl. Pyrolysis*. 57 (2001) 169–176. [https://doi.org/https://doi.org/10.1016/S0165-2370\(00\)00108-X](https://doi.org/https://doi.org/10.1016/S0165-2370(00)00108-X).
- [273] O. Sevastyanova, M. Helander, S. Chowdhury, H. Lange, H. Wedin, L. Zhang, M. Ek, J.F. Kadla, C. Crestini, M.E. Lindström, Tailoring the molecular and thermo-mechanical properties of kraft lignin by ultrafiltration, *J. Appl. Polym. Sci.* 131 (2014) 9505–9515. <https://doi.org/10.1002/app.40799>.
- [274] C. Schuerch, The Solvent Properties of Liquids and Their Relation to the Solubility, Swelling, Isolation and Fractionation of Lignin, *J. Am. Chem. Soc.* 74 (1952) 5061–5067. <https://doi.org/10.1021/ja01140a020>.
- [275] J. Sameni, S. Krigstin, M. Sain, Solubility of Lignin and Acetylated Lignin in Organic Solvents, *Bioresources*. 12 (2017) 1548–1565. <https://doi.org/10.15376/biores.12.1.1548-1565>.
- [276] H. Sadeghifar, D.S. Argyropoulos, Macroscopic Behavior of Kraft Lignin Fractions: Melt Stability Considerations for Lignin–Polyethylene Blends, *ACS Sustain. Chem. Eng.* 4 (2016) 5160–5166.

<https://doi.org/10.1021/acssuschemeng.6b00636>.

- [277] H. Liu, Z. Dai, Q. Cao, X. Shi, X. Wang, H. Li, Y. Han, Y. Li, J. Zhou, Lignin/Polyacrylonitrile Carbon Fibers: The Effect of Fractionation and Purification on Properties of Derived Carbon Fibers, *ACS Sustain. Chem. Eng.* 6 (2018) 8554–8562. <https://doi.org/10.1021/acssuschemeng.8b00868>.
- [278] Q. Li, W.K. Serem, W. Dai, Y. Yue, M.T. Naik, S. Xie, P. Karki, L. Liu, H.J. Sue, H. Liang, F. Zhou, J.S. Yuan, Molecular weight and uniformity define the mechanical performance of lignin-based carbon fiber, *J. Mater. Chem. A* 5 (2017) 12740–12746. <https://doi.org/10.1039/c7ta01187c>.
- [279] Q. Li, M. Li, H.-S. Lin, C. Hu, P. Truong, T. Zhang, H.-J. Sue, Y. Pu, A.J. Ragauskas, J.S. Yuan, Non-Solvent Fractionation of Lignin Enhances Carbon Fiber Performance, *ChemSusChem*. 12 (2019) 3249–3256. <https://doi.org/doi:10.1002/cssc.201901052>.
- [280] X. Shi, Z. Dai, Q. Cao, K. Chen, J. Zhou, Stepwise fractionation extracted lignin for high strength lignin-based carbon fibers, *New J. Chem.* 43 (2019) 18868–18875. <https://doi.org/10.1039/C9NJ04942H>.
- [281] A. Duval, F. Vilaplana, C. Crestini, M. Lawoko, Solvent screening for the fractionation of industrial kraft lignin, *Holzforschung*. 0 (2015). <https://doi.org/10.1515/hf-2014-0346>.
- [282] P. Mousavioun, W.O.S. Doherty, Chemical and thermal properties of fractionated bagasse soda lignin, *Ind. Crops Prod.* 31 (2010) 52–58. <https://doi.org/https://doi.org/10.1016/j.indcrop.2009.09.001>.
- [283] D. Fengel, G. Wegener, *Wood: chemistry, ultrastructure, reactions*, Walter de Gruyter, New York, 1984.
- [284] C. Peng, G. Zhang, J. Yue, G. Xu, Pyrolysis of lignin for phenols with alkaline additive, *Fuel Process. Technol.* 124 (2014) 212–221. <https://doi.org/https://doi.org/10.1016/j.fuproc.2014.02.025>.
- [285] P.R. Patwardhan, J.A. Satrio, R.C. Brown, B.H. Shanks, Influence of inorganic salts on the primary pyrolysis products of cellulose, *Bioresour. Technol.* 101 (2010) 4646–4655. <https://doi.org/https://doi.org/10.1016/j.biortech.2010.01.112>.
- [286] L. Sandström, A.-C. Johansson, H. Wiinikka, O.G.W. Öhrman, M. Marklund, Pyrolysis of Nordic biomass types in a cyclone pilot plant — Mass balances and yields, *Fuel Process. Technol.* 152 (2016) 274–284. <https://doi.org/https://doi.org/10.1016/j.fuproc.2016.06.015>.
- [287] T.G. Fox, Influence of Diluent and of Copolymer Composition on the Glass Temperature of a Poly-mer System, *Bull. Am. Phys. Soc.* 1 (1956) 123.
- [288] O. Faix, Condensation indices of lignins determined by FTIR-spectroscopy, *Holz Als Roh- Und Werkst.* 49 (1991) 356–356. <https://doi.org/10.1007/bf02662706>.
- [289] W. Fang, S. Yang, T.Q. Yuan, A. Charlton, R.C. Sun, Effects of Various Surfactants on Alkali Lignin Electrospinning Ability and Spun Fibers, *Ind. Eng. Chem. Res.* 56 (2017) 9551–9559. <https://doi.org/10.1021/acs.iecr.7b02494>.

- [290] C. Hansen, *Hansen Solubility Parameters: A User's Handbook*, Second Edition, 2012. <https://doi.org/10.1201/9781420006834>.
- [291] A. Bengtsson, J. Bengtsson, M. Sedin, E. Sjöholm, Carbon Fibers from Lignin-Cellulose Precursors: Effect of Stabilization Conditions, *ACS Sustain. Chem. Eng.* 7 (2019) 8440–8448. <https://doi.org/10.1021/acssuschemeng.9b00108>.
- [292] J. Catalán, C. Díaz, F. García-Blanco, Characterization of Binary Solvent Mixtures of DMSO with Water and Other Cosolvents, *J. Org. Chem.* 66 (2001) 5846–5852. <https://doi.org/10.1021/jo010415i>.
- [293] GaylordChemical, *DMSO Physical Properties*, (2019). <https://www.gaylordchemical.com/literature/dmso-physical-properties/>.
- [294] H. Sadeghifar, C. Cui, S. Sen, D. Argyropoulos, Toward thermoplastic lignin polymers; thermal & polymer characteristics of kraft lignin & its derivatives, 2012.
- [295] C. Cui, H. Sadeghifar, S. Sen, D. Argyropoulos, Toward Thermoplastic Lignin Polymers; Part II: Thermal & Polymer Characteristics of Kraft Lignin & Derivatives, *Bioresources.* 8 (1) (2013) 864–886. <https://doi.org/10.15376/biores.8.1.864-886>.
- [296] J.M. Goodman, P.D. Kirby, L.O. Haustedt, Some calculations for organic chemists: boiling point variation, Boltzmann factors and the Eyring equation, *Tetrahedron Lett.* 41 (2000) 9879–9882. [https://doi.org/https://doi.org/10.1016/S0040-4039\(00\)01754-8](https://doi.org/https://doi.org/10.1016/S0040-4039(00)01754-8).
- [297] K. Peredo, D. Escobar, J. Vega-Lara, A. Berg, M. Pereira, Thermochemical properties of cellulose acetate blends with acetosolv and sawdust lignin: A comparative study, *Int. J. Biol. Macromol.* 83 (2016) 403–409. <https://doi.org/10.1016/j.ijbiomac.2015.11.022>.
- [298] R. Rana, R. Langenfeld-Heyser, R. Finkeldey, A. Polle, FTIR spectroscopy, chemical and histochemical characterisation of wood and lignin of five tropical timber wood species of the family of Dipterocarpaceae, *Wood Sci. Technol.* 44 (2010) 225–242. <https://doi.org/10.1007/s00226-009-0281-2>.
- [299] V.N. Tsaneva, W. Kwapinski, X. Teng, B.A. Glowacki, Assessment of the structural evolution of carbons from microwave plasma natural gas reforming and biomass pyrolysis using Raman spectroscopy, *Carbon N. Y.* 80 (2014) 617–628. <https://doi.org/10.1016/j.carbon.2014.09.005>.
- [300] K. Ishimaru, T. Hata, P. Bronsveld, D. Meier, Y. Imamura, Spectroscopic analysis of carbonization behavior of wood, cellulose and lignin, *J. Mater. Sci.* 42 (2007) 122–129. <https://doi.org/10.1007/s10853-006-1042-3>.
- [301] L.S. Johansson, J.M. Campbell, K. Koljonen, P. Stenius, Evaluation of surface lignin on cellulose fibers with XPS, *Appl. Surf. Sci.* 144–145 (1999) 92–95. [https://doi.org/10.1016/S0169-4332\(98\)00920-9](https://doi.org/10.1016/S0169-4332(98)00920-9).
- [302] J. Bañuls-Ciscar, D. Pratelli, M.L. Abel, J.F. Watts, Surface characterisation of pine wood by XPS, in: *Surf. Interface Anal.*, 2016: pp. 589–592. <https://doi.org/10.1002/sia.5960>.
- [303] W. Li, Y. Zhang, L. Das, Y. Wang, M. Li, N. Wanninayake, Y. Pu, D.Y. Kim,

- Y.T. Cheng, A.J. Ragauskas, J. Shi, Linking lignin source with structural and electrochemical properties of lignin-derived carbon materials, *RSC Adv.* 8 (2018) 38721–38732. <https://doi.org/10.1039/c8ra08539k>.
- [304] S. Kim, S.C. Chmely, M.R. Nimlos, Y.J. Bomble, T.D. Foust, R.S. Paton, G.T. Beckham, Computational study of bond dissociation enthalpies for a large range of native and modified Lignins, *J. Phys. Chem. Lett.* 2 (2011) 2846–2852. <https://doi.org/10.1021/jz201182w>.
- [305] J. Rodríguez-Mirasol, T. Cordero, J.J. Rodríguez, High-temperature carbons from kraft lignin, *Carbon N. Y.* 34 (1996) 43–52. [https://doi.org/10.1016/0008-6223\(95\)00133-6](https://doi.org/10.1016/0008-6223(95)00133-6).
- [306] S. Aslanzadeh, B. Ahvazi, Y. Boluk, C. Ayranci, Carbon Fiber Production from Electrospun Sulfur Free Softwood Lignin Precursors, *J. Eng. Fiber. Fabr.* 12 (2017) 33–43. <https://doi.org/10.1177/155892501701200405>.
- [307] M. Nakamizo, R. Kammereck, P.L. Walker, Laser raman studies on carbons, *Carbon N. Y.* 12 (1974) 259–267. [https://doi.org/10.1016/0008-6223\(74\)90068-2](https://doi.org/10.1016/0008-6223(74)90068-2).
- [308] A. Cuesta, P. Dhamelincourt, J. Laureyns, A. Martínez-Alonso, J.M.D. Tascón, Raman microprobe studies on carbon materials, *Carbon N. Y.* 32 (1994) 1523–1532. [https://doi.org/10.1016/0008-6223\(94\)90148-1](https://doi.org/10.1016/0008-6223(94)90148-1).
- [309] F. Tuinstra, J.L. Koenig, Raman Spectrum of Graphite, *J. Chem. Phys.* 53 (1970) 1126–1130. <https://doi.org/10.1063/1.1674108>.
- [310] K. Ishimaru, T. Hata, P. Bronsveld, T. Nishizawa, Y. Imamura, Characterization of sp²- and sp³-bonded carbon in wood charcoal, *J. Wood Sci.* 53 (2007) 442–448. <https://doi.org/10.1007/s10086-007-0879-7>.
- [311] A. Sadezky, H. Muckenhuber, H. Grothe, R. Niessner, U. Pöschl, Raman microspectroscopy of soot and related carbonaceous materials: Spectral analysis and structural information, *Carbon N. Y.* 43 (2005) 1731–1742. <https://doi.org/10.1016/j.carbon.2005.02.018>.
- [312] X. Zhang, Q. Yan, W. Leng, J. Li, J. Zhang, Z. Cai, E.B. Hassan, Carbon nanostructure of kraft lignin thermally treated at 500 to 1000 °C, *Materials (Basel)*. 10 (2017) 1–14. <https://doi.org/10.3390/ma10080975>.
- [313] T. Jawhari, A. Roid, J. Casado, Raman spectroscopic characterization of some commercially available carbon black materials, *Carbon N. Y.* 33 (1995) 1561–1565. [https://doi.org/10.1016/0008-6223\(95\)00117-V](https://doi.org/10.1016/0008-6223(95)00117-V).
- [314] H. Sadeghifar, S. Sen, S. V Patil, D.S. Argyropoulos, Toward Carbon Fibers from Single Component Kraft Lignin Systems: Optimization of Chain Extension Chemistry, *ACS Sustain. Chem. Eng.* 4 (2016) 5230–5237. <https://doi.org/10.1021/acssuschemeng.6b00848>.
- [315] Q. Li, S. Xie, W.K. Serem, M.T. Naik, L. Liu, J.S. Yuan, Quality carbon fibers from fractionated lignin, *Green Chem.* 19 (2017) 1628–1634. <https://doi.org/10.1039/c6gc03555h>.
- [316] C. Kim, K.S. Yang, M. Kojima, K. Yoshida, Y.J. Kim, Y.A. Kim, M. Endo, Fabrication of Electrospinning-Derived Carbon Nanofiber Webs for the Anode

- Material of Lithium-Ion Secondary Batteries, *Adv. Funct. Mater.* 16 (2006) 2393–2397. <https://doi.org/10.1002/adfm.200500911>.
- [317] Y. Wang, S. Serrano, J.J. Santiago-Avilés, Raman characterization of carbon nanofibers prepared using electrospinning, *Synth. Met.* 138 (2003) 423–427. [https://doi.org/https://doi.org/10.1016/S0379-6779\(02\)00472-1](https://doi.org/https://doi.org/10.1016/S0379-6779(02)00472-1).
- [318] X. Zhou, F. Zheng, X. Liu, L. Tang, G. Xue, G. Du, Q. Yong, M. Chen, L. Zhu, Glass transition of oxygen plasma treated enzymatic hydrolysis lignin, *BioResources.* 7 (2012) 4776–4785. <https://doi.org/10.15376/biores.7.4.4776-4785>.
- [319] L. Klarhöfer, B. Roos, W. Viöl, O. Höfft, S. Dieckhoff, V. Kempter, W. Maus-Friedrichs, Valence band spectroscopy on lignin, *Holzforschung.* 62 (2008) 688–693. <https://doi.org/10.1515/HF.2008.116>.
- [320] Klarhöfer Lothar, V. Wolfgang, M.-F. Wolfgang, Electron spectroscopy on plasma treated lignin and cellulose, *Holzforschung.* 64 (2010) 331. <https://doi.org/10.1515/hf.2010.048>.
- [321] J. Liu, W. Qu, Y. Xie, B. Zhu, T. Wang, X. Bai, X. Wang, Thermal conductivity and annealing effect on structure of lignin-based microscale carbon fibers, *Carbon N. Y.* 121 (2017) 35–47. <https://doi.org/https://doi.org/10.1016/j.carbon.2017.05.066>.
- [322] M. Demir, A.A. Farghaly, M.J. Decuir, M.M. Collinson, R.B. Gupta, Supercapacitance and oxygen reduction characteristics of sulfur self-doped micro/mesoporous bio-carbon derived from lignin, *Mater. Chem. Phys.* 216 (2018) 508–516. <https://doi.org/10.1016/j.matchemphys.2018.06.008>.
- [323] J. Lin, S. Kubo, T. Yamada, K. Koda, Y. Uraki, Chemical thermostabilization for the preparation of carbon fibers from softwood lignin, *BioResources.* 7 (2012) 5634–5646. <https://doi.org/10.15376/biores.7.4.5634-5646>.
- [324] J. Lin, G. Zhao, Preparation and Characterization of High Surface Area Activated Carbon Fibers from Lignin, *Polymers (Basel).* 8 (2016) 369. <https://doi.org/10.3390/polym8100369>.
- [325] H. Chen, X. Huang, M. Zhang, F. Damanik, M.B. Baker, A. Leferink, H. Yuan, R. Truckenmüller, C. van Blitterswijk, L. Moroni, Tailoring surface nanoroughness of electrospun scaffolds for skeletal tissue engineering, *Acta Biomater.* 59 (2017) 82–93. <https://doi.org/https://doi.org/10.1016/j.actbio.2017.07.003>.
- [326] J. Bouajila, P. Dole, C. Joly, A. Limare, Some laws of a lignin plasticization, *J. Appl. Polym. Sci.* 102 (2006) 1445–1451. <https://doi.org/10.1002/app.24299>.

